TEXAS INSTRUMENTS
INCORPORATED

FINAL REPORT FOR AIRBORNE ELECTRONICALLY STEERABLE PHASED ARRAY (AESPA) PROGRAM

Prepared for:

NATIONAL AERONAUTICS AND SPACE ADMINISTRATION
Marshall Space Flight Center
Huntsville, Alabama 35812

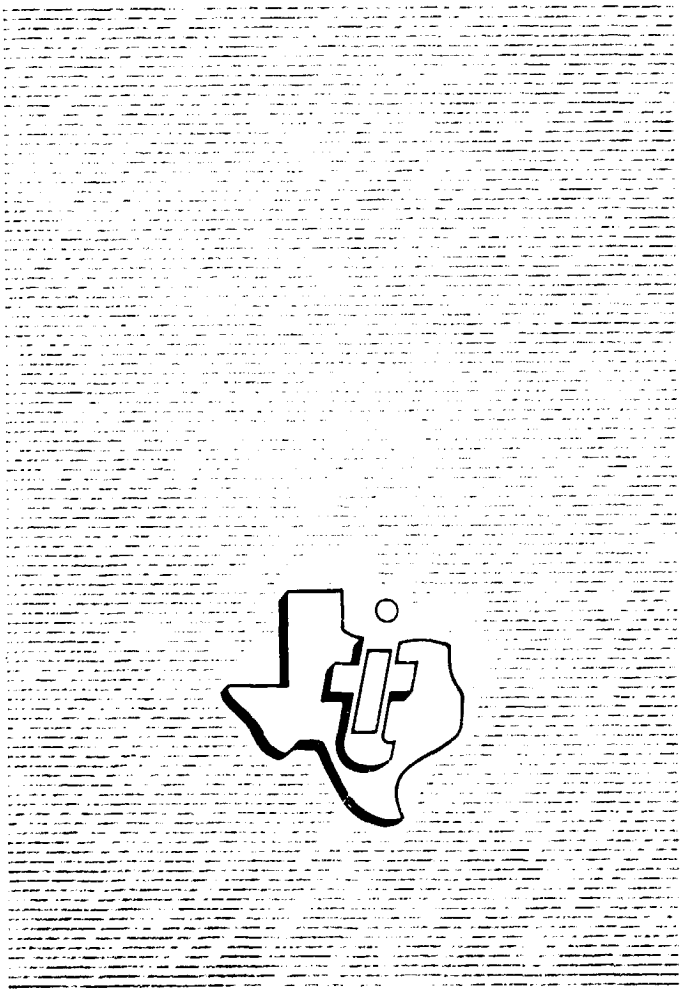

Contract No. NAS8-33116

Prepared by:

Equipment Group
Report No. U1-771401-F
November 1979

TEXAS INSTRUMENTS
INCORPORATED, Huntsville

TABLE OF CONTENTS

PRECEDING PAGE BLANK NOT FILMED

LIST OF ILLUSTRATIONS

LIST OF TABLES

SECTION I
INTRODUCTION

This report describes the work performed on the development and testing of a J-band transmissive array engineering model for the Airborne Electronically Steerable Phased Array (AESPA) program. This program, under Contract Number NAS8-33116, was sponsored by the Astrionics Division of NASA Marshall Space Flight Center.

The 19-element engineering model array was proposed as a means of demonstrating the performance capabilities of the transmissive array. The transmissive array approach was selected above two alternative approaches following an in-depth trade analysis. Key parameters of interest for the engineering array are gain, beamwidth, and sidelobe variation versus frequency and scan angle.

The AESPA program has included several study, design, and developmental tasks and has the following overall objectives:

- To develop a highly reliable solid-state communication terminal system applicable to low- and high-altitude, reusable and/or permanently placed satellites
- To provide high-gain electronic beamsteering without incurring a weight penalty
- To develop a highly efficient modular antenna concept applicable to moderate apertures driven by fully duplexed, electronic transceiver modules
- To extend these capabilities to J-band for high-data-rate (up to 10^8 bits per second) payloads.

A brief description of the various tasks performed to date on the program shows the progress achieved toward the overall objectives. In 1971, work was completed on the first phase of the program which was to provide a preliminary design of a spaceborne communications array. Key system parameters included the following:

- Light weight: under 50 pounds
- Simultaneous transmit and receive: 2282, 2101 MHz
- 60-degree conical coverage capable of automatic acquisition and tracking
- High gain: 60-percent antenna efficiency, 30-percent transmitter efficiency
- High sensitivity: 5-dB noise figure
- High reliability.

A system block diagram (Figure 1-1) and a system mechanical design concept (Figure 1-2) were configured during this first phase.

A full-scale 128-element array was designed, constructed, and tested as part of the second program phase. Also developed in this phase were an RF transmit manifold and a working electronics module integrating a duplexer, a transmitter, a receiver, and phase shifter circuits. A photograph of the array is included as Figure 1-3. A quarter section of the RF manifold is shown in Figure 1-4, while Figure 1-5 shows a prototype electronics module.

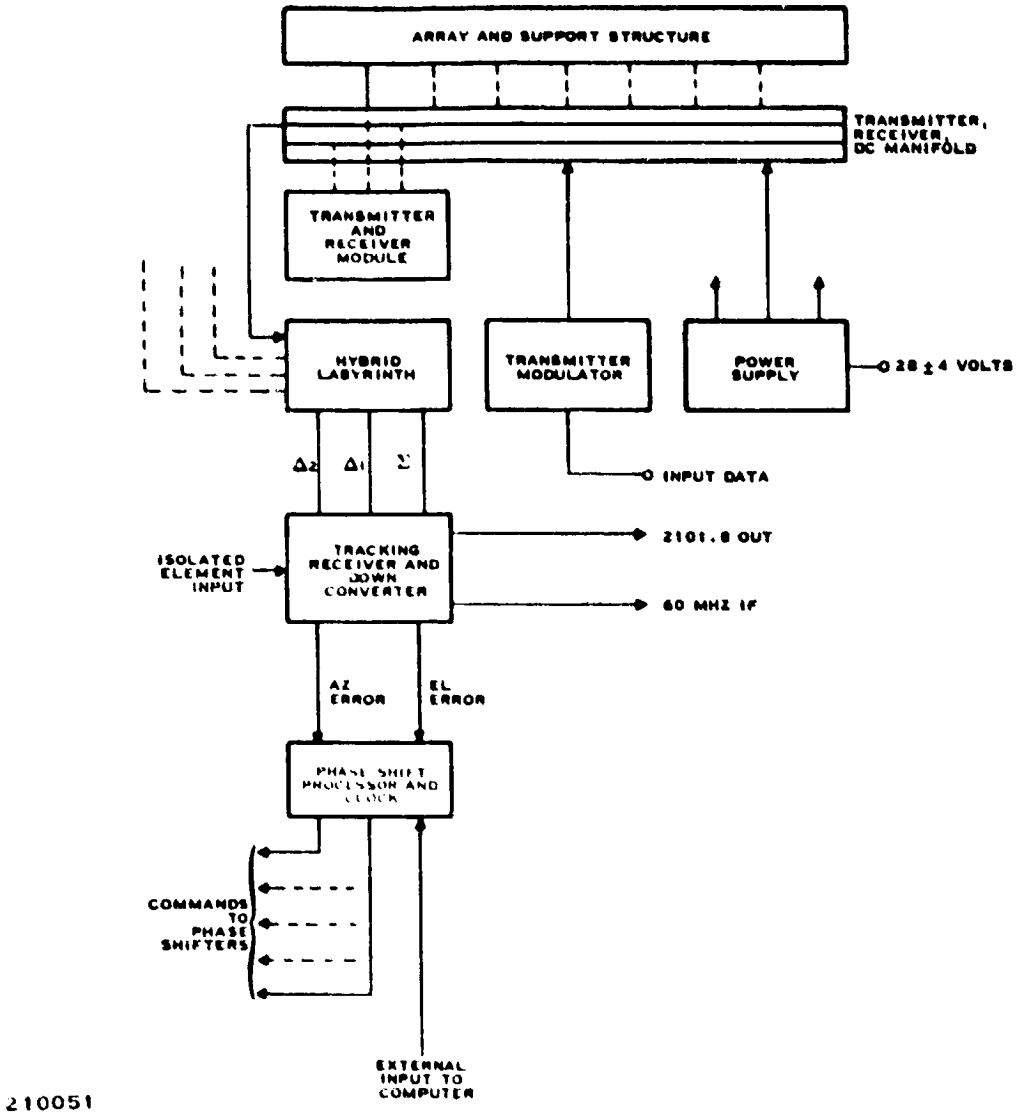

Figure 1-1. System Block Diagram

At this point, D.O. Lowery, NASA's cognizant engineer, suggested a development effort parallel to the S-band work, which would extend the technology to Ku-band and thus be applicable to the Tracking and Data Relay Satellite System (TDRSS). The scope of effort was increased to include development of components in this frequency band. A gallium arsenide diode to be used for power generation at J-band was developed for and delivered to NASA under this contract modification. Figure 1-6 shows the diode.

Phase III continued the parallel S-band/J-band development and included the following items:

Development of beamsteering logic

Development of a dc and logic manifold

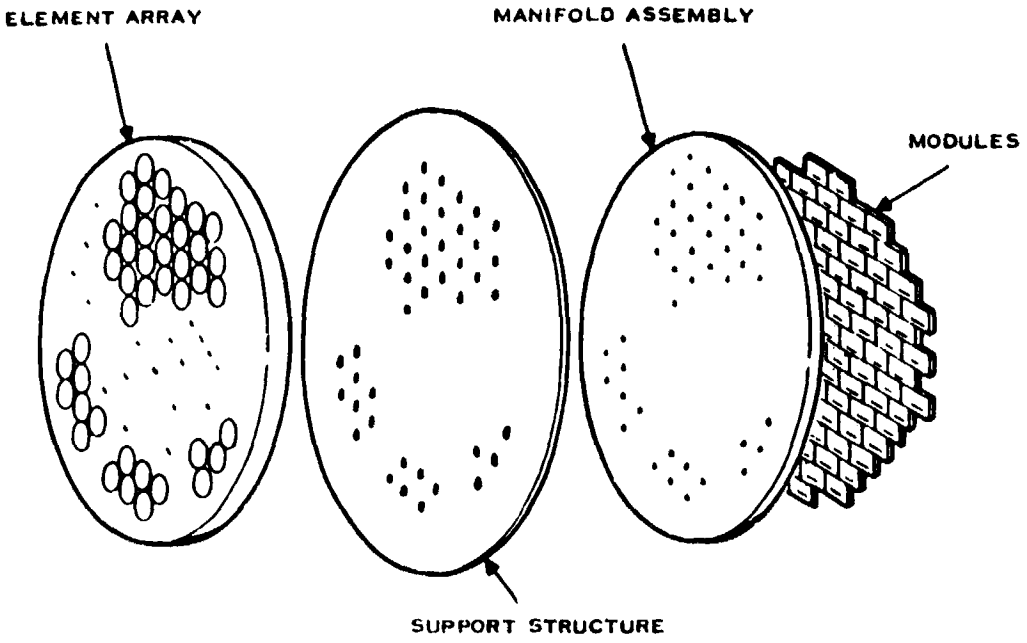

Figure 1-2. Array Assembly

Construction of 12 additional modules incorporating phase trim and a lower noise figure and capable of being hermetically sealed

Study of a J-band electronically steerable antenna system.

Also during this phase of the contract, members of the Pioneer Venus Orbiter study team showed interest in the application of the AESPA modular antenna concept to an electronically despun antenna (EDA) system. A study was initiated to look into the compatibility of AESPA components with various antenna configurations. Figure 1-7 shows the concept of a high-gain EDA placed on the top of a spacecraft. Two sizes of this configuration were considered for further study.

Figure 1-8 shows an alternate configuration where the antenna elements have been removed from the top of the spacecraft and integrated into a solar cell field on the outer diameter. Each of these configurations was to use the existing AESPA module. It was discovered during this phase of the EDA study that slight modifications of the fully duplexed AESPA module could result in its use as a radar module. This discovery led to the possibility of simultaneous radar mapping and communications functions by the EDA.

NASA Ames Research Center narrowed the various configurations and functions into three approaches and asked Texas Instruments to determine the viability of each. The three approaches include:

A fully integrated electronically despun antenna having a separate cylindrical aperture for communications with radar capability over an approximate 45-degree sector of that cylinder

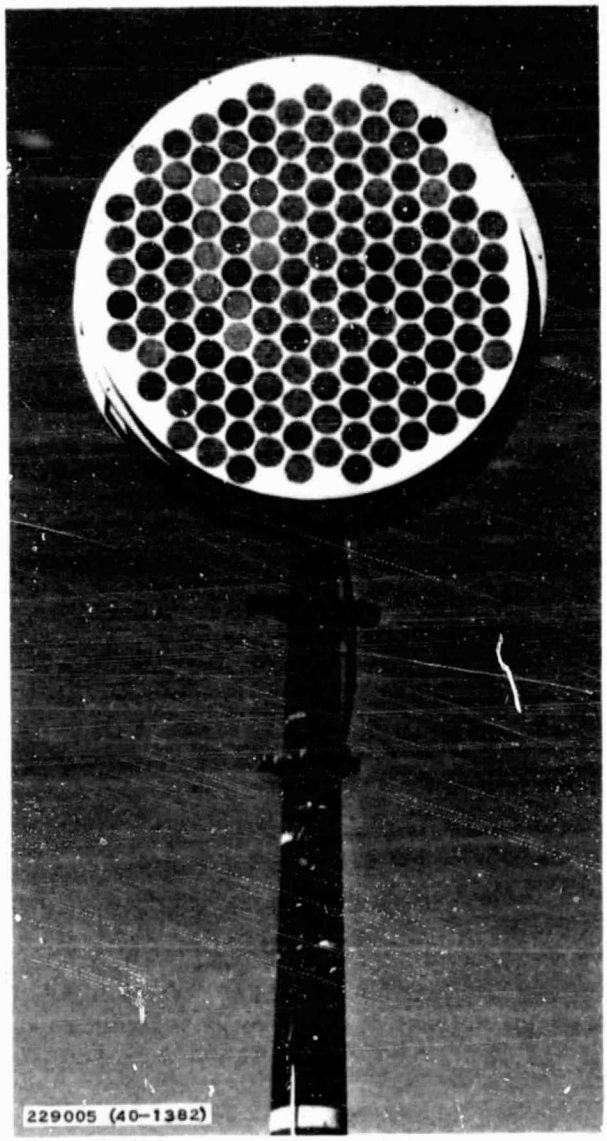

Figure 1-3. 128-Active-Element Antenna

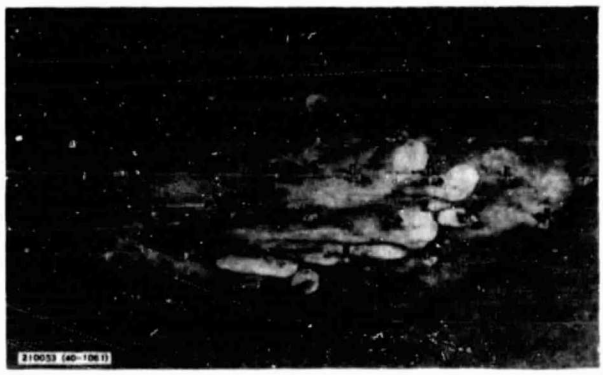

Figure 1-4. RF Manifold

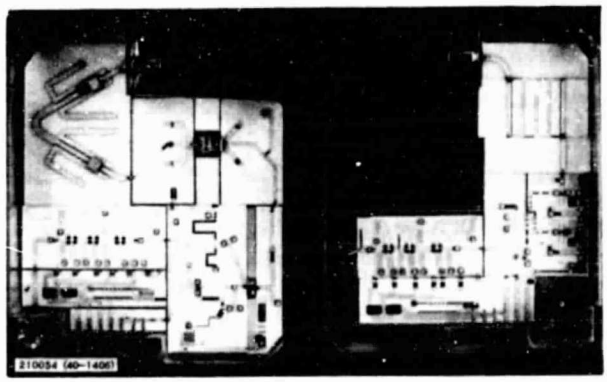

Figure 1-5. Electronics Module

A dedicated rectangular planar radar array using AESPA modules

A mechanically steered reflector system.

In parallel to the above efforts of AESPA Phase III, the J-band phased array study continued with the consideration of diodes in a power amplifier to obtain increased performance and reliability.

The fourth phase of AESPA continued the parallel S-band/J-band development and accomplished the following:

Completion of the 48 AESPA modules

Completion of a 48-element transmit manifold

Completion of a 48-element receive manifold

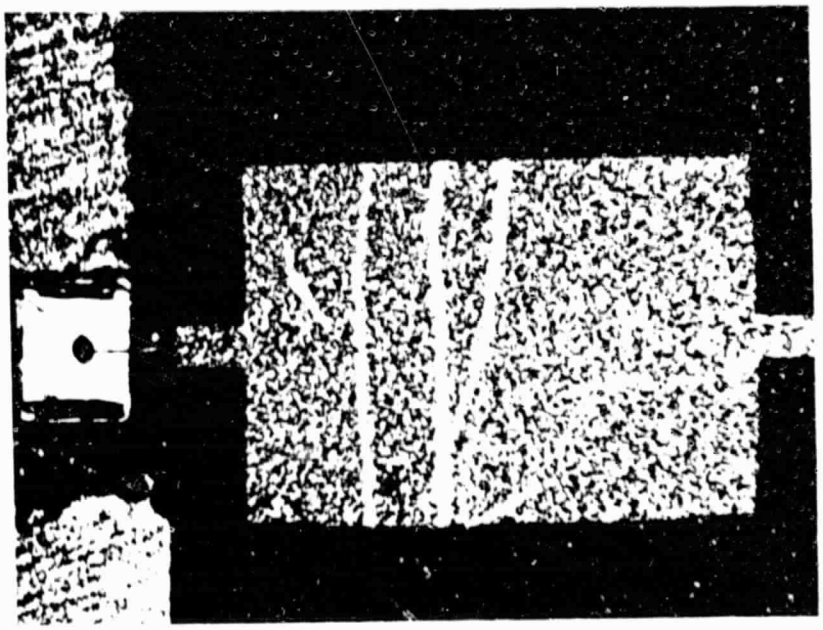

(B) DIODE PLACEMENT

Figure 1-6. Microstrip Circuit and Diode

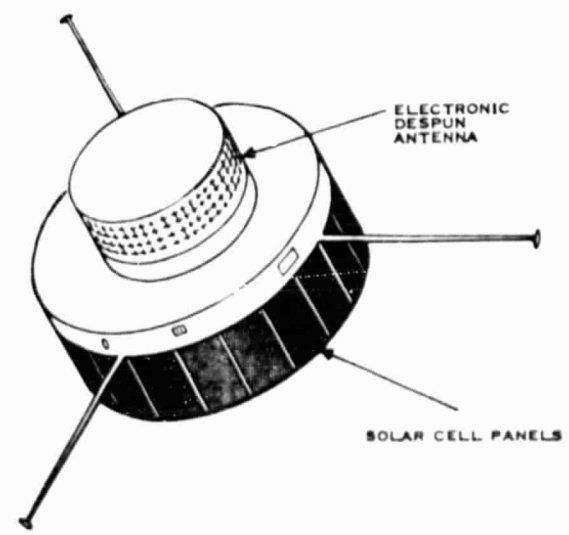

210059

Figure 1-7. Baseline System Concept

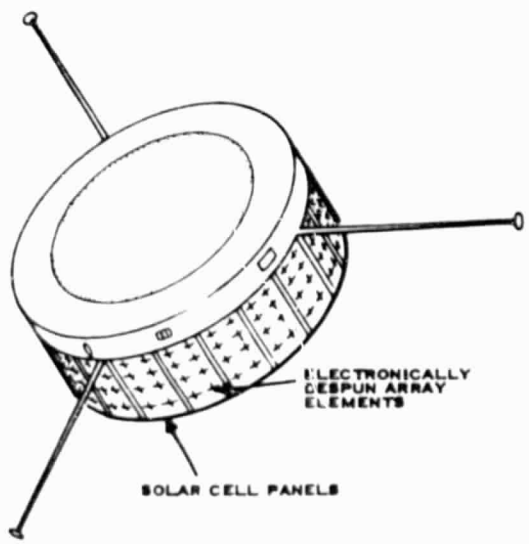

210060

Figure 1-8. Spacecraft Integrated Sytem

Completion of a 48-element dc logic manifold

Completion of a study of a Ku-band electronically steered phased array.

The completed S-band components were assembled, integrated, and tested. Results of those tests were published in Final Report DM75-05-10 in April 1975. Development also began on a J-band phase shifter. Progress on the overall program at this point is shown as the shaded portion of the system block diagram (Figure 1-9).

During the next phase, Texas Instruments performed preliminary design studies, circuit design, and fabrication of the monopulse receiver section. A four-channel monopulse receiver was designed and a single difference channel breadboarded. This single channel contained the majority of the basic circuitry of the receiver and was used to demonstrate beamtracking capability. Complete test results were included in Final Report DM76-06-05.

Contract modification 10 focused on the J-band development tasks. Under this contract, the aperture study was completed and an engineering model J-band phase shifter was fabricated. Figure 1-10 is a photograph of this prototype phase shifter module. The array study covered three different configurations that could be developed to meet the AESPA performance levels similar to those S-band parameters shown in Table 1-1. The three configurations studied were a flatplate-fed array (transmissive array), a reflector-fed array (reflective array), and a constrained feed array. The transmissive array and the reflective array were chosen as the best configurations on which to perform further study and trade analysis.

The trade analysis was performed and the transmissive array was selected as the most viable approach. A cross-sectional representation of the array is shown in Figure 1-11. Following selection of this configuration, work was performed to expand the mechanical design of the array. Further development of the phase shifter module and radiating dipole elements also took place. A complete description of the trade analysis, as well as development and testing of the phase shifter module, is given in Final Report CD77-08-01.

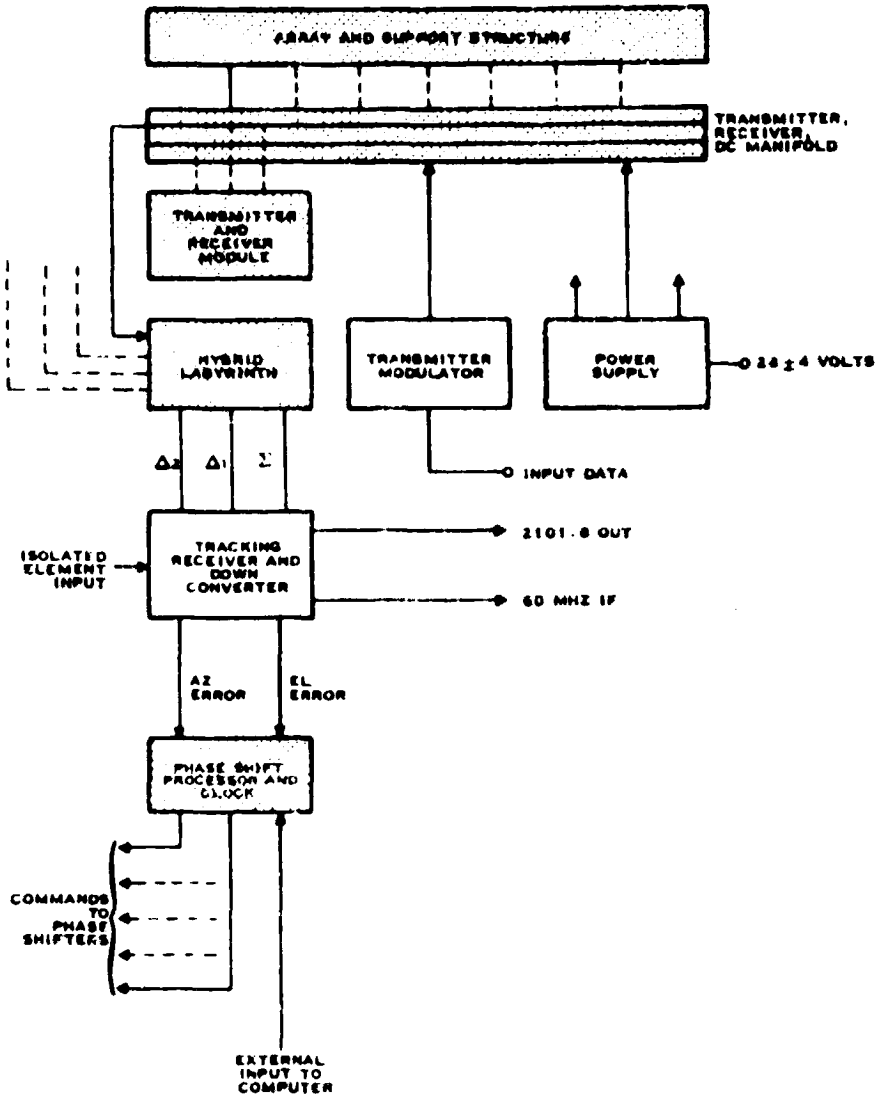

210061

Figure 1-9. System Block Diagram Showing Program Progress

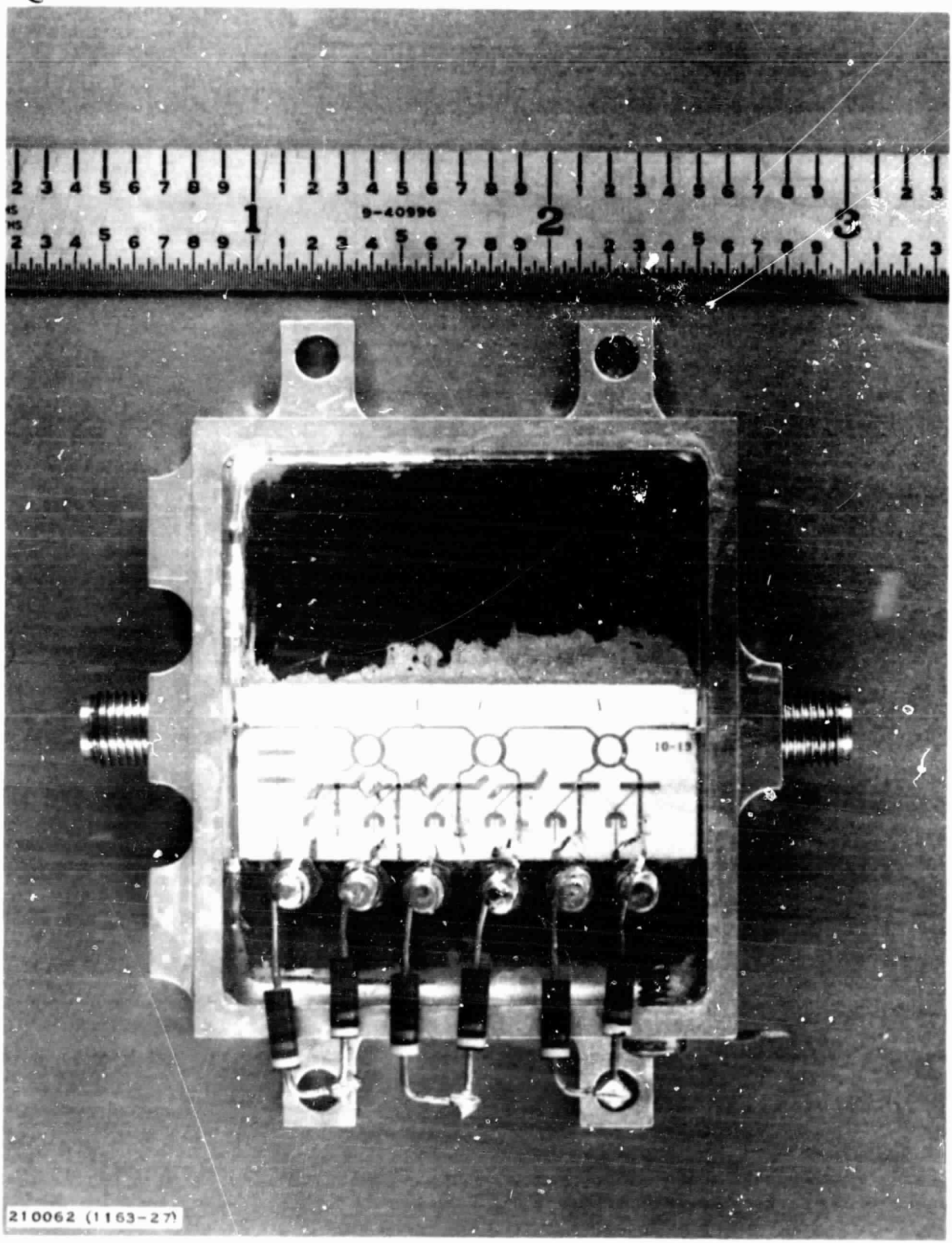

Figure 1-10. Prototype J-Band Phase Shifter Module

TABLE 1-1. PERFORMANCE SPECIFICATIONS

Scan angle: 60 degrees from broadside (maximum)

Scan increments: <2.5 degrees

Transmit frequency: 2282.5 MHz

Transmit gain: 20 dB at maximum scan

Frequency stability: ±0.003 percent

Input impedance: 50 ±3 ohms

Power output: >25 watts at 2282.5 MHz

Polarization: right-hand circular (RHCP)

Antenna efficiency: 60 percent or greater at f_o

Beamwidth: 10 degrees (60 degrees from broadside)

Sidelobes: 12 dB below mainlobe at maximum scan

Grating lobe: suppressed below maximum scan

Bandwidth (transmitter): 30 MHz (minimum); 60 MHz (maximum)

VSWR: 1.5 maximum at any scan angle

Modulation (transmitter): FM

Modulation input impedance: 10,000 ohms ($0 < f < 200$ kHz)

Modulation distortion: down 35 and 45 dB for 2nd and 3rd harmonics, respectively, at 300 to 500 MHz with peak deviation of 50 kHz

Intermodulation distortion: down 40 dB

Deviation sensitivity: 200 ±10 kHz/rms volt

Deviation linearity: ±1 percent, $\Delta < 200$ kHz; ±2 percent, $\Delta < 500$ kHz

Carrier deviation: ±500 kHz

Frequency response (transmitter): ±1.5 dB with respect to 50 kHz, $0 < f < 500$ kHz

Random motion: 25 g for 5 minutes in each of three orthogonal planes

Acoustical noise: 50M 71810

RFI: MIL-I-6181D

Incidental FM: 8 kHz maximum

Incidental AM: 5 percent maximum

Protection: capable of open circuit, short circuit, or ±28 volts applied to modulation input

Receive frequency: 2101.8 MHz

Receiver bandwidth: minimum, 30 MHz; maximum, 60 MHz

Receive gain: 25 dB at maximum scan

Noise figure: 10 dB, maximum

Output frequencies: IF, 60 MHz ; baseband, 2101.8 MHz

Output impedance: 50 ±3 ohms

Aperture: 225 elements (maximum)

Operational modes: self-focusing, pointing-logic controlled, hybrid

Prime power source: 28 ±4 volts ($Z_o < 1$ ohm)

Conversion efficiency (dc to RF): > 10 percent

Grounding: 10^7 ohms isolation

Polarity reversal (28 V): no effect

Radius of curvature: ≅ 300 cm

Mounting: flush mount

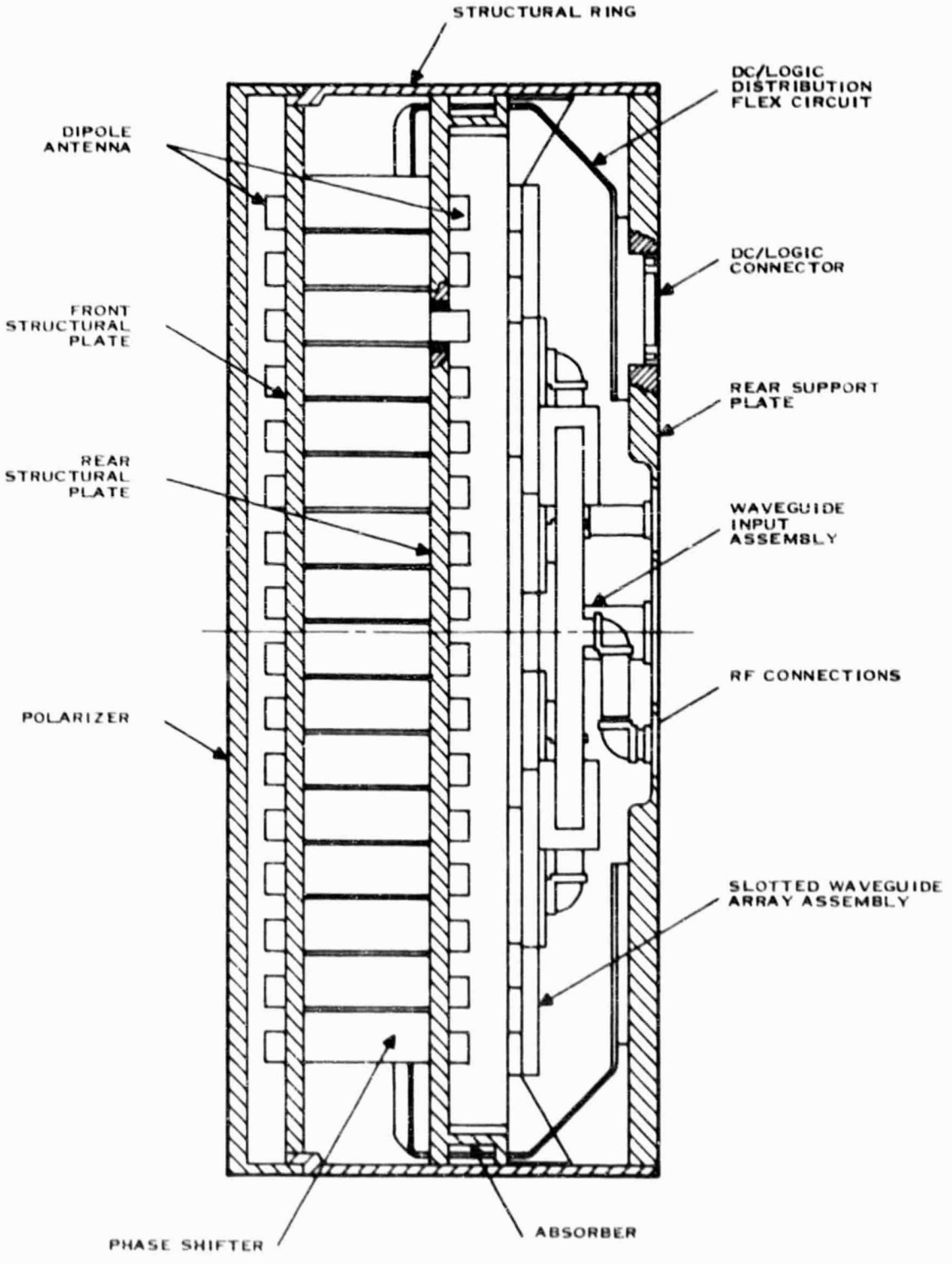

Figure 1-11. Transmissive Array

SECTION II
TRANSMISSIVE ARRAY CONCEPT

A. SUMMARY

This section contains information on the basic concept and design of the transmissive array. Included first is a summary of the system performance requirements. Much of this information is a review of material from previous phases but is fundamental to understanding the purpose of the development of an engineering array.

B. SYSTEM PERFORMANCE REQUIREMENTS

When the Ku-band array concept was first conceived, a set of design goals and preliminary performance specifications was established. These goals and specifications are shown in Table 2-1. Although these specifications are not firm, they were the basic constraints used for a trade study between the transmissive array approach and a reflective array approach. The trade parameters and the results of the trade analysis are shown in Table 2-2. The transmissive array proved to be the preferred approach.

C. CONCEPT AND DESCRIPTION

Figure 1-11 is a cross-sectional drawing of the transmissive array conceived in an earlier phase of the AESPA program. The inputs to the RF connections are divided in a three-channel monopulse comparator network feeding a conventional flatplate (slotted-waveguide) array. The amplitude and phase distribution of the array combine with the comparator network to give the desired four-lobe monopulse operation. The fields developed by this flatplate antenna are transferred to a broadside array of dipoles in proximity to the antenna. The signal captured by each dipole in the array is fed through a 3-bit dc-controlled phase shifter to another dipole at the opposite end that forms part of the radiating array. The phase shifters connected between the two dipole arrays control the beam pointing direction of the radiating array. A planar polarizer in front of the radiating array converts the linear polarization of the array to circular polarization.

TABLE 2-1. PRELIMINARY SPECIFICATIONS FOR Ku-BAND ANTENNA ARRAY

Frequency range	
Transmit	14.6 to 15.2 GHz
Receiver	13.4 to 14.0 GHz
Gain	
Transmit	Greater than 20 dB
Receive	Greater than 16 dB
Size	Less than 1 meter diameter and 10 cms thick
Weight	Less than 25 pounds
Scan area	Scan coverage shall be any point with a 120-degree cone of coverage
Radiating elements	Active spirals or waveguide ports

TABLE 2-2. TRADE PARAMETERS AND TRADE ANALYSIS RESULTS

20-dB Gain Transmit Array	Transmissive	Reflective	Preferred
Gain (dB) at 60 degrees	20.0	20.0	Equal
Phasors (required)	649	932	Transmissive
Size			
Diameter (centimeters)	38.4	43.2	Transmissive
Thickness (centimeters)	14.2	25.4	
Volume (liters)	16.4	22.1	
Weight (kilograms)	16.24	32.49	Transmissive
Vehicle opening (centimeters)	42.4 x 46.5	89.2 x 107.4	Transmissive
Input power (RF kilowatts)	1.95	1.69	Equal
(dc watts)	81	117	
Dissipated power (watts)	649	472	Reflective
Cooling system	Passive	Passive	Equal
Producibility	1	2	Transmissive
Reliability	1	2	Transmissive
Cost	72	104	Transmissive

30-Centimeter Transmit Array	Transmissive	Reflective	Preferred
Gain (dB) at 60 degrees	17.4	16.4	Transmissive
Phasors (required)	367	398	Equal
Size			
Diameter (centimeters)	30.0	30.0	Equal
Thickness (centimeters)	14.2	20.8	
Volume (liters)	9.9	9.6	
Weight (kilograms)	9.84	13.88	Transmissive
Vehicle opening (centimeters)	34.0 x 36.8	63.8 x 73.2	Transmissive
Input power (RF kilowatts)	1.10	1.09	Equal
(dc watts)	46	50	
Dissipated power (watts)	367	278	Reflective
Cooling system	Passive	Passive	Equal
Producibility	1	2	Transmissive
Reliability	1	2	Transmissive
Cost	41	44	Equal

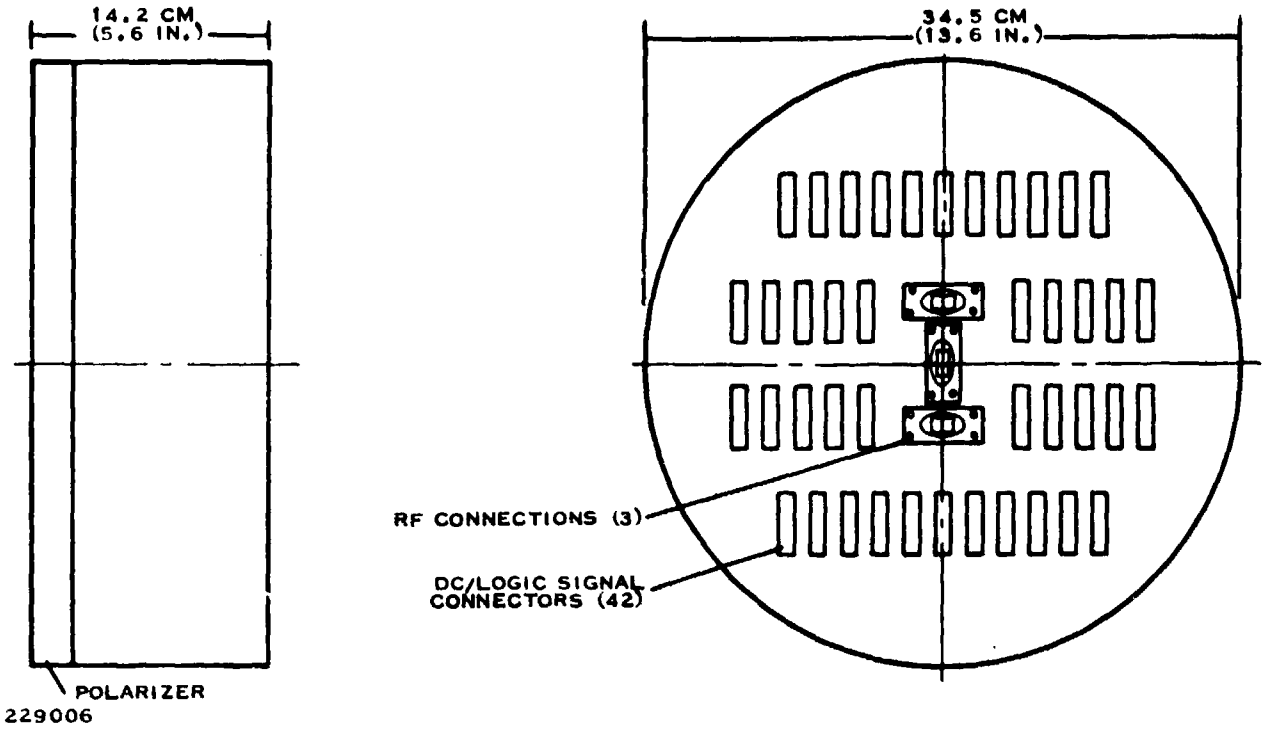

Figure 2-1. Flat Plate Fed Array Outline Dimensions

The basic mechanical configuration is shown in Figure 2-1. Best estimates indicate an overall thickness of 14.2 cm (5.6 in.), a diameter of 34.5 cm (13.6 in.), a volume of 0.013 m^3 (0.47 ft^3), and a weight of approximately 16.01 kg (35.3 lb). The planar polarizer is made up of etched copper-clad dielectric material 0.013 cm (0.005 in.) thick and is bonded to honeycomb to provide a rigid structure. The microstrip dipole elements are etched on copper-clad duroid material and are directly connected to the phase shifter circuit tc eliminate the need for an RF connector interface.

The phase shifter is a hermetically sealed package containing an etched ceramic microstrip reflective-type circuit incorporating chip PIN diodes and 3-dB hybrids. The dc/logic signals are supplied through a flexible printed circuit assembly.

The flatplate feed antenna is a circular, slotted-waveguide array. The power distribution in one plane is controlled at the rear plate of the antenna using inclined series slots in the broadwall of the waveguide. Power is coupled through each inclined series slot into an orthogonal waveguide section containing several longitudinal shunt slot elements. These shunt slots form the feed's radiating elements. The faceplate is etched aluminum and is bonded to the backplate, which can be either etched or machined construction.

SECTION III
ENGINEERING ARRAY DESIGN

A. SUMMARY

The engineering array was proposed as a means to demonstrate the performance capabilities of the transmissive array. The specific areas of concern are gain, beamwidth, and sidelobe level versus frequency and scan angle. (A photograph of the completed engineering array is shown in Figure 3-1.)

Some noteworthy differences exist between the engineering array and the proposed system array. The engineering array will operate in the transmit frequency band (14.6 to 15.2 GHz). The flatplate feed has a single channel providing only a sum beam rather than four-lobe monopulse capability. The primary scanning aperture and the secondary pickup aperture incorporate dipole elements spaced in a triangular grid as specified for the large array. This spacing is not optimum for the engineering array. However, changing the spacing for optimized performance is impractical (see Subsection III.B of this report). The 19 phase shifters are controlled by a manually operated switchbox rather than a computerized beamsteering unit. The planar polarizer proposed in the system array will not be used and, therefore, only linear polarization will be demonstrated. Mechanical design efforts for the engineering array have been limited to support and alignment structures and are not intended to be representative of the system mechanical design.

The design, fabrication, and testing of the major components of the array are discussed in the following subsections.

B. APERTURE DESIGN

The aperture geometry for the transmissive array was designed under Contract NAS8-32070 and specified in Final Report CD77-08-01. A triangular grid spacing was selected for use over a rectangular grid because it results in fewer elements for a given area. A prime consideration in selecting the element spacing is to allow an array scan volume of ±60 degrees about the array normal without the appearance of grating lobes in the visible space region. The relationship that must be satisfied to meet this criterion is given in the expressions below:

$$d_R = \frac{\lambda(1 - 1/N)}{1 + \sin \theta_{max}}$$

$$d_T = \frac{d_R}{\sin 60^\circ}$$

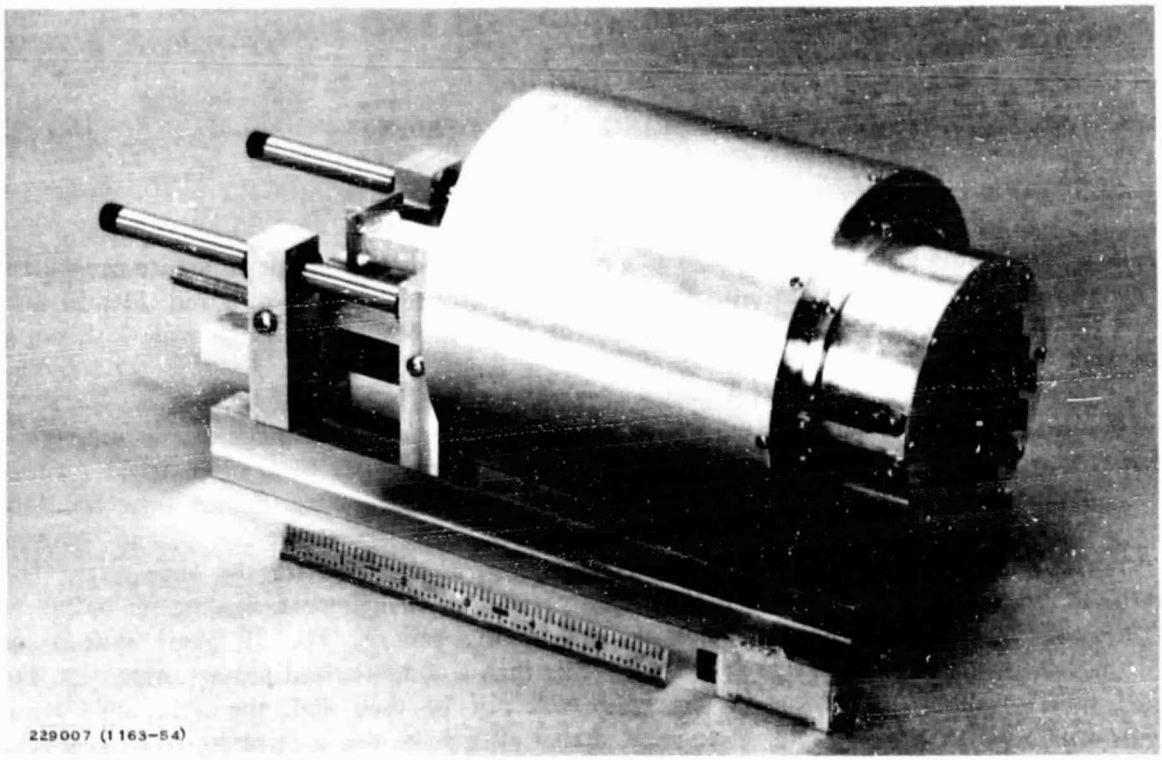

Figure 3-1. AESPA Engineering Model Array

where

d_R = rectangular element spacing

λ = wavelength

N = number of array elements

θ_{max} = maximum scan angle

d_T = triangular element spacing (equilateral).

For large arrays, the 1/N term may be ignored. Worst case (d_T = minimum) occurs for the highest frequency and largest scan angle. Evaluating the expressions for these conditions results in the dimensions shown in Figure 3-2. These dimensions, along with the required clearances for wiring and assembly, were used to establish the phase shifter module package size.

For the engineering array, however, the 1/N term in the original constraining equation may not be ignored since N is no longer large. Including the 1/N term reduces the element spacing. This is impractical for the engineering array since reduced element spacing requires a reduced phase shifter package size and, thus, a redesign of the module itself. By leaving the element spacing at the values obtained for the larger array, the engineering array will experience the appearance of grating lobes for angles less than the ±60-degree scan limit. The grating lobe locations for an equilateral triangular grid are shown in Figure 3-3. As long as it is realized that this will not occur in the larger array, the appearance of grating lobes in the engineering array will not degrade the performance demonstration.

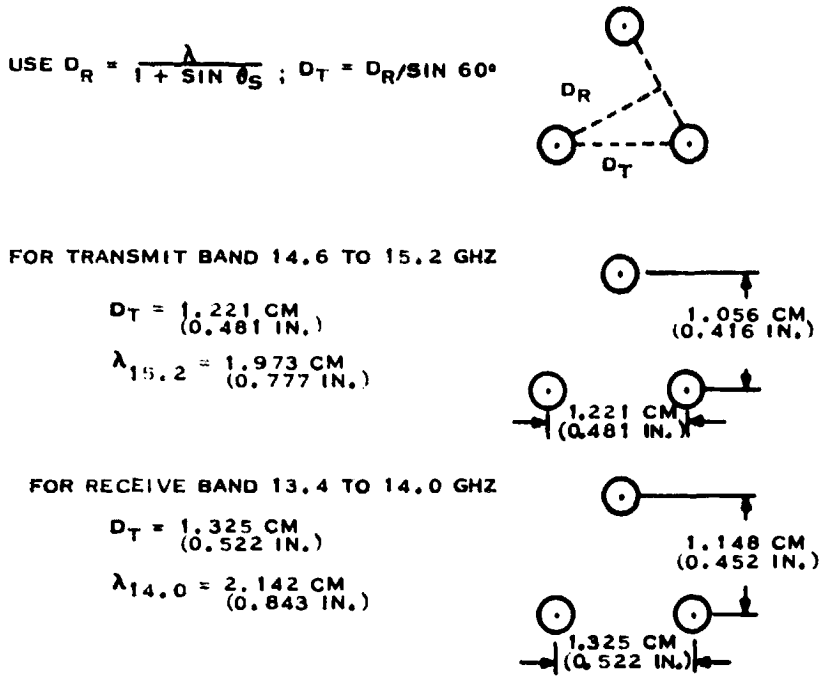

Figure 3-2. Array Element Spacings

C. RADIATING ELEMENT

1. Summary

The radiating element selected for use in the transmissive array is a thin half-wavelength dipole. It is the most widely used radiating element in scanning phased arrays. This fact and the vast amount of published design data available led to the proposal for its use under a previous AESPA contract (NAS8-25847). Further investigation in a follow-on contract (NAS8-32070) showed it was indeed suitable for use in the transmissive array application. In-depth design and development details were published in Final Report CD77-08-01. Highlights from that report are repeated in the following design and performance subsections.

2. Design Review

Since the radiating element is in an array environment, the effects of mutual coupling must not be ignored. Strong coupling can exist, especially as the beam is scanned in the H-plane, and the possibility of "holes" in the pattern exists if the impedance function reaches a singularity point. To avoid this problem, the dipole may be slightly mismatched at broadside, making performance more uniform as the beam is scanned.

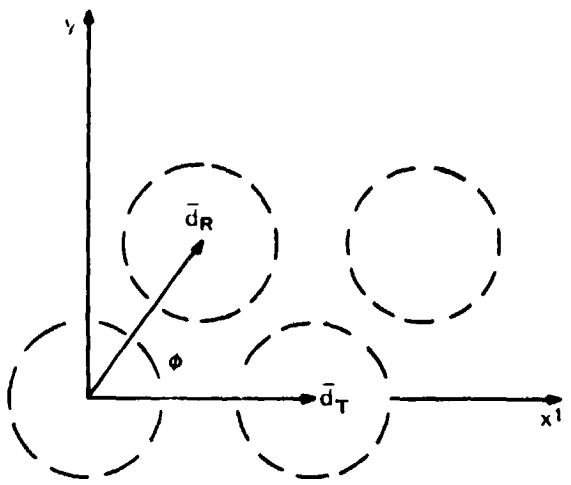

A. TRIANGULAR GRID (EQUILATERAL)

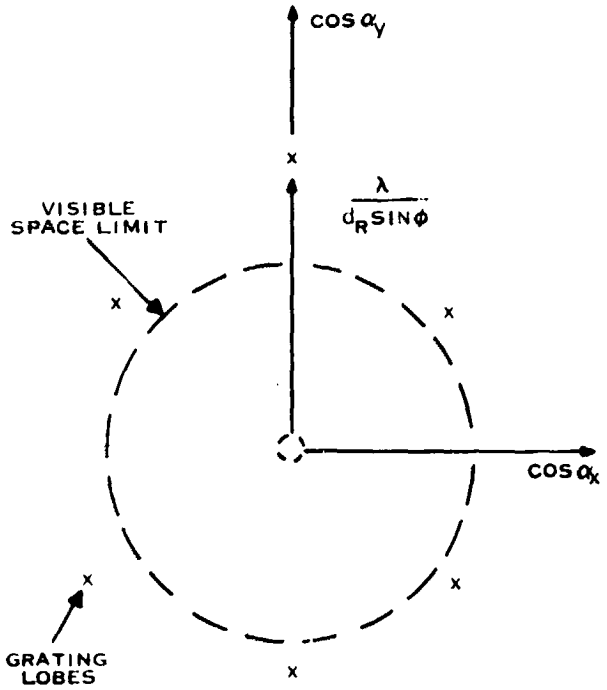

B. GRATING LOBE LOCATIONS FOR EQUILATERAL TRIANGULAR GRID

217500A

Figure 3-3. Triangular Grid Geometries and Grating Lobe Structures

A mutual coupling analysis was performed for the particular constraints AESPA presented. Several array configurations were computer-modeled and analyzed. Complete details of the analysis can be found in Final Report CD77-08-01. Results indicated that an isolated dipole VSWR match of 1.3:1 is optimum for this application.

In the task to determine the physical configuration, various forms considered included cylindrical, conical, rectangular, and printed circuit. The latter was chosen primarily because of the capability to adapt it for direct connection to the phase shifter rather than having to use an RF connector for the interface. The element is also small, lightweight, and easily fabricated. Design dimensions were chosen to acquire the proper impedance for the desired mismatch.

The various dimensions are shown in Figure 3-4. A photograph of the prototype dipole as fabricated is shown in Figure 3-5.

The dipole phase shifter interface can be seen in Figure 3-6. Low-temperature indium solder is used to attach the dipole to the phase shifter. Care must be taken to ensure good ground contact to minimize cross-polarization.

3. Performance

Following the completion of the design, several dipoles were fabricated and tested. Comparisons were made between calculated and measured E- and H-plane patterns. Results are shown in Figures 3-7 through 3-10. Close agreement can be seen in the patterns. The measured impedance of the dipole is shown in Figure 3-11 in the form of a Smith chart. A nearly constant VSWR at 1.3:1 is maintained from 14.6 to 15.2 GHz.

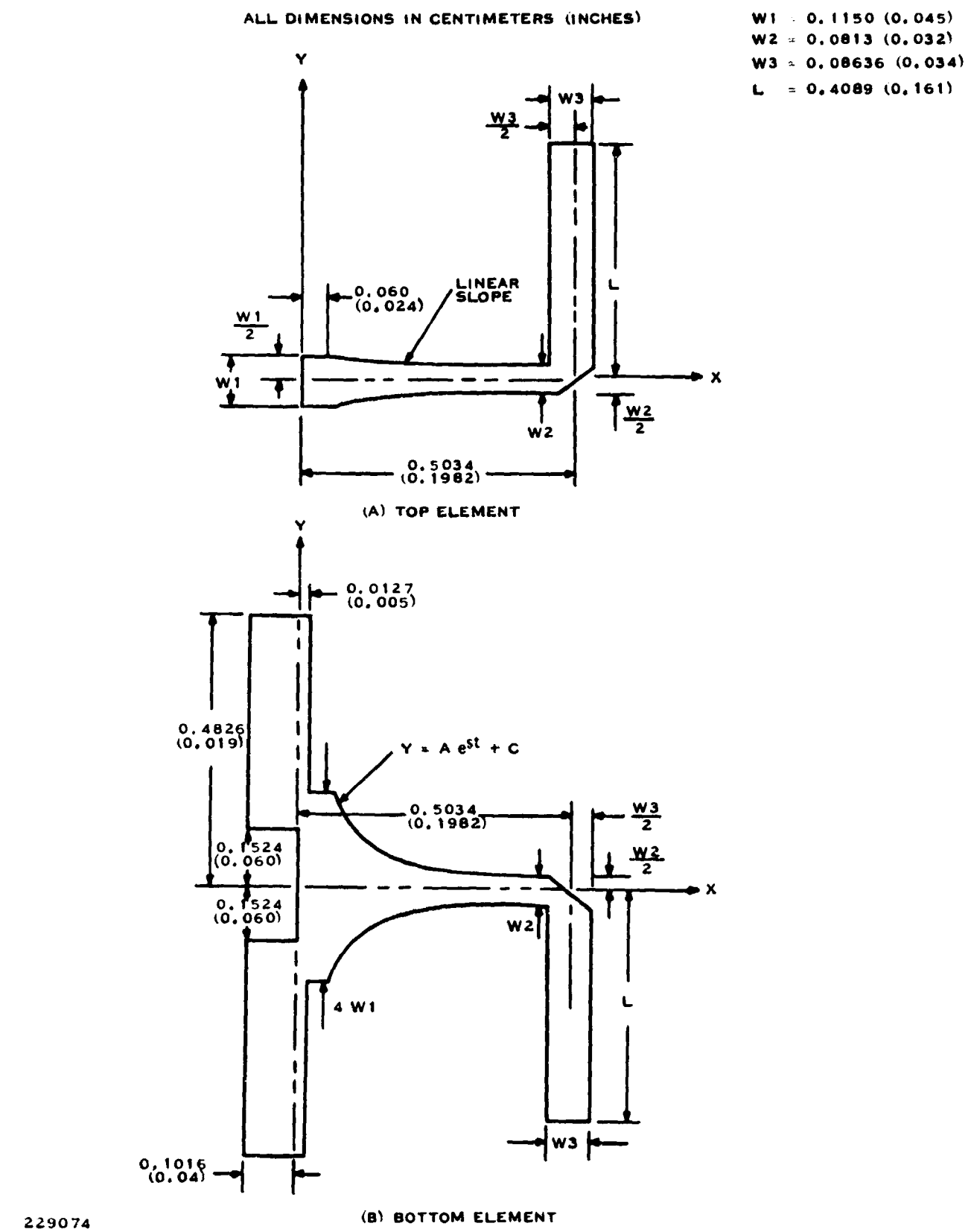

Figure 3-4. AESPA Dipole Dimensions

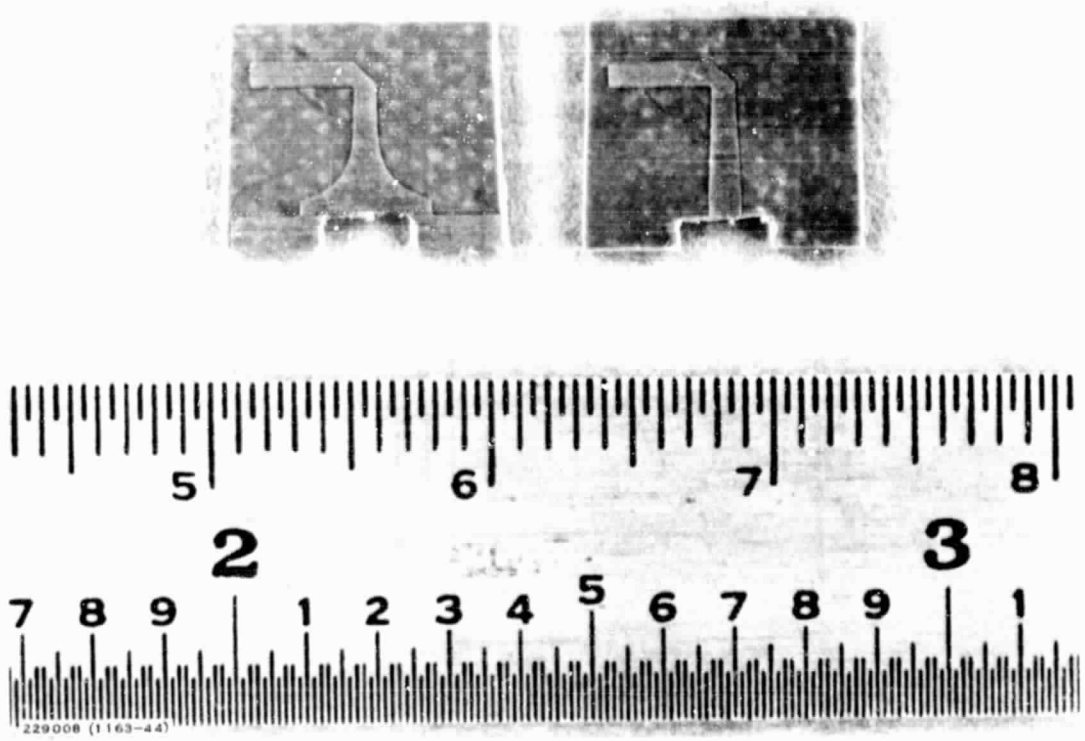

Figure 3-5. AESPA J-Band Dipole

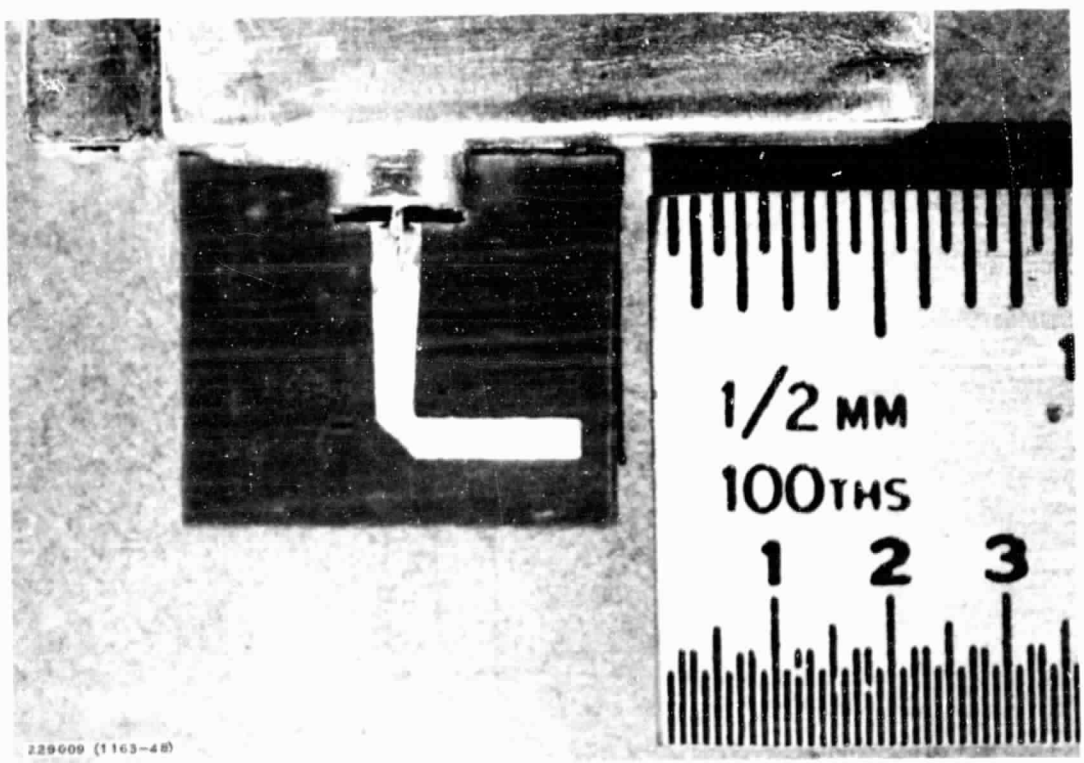

Figure 3-6. Dipole/Phase Shifter Interface

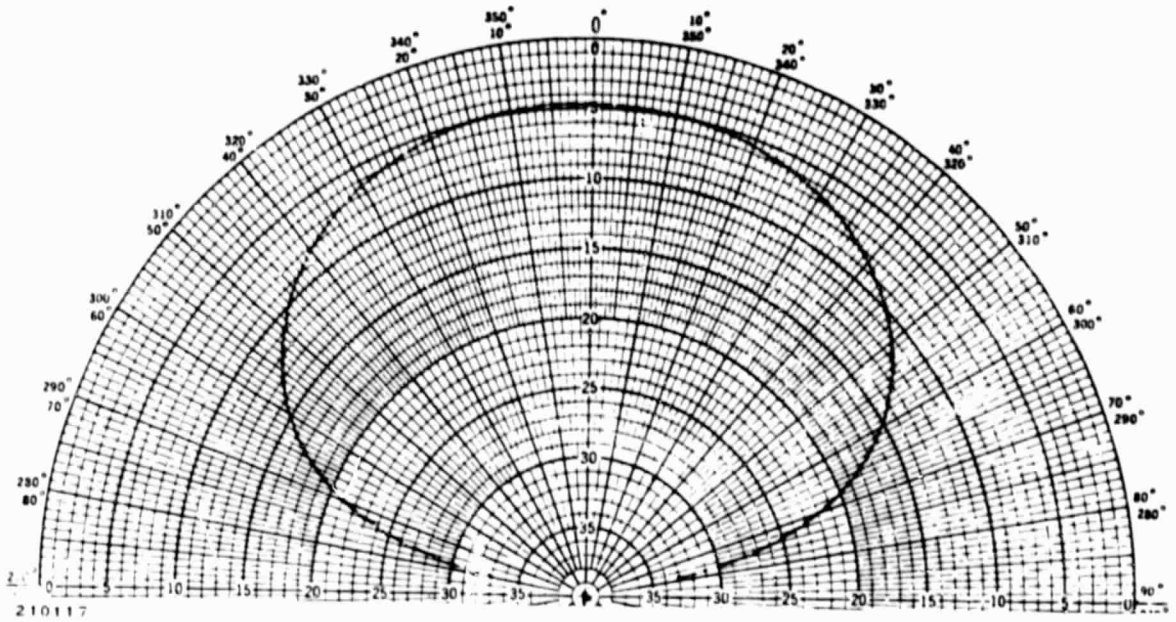

Figure 3-7. Calculated E-Plane Pattern at 14.9 GHz

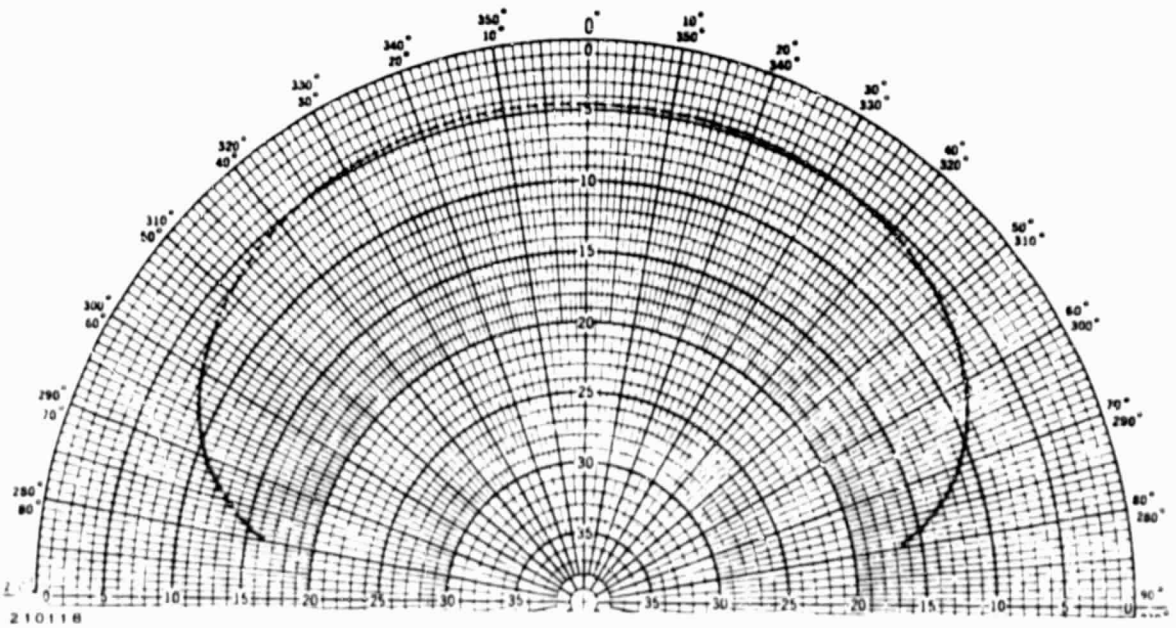

Figure 3-8. Calculated H-Plane Pattern at 14.9 GHz

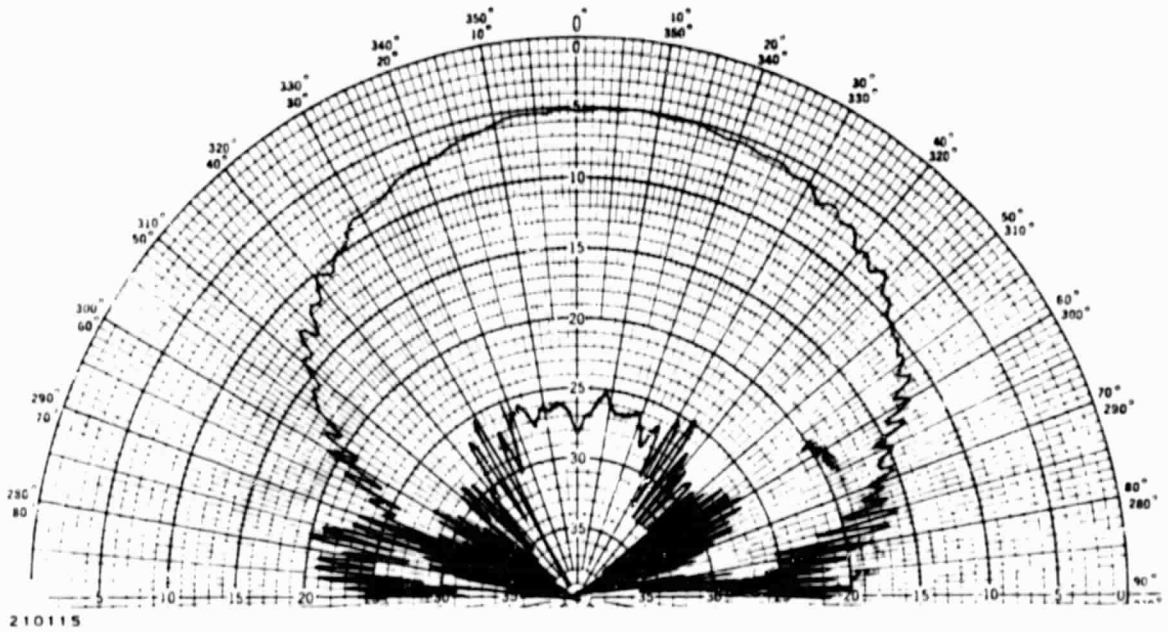

Figure 3-9. Measured E-Plane Pattern at 14.9 GHz

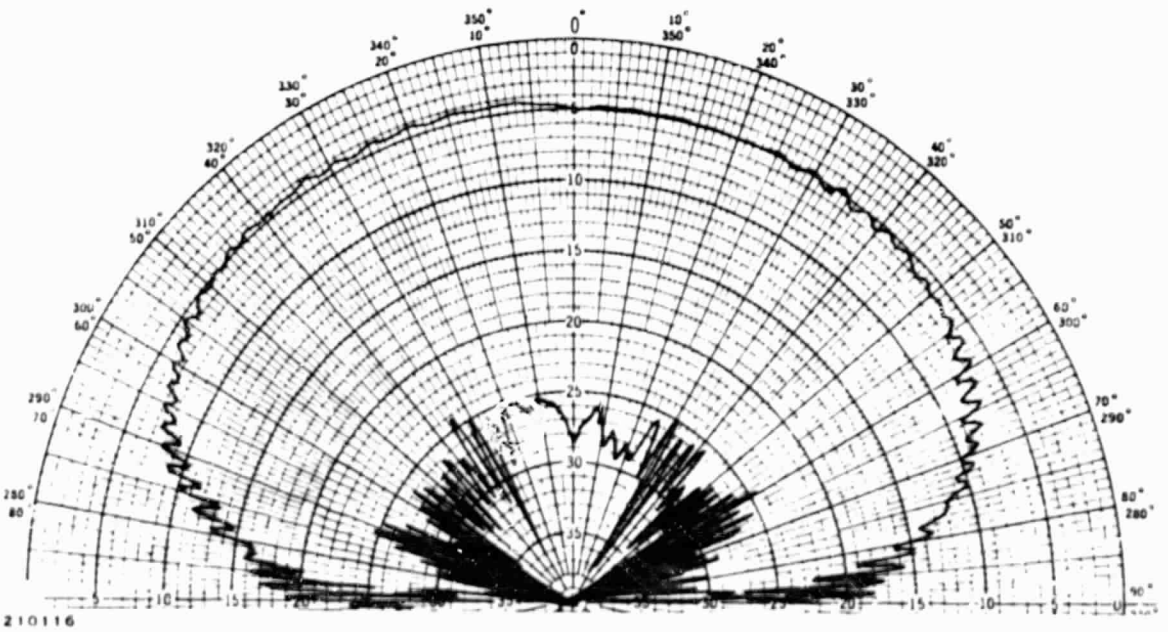

Figure 3-10. Measured H-Plane Pattern at 14.9 GHz

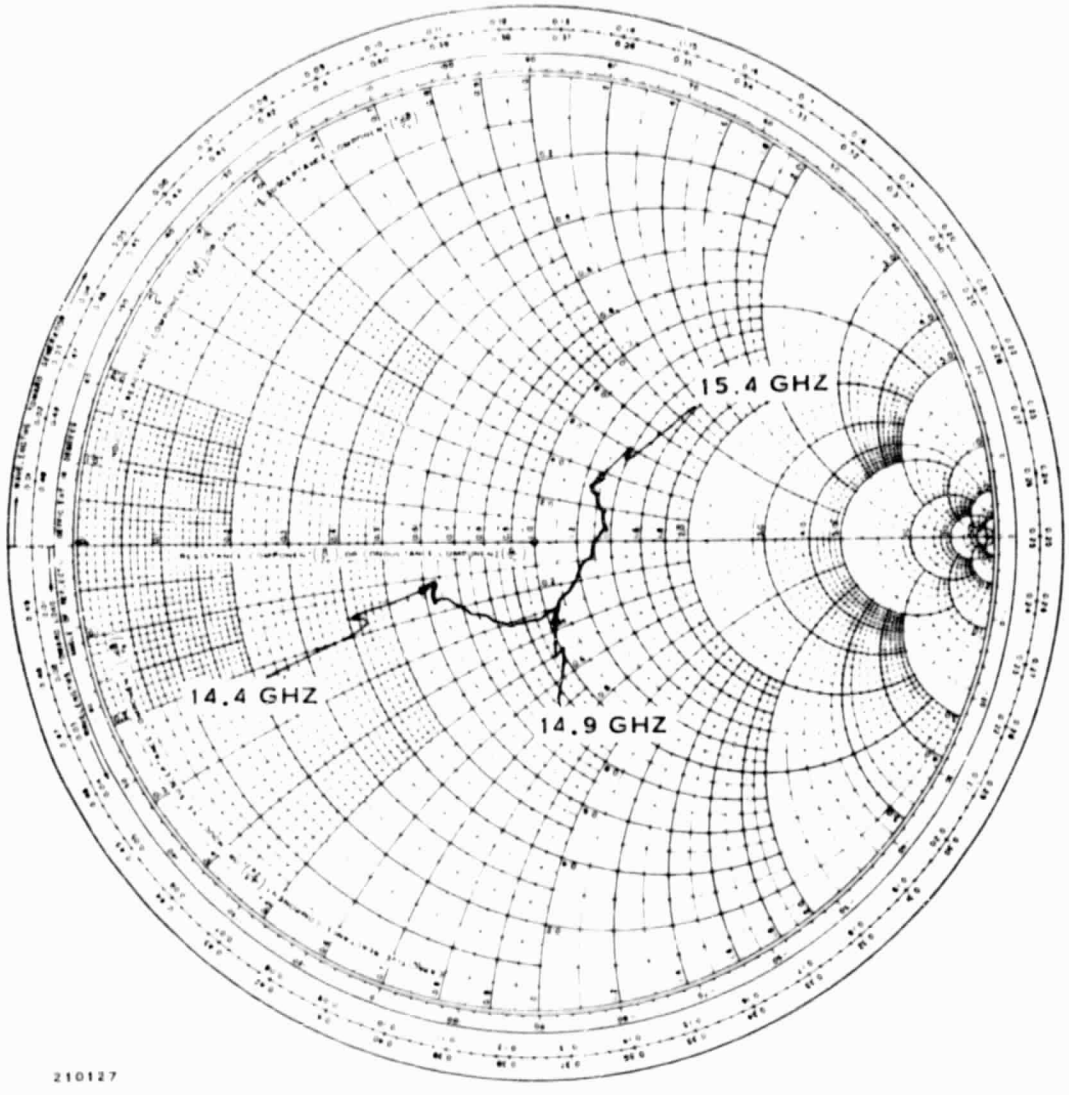

Figure 3-11. AESPA Dipole Isolated VSWR Versus Frequency

D. PHASE SHIFTER

1. Summary

Design and development work for the phase shifter module was completed under a previous AESPA contract (NAS8-32070). At completion, detailed fabrication drawings were made and the manufacturing assembly methods were defined. Complete design and development details may be found in the final report of the contract. A basic review of the design is given in Subsection III.D.2, followed by a discussion of the performance obtained.

2. Design Review

Initial development efforts for the phase shifter centered on selecting the design approach and on analysis of component parts that would be incorporated in each design. Size and weight were perhaps the two most stringent restrictions on the module package. The package must be small, indicating the need for high dielectric substrates for etched circuits. The use of chip diodes for small size as well as reproducibility was also indicated. This initial development effort resulted in the selection of microstrip construction and the use of 10-mil-thick alumina as a substrate material. Established thin-film circuit production techniques can be used to etch circuits on this material with good reproducibility.

In addition to the physical size and weight constraints, a set of electrical performance goals was established, as shown in Table 3-1. Also shown in Table 3-1 is the performance achieved by the prototype module.

TABLE 3-1. PHASE SHIFTER PERFORMANCE CHARACTERISTICS

Performance Parameter	Design Goal	Performance Obtained
Frequency range		
Transmit	14.6 to 15.2 GHz	14.6 to 15.2 GHz
Receive	13.4 to 14.0 GHz	–
Insertion loss		
Transmit	5.0 dB maximum	4.96 dB maximum
	4.3 dB average	4.04 dB average
Power level		
Transmit	0.5 watt	0.5 watt
Control power	0.25 watt maximum	0.23 watt maximum
DC drive		I_f = 90 milliamperes at 2.5 volts
		V_r = 15 volts
VSWR	1.8:1	1.89:1
Weight	0.6 ounce (17.0 grams)	0.48 ounce (13.6 grams)
Bits	3	3
Amplitude tracking versus phase state	1.0 dB maximum	1.4 dB maximum
Phase tracking versus phase state	20 degrees rms	11.5 degrees rms

The phase shifter circuit developed is a 3-bit reflective type using 3-dB hybrids and chip PIN diodes to switch the signal in or out of delay lines to achieve the desired shift in phase state. Figure 3-12 shows the basic circuit layout and component parts. As mentioned previously, the network making up the hybrids, transmission lines, and delay lines consists of etched gold circuits on a 10-mil-thick alumina substrate. The thin-film resistors and PIN diodes are alloyed to the circuits to provide good electrical contact. The RF feedthroughs are connected to the circuit by welded gold ribbons.

Figures 3-13 and 3-14 are photographs showing the phase shifter circuit and a completed module (without the dipoles).

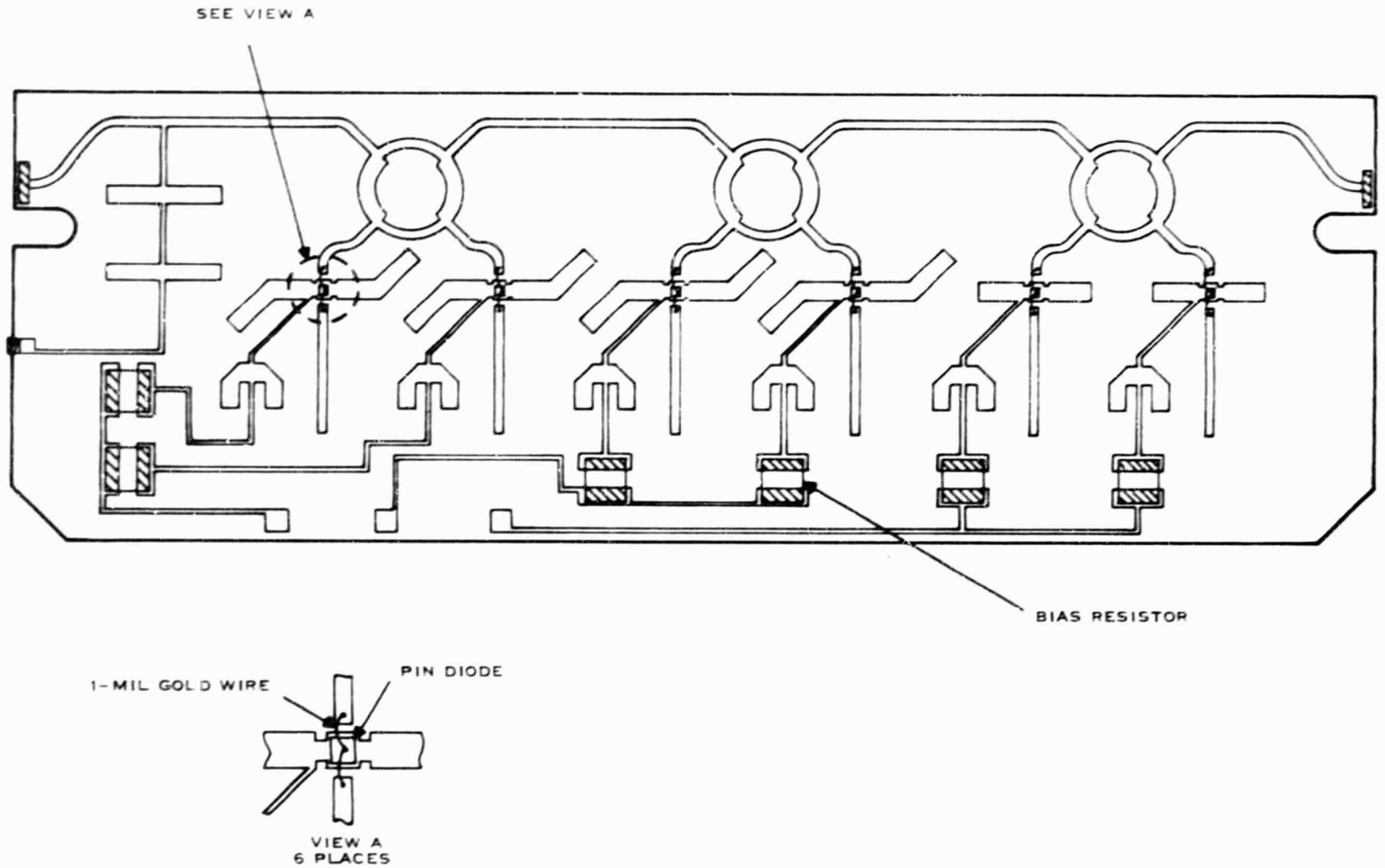

Figure 3-12. Phase Shifter Network

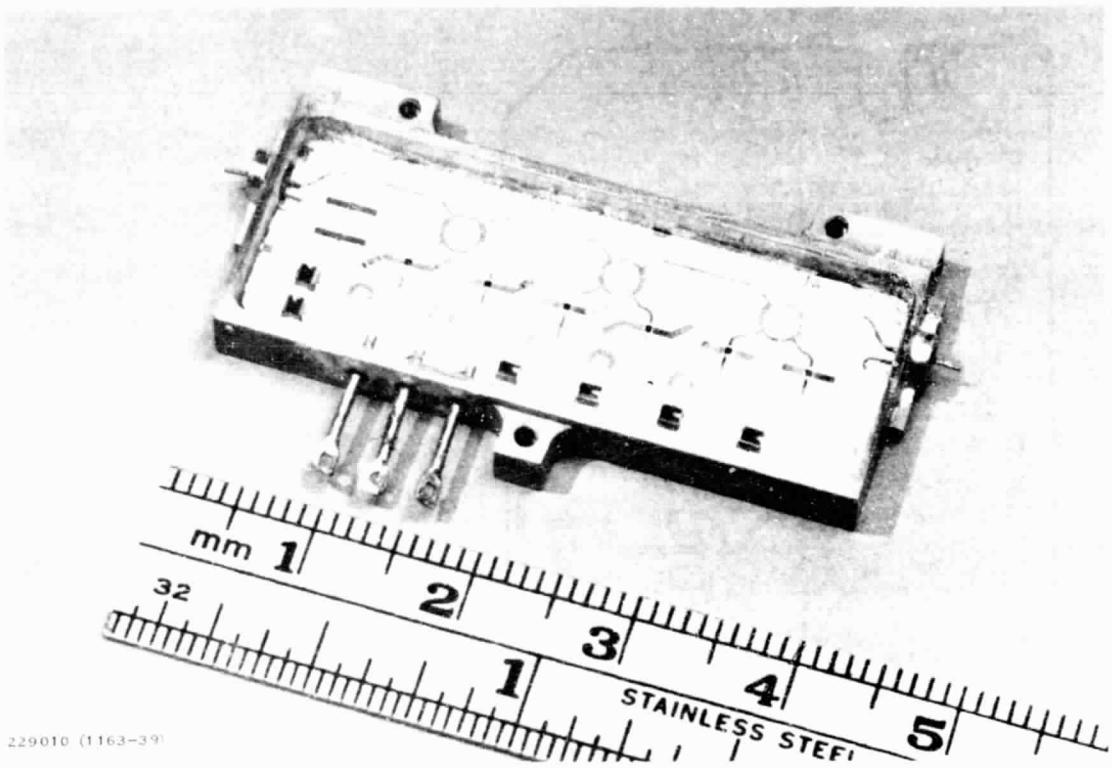

Figure 3-13. Ku-Band Phase Shifter

ORIGINAL PAGE IS
OF POOR QUALITY

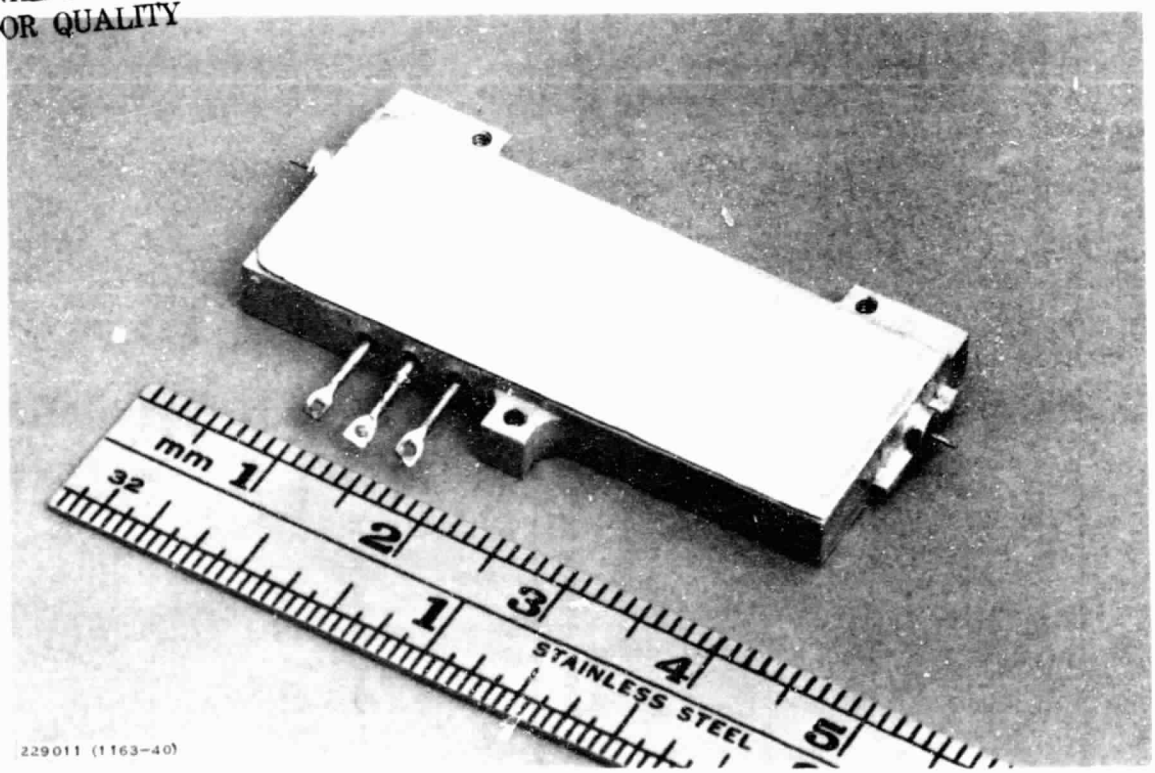

Figure 3-14. Phase Shifter Module

3. Performance

Since the feedthroughs on the phase shifter were designed for direct interconnection to the dipoles and were not directly compatible with any RF connectors, a special test fixture was designed and built for use during the test phase of the phase shifter fabrication cycle. A complete description of the test fixture design and tuning can be found in Final Report CD77-08-01 for Contract NAS8-32070.

The test fixture and test procedures developed for use on the prototype model phase shifter were used for testing of the 19 units needed for the array. Following this testing, the dipoles were attached to the phase shifter and additional testing of the completed module was performed. As part of this cycle, another special test chamber was built to make the necessary RF measurements. Two views of the test chamber are shown in Figures 3-15 and 3-16. Energy is radiated from a horn antenna in one end of the test chamber to one of the dipoles on the phase shifter. The signal is passed through the module to the dipole at the other end where it is radiated and then received by another horn antenna in the opposite end of the test chamber. Test chamber, cable, and connector characteristics may be calibrated from the measurement using an automatic network analyzer.

The 19 modules necessary for the array followed the same basic fabrication, assembly, and test cycle as the prototype module. Final insertion loss and phase data on those modules are shown in the appendix as Tables A-1 and A-2, respectively. Table A-1 includes each module's average and peak loss versus frequency and phase state. At the end of Table A-1 is the lens loss at broadside versus frequency. This value is the average loss of the 19 modules in the 0-degree state calculated at the five array test frequencies. This number is used later in the array gain calculations. Table A-2 shows the module phase performance versus frequency and phase state. Also shown is each module's rms phase tracking error with respect to its measured insertion phase.

The variation in insertion phase among the 19 modules is shown in Table 3-2. When considering the performance of the 19 modules as a group, this variation must also be included. In this demonstration, however, array patterns will be calculated for the ideal error-free case. Radiation patterns for the large array, including random errors in both phase and amplitude, were included as part of the final report published in April 1976 for Contract NAS8-25847.

E. FLATPLATE FEED

1. Summary

A conventional flatplate antenna is used to space feed the secondary dipole pickup aperture. A sketch of the feed is shown in Figure 3-17. Figures 3-18 and 3-19 show front and rear views of the key components. The main body of the feed is machined aluminum and makes up the major portion of a single vertical waveguide section and five horizontal waveguide sections. The orthogonal waveguides are coupled by five inclined broadwall series slots. The vertical waveguide section is center fed by a tapered waveguide that converts standard Ku-band waveguide to the series waveguide dimensions. Attached to the tapered waveguide is a 50-mil aluminum plate that forms the fourth wall of the series waveguide. The "feedthrough hole" in this plate may be used as an electrical matching device by varying the "a" and "b' dimensions of the hole. A

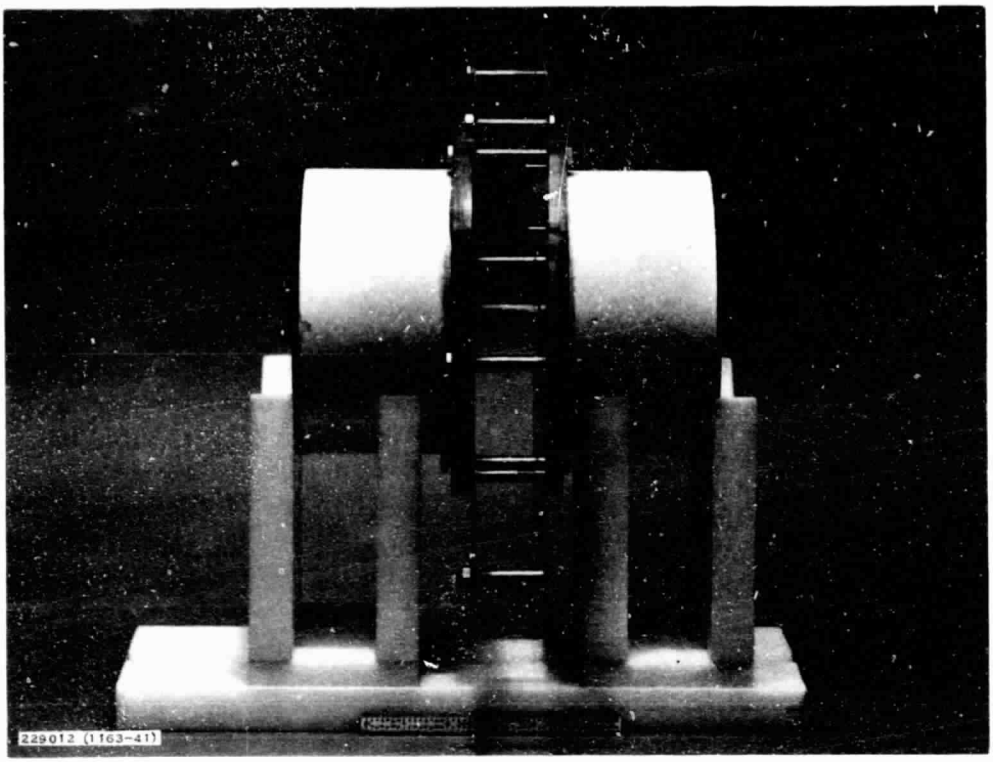

Figure 3-15. Assembled Test Chamber and J-Band Module

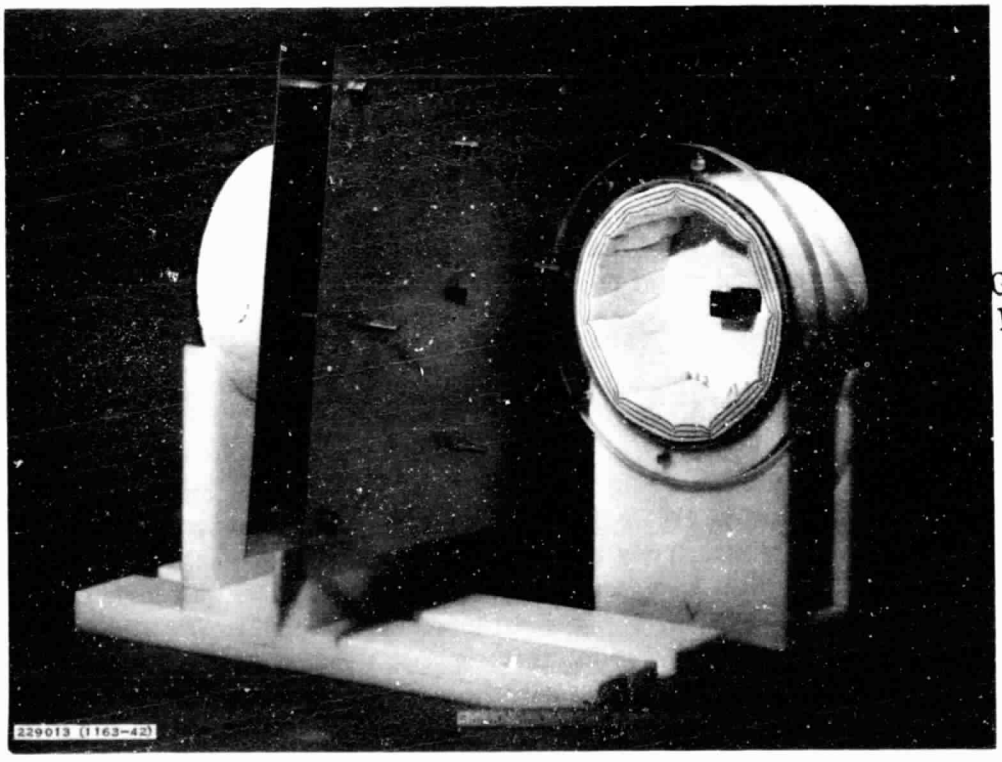

Figure 3-16. Disassembled Test Chamber and J-Band Module

TABLE 3-2. INSERTION PHASE VERSUS FREQUENCY

Frequency (GHz)	Module Number 1	2	4	5	6	7	9	10	11	12
14.60	0.0	32.0	−5.4	−18.1	−1.0	−8.3	4.5	−1.0	−35.5	22.9
14.76	0.0	23.7	−14.5	−21.8	−12.7	−20.4	−1.7	−14.5	−51.0	−8.6
14.90	0.0	23.5	−20.5	−23.4	−15.7	−26.3	−4.0	−23.7	−56.2	−3.5
15.04	0.0	14.7	−26.3	−26.5	−25.0	−28.3	−14.7	−26.0	−60.0	−13.9
15.20	0.0	20.3	−16.4	−14.9	−20.4	−24.1	−3.8	−10.3	−59.3	−17.7

Frequency (GHz)	Module Number 13	14	15	16	18	19	20	22	23
14.60	10.4	15.1	11.5	18.6	−2.1	−3.3	−12.6	−16.0	11.2
14.76	−1.7	−0.0	−1.1	−7.5	−23.4	−24.2	−3.0	−35.0	−16.2
14.90	−8.7	−9.1	−16.0	−23.5	−37.5	−32.2	−12.2	−40.0	−32.9
15.04	−12.4	−11.8	−20.5	−32.3	−52.9	−39.7	−20.1	−51.2	−44.3
15.20	0.1	−2.6	−14.2	−29.6	−60.2	−30.6	−19.8	−62.9	−46.4

10-mil-thick, Kapton-covered aluminum faceplate forms the fourth wall of the five horizontal waveguide sections when bonded to the main body. The faceplate contains 20 chemically milled radiating broadwall shunt slot elements.

The feed is designed for uniform phase and amplitude on all radiating elements and has a 3-dB beamwidth of approximately 20 degrees in each principal plane.

2. Design Review

Several tasks are involved in the design of the feed and include:

- Solving for array lattice spacing
- Solving for shunt slot conductance and resonant length versus offset from waveguide centerline
- Solving for series slot resistance and resonant length versus angle of inclination
- Design of input waveguide section.

Each of these tasks is discussed sequentially in the following paragraphs.

The radiating slots are placed in a basic rectangular grid. Figure 3-20 depicts a typical radiation cell and its geometry.

The shunt slots are placed one-half wavelength apart. The 180-degree phase reversal obtained from this condition is counteracted by placing the radiating slots on opposite sides of the waveguide centerline, thus achieving another 180-degree shift. One-half wavelength spacing is also used for the series slot spacing. The added 180-degree phase shift necessary to bring each element back to a 0-degree condition is obtained by reversing the direction of inclination of each alternating slot.

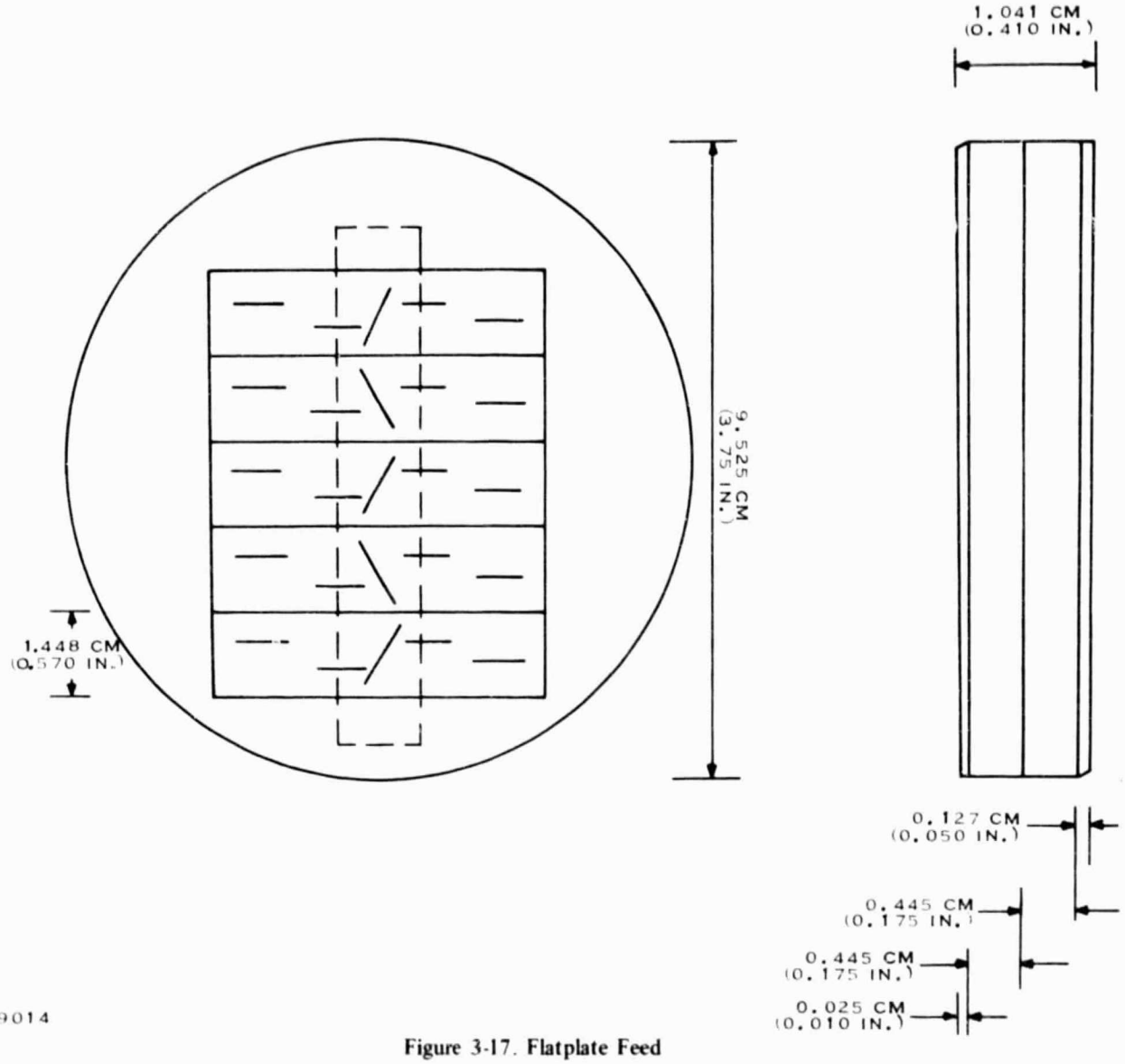

Figure 3-17. Flatplate Feed

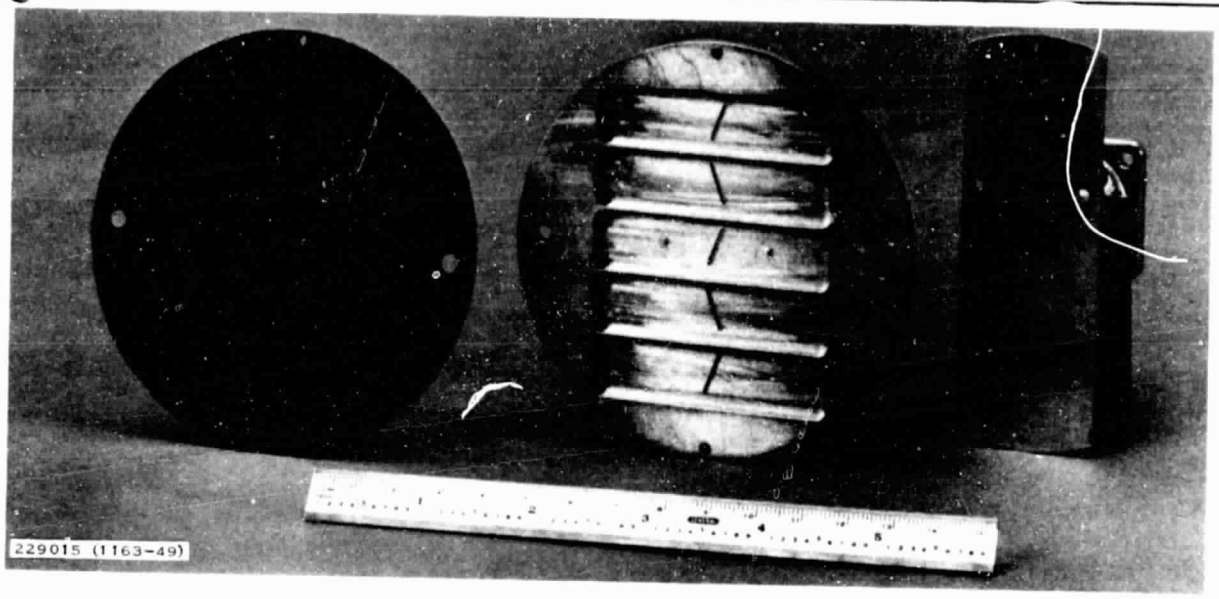

Figure 3-18. Flatplate Feed Components, Front View

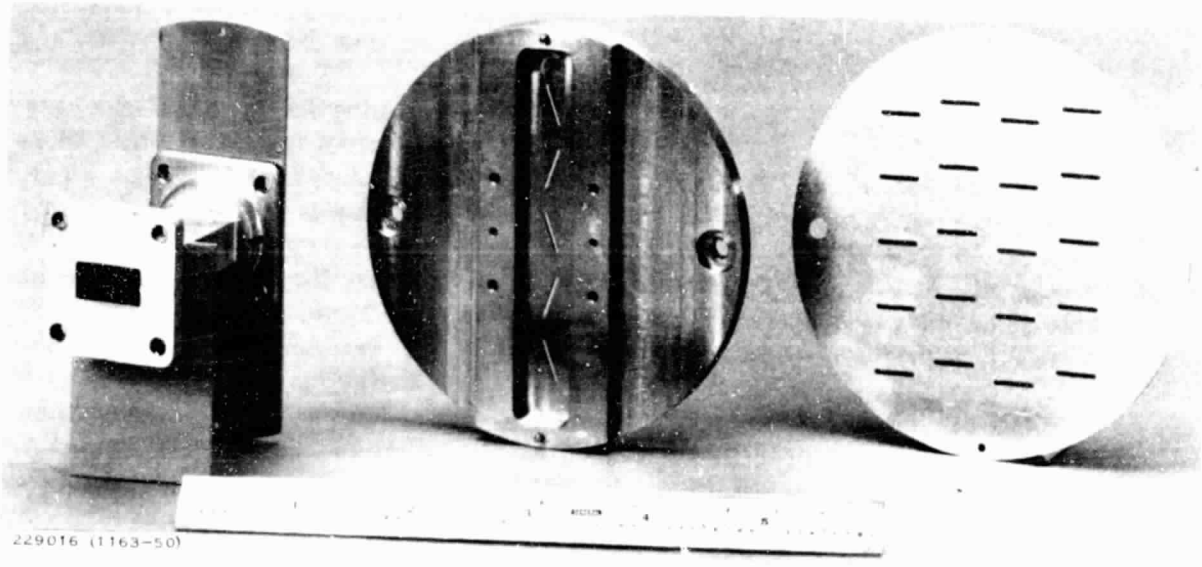

Figure 3-19. Flatplate Feed Components, Rear View

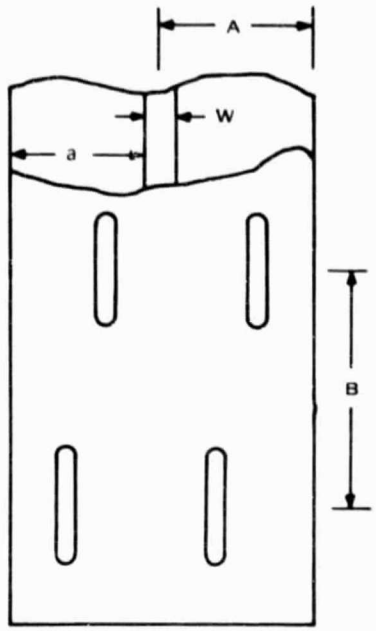

229017

Figure 3-20. Slot Array Radiation Cell Geometry

Equations that must be enforced and that define the lattice spacing are:

$$A = B$$

$$A = a + w$$

$$a + w = \frac{\lambda_g}{2}$$

$$\lambda_g = \frac{\lambda_o}{\sqrt{1 - \left(\frac{\lambda_o}{2a}\right)^2}}$$

The terms A, B, a, and w are defined in Figure 3-20. The terms λ_g and λ_o are the wavelengths in the waveguide and freespace, respectively. If a typical wall thickness of 0.046 cm (0.018 in.) is chosen, solving for A at center frequency gives a grid spacing of 1.448 cm (0.570 in.). The basic waveguide dimensions are now defined.

Before solving for the shunt slot conductances and series resistances, some background on the design should be given. Figure 3-21 shows two layers of the array. The first division occurs at the E-plane tee at the center of the vertical waveguide. This junction is designed to be matched at the center frequency by terminating the vertical guide in its characteristic impedance Z_{o2} in the absence of coupling slots. This shunt-connected junction will operate identically if the total admittance at the center of the waveguide resulting from the coupling slots is made $2Y_o$ in the absence of waveguide loads. Energy input to this section may then be reactively transferred to the next layer with a uniform transfer phase. The equivalent resistance of each slot is determined by the desired percent power to be coupled by that slot. The same requirement (composite admittance = $2Y_o$) is placed on each of the radiating shunt slot waveguide sections. The percent power radiated by each slot is determined by the slot conductance. Thus, the vertical distribution is controlled by the series slot waveguide and the horizontal distribution is controlled by the shunt slot waveguide sections.

For the case of uniform amplitude, the solution to the problem becomes trivial. The five series slots will all have the same resistance and the composite will equal 2. Each series slot will have a resistance of 0.4 ohm. Each shunt waveguide will have four elements with a conductance of 0.5 mho each.

3. Performance

Following the design and fabrication of the component parts, the feed antenna was assembled and tested. A photograph of the fully assembled flatplate is shown in Figure 3-22. Testing of the feed included measurement of VSWR and of near-field amplitude and phase.

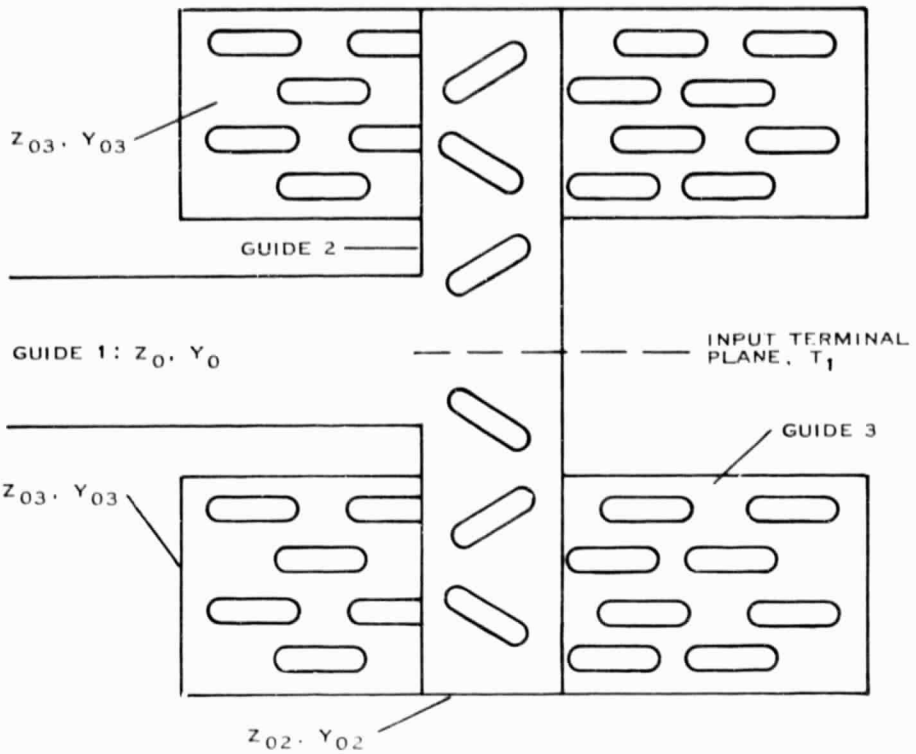

Figure 3-21. Subarray Development

ORIGINAL PAGE IS
OF POOR QUALITY

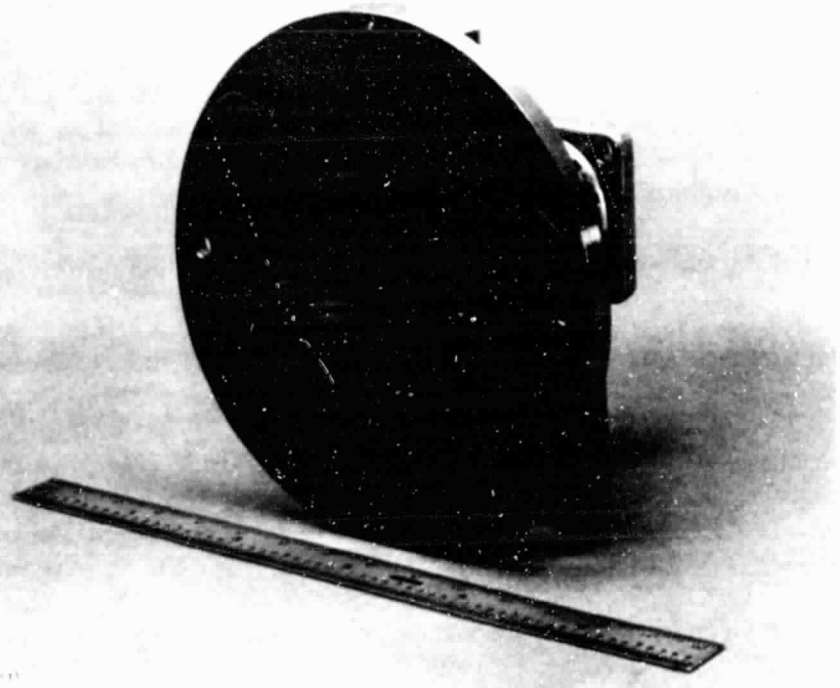

Figure 3-22. Assembled Flatplate

VSWR was measured and is shown in the form of a Smith chart in Figure 3-23. A match of ≤1.5:1 was obtained over the 14.6- to 15.2-GHz frequency band. This measurement was performed with the flatplate feed in an unobstructed freespace environment.

Near-field amplitude and phase measurements were performed using the Texas Instruments Antenna Laboratory's planar near-field probe facility. The engineering array was designed so that the distance between the feed aperture and the secondary dipole feed aperture could be varied from approximately 0.1 to 10.2 cm (0.040 to 4.000 in.). It would be desirable to know the near-field distribution at a distance approximating the smallest distance possible.

A practical limit exists, however, mainly because of a scattering effect caused by the near-field probe itself. The first step in the measurement process then becomes finding the region where scattering is minimized by probing the antenna in the direction along the normal to the aperture. The region closest to the aperture will show a ripple effect caused by the constructive and destructive scattered components. As the probe is moved farther from the aperture, a region of rather smooth decay is encountered. Figure 3-24 is a plot of the data acquired when the "z scan" or scan along the normal was performed on the feed antenna. The region less than 5 cm (2 in.) from the aperture shows heavy scattering effects. Attempting to take measurements in this region would result in unreliable data. A distance of 5.4 cm (2.125 in.) was selected as the fixed z distance while performing a planar x,y scan. Some beam focusing will be evident at this distance; however, the aperture can still be qualitatively examined for uniformity and symmetry. The planar scan covered a square grid approximately 10.2 cm (4 in.) on a side centered on the feed aperture. The probe was stepped in x and y in $\lambda/4$ increments. Figure 3-25 is a three-dimensional plot of the amplitude data as measured at center frequency. Figure 3-26 shows the normalized data as a contour plot. Superimposed on the plot is the outline of the secondary pickup aperture area. Figure 3-27 is a three-dimensional plot of the phase data taken over the same region, while Figure 3-28 shows the normalized phase data in contour form. Again, the pickup aperture area is superimposed on the contour plot.

Data were recorded at the frequency band edges as well as at center frequency for several other "z" distances. Additional beam focusing became more evident as the measurement was taken at distances farther from the aperture. The flatplate measurement data showed the feed to be operating acceptably over the entire region of interest.

F. MECHANICAL SUPPORT STRUCTURE

The mechanical design effort for the engineering model array was limited to the creation of a suitable support and alignment structure and in no way was intended to be representative of the proposed system design.

Two photographs of the fully assembled engineering array are shown in Figures 3-29 and 3-30. The support structure is composed of four major parts. The first of these is the lens support. It is the smaller of the two cylindrical cavities and houses the 19 phase shift modules and their associated dc control wiring and output connectors. The support and alignment of the modules is controlled by this structure. The modules are first attached to nine vertical alignment panels. The panel-mounted modules are then attached to an etched aluminum dipole ground plane that contains close tolerance passages for the module feedthrough, dipole, and alignment foot. The ground plane is then attached to the outer support ring. A front view of the assembled

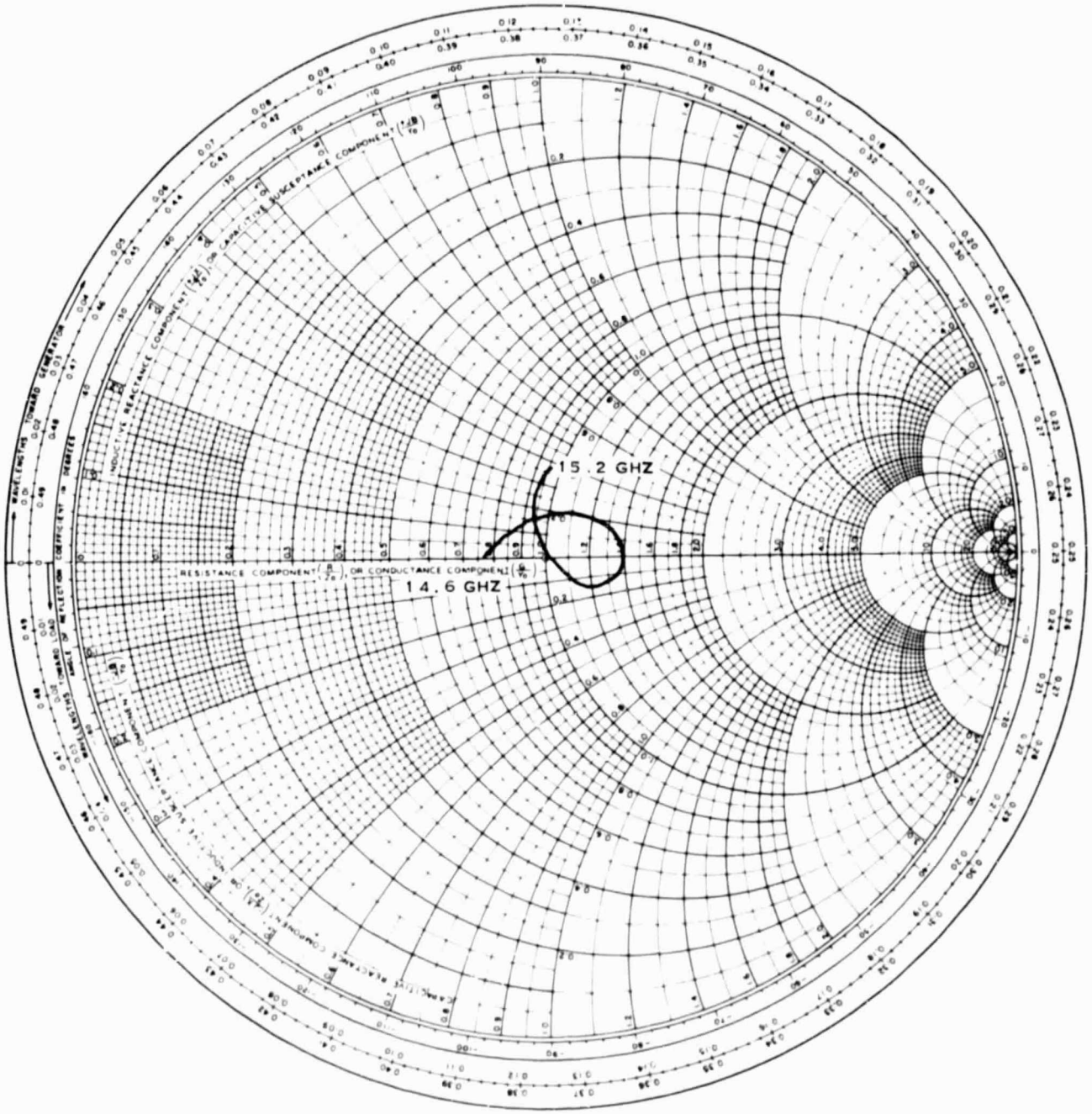

ORIGINAL PAGE IS
OF POOR QUALITY

229020

Figure 3-23. Smith Chart of VSWR Data

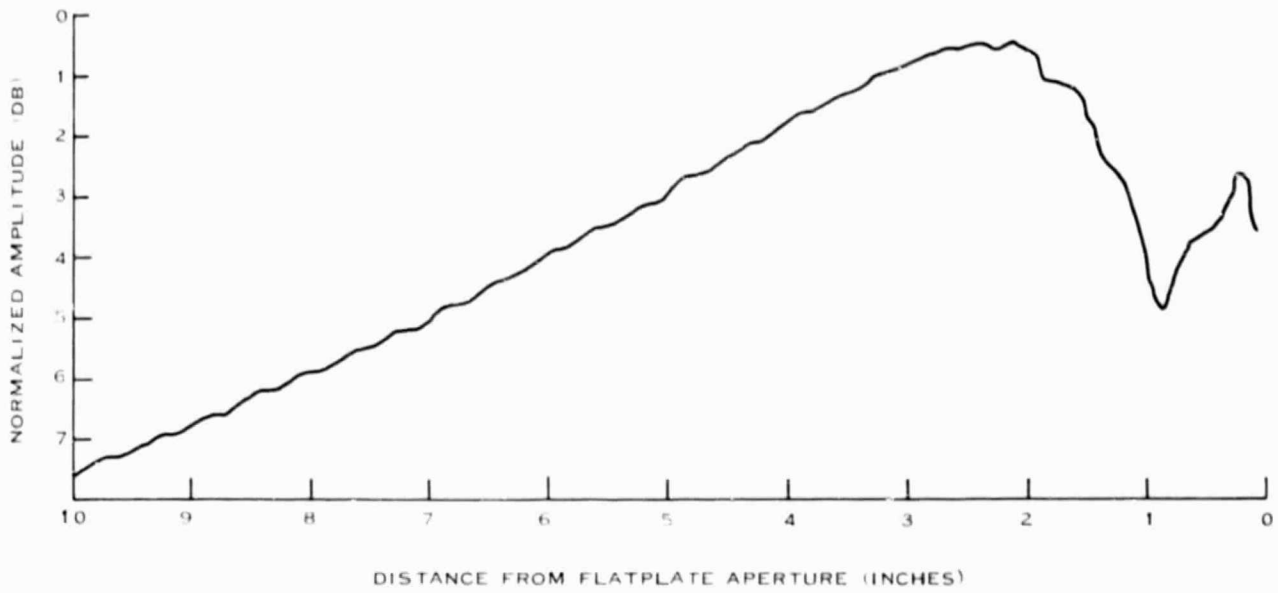

229021

Figure 3-24. Z Scan of Feed Antenna

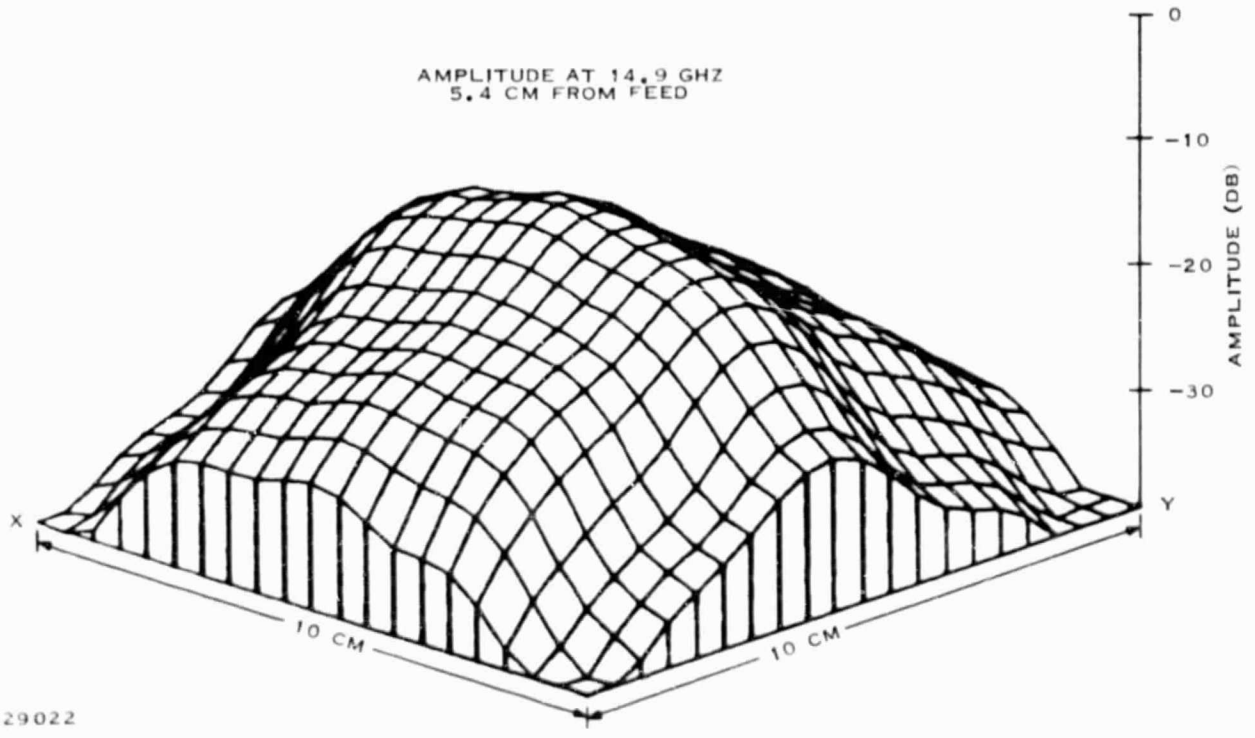

229022

Figure 3-25. Three-Dimensional Plot of Amplitude Data Measured at Center Frequency

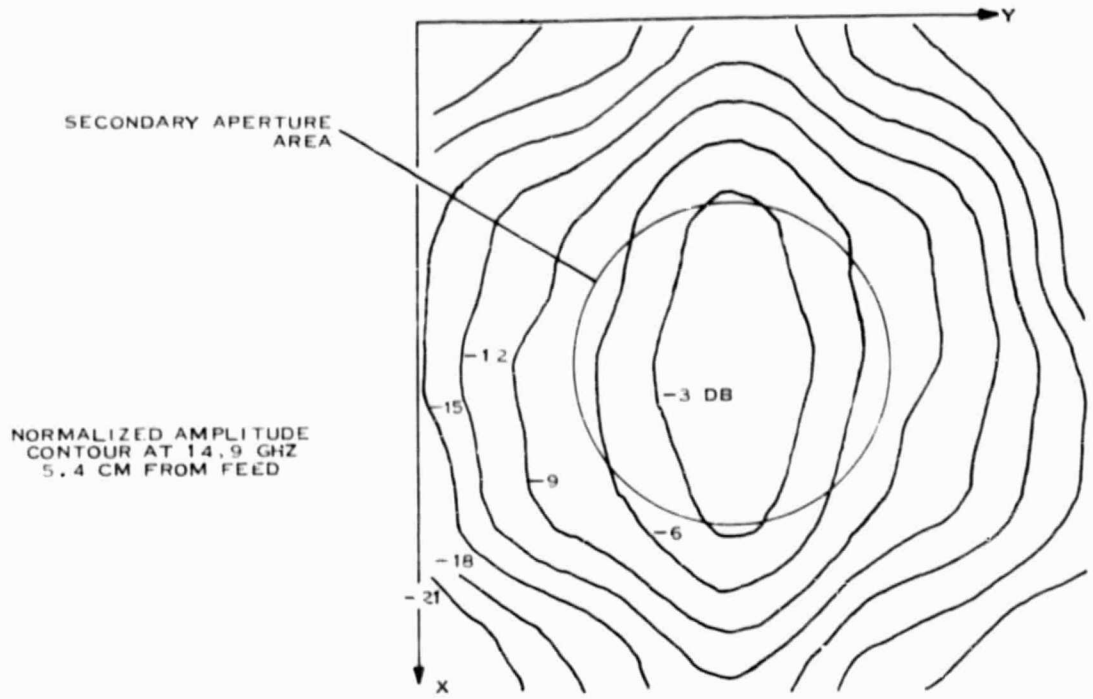

Figure 3-26. Contour Plot of Normalized Amplitude Data

lens with the front ground plane removed is shown in Figure 3-31. The vertical panels and the dc control wiring are evident. The larger cylindrical cavity houses the flatplate feed and secondary pickup aperture. The cavity is lined with AN-73 absorber to reduce the various reflected signals in the feed region. The feed antenna and absorber are partially visible through the open lens assembly in Figure 3-32. In the large system array, this region would also provide the rigid support for the feed antenna.

For the engineering array, provisions were made to allow variation of the separation between the flatplate feed and the pickup array. The flatplate was designed to be mounted on two rods that slide in a set of linear bearings, allowing front-to-rear movement while remaining rather rigid in the vertical and horizontal directions. The rods are visible in Figure 3-29.

The remaining portion of the structure consists of the supporting baseplate that holds and aligns the previously mentioned parts and provides attachment points for range mounting of the antenna for pattern testing.

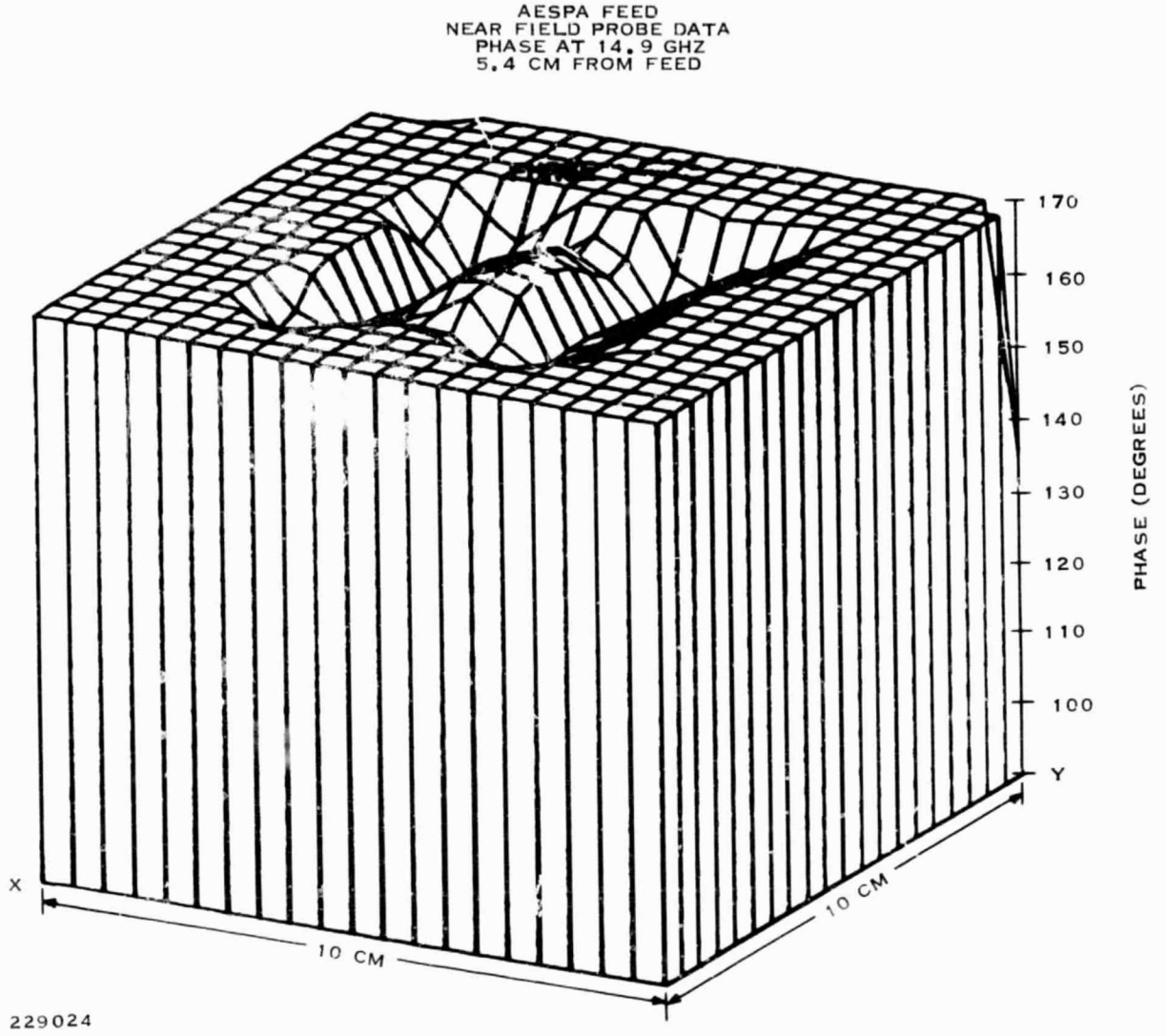

Figure 3-27. Three-Dimensional Plot of Phase Data Measured at Center Frequency

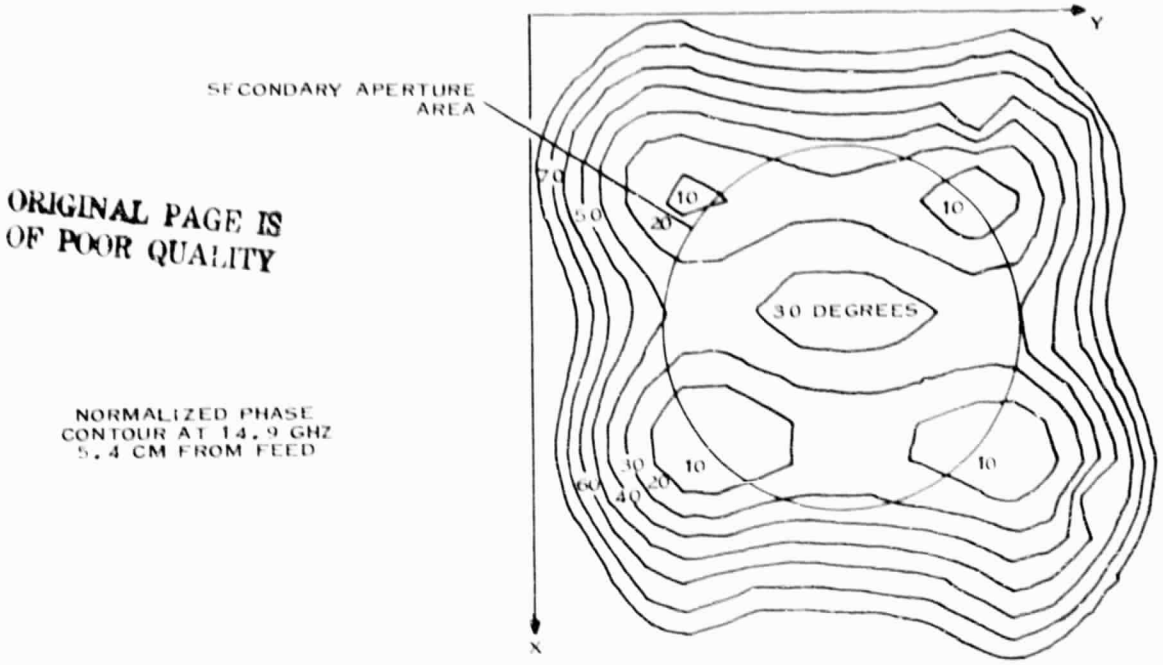

Figure 3-28. Contour Plot of Normalized Phase Data

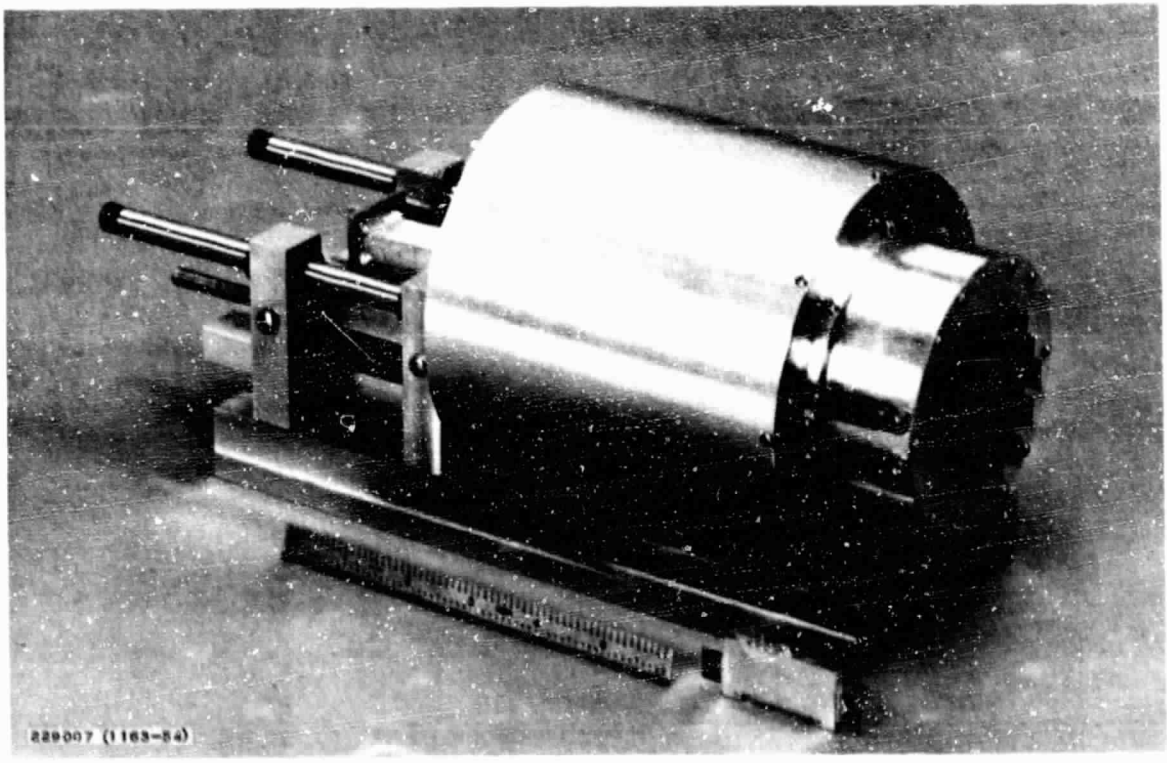

Figure 3-29. AESPA Array and Phase Shifter Module

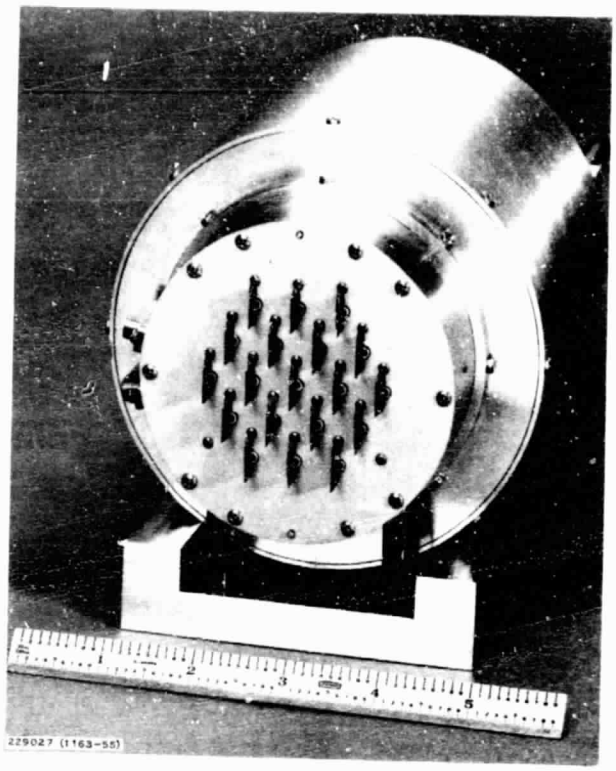

Figure 3-30. AESPA Engineering Model Array

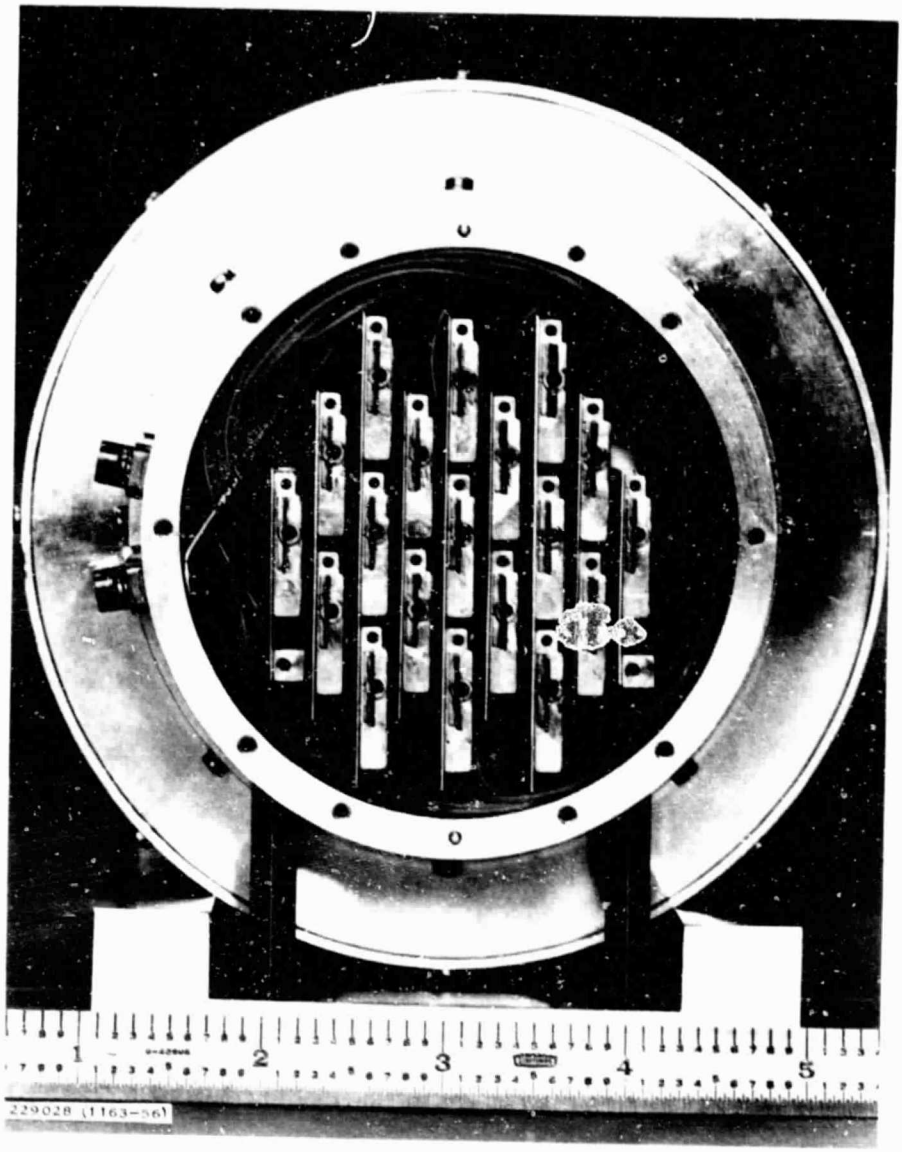

Figure 3-31. Assembled Lens With Front Ground Plane Removed (Front View)

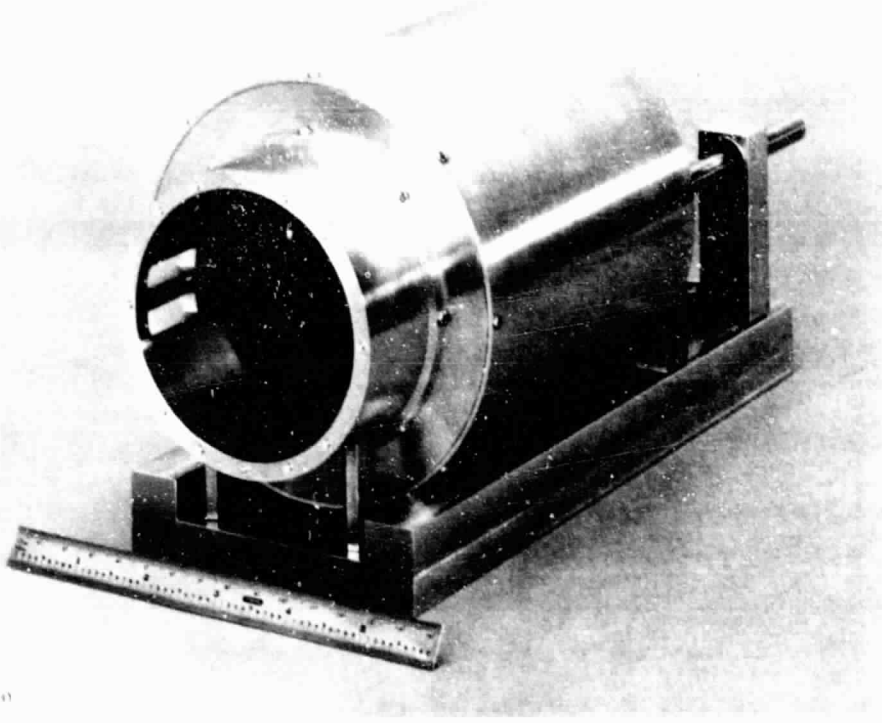

Figure 3-32. Open Lens Assembly Showing Feed Antenna and Absorber

SECTION IV
ARRAY PERFORMANCE AND TESTING

A. SUMMARY

The engineering array was proposed, designed, and fabricated to demonstrate some of the performance capabilities of the transmissive array. Of particular interest are the gain, beamwidth, and sidelobe variation versus frequency and scan angle. This section contains discussions of calculated array patterns and measured performance data. Subsection IV.D summarizes the results in a performance comparison matrix.

B. CALCULATED PERFORMANCE

1. Patterns

As part of the calculated performance, array radiation patterns were computed and plotted for several scan angles at five nearly evenly spaced frequencies throughout the 14.6- to 15.2-GHz band. Patterns were computed for the ideal error-free case and did not include mutual coupling effects.

Figures A-1 through A-35, shown in the appendix, are the computed planar radiation patterns. The patterns are grouped according to frequency and begin at the low end of the band. At each frequency, seven patterns are shown. The first three patterns shown are azimuthal. The first azimuth pattern is the broadside case where no phase gradient is introduced across the aperture. The second pattern shows the beam scanned approximately 23 degrees and is obtained by putting a 45-degree linear phase gradient in the horizontal direction. Increasing the gradient to 90 degrees causes the beam to steer to approximately 50 degrees. The last four patterns in each frequency group are elevation cuts. Phase gradients of 0, 45, 90, and 135 degrees are used to steer the beam from broadside to 13, 27, and 43 degrees, respectively.

Recall from the discussion in Subsection III.B that pattern degradation in the form of grating lobes is unavoidable in the engineering array and becomes evident at angles less than 60 degrees. Figures 4-1 through 4-5 are three-dimensional patterns that demonstrate the problem. Figure 4-1 shows the broadside pattern, while Figures 4-2 and 4-3 show the patterns for a small scan angle in azimuth and elevation, respectively. Figures 4-4 and 4-5 show larger scan angles in each plane and clearly show the grating lobes.

2. Gain

The aperture gain is related to the active aperture area A by

$$G_A = 10 \log \left(\frac{4\pi A}{\lambda^2} \right)$$

Using the dimensions of the engineering array yields G_A = 19.4 dB. The various losses associated with the array must be subtracted from this value. A loss budget for the engineering array is shown in Table 4-1. The values in the table are measured where possible and estimated where

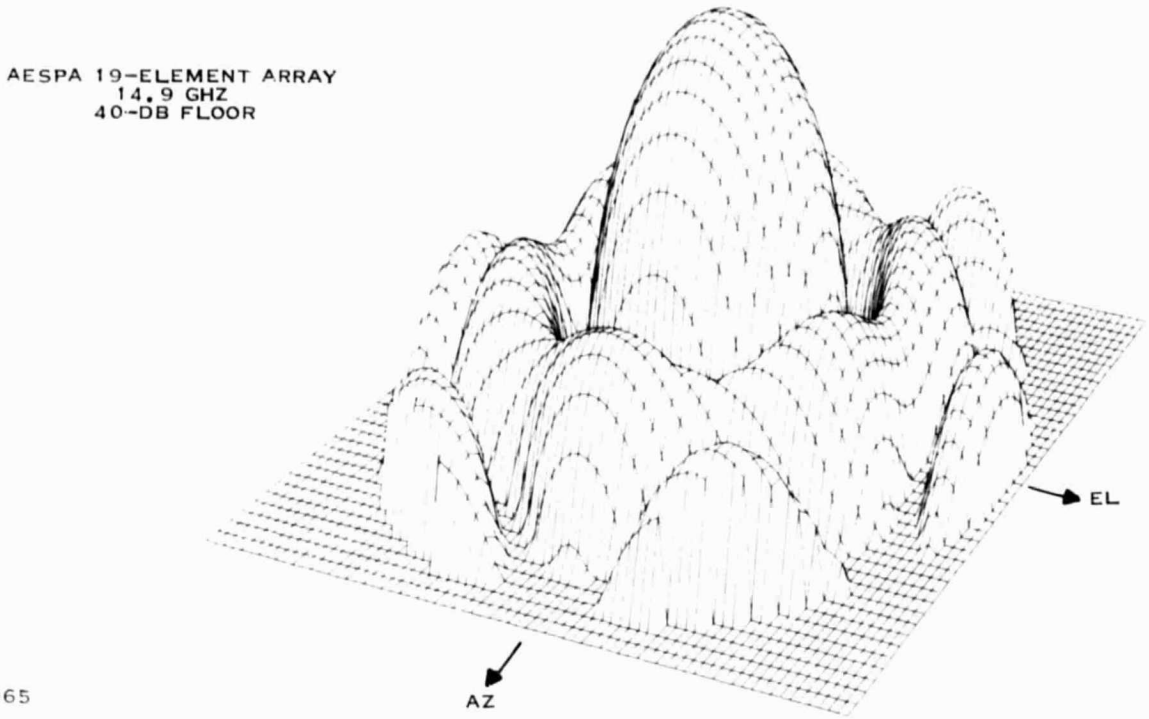

Figure 4-1. Three-Dimensional Plot, No Scan

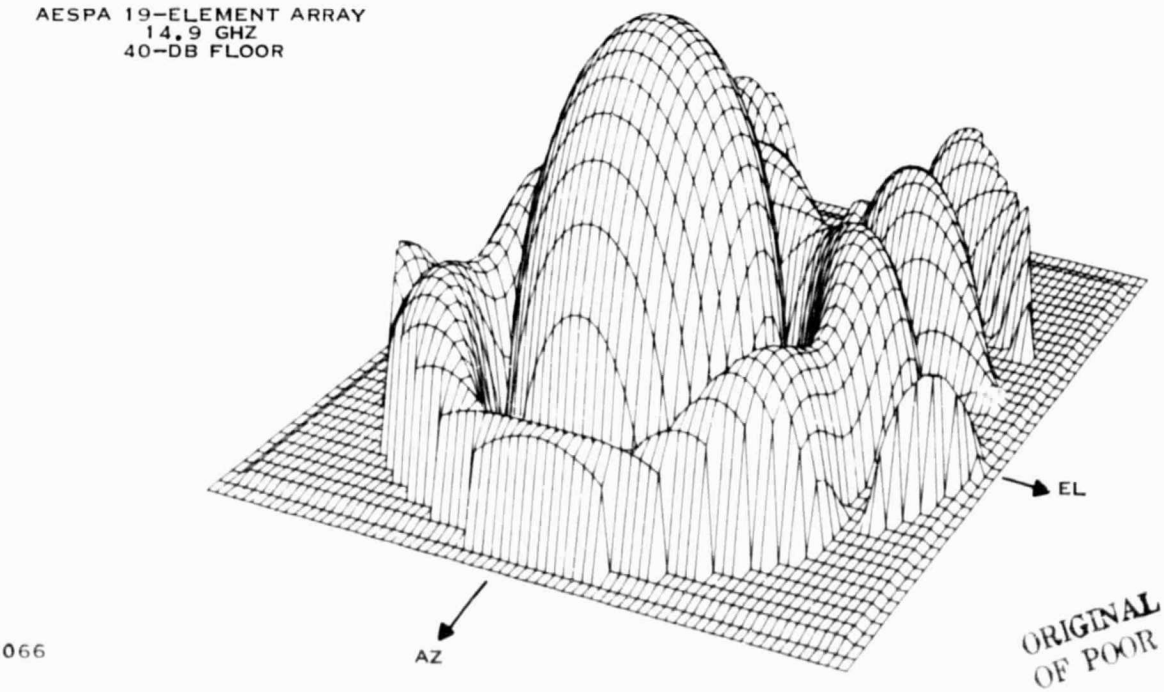

Figure 4-2. Three-Dimensional Plot, Beam Scanned 23.5 Degrees in Azimuth

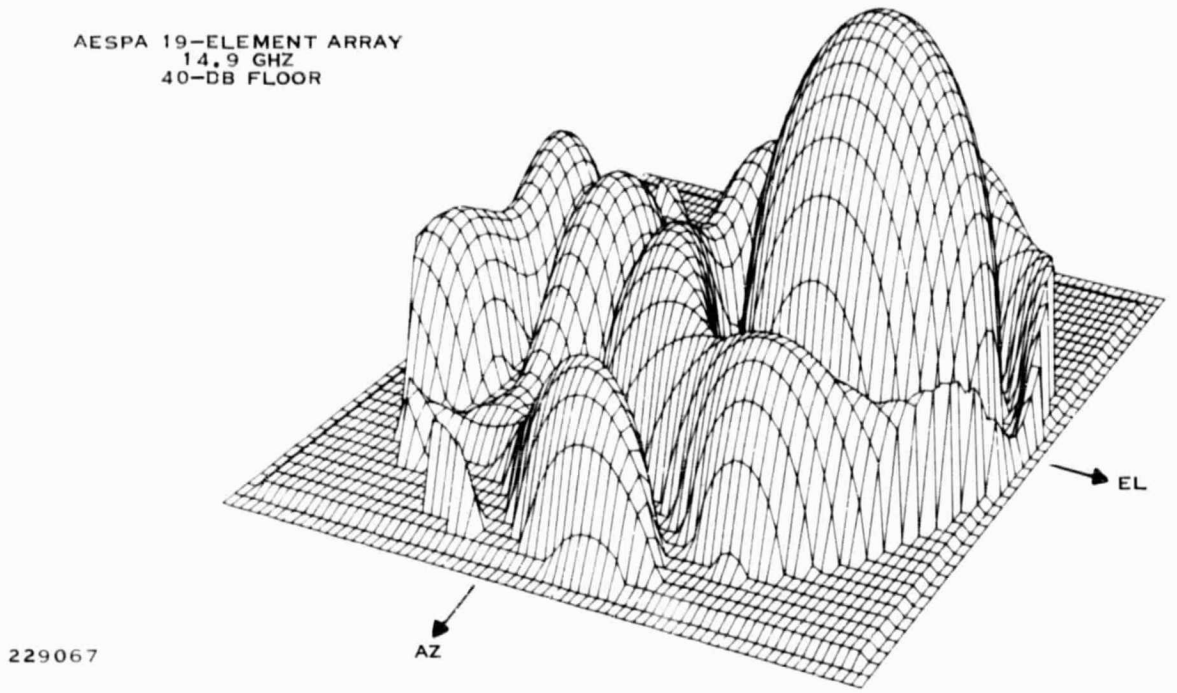

Figure 4-3. Three-Dimensional Plot, Beam Scanned 27 Degrees in Elevation

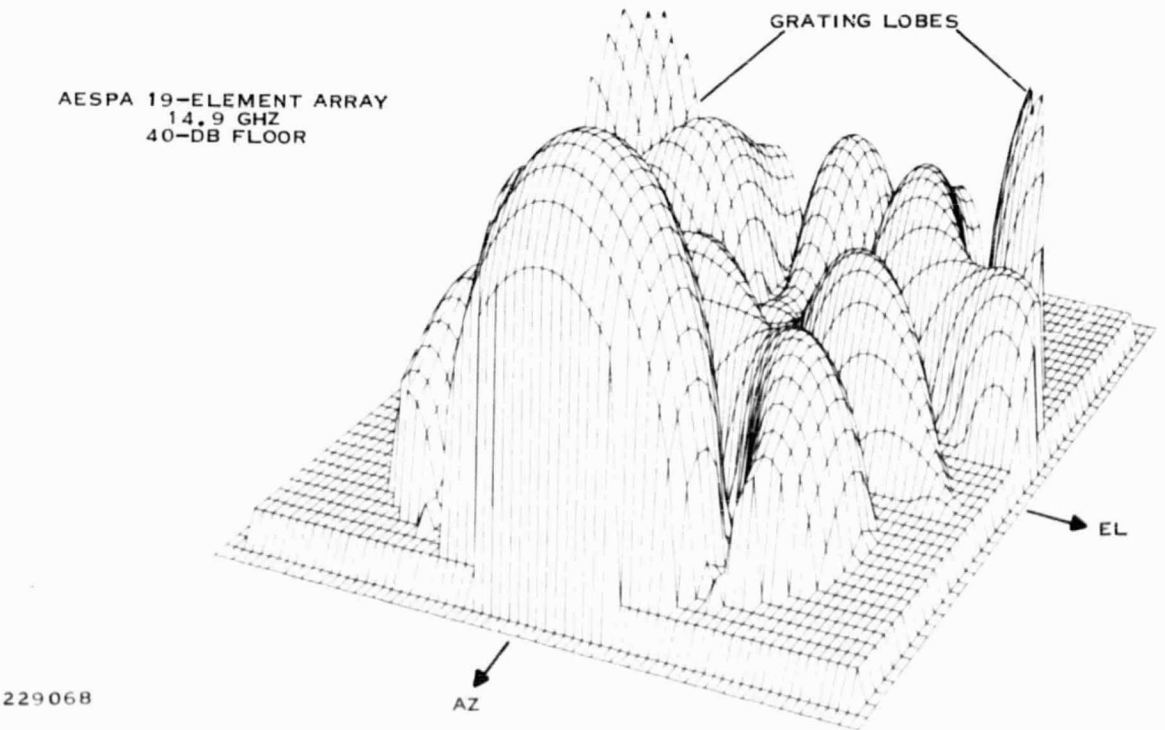

Figure 4-4. Three-Dimensional Plot, Beam Scanned 51 Degrees in Azimuth

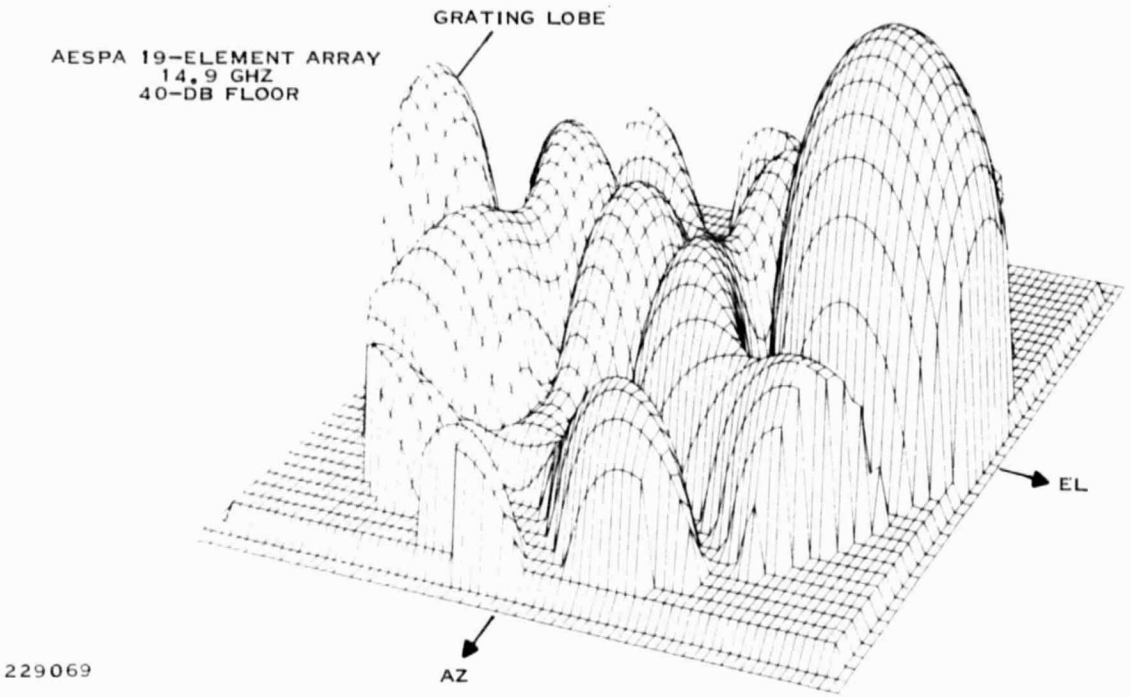

Figure 4-5. Three-Dimensional Plot, Beam Scanned 43 Degrees in Elevation

TABLE 4-1. LOSS BUDGET

	Loss (dB)
Flatplate array	
Mismatch	0.20
Waveguide (1 foot at 0.15 dB/foot)	0.15
Slots (two at 0.4 dB)	0.80
Kapton	0.30
Feed junction	0.20
	1.65
Space transition	0.80
Receive dipole array	
Mismatch	0.50
Phase shifter	4.9
Radiating dipole array	
Mismatch	0.50
Total Loss	8.35

necessary. When the losses are taken into account, the engineering array gain is reduced to approximately 11.1 dB. This calculation neglects amplitude and phase errors present in the system. The calculated aperture gain varies a small amount with frequency because of the change in wavelength (λ). The variation is shown in the performance comparison matrix of Subsection IV.D.

C. MEASURED PERFORMANCE

1. Summary

The engineering array was tested extensively following final assembly. The impedance match was measured and data generated in the form of Smith charts and

return loss plots. The array was given a cursory examination using a near-field probe to ensure all 19 elements were functioning. Following these measurements, the planar radiation patterns were measured. Information pulled from the patterns is compared to calculated values in the performance comparison matrix (Subsection IV.D).

2. Impedance Testing

The first test performed on the array were done to examine the impedance match versus frequency and feed-pickup aperture spacing. A swept-frequency Smith chart was plotted as the separation was varied in approximately $\lambda/8$ (0.1 inch) intervals. These tests unsurprisingly show the VSWR to be sensitive to the variation in separation and to be periodic by $\lambda/2$. Figures 4-6 through 4-9 are examples of the collected data. Figure 4-6 shows the impedance with minimum separation between the feed and pickup array. An actual separation of 0.102 cm (0.040 in.) exists at this "0.0"-inch spacing. Figure 4-7 shows the plot at the array's first optimum separation and Figure 4-8 at the second optimum. VSWR values at the optimum separations were typically 1.8:1. Figure 4-9 is a typical plot midway between two optimum values. VSWR at these points approached 3:1 or worse.

The periodic nature of the VSWR is further evident in Figures 4-10 through 4-12, which are plots of measured return loss versus feed-pickup aperture separation at 14.6, 14.9, and 15.2 GHz, respectively.

3. Pattern Measurements

Following VSWR testing, the array's near-field amplitude and phase distributions were briefly examined to ensure all the radiating elements were functioning properly. Both distributions had a smooth taper across the aperture and showed good symmetrical characteristics. The array was then mounted on a far-field range so that pattern testing could begin.

The first pattern tests performed involved pattern shape versus feed-pickup aperture separation. The feed was placed as close to the pickup as possible (0.040 inch) and the pattern recorded. The feed was then moved rearward to each of the VSWR optimum points. Patterns obtained are shown in Figures 4-13 and 4-14. The shape of the main beam remained nearly constant while the sidelobe level dropped as the separation increased. This result was not surprising since the energy from the feed is better focused as separation increases and effectively places a taper on the amplitude distribution at the pickup aperture. One nonoptimum VSWR point was also recorded and is shown in Figure 4-14. Recall that VSWR at the nonoptimum points approached 3:1 and, thus, the 1.5-dB drop in gain is also not surprising.

From a system standpoint it is desirable that the feed-pickup aperture separation be minimized to reduce antenna volume. The second VSWR optimum point yielded symmetrical azimuth sidelobe levels (within 1.0 dB) and was selected for further pattern testing. Figures A-36 through A-70, shown in the appendix, are the measured patterns corresponding to the calculated patterns shown earlier. The measured patterns are grouped in the same manner as the calculated patterns (seven plots per frequency group beginning at 14.6 GHz). Beamwidths and sidelobe levels were extracted from the measured patterns and are summarized in the comparison matrix in Subsection IV.D. Array gain was extracted from Figure A-71 and is also shown in Subsection IV.D.

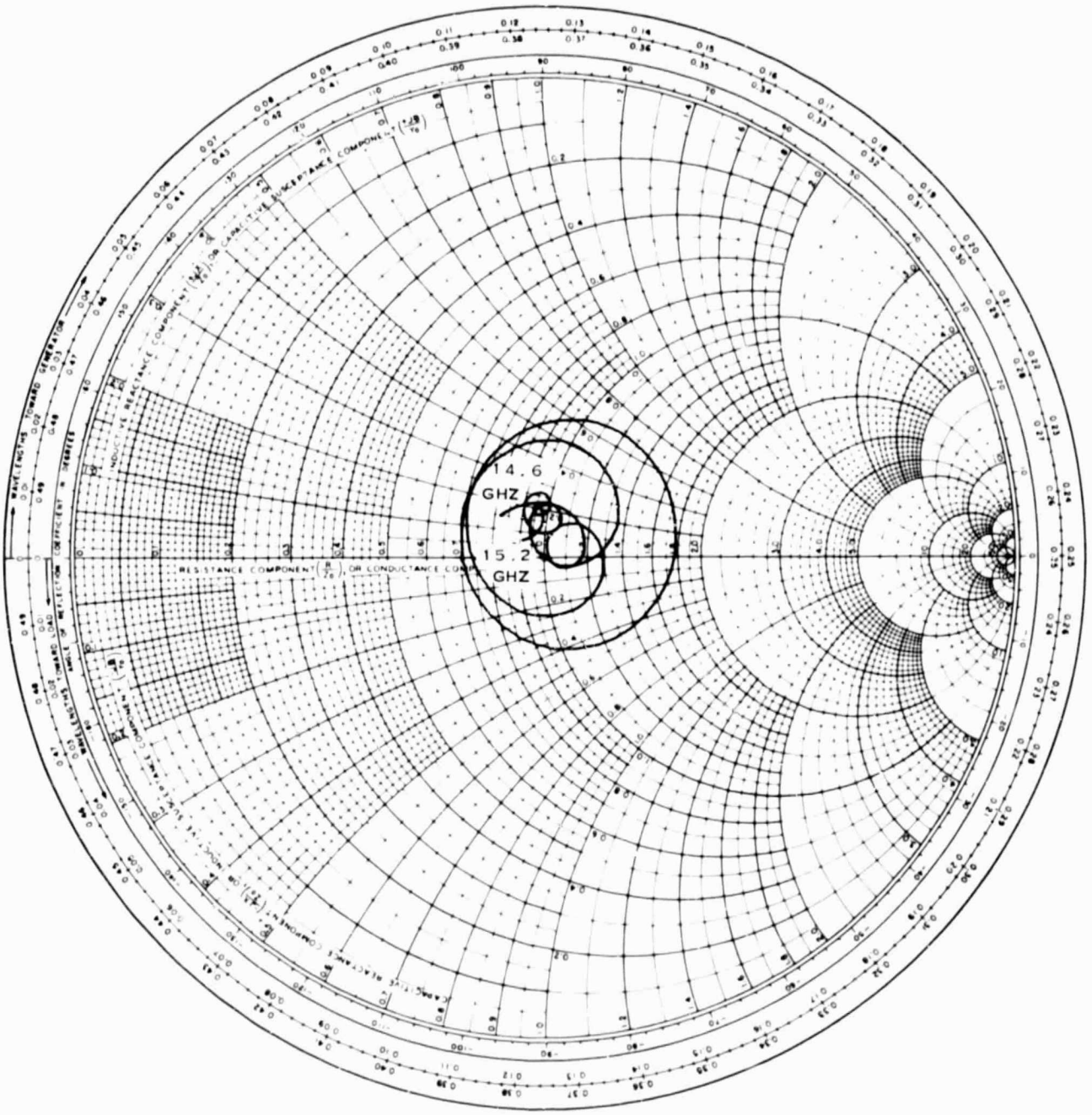

FEED SPACING = 0.0 IN.

229070

Figure 4-6. Impedance Match Versus Frequency and Feed-Pickup Aperture Spacing, Minimum Separation

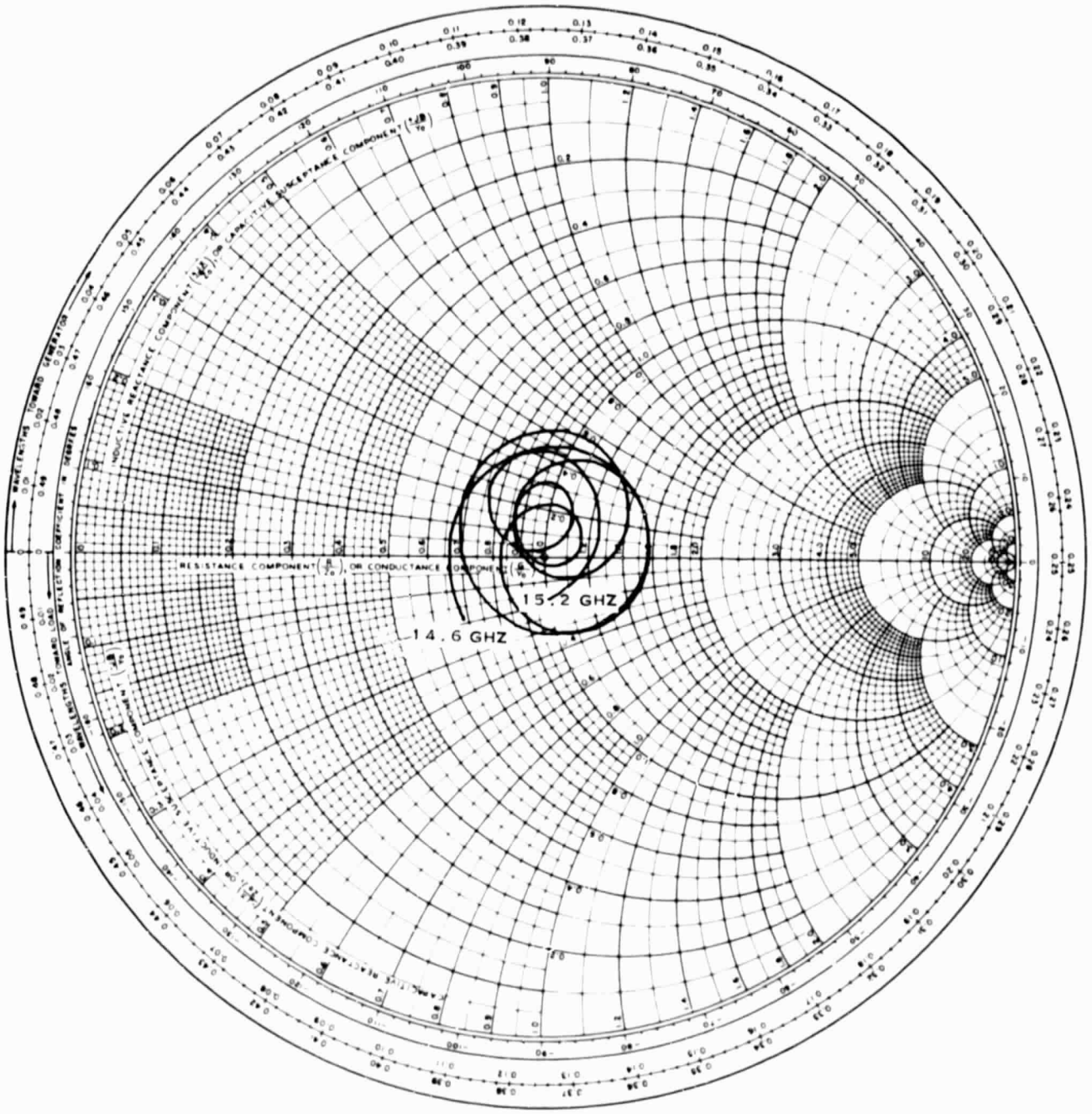

FEED SPACING 0.35 IN.

229071

Figure 4-7. Impedance Match Versus Frequency and Feed-Pickup Aperture Spacing, First Optimum Separation

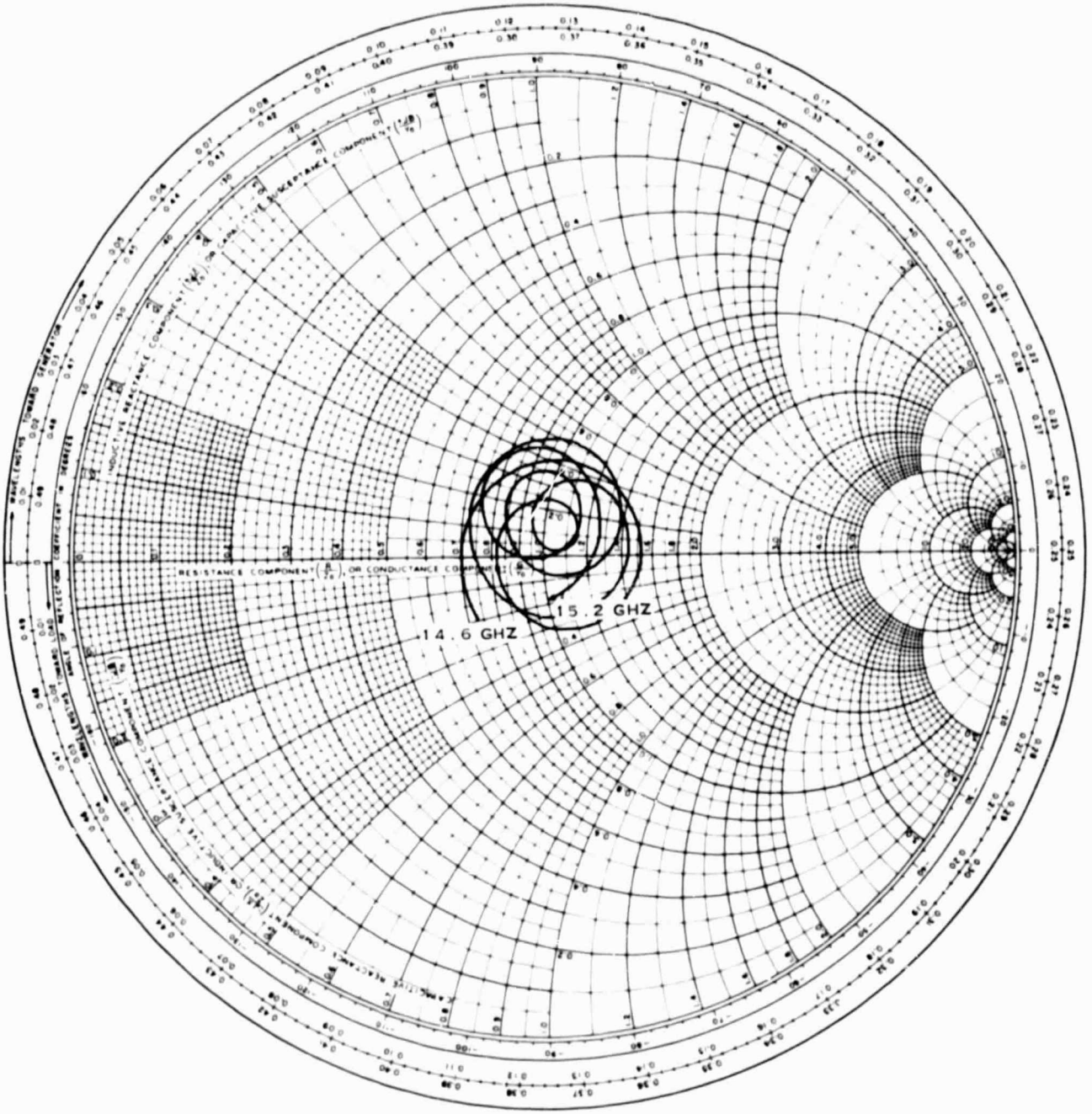

FEED SPACING 0.74 IN.

229072

Figure 4-8. Impedance Match Versus Frequency and Feed-Pickup Aperture Spacing, Second Optimum Separation

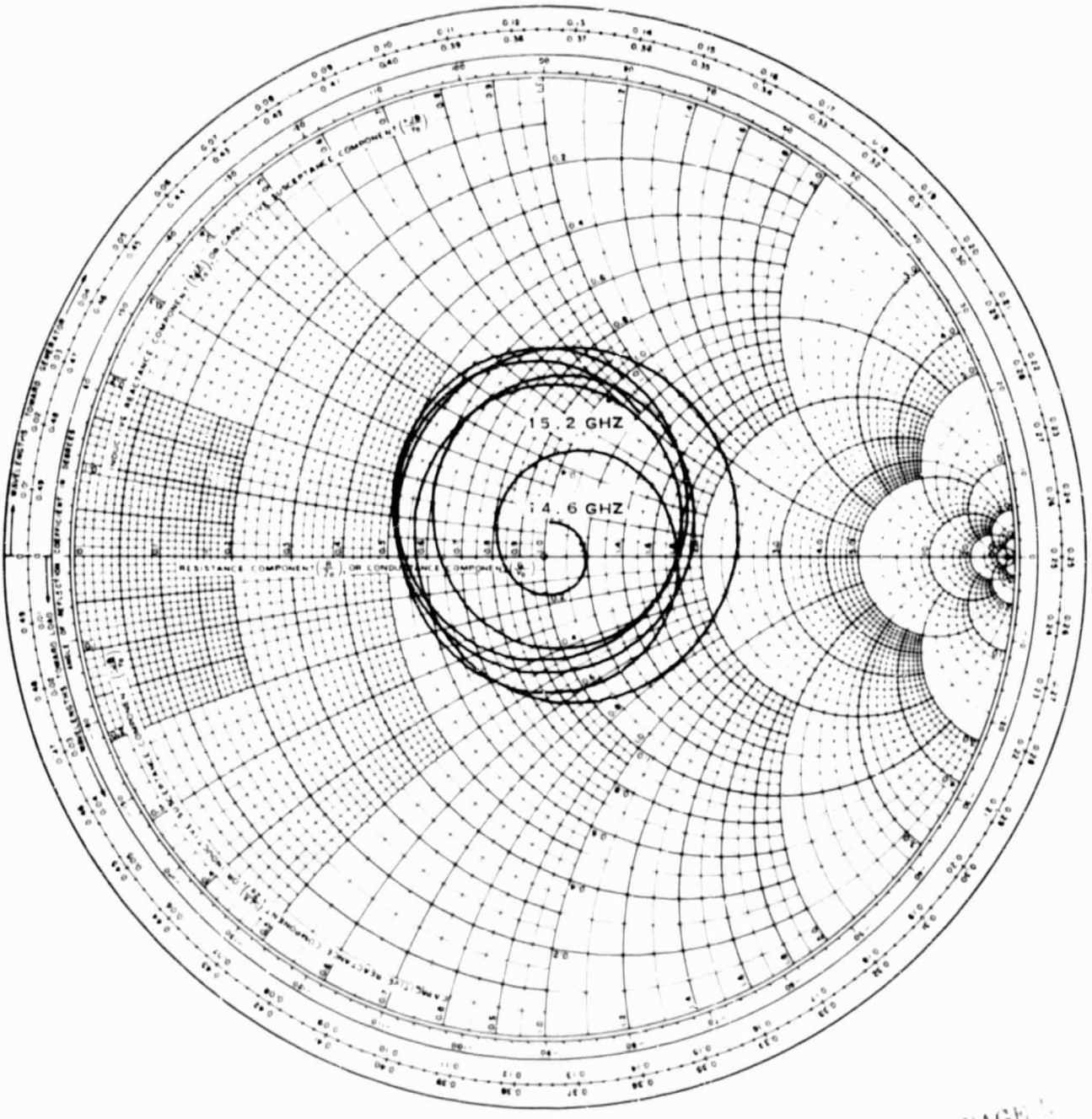

FEED SPACING - 2.49 IN.

229073

Figure 4-9. Impedance Match Versus Frequency and Feed Pickup Aperture Spacing, Separation Midway Between Two Optimum Values

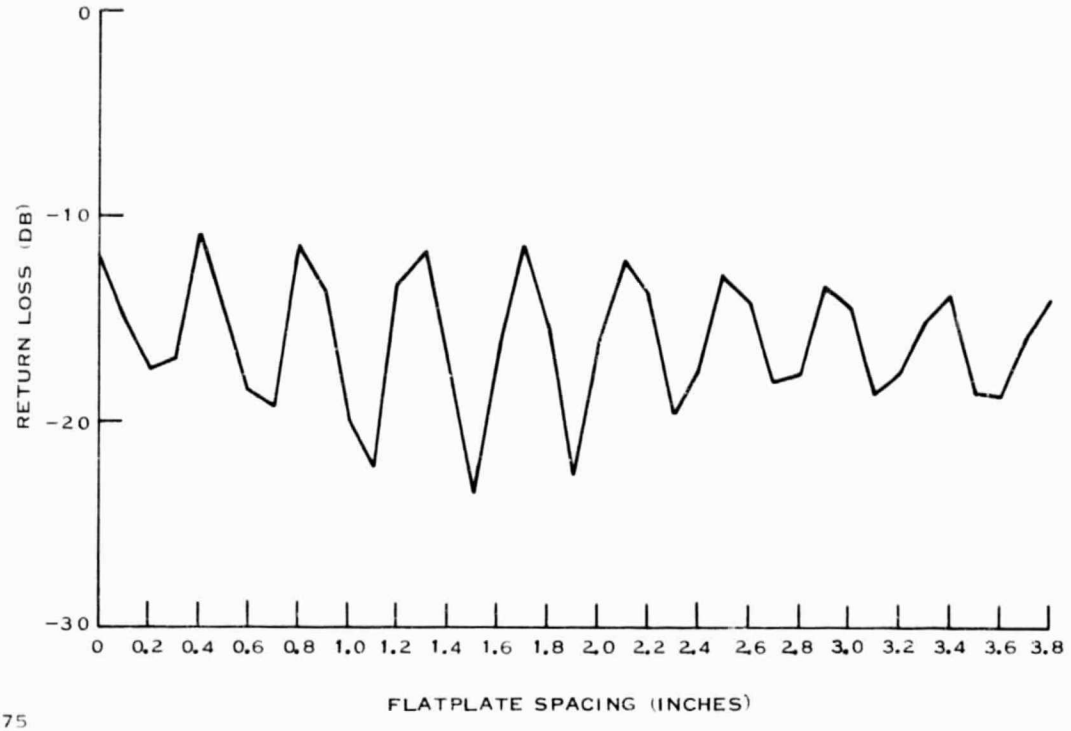

Figure 4-10. Measured Return Loss Versus Feed-Pickup Aperture Spacing at 14.6 GHz

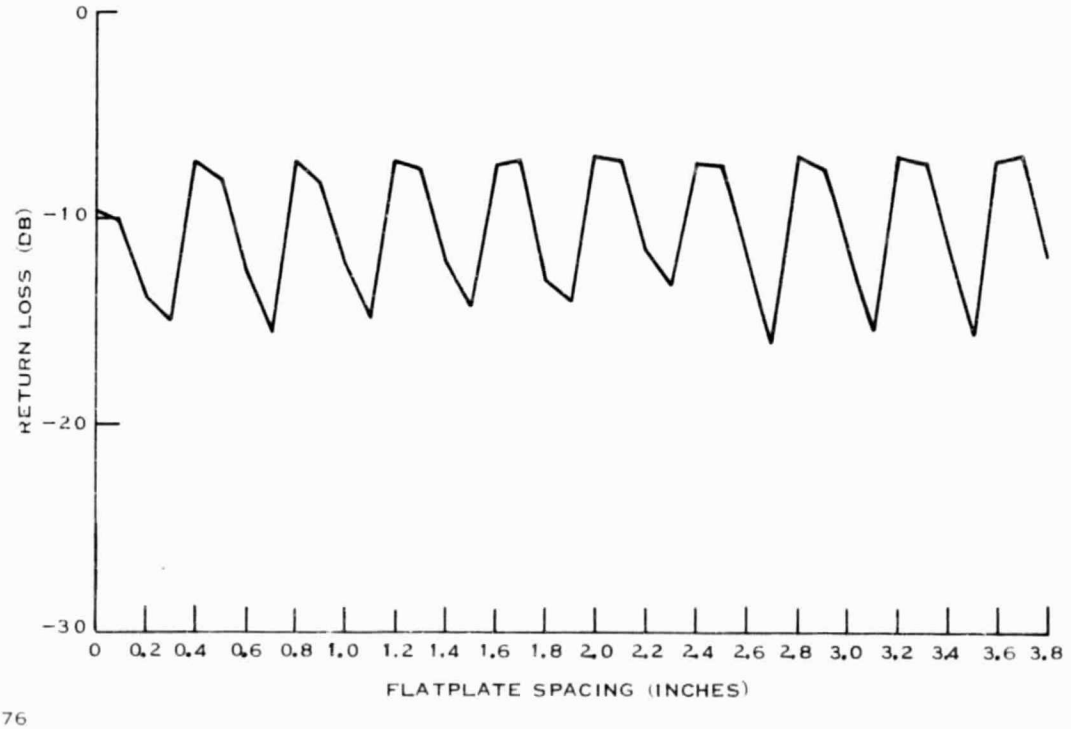

Figure 4-11. Measured Return Loss Versus Feed-Pickup Aperture Spacing at 14.9 GHz

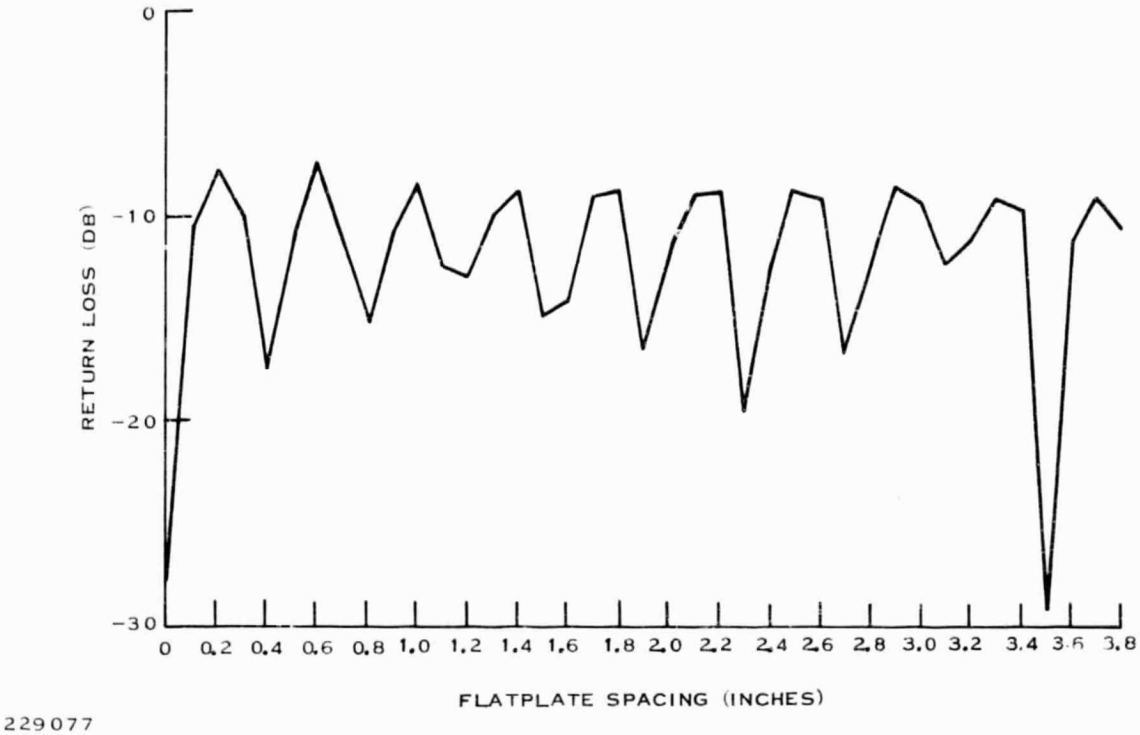

Figure 4-12. Measured Return Loss Versus Feed-Pickup Aperture Spacing at 15.2 GHz

D. COMPARISON MATRIX

This subsection contains several tables that summarize the results of the array calculations versus array performance. In order to help reduce the large amount of data, this subsection shows the various performance parameters at the frequency band edges (14.6 and 15.2 GHz) and at center band (14.9 GHz) only. Values at the other two frequencies may be obtained from the patterns shown in the appendix.

Table 4-2 is a summary of the calculated and measured array beamwidths versus frequency and scan angle. Two numbers are given for each scan-frequency combination. The first number represents the measured value, while the second number (in parentheses) represents the calculated value. Values compare reasonably well as would be expected since beamwidth is most heavily dependent on physical size of the array. Some error exists because of amplitude and phase errors in the system, causing some beam defocusing.

Table 4-3 is a similar summary for peak sidelobe level versus frequency and scan angle. A notable difference is evident at first glance: measured values are considerably higher than calculated values. Recall, however, that the calculated values are for the ideal error-free case. Sidelobes in a small array are readily degraded by amplitude and phase errors. The same amplitude and phase errors would have less effect on a larger array. The table also illustrates increasing degradation of sidelobes as scan angle is increased.

TABLE 4-2. MEASURED AND CALCULATED ARRAY BEAMWIDTH (DEGREES) VERSUS FREQUENCY AND SCAN ANGLE

	Scan Angle (degrees)	Frequency (GHz) 14.6	14.9	15.2
Azimuth	0	26 (22)	26.5 (21.5)	25 (21)
	23	25 (23.8)	26.5 (23.3)	26.5 (22.7)
	51	30.5 (32)	29 (31.2)	29 (30.4)
Elevation	0	18.5 (22)	22.5 (21.5)	22.5 (21)
	13	20 (22.5)	22 (22)	24 (21.6)
	27	21 (24.4)	23.5 (23.9)	25.5 (25.3)
	43	21 (29.1)	23 (28.3)	25 (27.6)

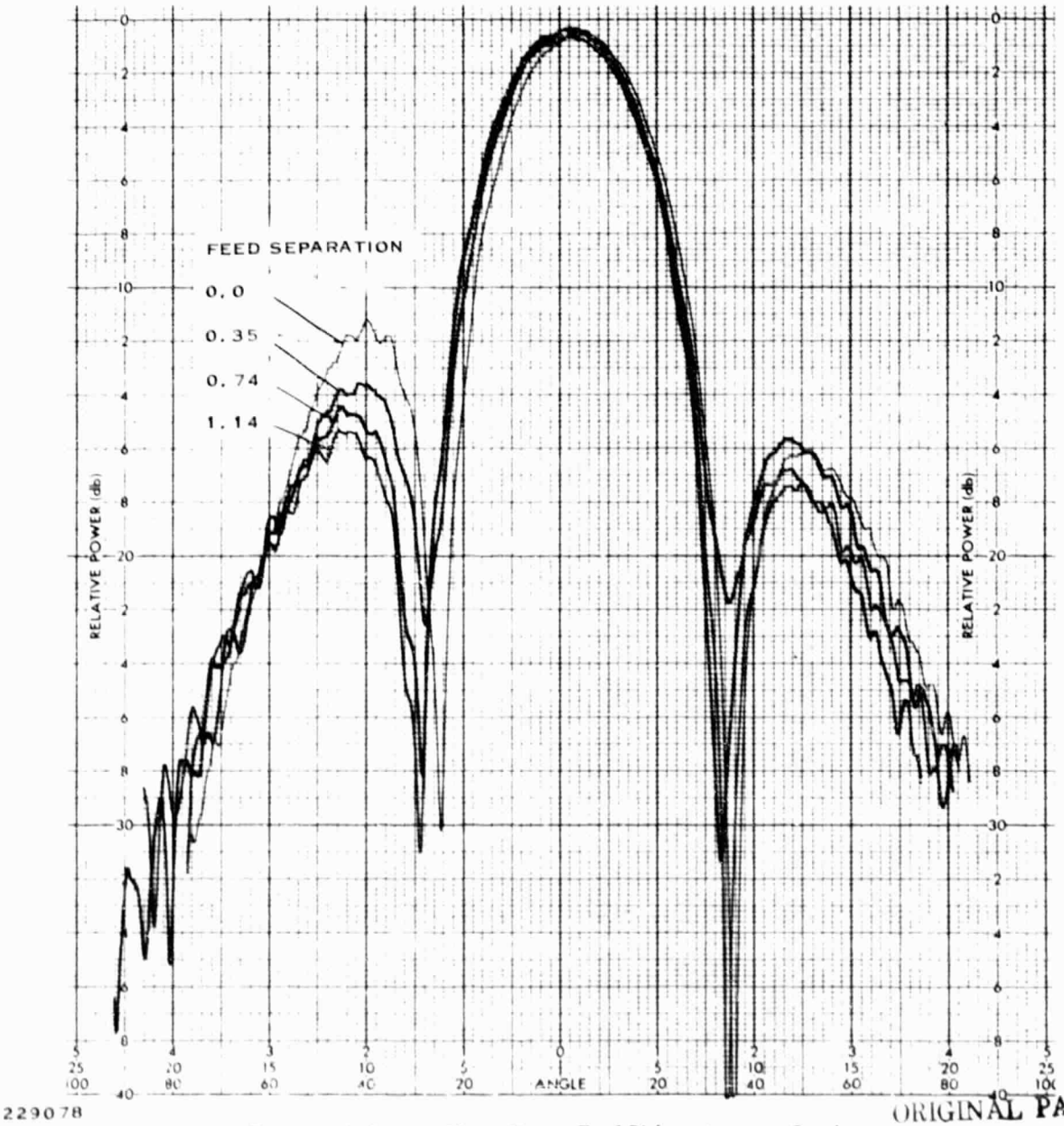

Figure 4-13. Pattern Shape Versus Feed-Pickup Aperture Spacing First Optimum Separation

TABLE 4-3. MEASURED AND CALCULATED PEAK SIDELOBE (dB) LEVEL VERSUS FREQUENCY AND SCAN ANGLE

	Scan Angle (degrees)	Frequency (GHz) 14.6	14.9	15.2
Azimuth	0	10.4 (16)	13.6 (16)	11.7 (16)
	23	8.9 (14.6)	13.1 (14.6)	12.4 (14.6)
	51	9.7 (12.7)	12.9 (12.8)	9.3 (13)
Elevation	0	9.1 (19)	14.3 (19)	16.8 (19)
	13	8.3 (17.5)	14.0 (17.4)	17.2 (17.4)
	27	6.9 (16)	15.0 (16)	14.3 (16.1)
	43	7.5 (14.7)	12.9 (14.7)	12.8 (14.8)

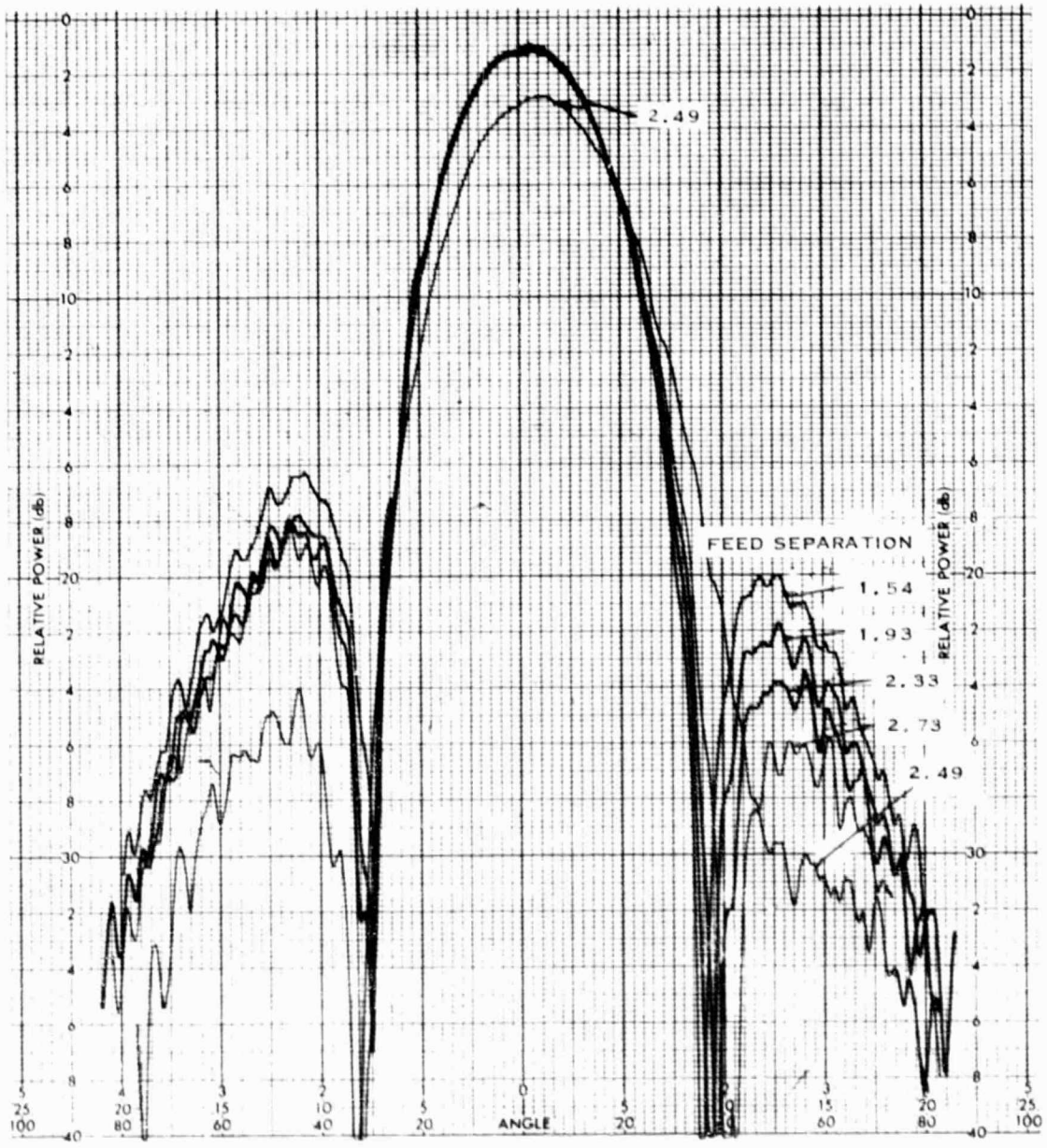

229079

Figure 4-14. Pattern Shape Versus Feed-Pickup Aperture Spacing
Second Optimum Spacing

Gain loss versus scan angle is shown in Table 4-4. In this table, values are normalized to the broadside case at each frequency. Values in this table show good correspondence, again as expected since the loss with scan is primarily the result of the radiating element pattern. The array gain at broadside versus frequency is shown in Table 4-5. Again, system errors have a larger effect on this measurement. The losses shown in Table 4-1 were used to obtain the calculated values for absolute gain. Beam defocusing caused by the various phase errors also contributes to increased losses as does increased power in the sidelobes. The latter two items should be less a problem in a larger array. Array gain appeared to be sensitive to feed-array aperture separation and showed some dispersive effects because of the change in separation relative to wavelength.

Table 4-6 compares the calculated beamsteering angle with the measured angle. The values in this table show close agreement and are, therefore, insensitive to the system amplitude and phase errors.

TABLE 4-4. NORMALIZED MEASURED AND CALCULATED GAIN LOSS (dB) VERSUS SCAN ANGLE

	Scan Angle (degrees)	Frequency (GHz) 14.6	14.9	15.2
Azimuth	0	0 (0)	0 (0)	0 (0)
	23	1.0 (0.4)	0.3 (0.4)	0.0 (0.4)
	51	2.4 (2.3)	1.4 (2.1)	1.0 (2.0)
Elevation	0	0 (0)	0 (0)	0 (0)
	13	0.2 (0.1)	0.4 (0.1)	0.0 (0.1)
	27	0.8 (0.6)	0.0 (0.5)	0.2 (0.5)
	43	2.0 (1.5)	1.3 (1.4)	0.5 (1.4)

TABLE 4-5. MEASURED AND CALCULATED GAIN (dB) WITH ARRAY AT BROADSIDE

Frequency (GHz)	Gain (dB)
14.60	9.0 (10.9)
14.76	10.3 (11.0)
14.90	9.6 (11.1)
15.04	12.3 (11.2)
15.20	10.6 (11.3)

TABLE 4-6. MEASURED AND CALCULATED BEAMSTEERING ANGLE (DEGREES)

	Frequency (GHz) 14.6	14.9	15.2
Azimuth	−0.5 (0)	−0.5 (0)	−2.0 (0)
	24.5 (24)	25.5 (23.5)	24 (23)
	51.5 (51.5)	51.5 (51)	50.5 (49.5)
Elevation	1.0 (0)	−0.5 (0)	(0)
	15.0 (13)	13.5 (13.5)	14 (14)
	30.5 (28)	26.5 (27)	26.5 (27)
	44.5 (44)	42.5 (43)	40.5 (42)

SECTION V
CONCLUSIONS AND RECOMMENDATIONS

A. CONCLUSIONS

The engineering array was successfully designed, fabricated, and tested and demonstrated the performance capabilities of the transmissive array.

Of the three major parameters of interest, beamwidth was shown to be the least sensitive to system amplitude and phase errors. This result was expected since beamwidth is primarily dependent on aperture size. Although not a major parameter, beam pointing angle was also shown to be relatively insensitive to errors. Measured and calculated values for this parameter were nearly identical.

Array gain also showed close agreement between measured and calculated values. Recall that the calculated values did not account for any amplitude or phase errors nor the slight beam widening they cause. Including these effects will reduce the calculated value approximately 1.0 dB. The somewhat dispersive nature of the measured gain was caused by variation in reflection components within the feed-pickup aperture region. This may or may not be a cause for concern, depending on the system instantaneous bandwidth being considered.

Array sidelobe level unsurprisingly showed the greatest difference between measured and calculated values. Recall that the calculated values were for the error-free case. Amplitude and phase errors found in the feed antenna and the phase shifter modules were, for the most part, within design limits established for the larger array. These errors have a much larger effect on a small array, however, because of the smaller number of sidelobes present. In the larger array, the errors tend to average out and degrade a larger number of sidelobes by a smaller amount.

B. RECOMMENDATIONS

The development of the transmissive array for the transmit band has successfully demonstrated this array concept for the AESPA program. Extension of the antenna design to an active array configuration is the recommended development for the next program activity. The maturing GaAs FET technology has made possible direct J-band power generation and low-noise small-signal amplification that can be used in active module development. The active array offers a potential cost-effective system approach by providing long-term reliability.

The recommended program, with a moderate level of contract funding, is the development of the low-noise amplifier for receive and the power amplifier for transmit. These would then be integrated with the phase shifters and module performance demonstrated. Using present GaAs FETs and low-noise design techniques, the proposed receive amplifier would have a 4.5-dB noise figure as a goal. The amplifier would require two to three stages and would be integrated in front of the phase shifter in the receive module. The power amplifier would be a three-stage circuit with a goal of 1 watt output power. This amplifier would be integrated after the phase shifter in the transmit module.

With an adequate level of funding, the recommended program is the development of an active transmissive array for the receive band. The antenna would be a 19-element array similar in design to the present transmit array but with active receive modules. The array would be assembled and tested to the same procedure as the transmit array. This would provide both transmit and receive arrays that could later be used in a link demonstration.

APPENDIX
DATA

TABLE A-1. AESPA PHASE SHIFTER MODULE INSERTION LOSS (dB)

Frequency (GHz)	Scan Angle (degrees) 0	45	90	135	180	215	270	315
Module No. 1								
14.60	4.46	5.12	5.64	7.14	6.15	5.85	5.09	5.34
14.76	2.41	2.90	3.61	4.41	2.56	3.32	3.69	3.64
14.90	2.61	3.22	3.92	4.57	3.29	4.03	3.72	3.89
15.04	2.23	2.51	2.49	3.28	2.74	3.70	3.80	3.96
15.20	4.90	5.40	5.28	5.80	4.84	5.04	4.87	5.51
	Average loss = 4.17 dB		Peak loss = 7.14 dB					
Module No. 2								
14.60	5.71	9.31	8.78	10.18	7.26	8.15	6.82	7.98
14.76	4.88	6.65	6.47	5.77	4.92	5.33	5.50	6.46
14.90	5.48	5.94	7.04	6.51	6.41	6.21	7.05	7.78
15.04	5.90	5.05	7.49	7.09	6.55	5.89	6.75	6.31
15.20	9.33	7.72	9.47	10.01	8.79	7.71	8.41	8.43
	Average loss = 7.09 dB		Peak loss = 10.18 dB					
Module No. 4								
14.60	2.53	4.47	4.33	7.04	5.38	6.14	3.99	5.18
14.76	1.56	3.06	2.98	3.57	1.63	2.98	2.22	3.67
14.90	2.69	3.36	3.76	4.57	2.52	3.80	3.53	4.71
15.04	3.62	3.47	3.13	4.37	2.84	3.34	2.78	4.45
15.20	5.78	6.73	5.42	6.26	5.34	5.83	4.39	5.37
	Average loss = 4.07 dB		Peak loss = 7.04 dB					
Module No. 5								
14.60	3.28	3.77	4.87	5.85	5.70	5.11	4.89	4.03
14.76	1.41	1.75	3.18	3.05	2.69	2.61	3.38	3.17
14.90	2.71	2.71	4.45	4.45	3.84	4.08	4.13	4.10
15.04	2.84	2.71	2.50	3.14	3.71	3.65	3.60	3.85
15.20	5.14	5.37	4.77	5.35	5.62	6.21	6.02	5.92
	Average loss = 3.99 dB		Peak loss = 6.21 dB					
Module No. 6								
14.60	9.54	8.69	9.42	11.59	11.83	13.28	10.07	11.33
14.76	6.64	6.79	6.60	6.98	6.99	7.70	6.73	6.89
14.90	7.28	8.36	9.26	8.18	7.52	8.22	8.44	8.01
15.04	7.12	7.28	8.76	8.64	6.98	6.99	6.98	6.99
15.20	10.60	9.62	9.90	10.88	10.26	9.81	9.73	10.47
	Average loss = 8.68 dB		Peak loss = 13.28 dB					
Module No. 7								
14.60	4.71	4.42	4.19	5.22	6.13	6.17	5.66	5.06
14.76	2.69	3.08	3.66	3.09	2.66	3.25	3.35	2.79
14.90	4.27	3.90	4.81	5.13	3.59	3.87	4.53	4.62
15.04	4.40	3.70	3.26	4.11	4.05	4.28	4.20	4.23
15.20	6.51	7.36	6.62	6.29	6.22	6.77	6.03	5.81
	Average loss = 4.62 dB		Peak loss = 7.36 dB					

TABLE A-1. AESPA PHASE SHIFTER MODULE INSERTION LOSS (dB) (Continued)

Frequency (GHz)	Scan Angle (degrees) 0	45	90	135	180	215	270	315
Module No. 9								
14.60	7.80	6.81	6.66	9.23	10.13	10.16	8.45	9.37
14.76	5.84	7.08	6.98	5.89	6.80	7.86	6.91	6.03
14.90	5.54	7.41	9.81	8.52	6.40	7.91	9.13	7.99
15.04	6.44	5.15	7.87	7.94	6.15	6.01	8.97	8.98
15.20	9.99	9.05	8.71	10.52	10.04	8.79	8.57	10.11
	Average loss = 7.95 dB		Peak loss = 10.52 dB					
Module No. 10								
14.60	3.28	3.21	3.02	3.99	4.26	5.76	5.37	4.99
14.76	1.23	1.88	2.48	2.49	2.08	3.19	3.38	2.56
14.90	2.89	2.79	4.65	5.39	4.34	3.49	3.53	3.70
15.04	4.06	2.90	2.88	4.03	4.04	3.26	2.73	3.51
15.20	6.04	6.23	4.92	5.66	6.70	7.09	5.24	4.81
	Average loss = 3.95 dB		Peak loss = 7.09 dB					
Module No. 11								
14.60	4.21	3.96	3.63	4.06	4.21	5.38	6.21	6.18
14.76	2.19	1.98	2.14	2.66	3.04	3.54	4.10	3.79
14.90	3.29	3.57	3.83	4.64	4.75	4.84	4.57	4.11
15.04	3.27	3.26	3.56	3.90	4.06	4.01	4.03	3.98
15.20	6.09	5.93	5.91	6.06	6.26	7.44	7.20	6.72
	Average loss = 4.41 dB		Peak loss = 7.44 dB					
Module No. 12								
14.60	3.30	2.74	3.44	3.84	6.06	5.65	4.78	3.96
14.76	1.84	1.43	1.80	1.89	3.19	3.27	2.75	2.04
14.90	3.46	3.39	3.42	3.47	3.60	3.61	3.16	2.94
15.04	3.33	3.18	2.58	2.91	3.42	3.24	2.75	2.62
15.20	6.30	6.49	5.76	5.39	5.60	5.49	4.77	4.71
	Average loss = 3.69 dB		Peak loss = 6.49 dB					
Module No. 13								
14.60	3.58	3.13	3.46	4.40	5.93	6.21	5.33	4.70
14.76	1.55	2.47	3.77	3.11	2.36	3.14	3.37	2.57
14.90	2.71	3.49	5.85	5.46	3.70	4.16	4.73	4.12
15.04	3.76	2.82	4.23	4.58	3.41	3.13	4.07	4.13
15.20	6.56	6.01	5.30	6.03	6.39	5.63	5.03	5.45
	Average loss = 4.25 dB		Peak loss = 6.56 dB					
Module No. 14								
14.60	2.73	4.38	4.27	3.91	3.51	3.91	3.71	4.02
14.76	0.62	2.27	2.34	2.14	1.32	2.28	1.61	1.68
14.90	2.11	2.24	3.94	4.20	1.85	2.46	2.13	1.92
15.04	2.74	1.68	2.65	4.16	1.72	1.93	2.10	1.79
15.20	5.69	5.43	4.83	5.63	4.20	3.74	3.84	4.10
	Average loss = 3.04 dB		Peak loss = 5.69 dB					

TABLE A-1. AESPA PHASE SHIFTER MODULE INSERTION LOSS (dB) (Continued)

Frequency (GHz)	Scan Angle (degrees) 0	45	90	135	180	215	270	315
Module No. 15								
14.60	5.06	4.72	4.21	5.81	7.25	8.04	5.67	5.54
14.76	2.81	3.78	3.25	2.89	4.09	5.51	4.09	2.78
14.90	4.02	4.74	5.41	4.92	4.93	4.97	4.48	3.88
15.04	4.69	3.47	3.59	4.22	5.36	4.31	4.04	4.07
15.20	7.75	6.74	5.18	5.79	7.86	6.90	5.70	5.62
	Average loss = 4.95 dB		Peak loss = 8.04 dB					
Module No. 16								
14.60	4.19	4.22	3.83	4.55	5.20	6.85	5.68	4.74
14.76	3.07	3.15	3.12	2.56	2.59	3.57	3.26	2.90
14.90	4.92	4.74	5.06	5.29	4.85	4.33	3.99	3.85
15.04	6.60	5.36	3.42	4.45	4.77	4.40	3.43	3.93
15.20	8.40	8.63	5.96	6.06	7.25	7.76	5.00	5.15
	Average loss = 4.78 dB		Peak loss = 8.63 dB					
Module No. 18								
14.60	5.02	4.52	5.32	5.50	4.31	4.44	5.24	5.72
14.76	2.91	2.41	3.14	2.52	1.59	1.43	2.98	3.10
14.90	4.14	3.89	4.98	4.59	3.61	3.01	3.79	3.19
15.04	4.57	4.13	4.44	3.98	3.75	3.16	3.42	3.13
15.20	7.71	7.26	7.64	6.77	5.98	5.28	5.79	5.93
	Average loss = 4.36 dB		Peak loss = 7.71 dB					
Module No. 19								
14.60	3.15	4.54	3.59	5.96	5.07	7.93	5.53	5.81
14.76	1.85	2.85	2.44	2.92	1.75	3.26	2.85	4.10
14.90	3.02	3.40	3.26	4.08	3.70	4.26	3.54	4.42
15.04	2.80	2.51	2.37	2.97	3.15	3.36	3.27	3.77
15.20	5.35	4.93	4.96	5.18	5.57	6.05	6.26	5.77
	Average loss = 4.04 dB		Peak loss = 7.93 dB					
Module No. 20								
14.60	3.57	3.63	2.98	5.78	5.36	7.98	6.53	7.23
14.76	1.84	1.79	1.31	2.33	1.96	3.82	3.48	3.82
14.90	2.55	3.38	3.46	4.15	3.36	3.89	3.52	3.58
15.04	2.44	2.79	2.80	3.00	2.25	2.82	2.71	3.44
15.20	4.96	5.14	5.01	5.40	5.00	5.40	5.20	5.36
	Average loss = 3.88 dB		Peak loss = 7.98 dB					
Module No. 22								
14.60	6.59	5.64	5.59	5.99	6.97	6.98	6.32	6.28
14.76	5.90	5.38	2.41	2.72	4.41	4.71	3.08	4.01
14.90	5.91	6.25	3.63	8.11	5.66	5.96	3.40	3.54
15.04	4.79	5.13	3.76	3.32	4.97	5.46	3.70	3.39
15.20	7.08	7.66	7.51	6.36	6.59	6.74	6.22	6.15
	Average loss = 5.36 dB		Peak loss = 8.11 dB					

TABLE A-1. AESPA PHASE SHIFTER MODULE INSERTION LOSS (dB) (Continued)

Frequency (GHz)	Scan Angle (degrees) 0	45	90	135	180	215	270	315
Module No. 23								
14.60	4.20	3.97	5.25	7.12	5.84	7.79	7.58	7.14
14.76	2.61	2.88	3.82	3.87	3.11	4.30	5.19	3.93
14.90	4.59	3.73	5.77	4.82	4.90	4.46	5.58	4.21
15.04	5.73	2.48	4.71	3.49	4.89	3.20	5.63	3.65
15.20	8.27	5.26	8.85	5.80	7.75	5.36	8.40	5.74

Average loss = 5.15 dB Peak loss = 8.85 dB

Lens Loss at Broadside	
Frequency (GHz)	Loss (dB)
14.60	4.57
14.76	2.83
14.90	3.90
15.04	4.28
15.20	6.97

TABLE A-2. AESPA PHASE SHIFTER MODULE INSERTION PHASE (DEGREES)

Frequency (GHz)	Scan Angle (degrees) 0	45	90	135	180	215	270	315
Module No. 1								
14.60	0.0	46.28	87.86	137.53	177.79	228.39	269.13	315.42
14.76	0.0	45.18	89.04	135.52	173.13	217.62	262.62	308.81
14.90	0.0	43.78	88.50	134.79	174.90	224.32	267.03	310.96
15.04	0.0	39.92	83.40	123.51	167.47	215.40	265.13	310.96
15.20	0.0	42.66	91.08	132.58	184.62	225.35	274.51	316.31
rms error = 4.86 degrees								
Module No. 2								
14.60	0.0	45.21	93.71	155.01	184.90	240.39	282.01	317.82
14.76	0.0	56.34	91.43	140.10	179.19	228.64	274.68	315.31
14.90	0.0	53.44	93.81	134.73	179.43	226.46	274.16	318.97
15.04	0.0	50.44	99.80	135.99	187.94	233.23	285.85	324.69
15.20	0.0	37.43	105.05	142.64	202.10	240.77	293.49	328.19
rms error = 10.07 degrees								
Module No. 4								
14.60	0.0	48.48	89.43	147.29	180.14	241.92	282.79	329.80
14.76	0.0	49.82	91.94	142.60	182.61	231.86	274.37	322.05
14.90	0.0	52.92	99.43	140.15	185.56	234.30	282.81	329.29
15.04	0.0	46.12	100.36	143.13	190.50	235.59	288.05	334.13
15.20	0.0	38.78	88.85	139.52	198.58	238.69	288.33	334.52
rms error = 10.83 degrees								
Module No. 5								
14.60	0.0	47.02	83.80	141.89	170.83	225.18	268.11	314.88
14.76	0.0	47.88	83.64	132.68	163.44	212.13	255.98	302.48
14.90	0.0	48.05	89.42	134.52	164.45	212.87	261.15	305.60
15.04	0.0	44.79	90.64	135.85	167.54	212.59	260.69	305.20
15.20	0.0	43.54	82.90	129.37	167.34	214.88	257.07	301.93
rms error = 8.89 degrees								
Module No. 6								
14.60	0.0	42.21	82.44	117.61	169.21	215.22	269.83	324.42
14.76	0.0	39.09	76.61	128.82	175.49	219.60	260.52	315.83
14.90	0.0	44.61	80.37	125.30	181.85	229.44	267.51	313.33
15.04	0.0	53.39	94.51	130.86	185.49	232.54	277.55	320.02
15.20	0.0	45.12	94.64	137.64	195.31	238.74	289.76	331.92
rms error = 8.76 degrees								
Module No.7								
14.60	0.0	33.14	79.82	126.06	158.87	202.29	256.26	303.83
14.76	0.0	40.54	82.81	124.30	169.61	211.49	256.28	298.77
14.90	0.0	43.02	90.23	125.73	175.11	218.39	266.96	305.00
15.04	0.0	36.67	85.36	123.77	173.27	215.96	270.89	315.61
15.20	0.0	36.92	79.18	125.15	189.41	230.86	276.10	320.46
rms error = 10.13 degrees								

TABLE A-2. AESPA PHASE SHIFTER MODULE INSERTION PHASE (DEGREES) (Continued)

Frequency (GHz)	Scan Angle (degrees) 0	45	90	135	180	215	270	315
Module No. 9								
14.60	0.0	36.05	88.17	135.08	169.59	206.84	278.41	328.13
14.76	0.0	36.50	77.17	132.31	179.25	214.67	257.14	308.93
14.90	0.0	47.01	85.14	123.77	183.55	229.13	268.77	307.20
15.04	0.0	50.09	106.45	135.40	178.99	243.87	287.70	320.80
15.20	0.0	32.75	101.60	144.93	188.07	227.74	292.97	329.14
rms error = 10.35 degrees								
Module No. 10								
14.60	0.0	40.42	76.57	122.18	157.27	204.85	257.22	309.29
14.76	0.0	43.89	79.14	120.86	165.24	217.89	264.91	309.94
14.90	0.0	47.06	89.75	130.70	177.96	231.80	283.33	320.62
15.04	0.0	41.27	94.32	135.90	181.12	224.26	281.16	326.37
15.20	0.0	33.66	76.65	125.19	183.62	226.99	274.84	324.03
rms error = 9.59 degrees								
Module No. 11								
14.60	0.0	42.40	86.23	131.22	176.23	226.58	276.44	321.74
14.76	0.0	43.53	85.53	128.81	164.70	212.05	266.15	315.71
14.90	0.0	38.26	80.66	124.49	169.48	214.59	264.84	314.70
15.04	0.0	42.98	87.17	132.32	180.82	228.08	280.15	328.20
15.20	0.0	43.12	86.61	128.25	183.43	230.40	287.73	338.64
rms error = 8.26 degrees								
Module No. 12								
14.60	0.0	38.53	77.35	115.80	163.28	207.07	258.32	301.49
14.76	0.0	38.77	80.72	118.98	172.79	213.27	258.95	301.87
14.90	0.0	41.26	90.44	132.55	184.45	226.81	271.36	310.13
15.04	0.0	41.55	90.29	135.84	183.54	230.67	281.46	322.68
15.20	0.0	47.73	95.04	141.95	188.56	237.28	291.11	337.45
rms error = 10.59 degrees								
Module No. 13								
14.60	0.0	34.31	69.34	112.57	161.49	206.30	260.09	307.05
14.76	0.0	37.22	73.80	115.68	176.41	216.35	260.10	300.46
14.90	0.0	43.12	85.47	120.85	183.67	228.27	276.04	309.31
15.04	0.0	40.46	94.71	127.14	180.61	225.77	283.09	317.33
15.20	0.0	32.36	88.79	126.25	185.50	223.99	284.46	321.12
rms error = 10.83 degrees								
Module No. 14								
14.60	0.0	42.52	82.25	133.06	153.32	202.38	259.90	306.11
14.76	0.0	48.51	87.04	129.01	164.05	211.06	263.28	312.79
14.90	0.0	52.10	98.56	137.92	176.90	226.52	275.05	320.11
15.04	0.0	43.69	95.38	135.98	174.12	227.51	280.94	324.08
15.20	0.0	37.09	89.53	138.08	179.55	227.03	283.03	326.44
rms error = 9.07 degrees								

TABLE A-2. AESPA PHASE SHIFTER MODULE INSERTION PHASE (DEGREES) (Continued)

Frequency (GHz)	Scan Angle (degrees) 0	45	90	135	180	215	270	315
Module No. 15								
14.60	0.0	34.37	75.16	123.97	177.38	221.62	272.84	322.73
14.76	0.0	39.82	70.94	120.95	175.76	224.98	267.08	316.21
14.90	0.0	53.97	87.52	131.47	185.19	242.39	280.52	322.52
15.04	0.0	50.88	92.89	134.47	179.27	234.12	283.15	328.84
15.20	0.0	43.16	87.93	140.38	184.86	232.33	280.25	333.87
rms error = 8.97 degrees								
Module No. 16								
14.60	0.0	41.52	72.10	116.82	156.16	205.09	255.02	305.45
14.76	0.0	51.98	91.40	132.47	168.78	217.53	266.56	312.61
14.90	0.0	51.02	104.96	146.53	178.31	231.76	287.93	329.43
15.04	0.0	44.91	109.14	157.19	177.83	224.06	294.41	340.97
15.20	0.0	42.86	103.30	159.10	179.80	226.48	301.88	355.96
rms error = 15.82 degrees								
Module No. 18								
14.60	0.0	43.31	80.40	120.81	175.03	218.00	258.00	302.33
14.76	0.0	45.75	84.48	129.30	179.03	222.34	261.83	310.72
14.90	0.0	45.07	87.59	136.57	190.52	237.12	277.74	324.08
15.04	0.0	50.96	88.89	138.82	194.74	244.79	285.37	333.96
15.20	0.0	58.26	95.42	151.40	206.73	259.28	293.89	348.60
rms error = 13.69 degrees								
Module No. 19								
14.60	0.0	50.35	77.74	131.66	170.86	230.55	296.75	329.36
14.76	0.0	58.21	88.84	140.88	176.65	231.67	265.68	322.38
14.90	0.0	57.05	89.18	141.21	179.92	235.61	272.58	326.03
15.04	0.0	51.40	85.41	137.79	178.69	231.39	270.03	325.51
15.20	0.0	49.21	87.31	137.36	181.44	233.24	278.45	329.50
rms error = 8.61 degrees								
Module No. 20								
14.60	0.0	43.27	63.60	108.02	143.64	194.28	225.14	293.27
14.76	0.0	41.14	63.68	108.26	145.95	194.40	222.74	278.76
14.90	0.0	40.94	66.39	114.42	158.75	207.78	236.77	281.06
15.04	0.0	43.71	71.49	113.99	158.56	203.31	234.99	280.90
15.20	0.0	44.11	74.81	117.00	166.01	210.22	243.02	288.07
rms error = 26.04 degrees								
Module No. 22								
14.60	0.0	33.65	101.69	130.57	181.40	214.93	284.73	320.22
14.76	0.0	35.47	106.72	139.40	183.08	213.84	284.30	322.85
14.90	0.0	34.95	96.52	137.64	188.77	221.97	286.49	323.97
15.04	0.0	35.09	94.15	134.91	187.19	223.85	288.95	327.46
15.20	0.0	41.67	116.71	154.13	196.17	236.13	308.43	344.70
rms error = 13.66 degrees								

TABLE A-2. AESPA PHASE SHIFTER MODULE INSERTION PHASE (DEGREES) (Continued)

Frequency (GHz)	Scan Angle (degrees) 0	45	90	135	180	215	270	315
Module No. 23								
14.60	0.0	37.00	84.50	126.91	171.79	225.06	286.66	335.96
14.76	0.0	48.65	88.20	140.58	178.78	234.43	282.58	337.43
14.90	0.0	59.10	91.80	148.09	187.78	253.26	292.29	344.64
15.04	0.0	60.83	86.72	145.30	183.67	252.00	288.31	347.3 /
15.20	0.0	60.06	84.91	146.69	193.50	256.23	285.84	352.12

rms error = 16.92 degrees

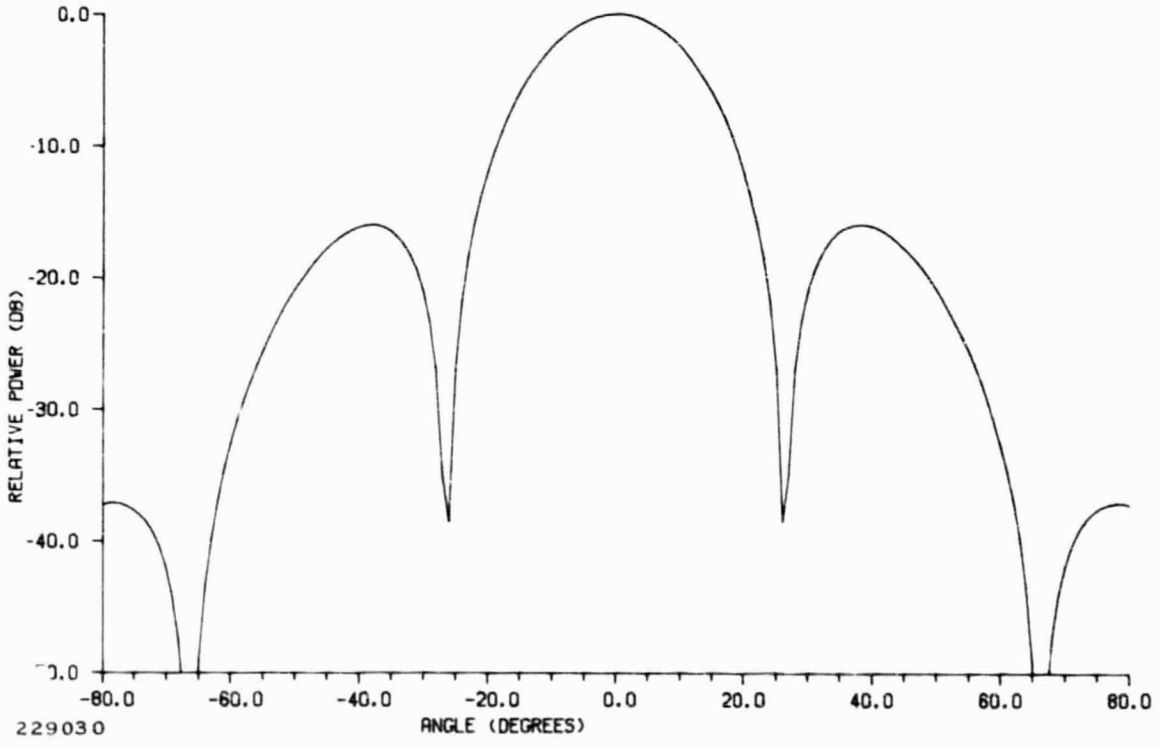

Figure A-1. Computed 14.6-GHz Planar Radiation Pattern, Azimuth, No Scan

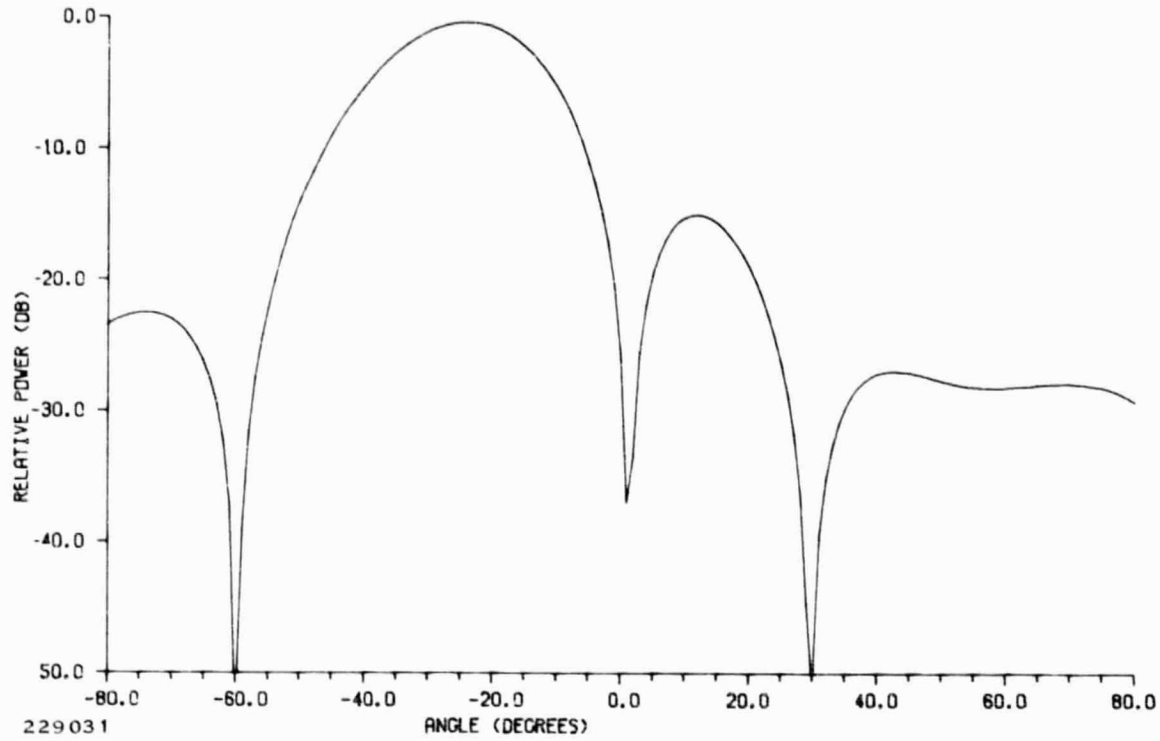

Figure A-2. Computed 14.6-GHz Planar Radiation Pattern, Beam Scanned 24.0 Degrees in Azimuth

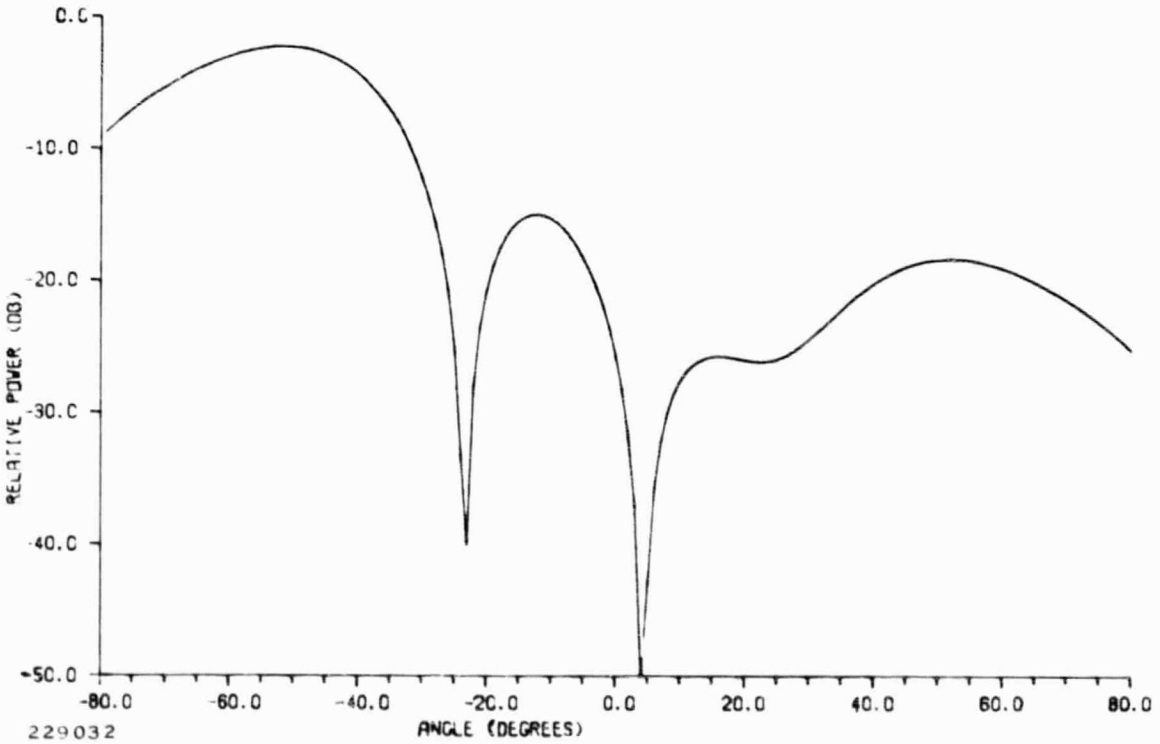

Figure A-3. Computed 14.6-GHz Planar Radiation Pattern, Beam Scanned 52.0 Degrees in Azimuth

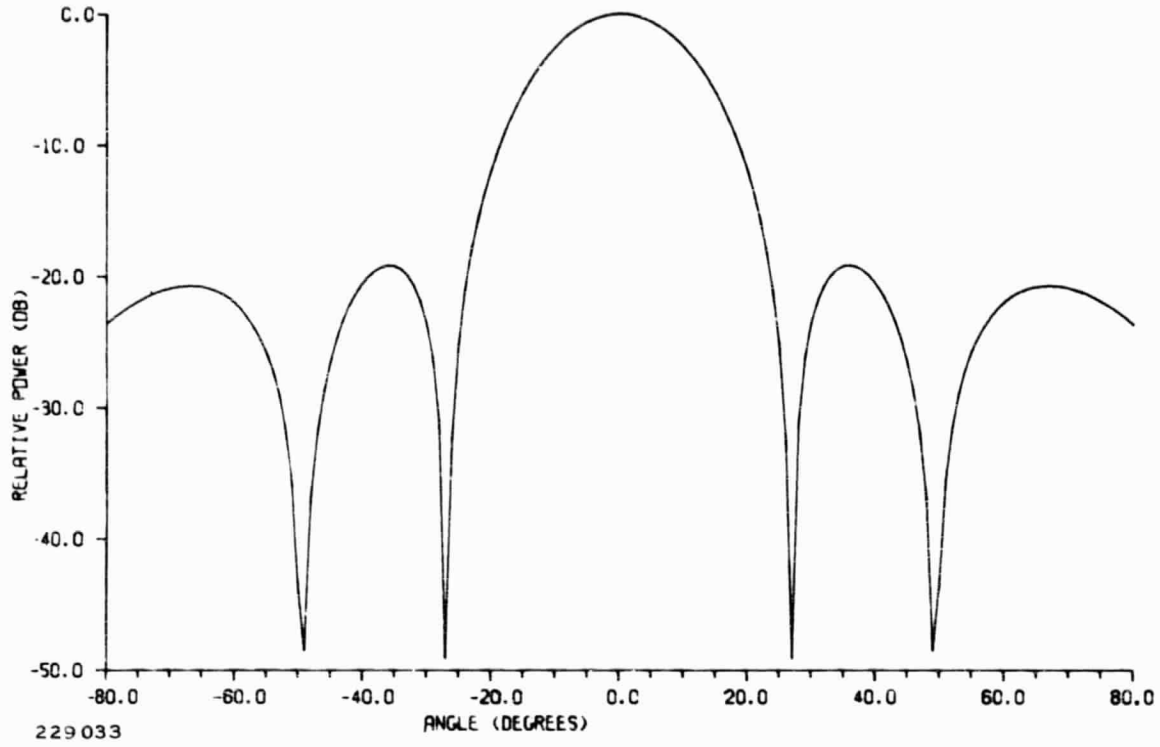

Figure A-4. Computed 14.6-GHz Planar Radiation Pattern, Elevation, No Scan

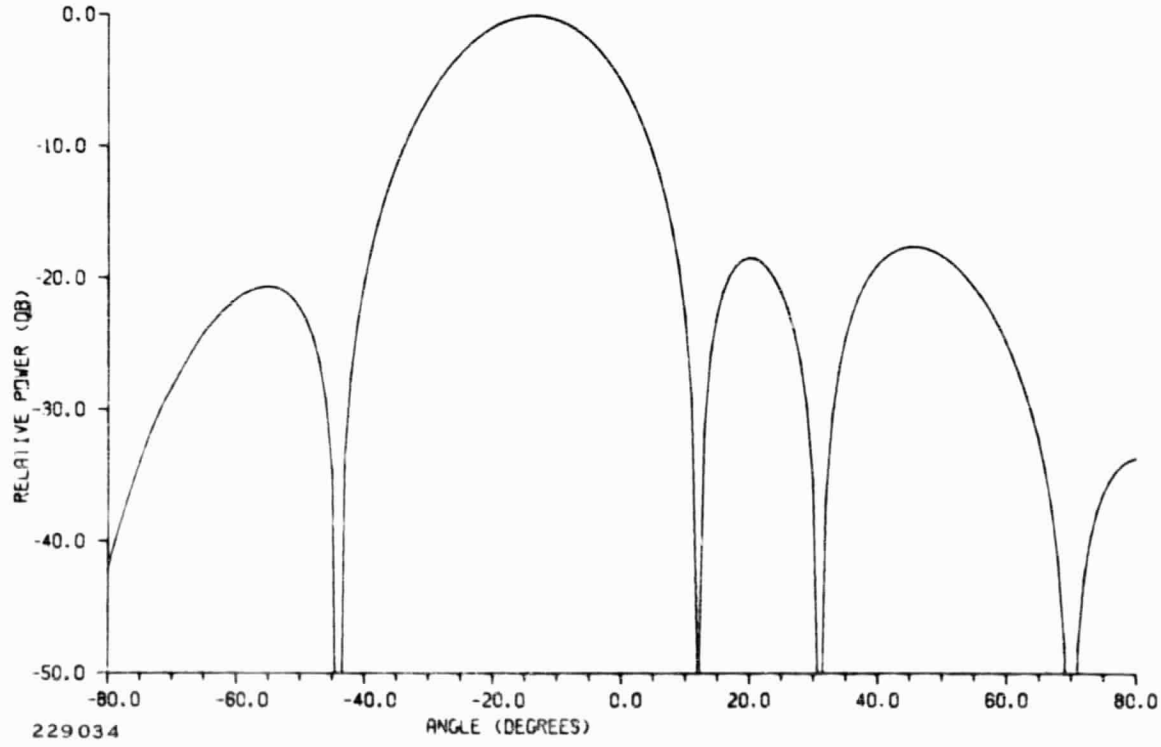

Figure A-5. Computed 14.6-GHz Planar Radiation Pattern, Beam Scanned 14.0 Degrees in Elevation

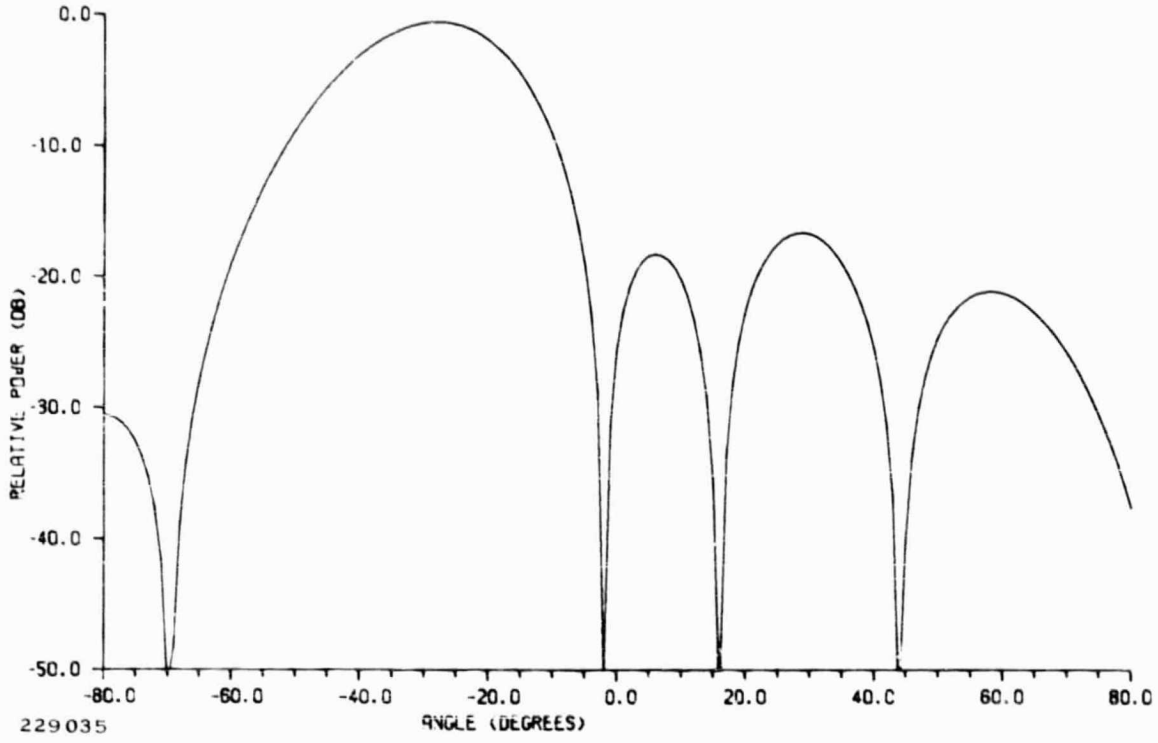

Figure A-6. Computed 14.6-GHz Planar Radiation Pattern, Beam Scanned 28.0 Degrees in Elevation

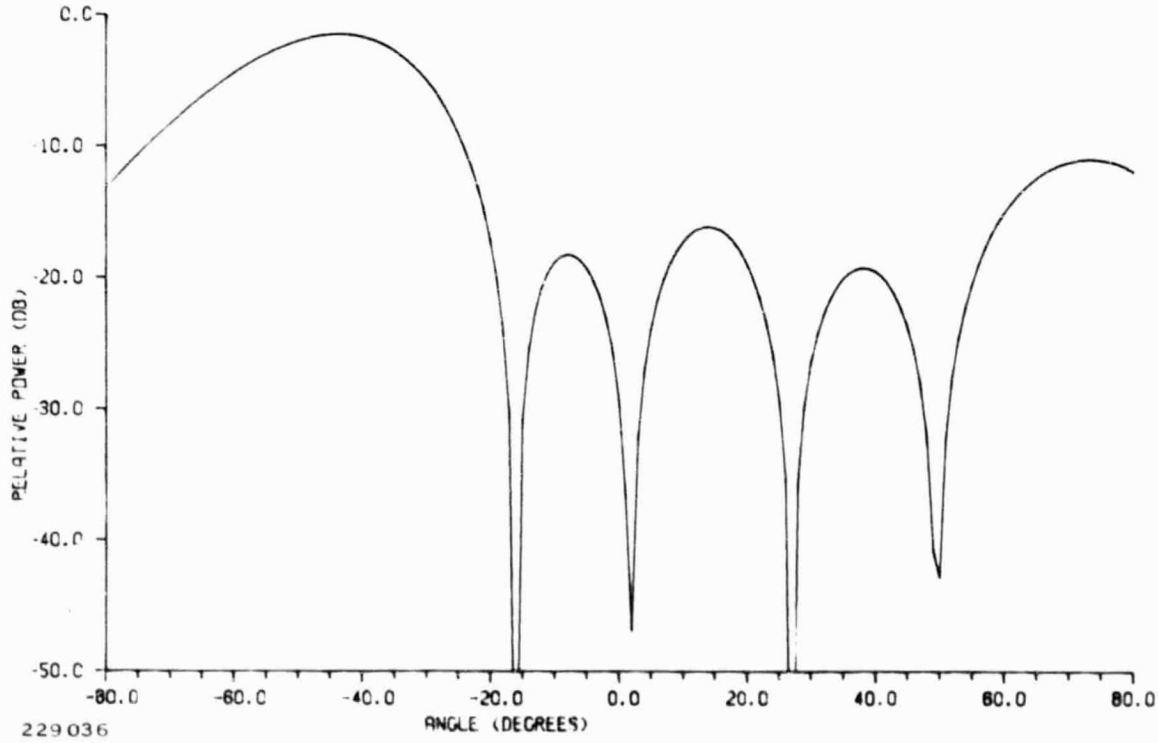

Figure A-7. Computed 14.6-GHz Planar Radiation Pattern, Beam Scanned 44.0 Degrees in Elevation

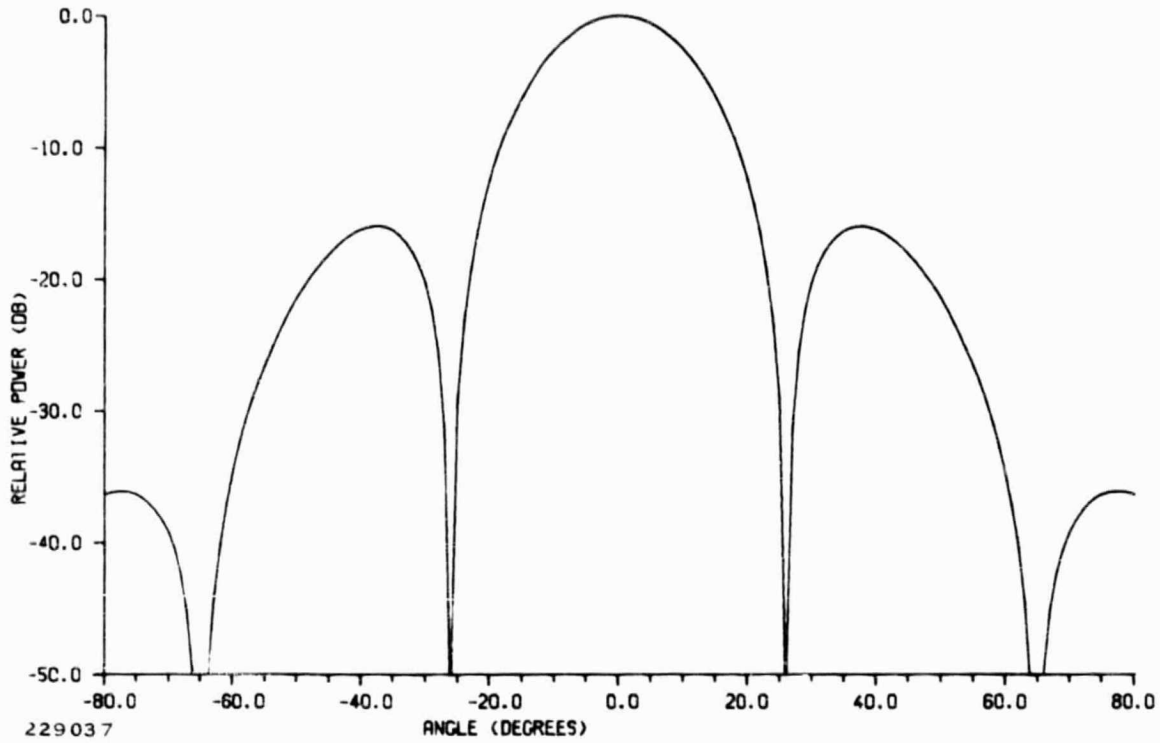

Figure A-8. Computed 14.76-GHz Planar Radiation Pattern, Azimuth, No Scan

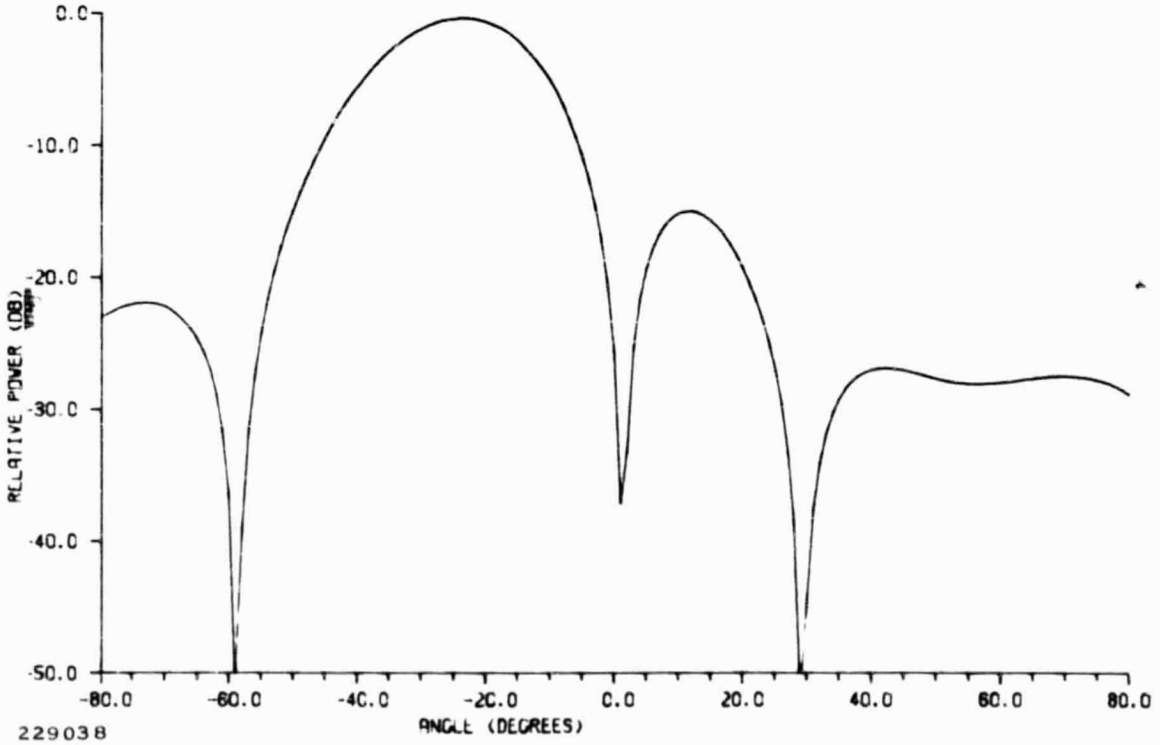

Figure A-9. Computed 14.76-GHz Planar Radiation Pattern, Beam Scanned 24.0 Degrees in Azimuth

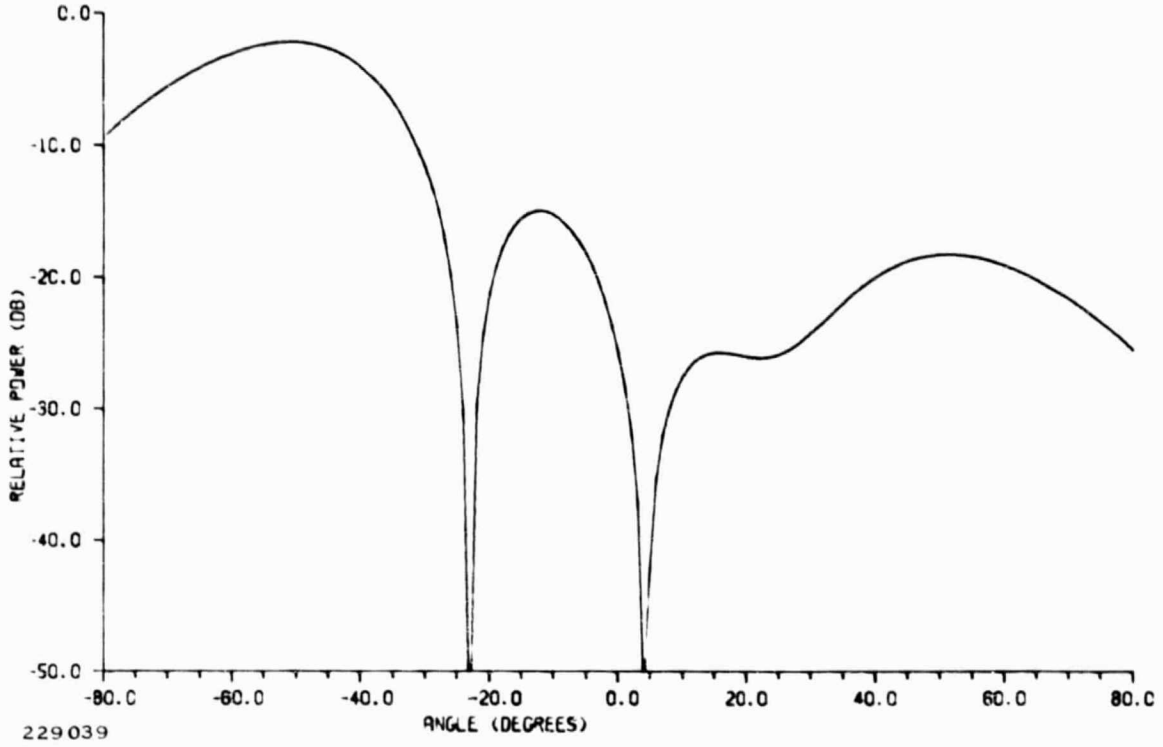

Figure A-10. Computed 14.76-GHz Planar Radiation Pattern, Beam Scanned 51.0 Degrees in Azimuth

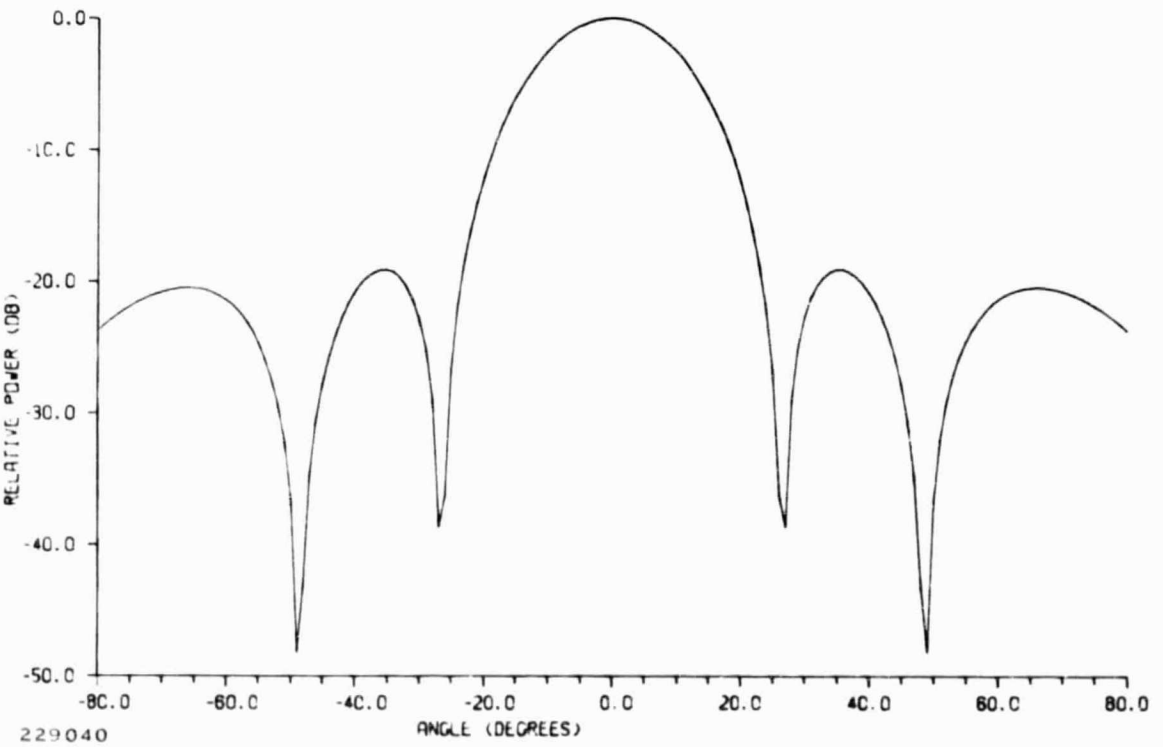

Figure A-11. Computed 14.76-GHz Planar Radiation Pattern, Elevation, No Scan

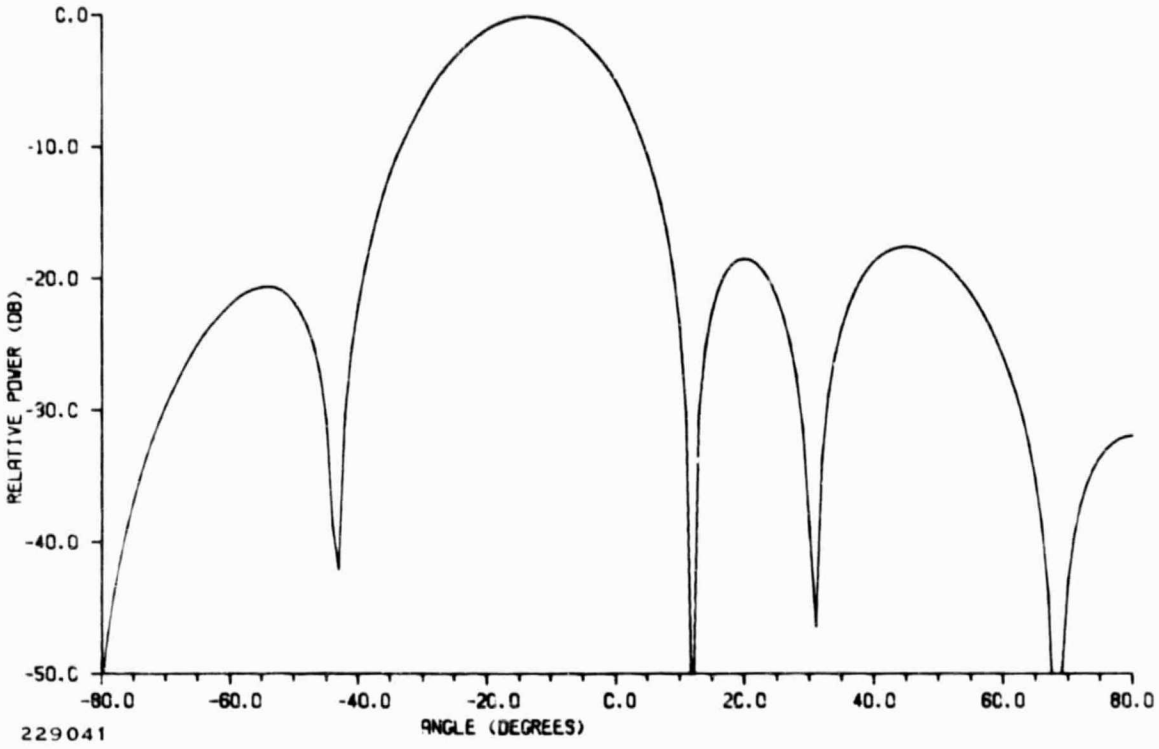

Figure A-12. Computed 14.76-GHz Planar Radiation Pattern, Beam Scanned 13.5 Degrees in Elevation

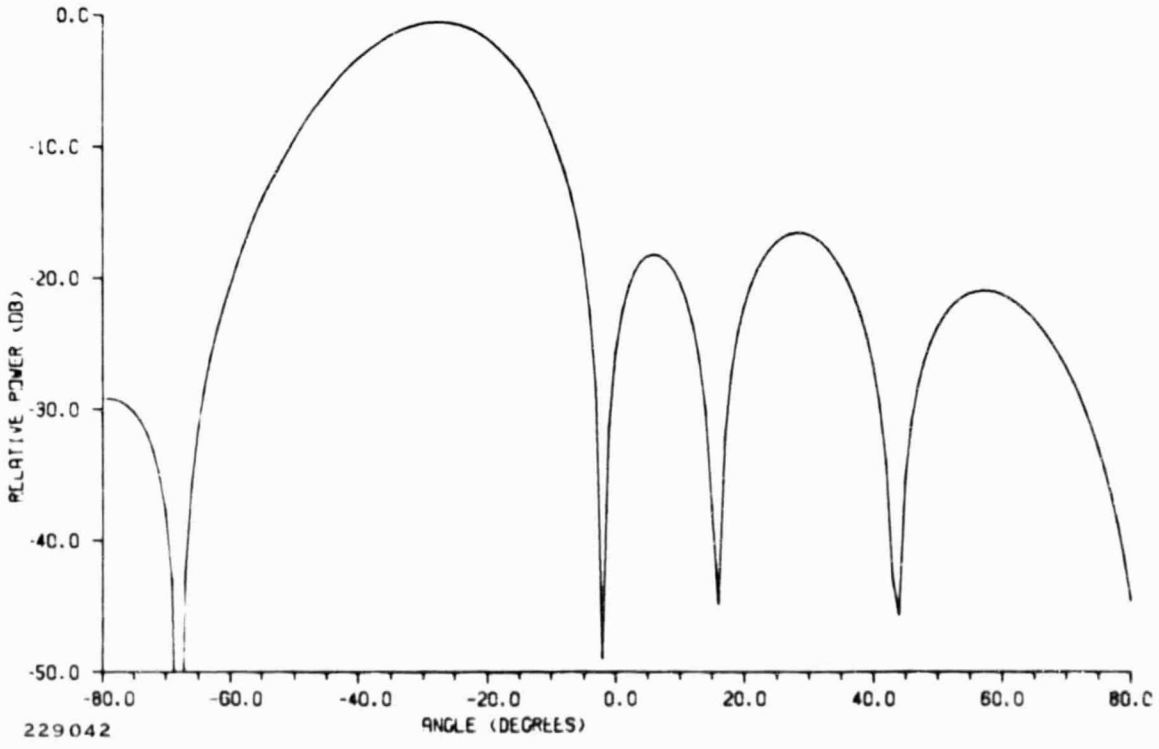

Figure A-13. Computed 14.76-GHz Planar Radiation Pattern, Beam Scanned 28.0 Degrees in Elevation

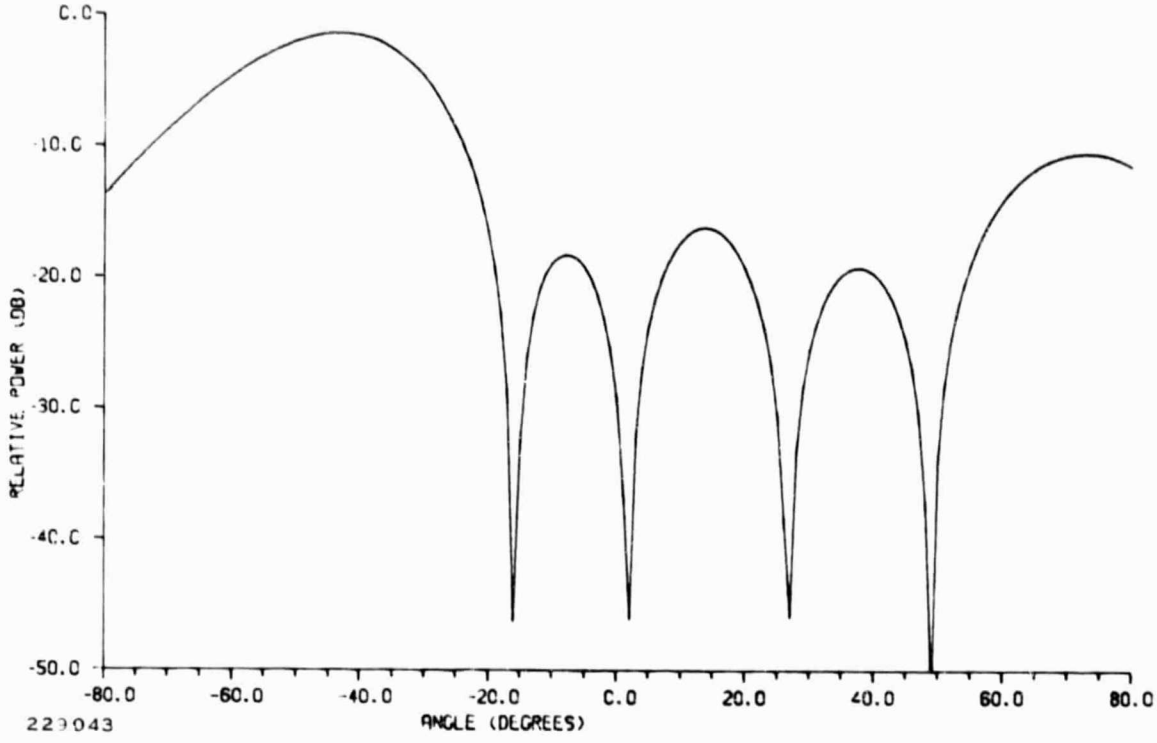

Figure A-14. Computed 14.76-GHz Planar Radiation Pattern, Beam Scanned 43.0 Degrees in Elevation

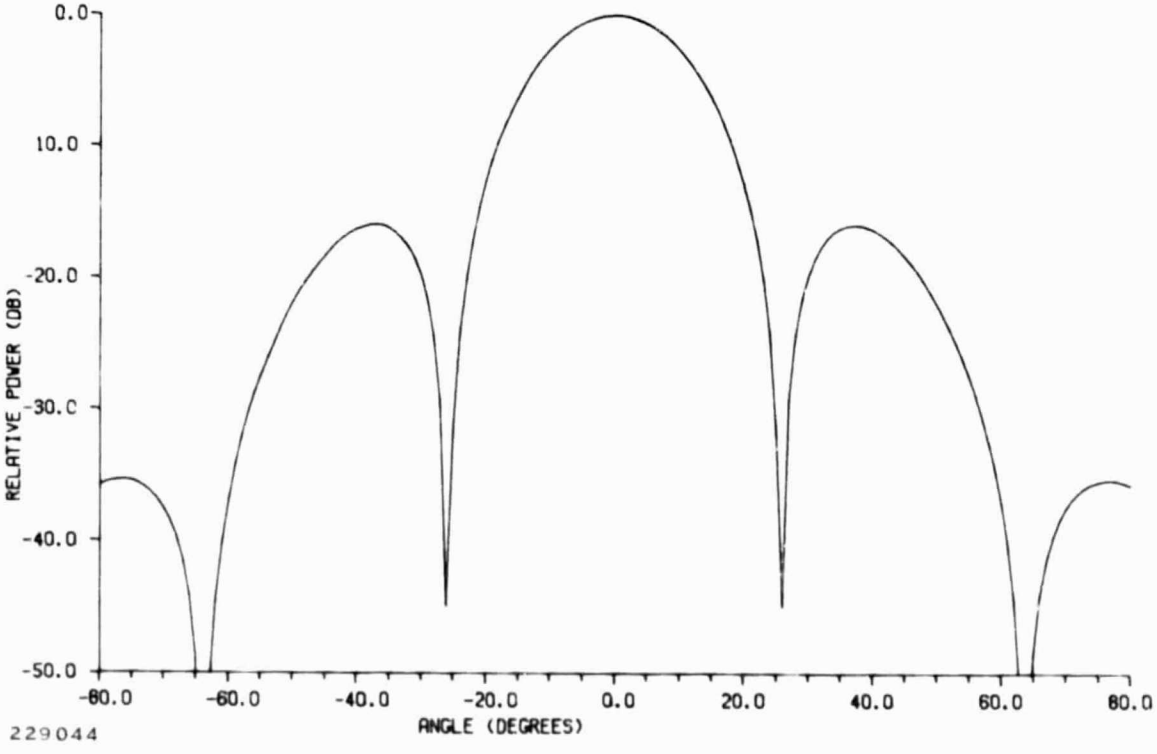

Figure A-15. Computed 14.9-GHz Planar Radiation Pattern, Azimuth, No Scan

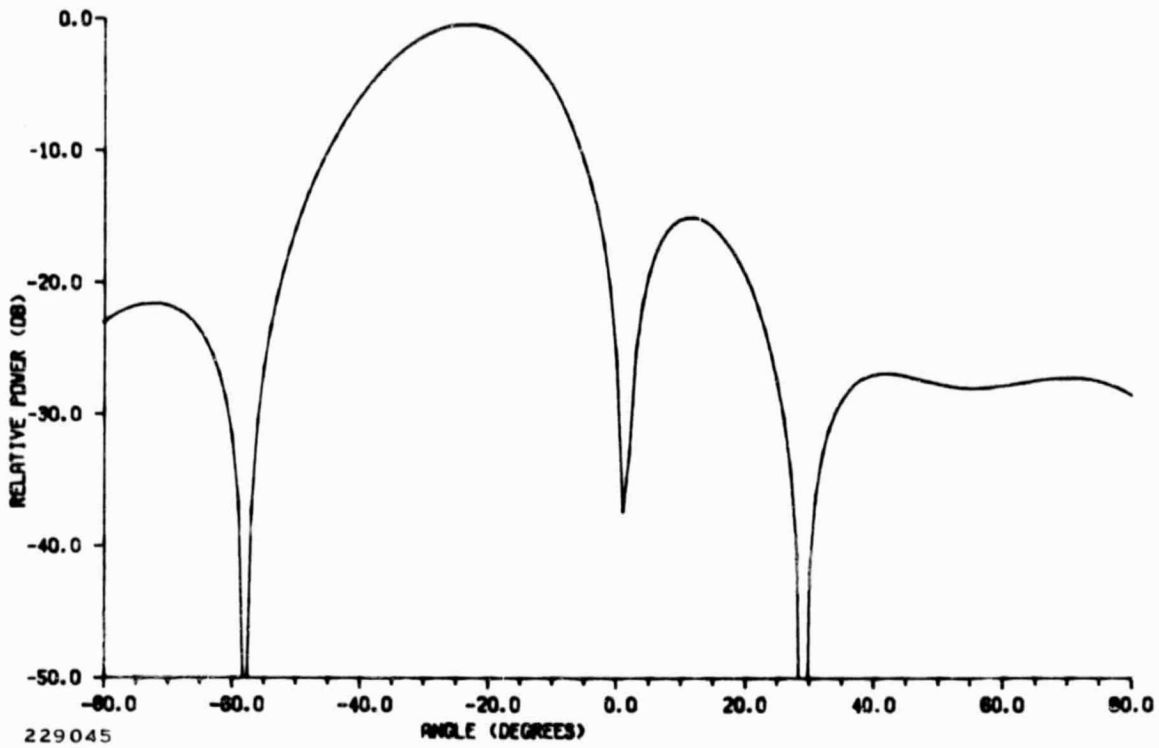

Figure A-16. Computed 14.9-GHz Planar Radiation Pattern, Beam Scanned 23.5 Degrees in Azimuth

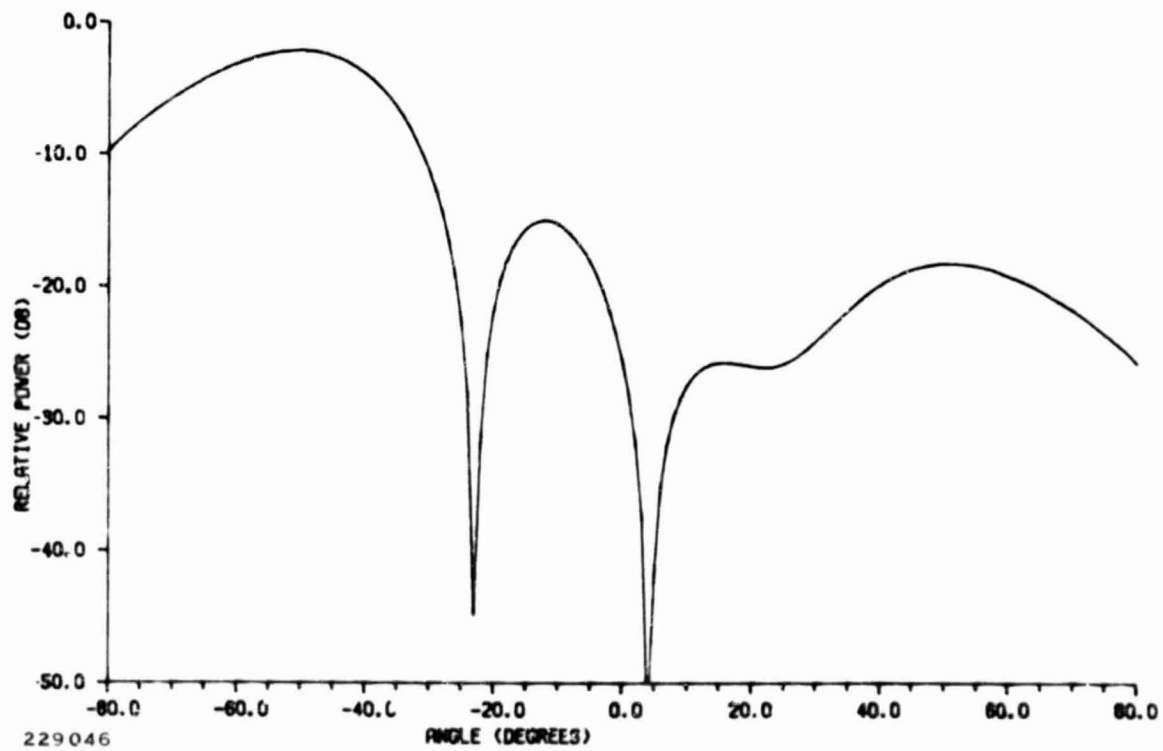

Figure A-17. Computed 14.9-GHz Planar Radiation Pattern, Beam Scanned 51.0 Degrees in Azimuth

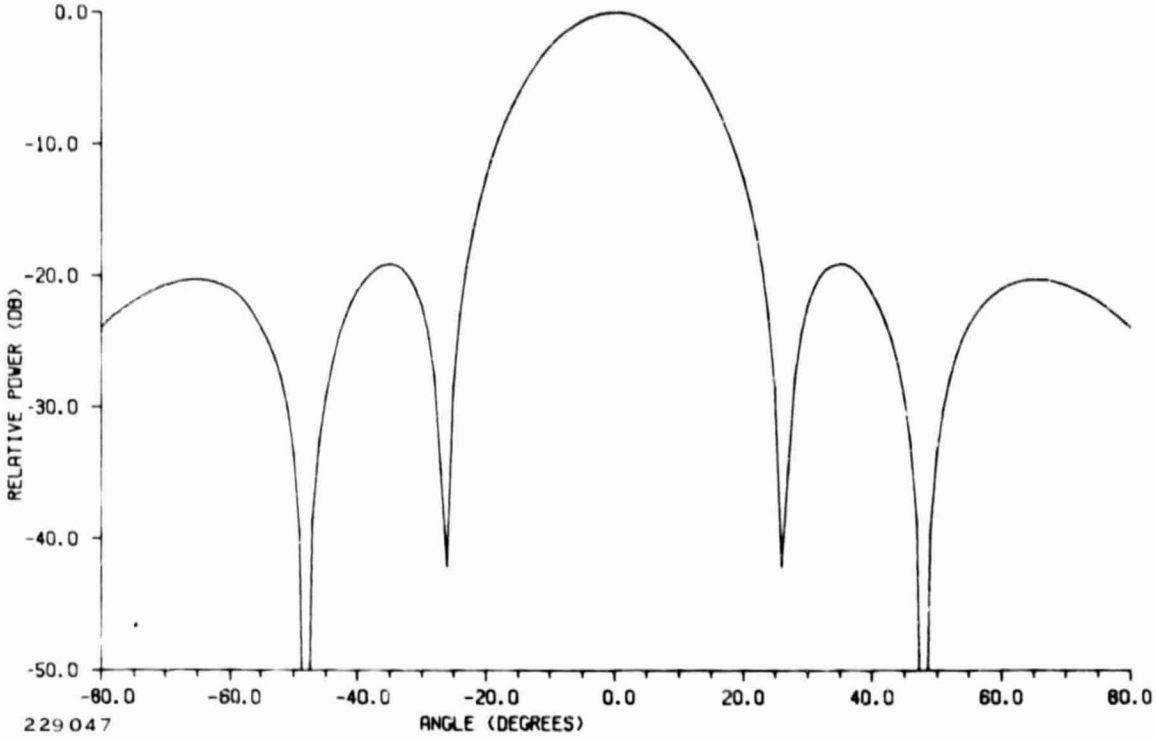

Figure A-18. Computed 14.9-GHz Planar Radiation Pattern, Elevation, No Scan

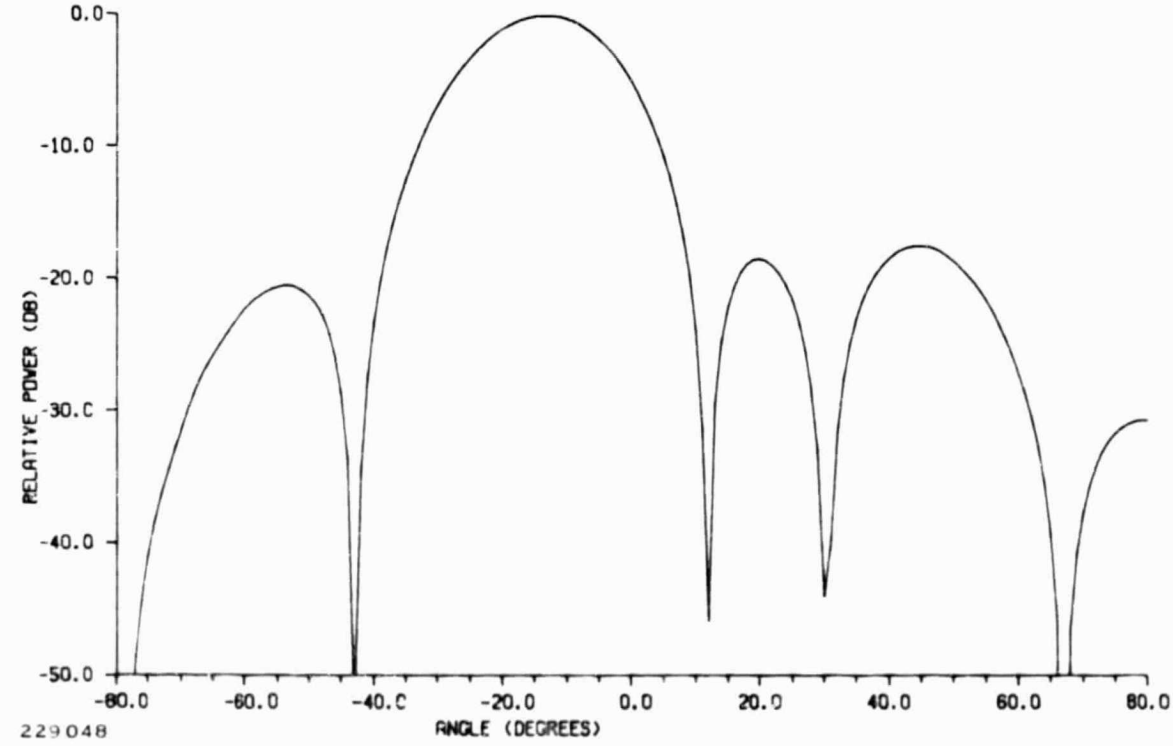

Figure A-19. Computed 14.9-GHz Planar Radiation Pattern, Beam Scanned 13.0 Degrees in Elevation

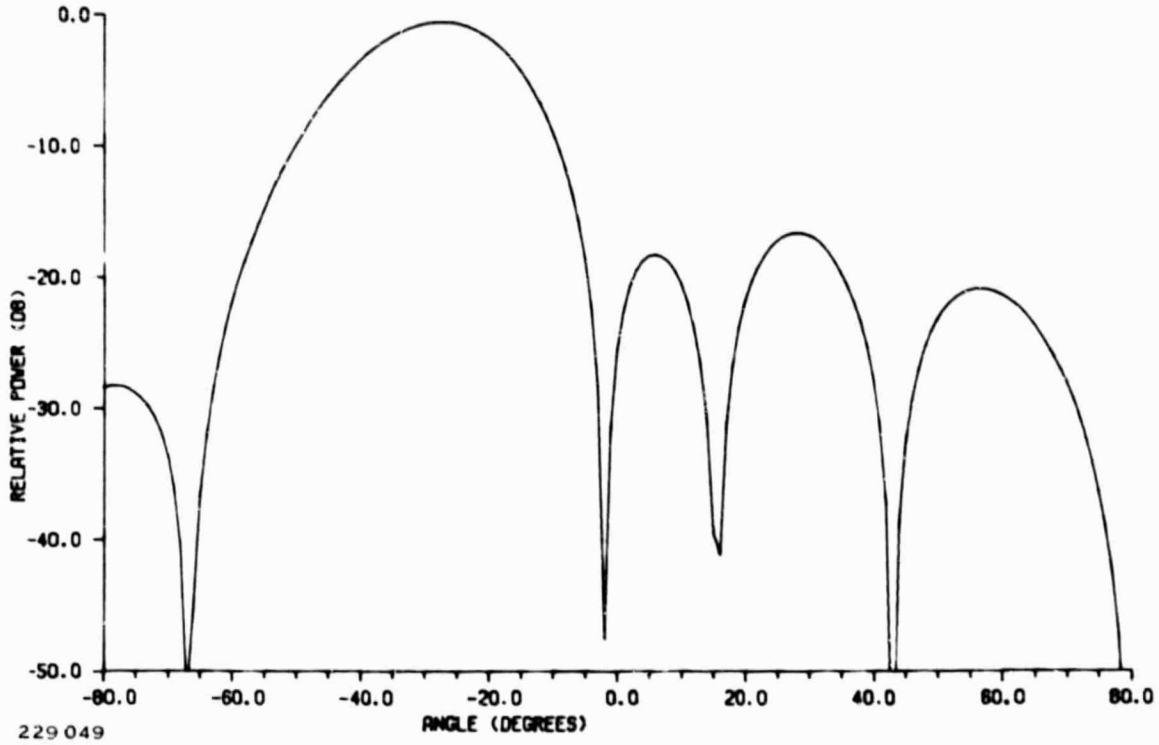

Figure A-20. Computed 14.9-GHz Planar Radiation Pattern, Beam Scanned 27.0 Degrees in Elevation

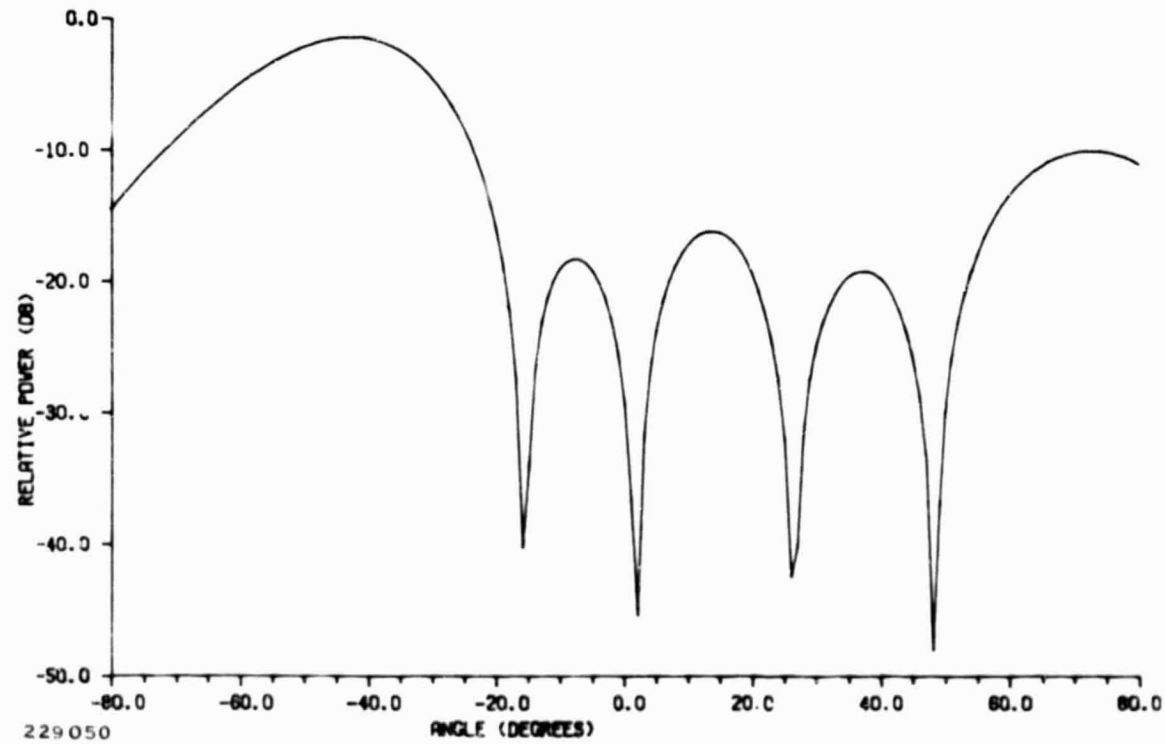

Figure A-21. Computed 14.9-GHz Planar Radiation Pattern, Beam Scanned 43.0 Degrees in Elevation

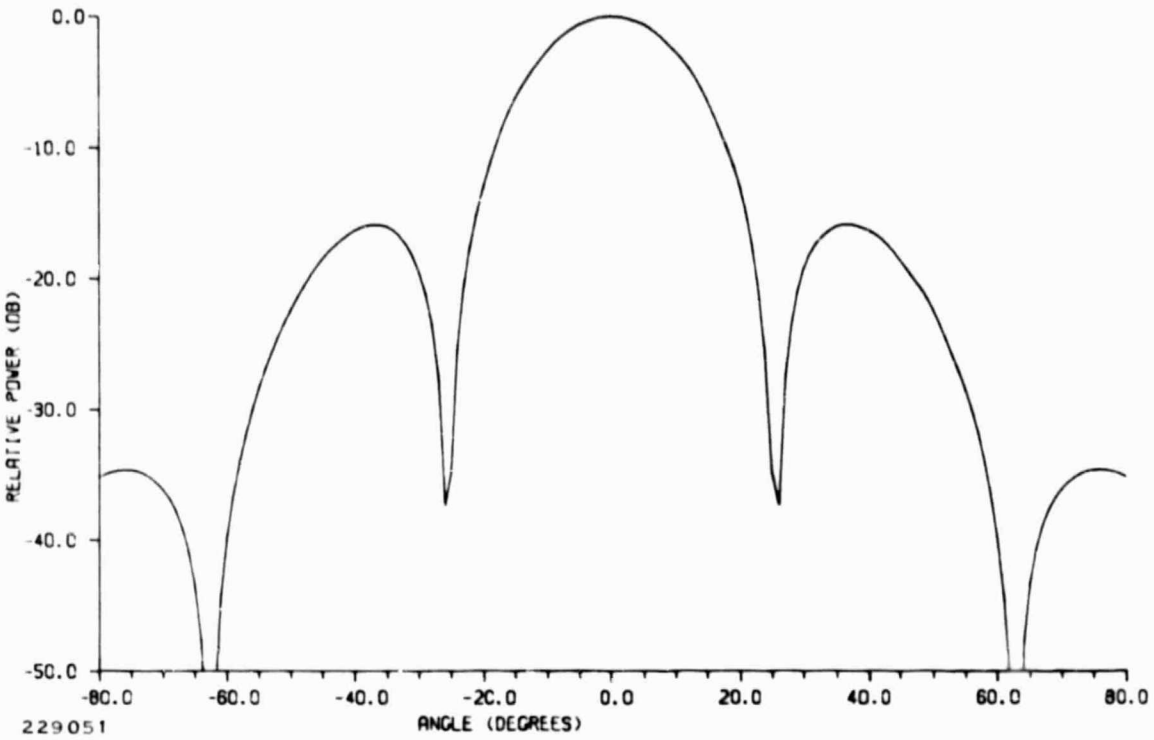

Figure A-22. Computed 15.04-GHz Planar Radiation Pattern, Azimuth, No Scan

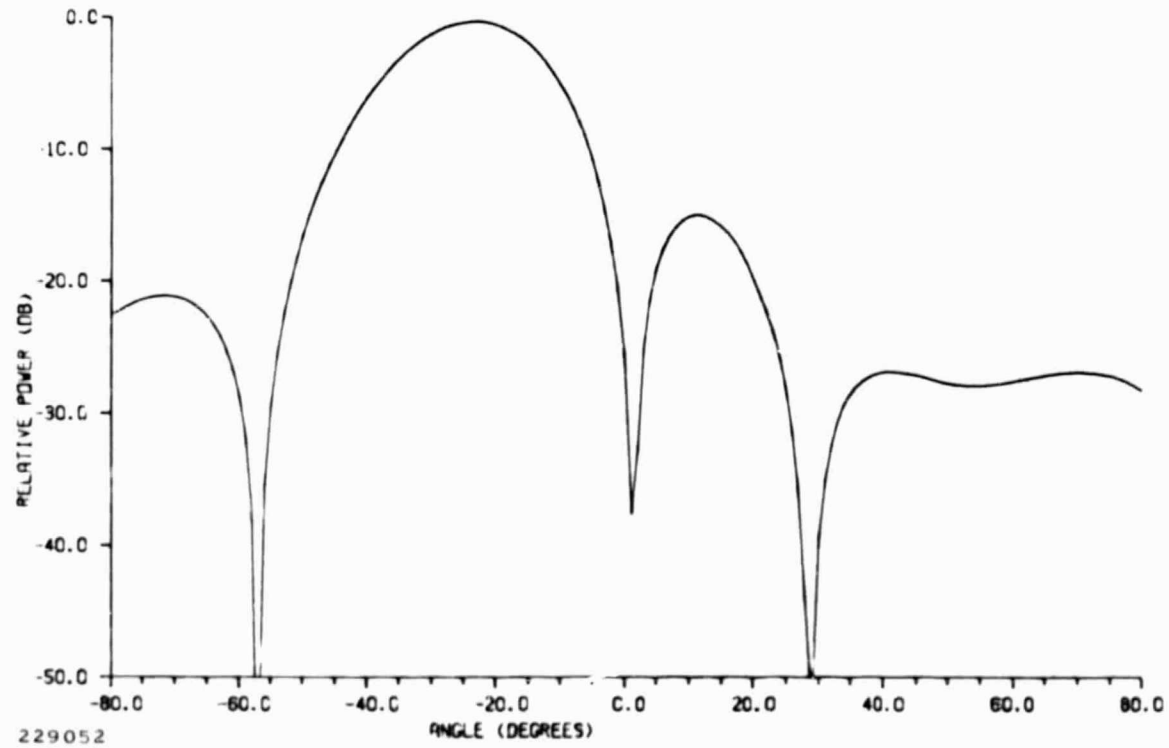

Figure A-23. Computed 15.04-GHz Planar Radiation Pattern, Beam Scanned 23.0 Degrees in Azimuth

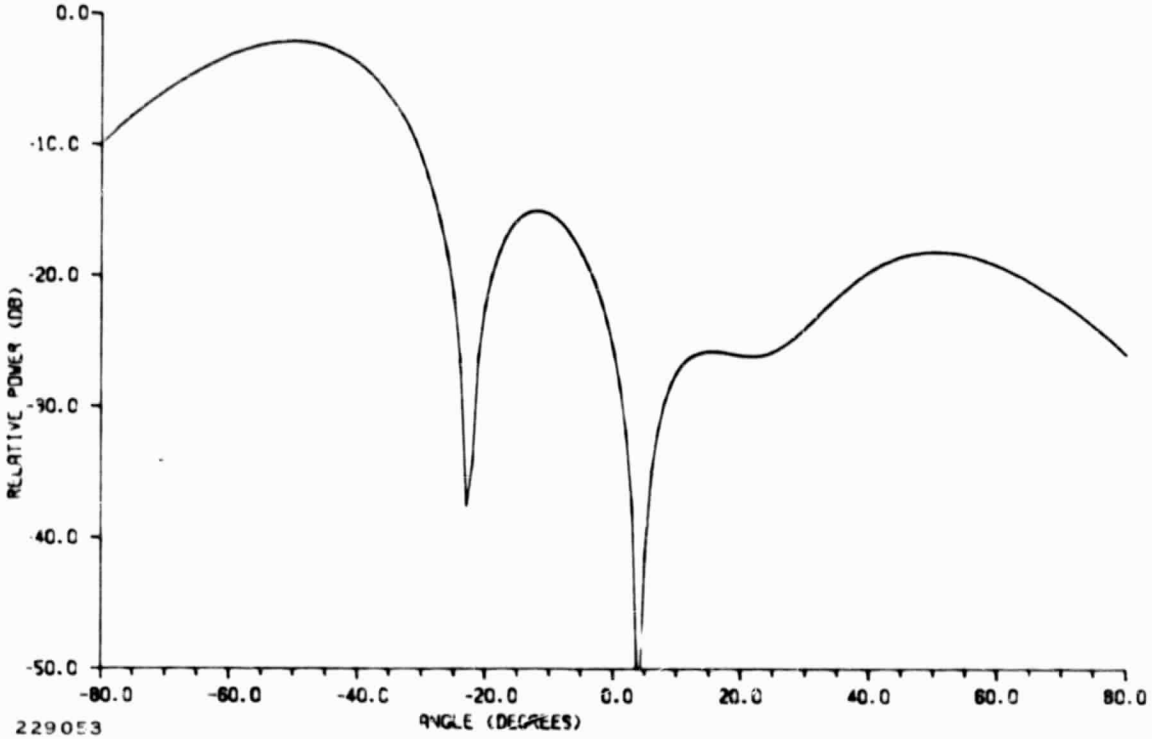

Figure A-24. Computed 15.04-GHz Planar Radiation Pattern, Beam Scanned 50.0 Degrees in Azimuth

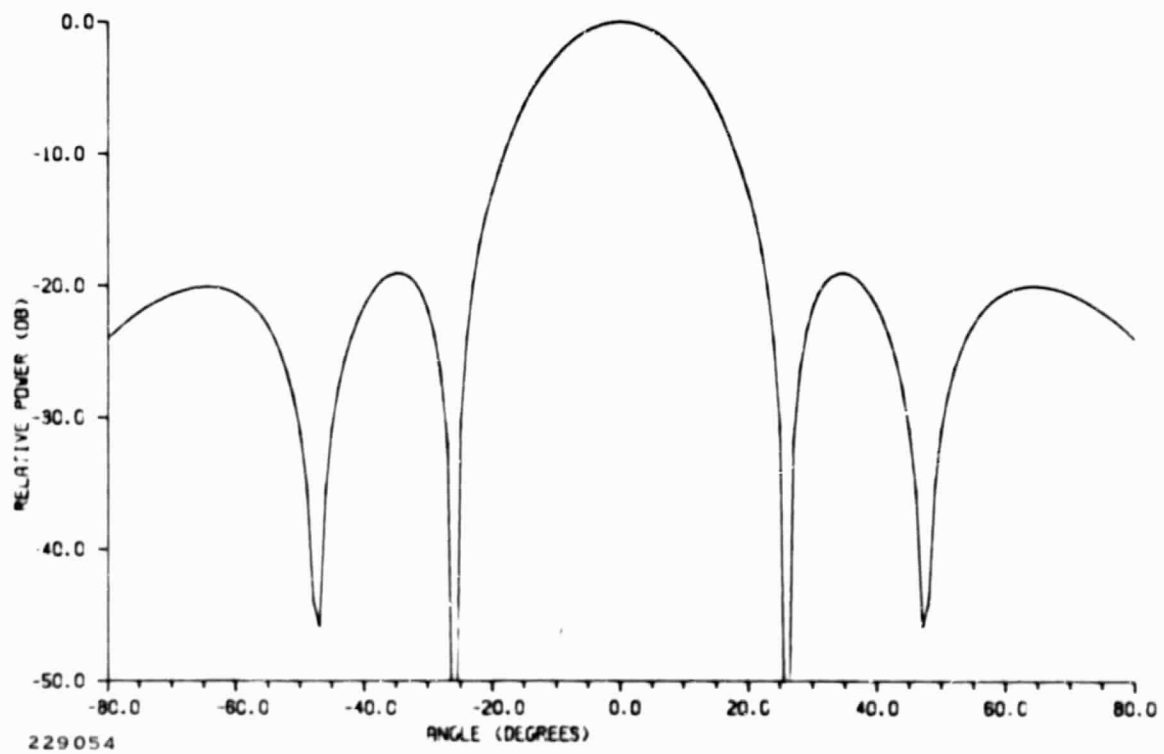

Figure A-25. Computed 15.04-GHz Planar Radiation Pattern, Elevation, No Scan

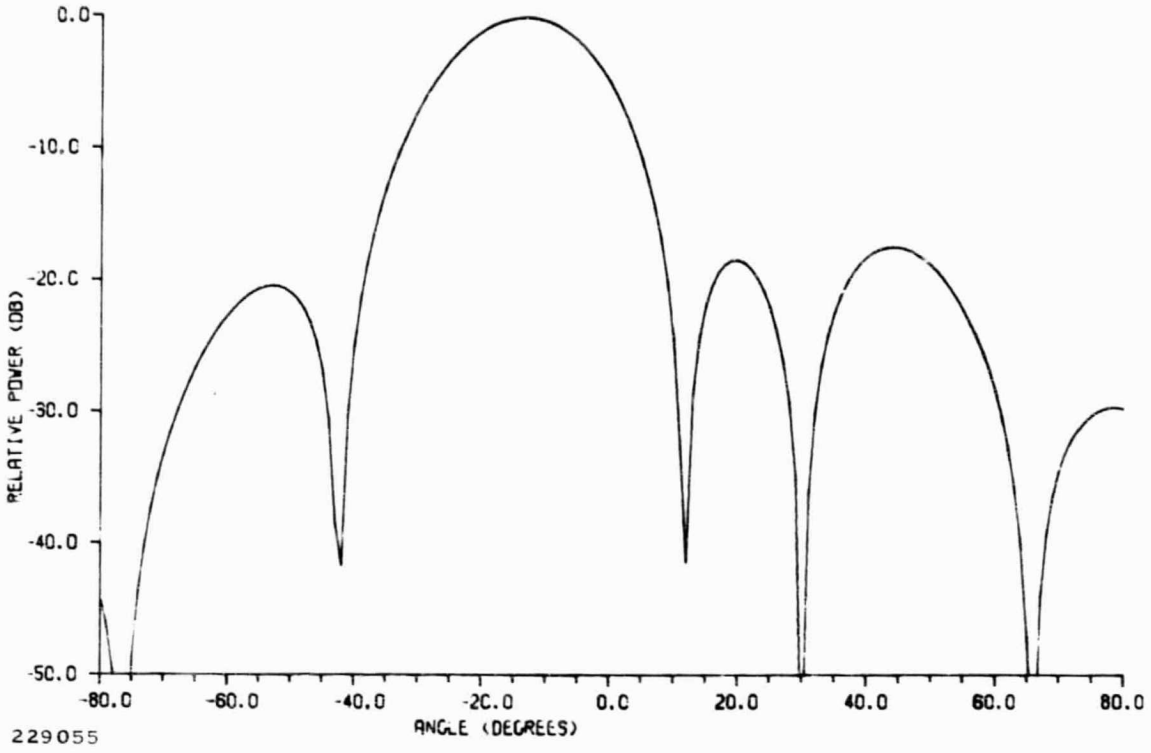

Figure A-26. Computed 15.04-GHz Planar Radiation Pattern, Beam Scanned 13.0 Degrees in Elevation

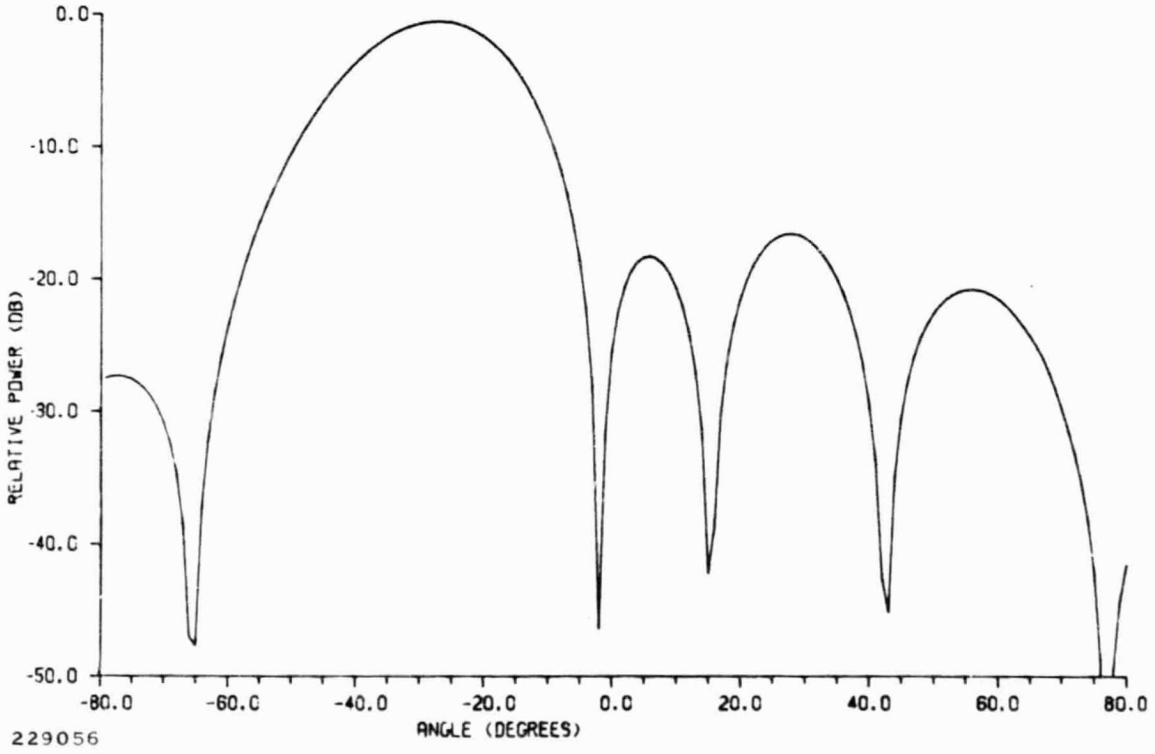

Figure A-27. Computed 15.04-GHz Planar Radiation Pattern, Beam Scanned 27.0 Degrees in Elevation

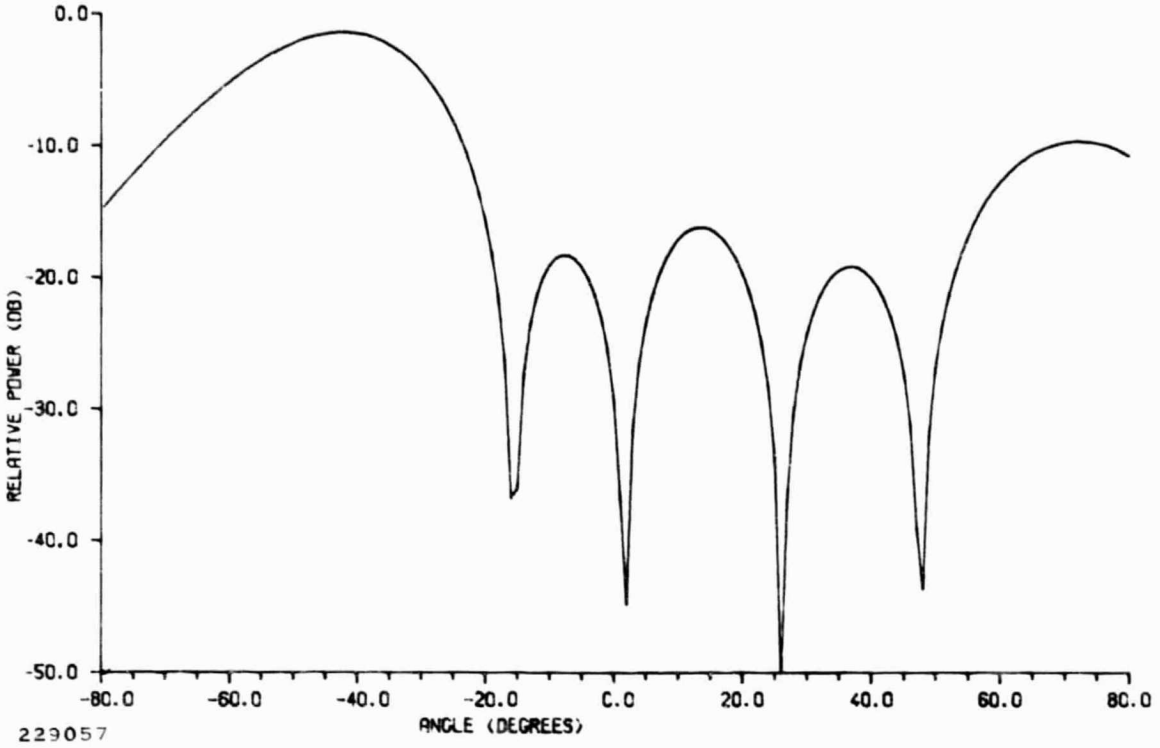

Figure A-28. Computed 15.04-GHz Planar Radiation Pattern, Beam Scanned 42.0 Degrees in Elevation

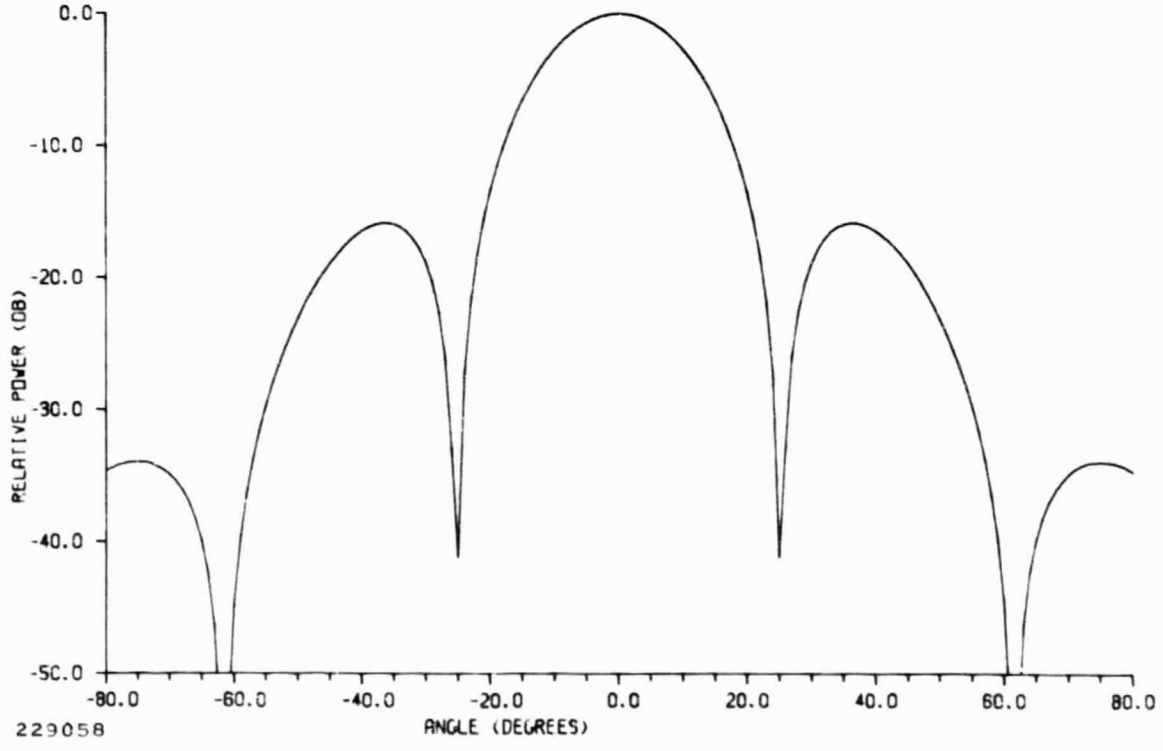

Figure A-29. Computed 15.2-GHz Planar Radiation Pattern, Azimuth, No Scan

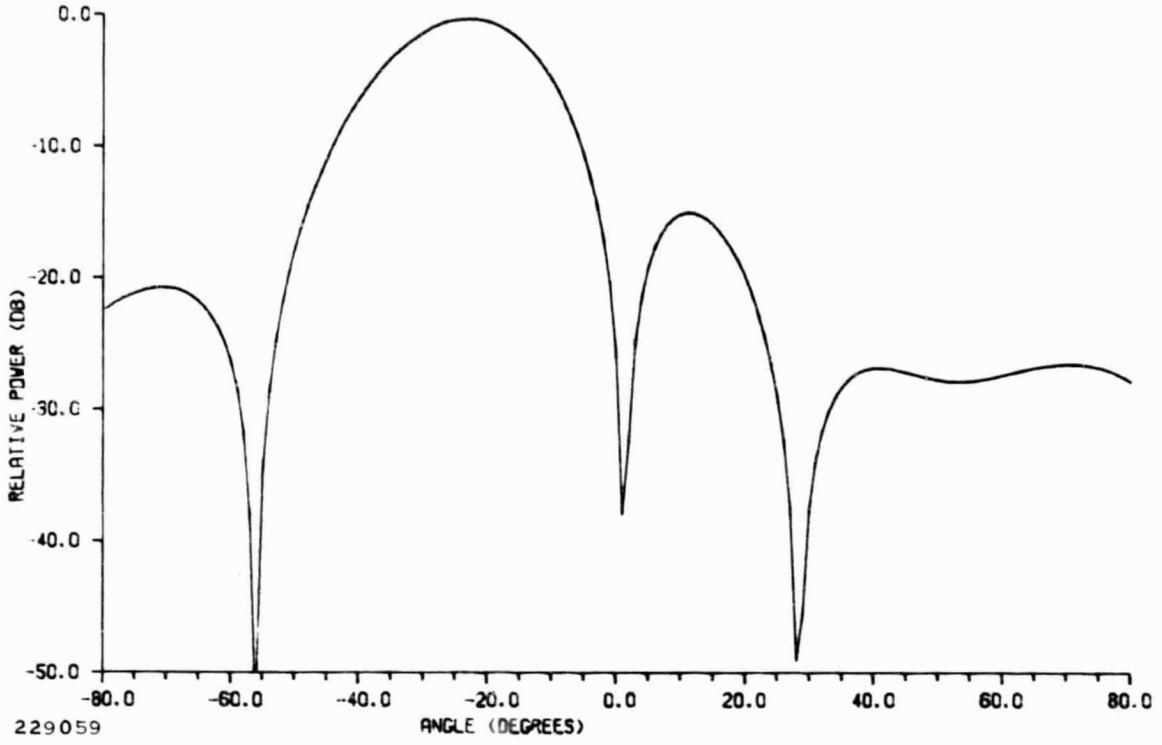

Figure A-30. Computed 15.2-GHz Planar Radiation Pattern, Beam Scanned 23.0 Degrees in Azimuth

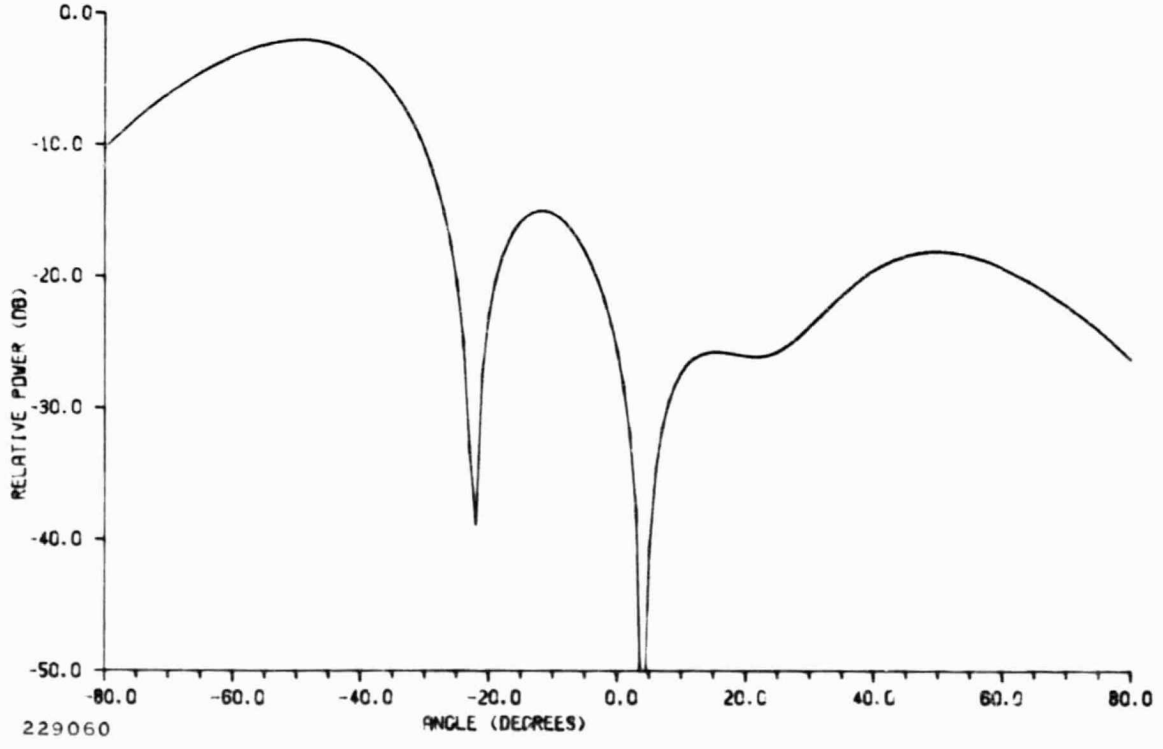

Figure A-31. Computed 15.2-GHz Planar Radiation Pattern, Beam Scanned 49.5 Degrees in Azimuth

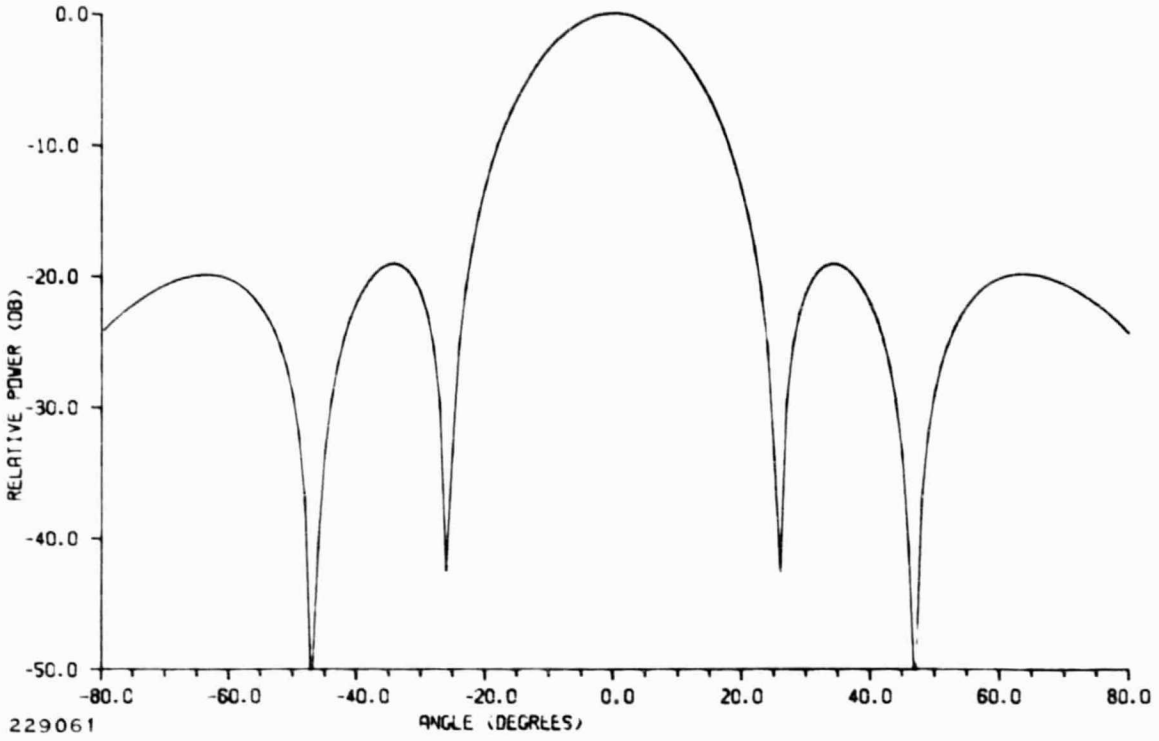

Figure A-32. Computed 15.2-GHz Planar Radiation Pattern, Elevation, No Scan

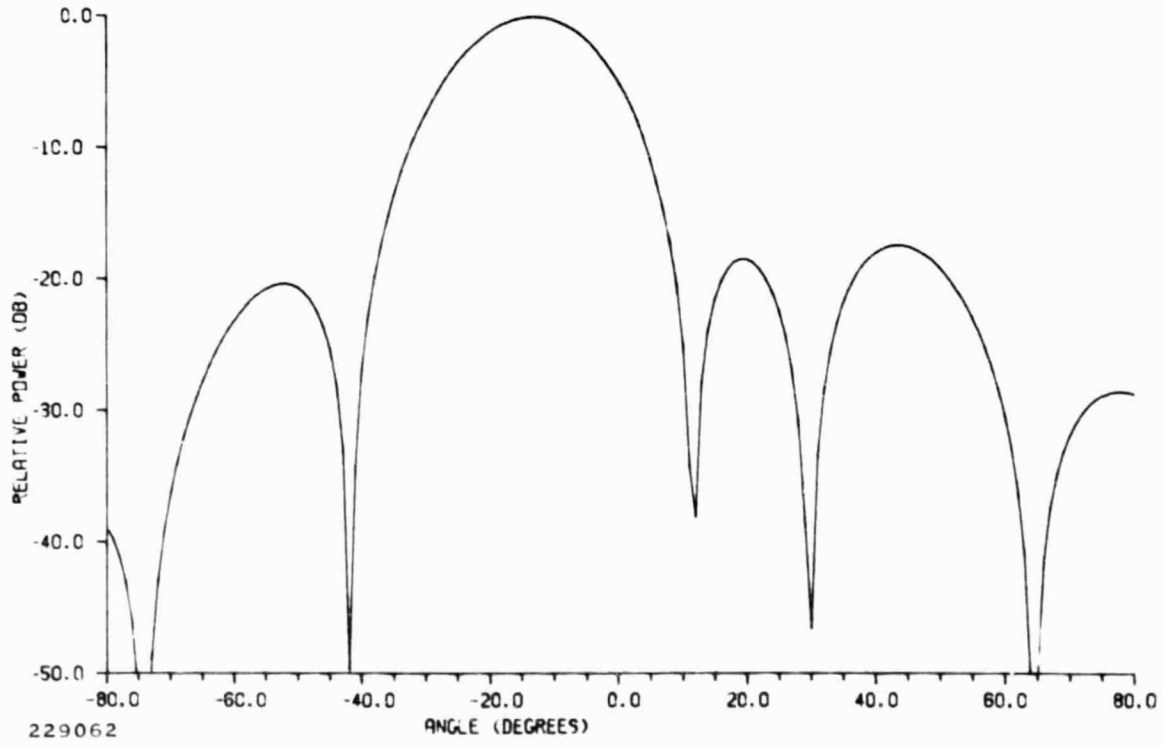

Figure A-33. Computed 15.2-GHz Planar Radiation Pattern, Beam Scanned 13.0 Degrees in Elevation

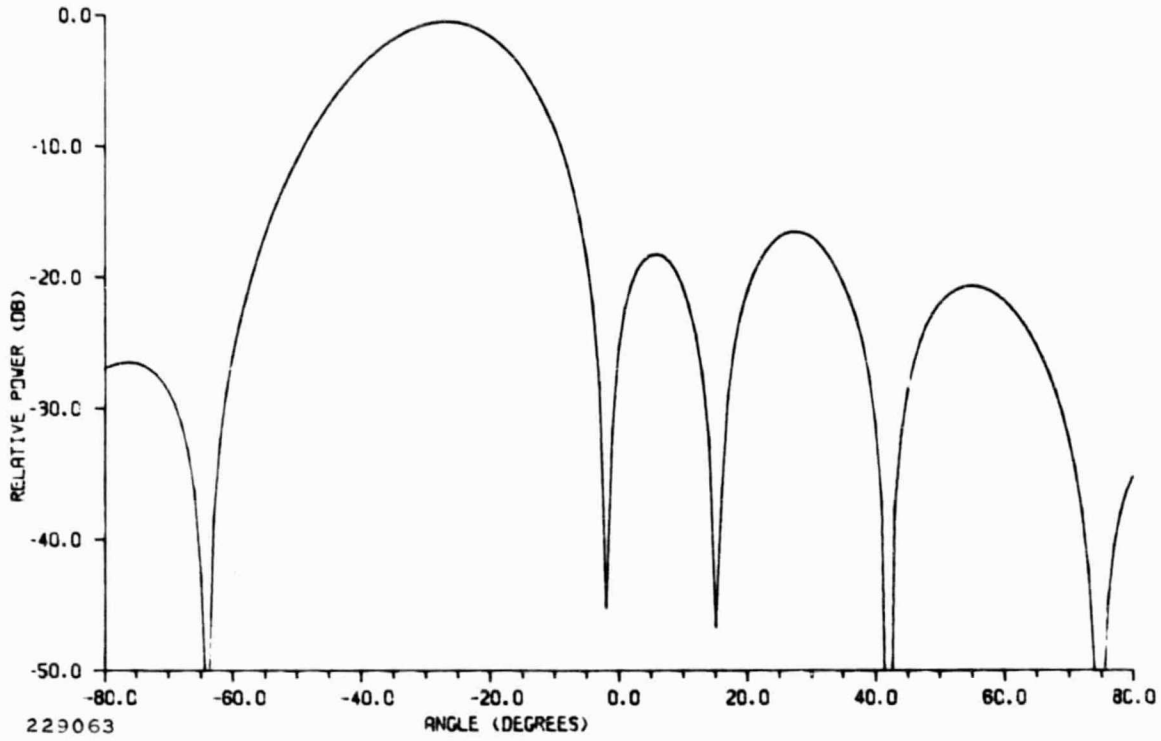

Figure A-34. Computed 15.2-GHz Planar Radiation Pattern, Beam Scanned 27.0 Degrees in Elevation

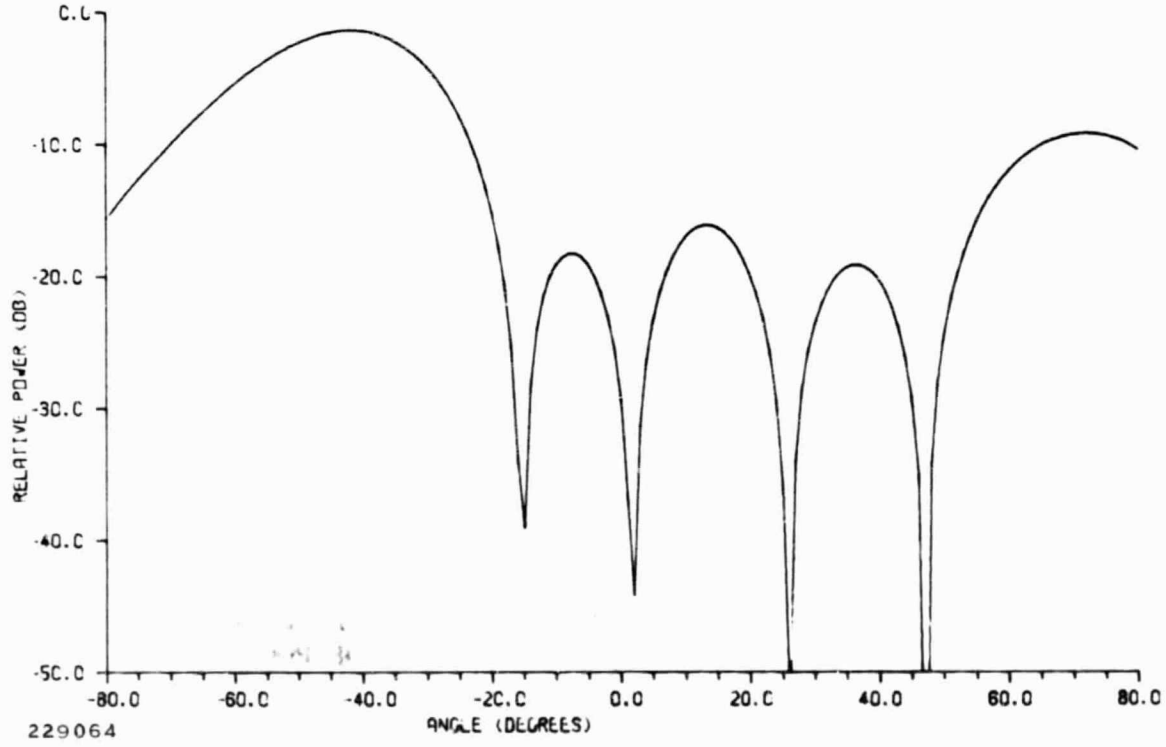

Figure A-35. Computed Computed 15.2-GHz Planar Radiation Pattern, Beam Scanned 42.0 Degrees in Elevation

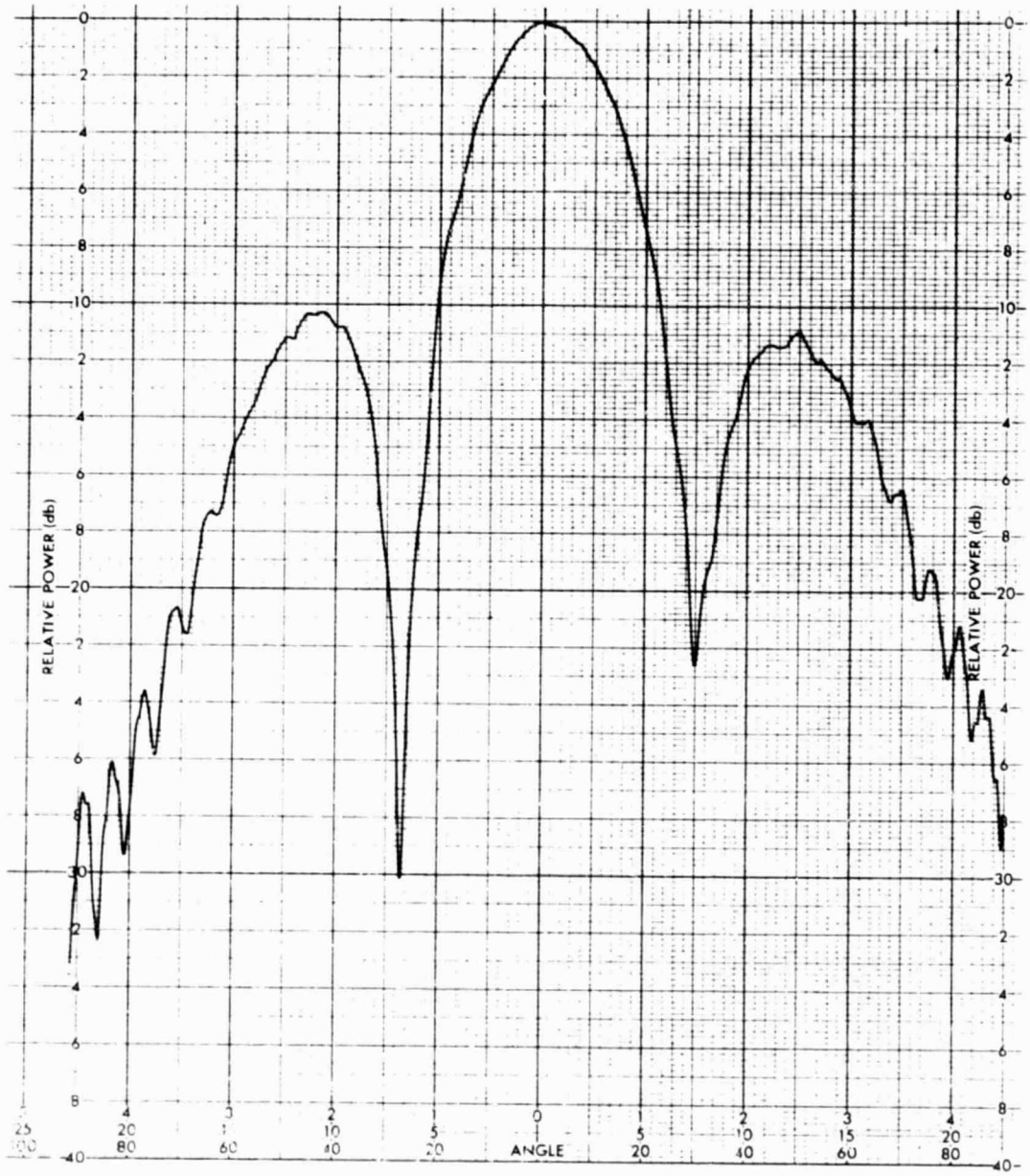

229080

ORIGINAL PAGE IS
OF POOR QUALITY

Figure A-36. Measured 14.6-GHz Pattern, Azimuth, No Scan

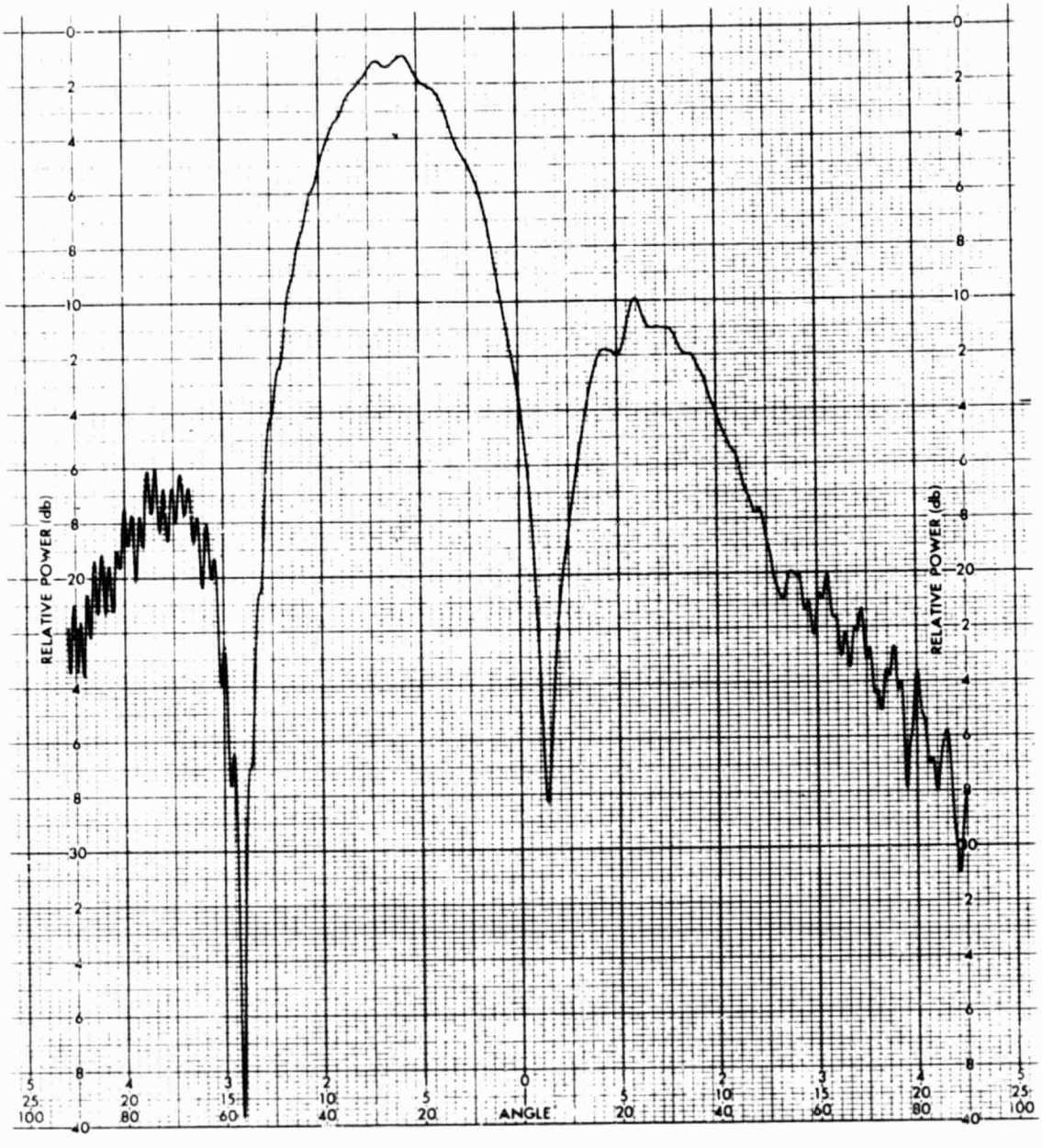

229081

Figure A-37. Measured 14.6-GHz Pattern, Beam Scanned 23 Degrees in Azimuth

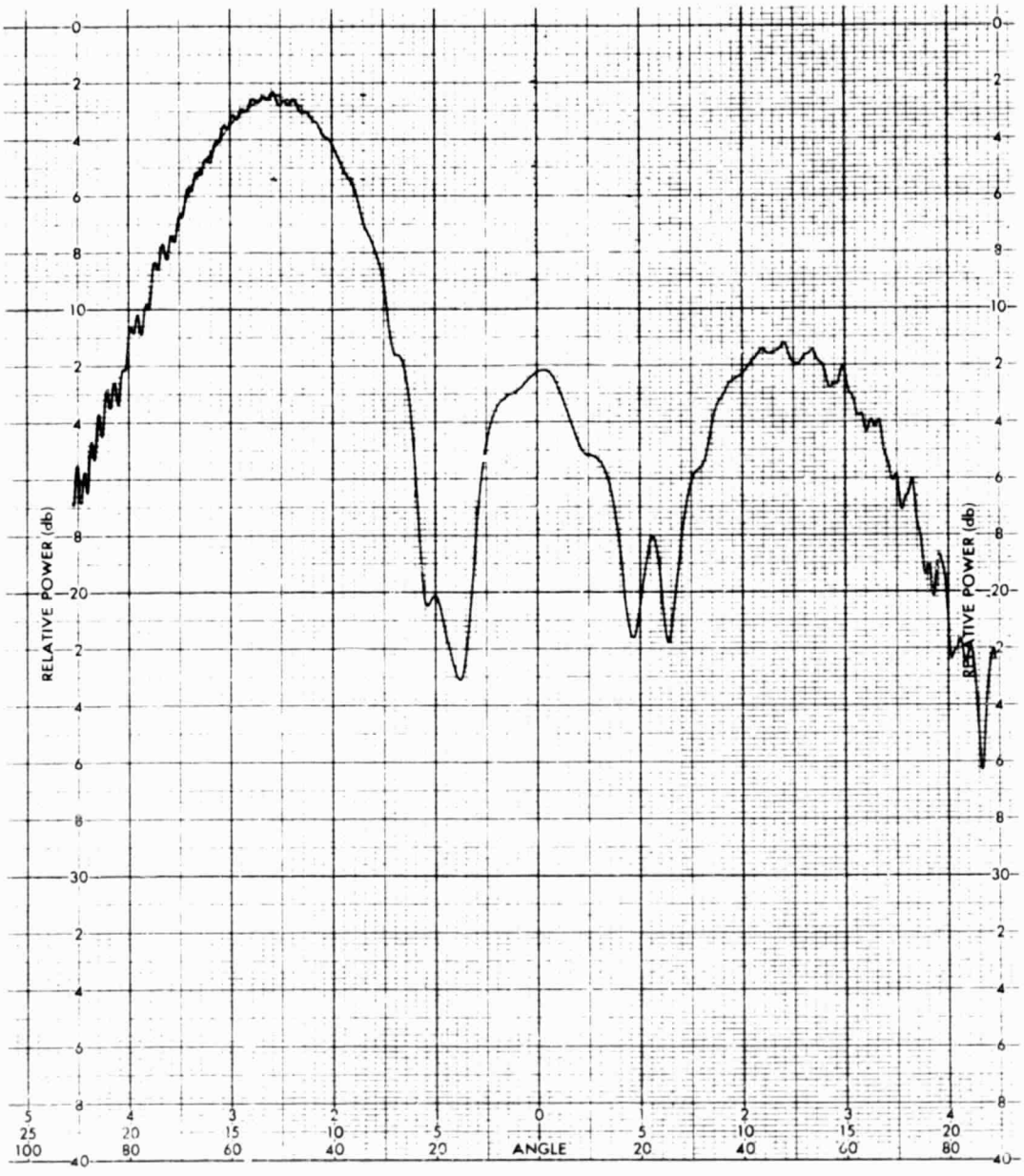

229082

Figure A-38. Measured 14.6-GHz Pattern, Beam Scanned 51 Degrees in Azimuth

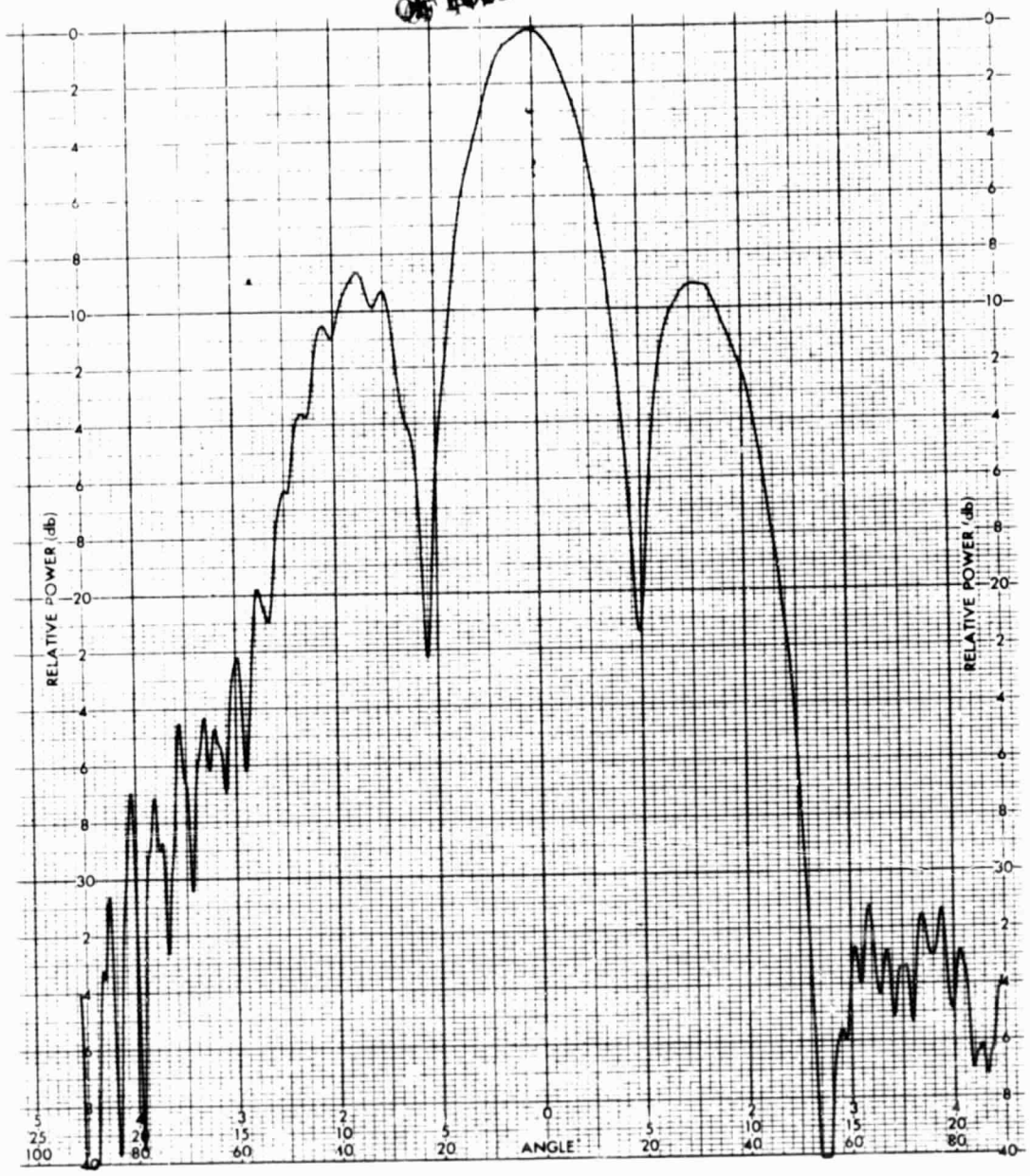

229093

Figure A-39. Measured 14.6-GHz Pattern, Elevation, No Scan

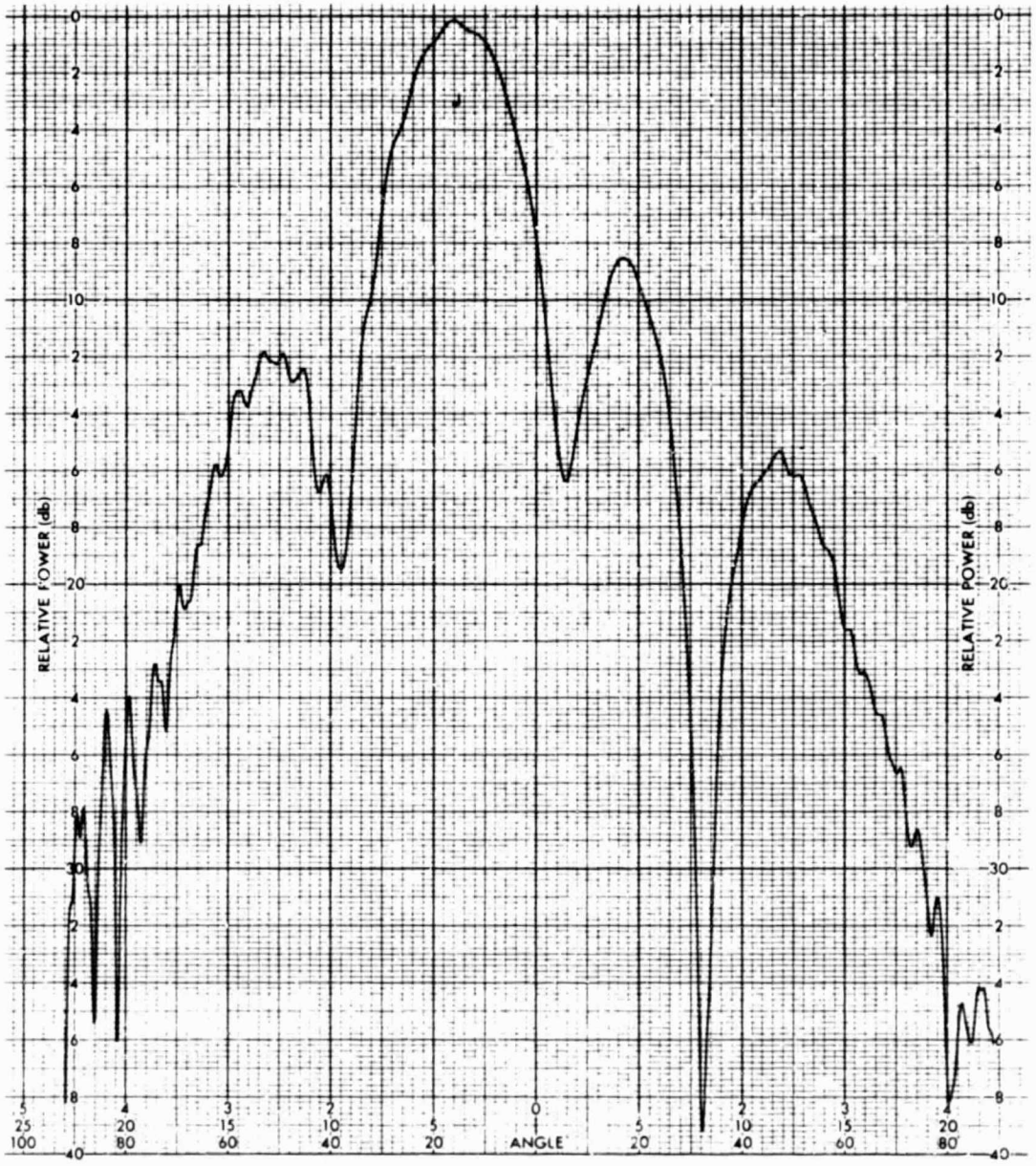

229084

Figure A-40. Measured 14.6-GHz Pattern, Beam Scanned 13 Degrees in Elevation

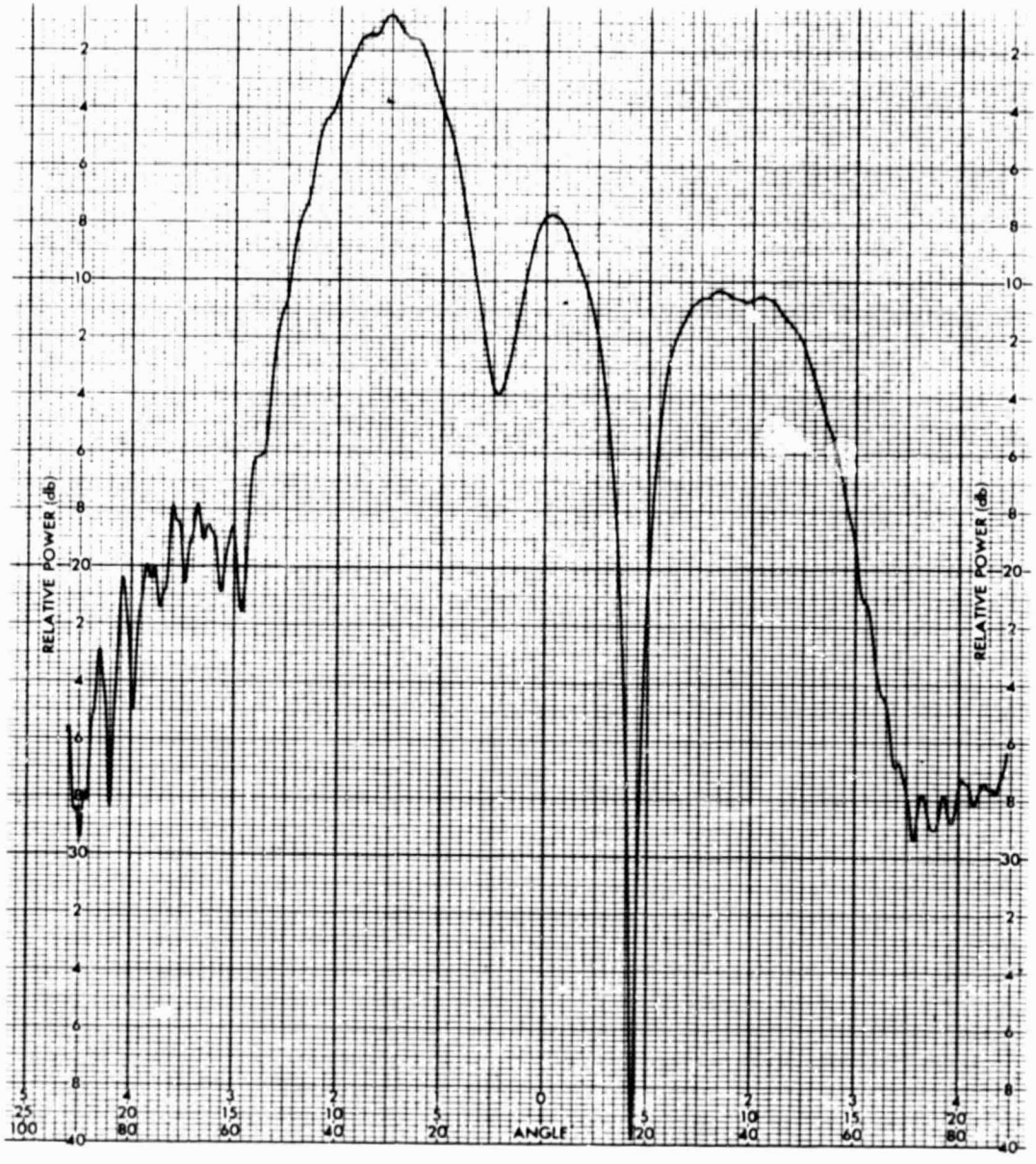

229085

Figure A-41. Measured 14.6-GHz Pattern, Beam Scanned 27 Degrees in Elevation

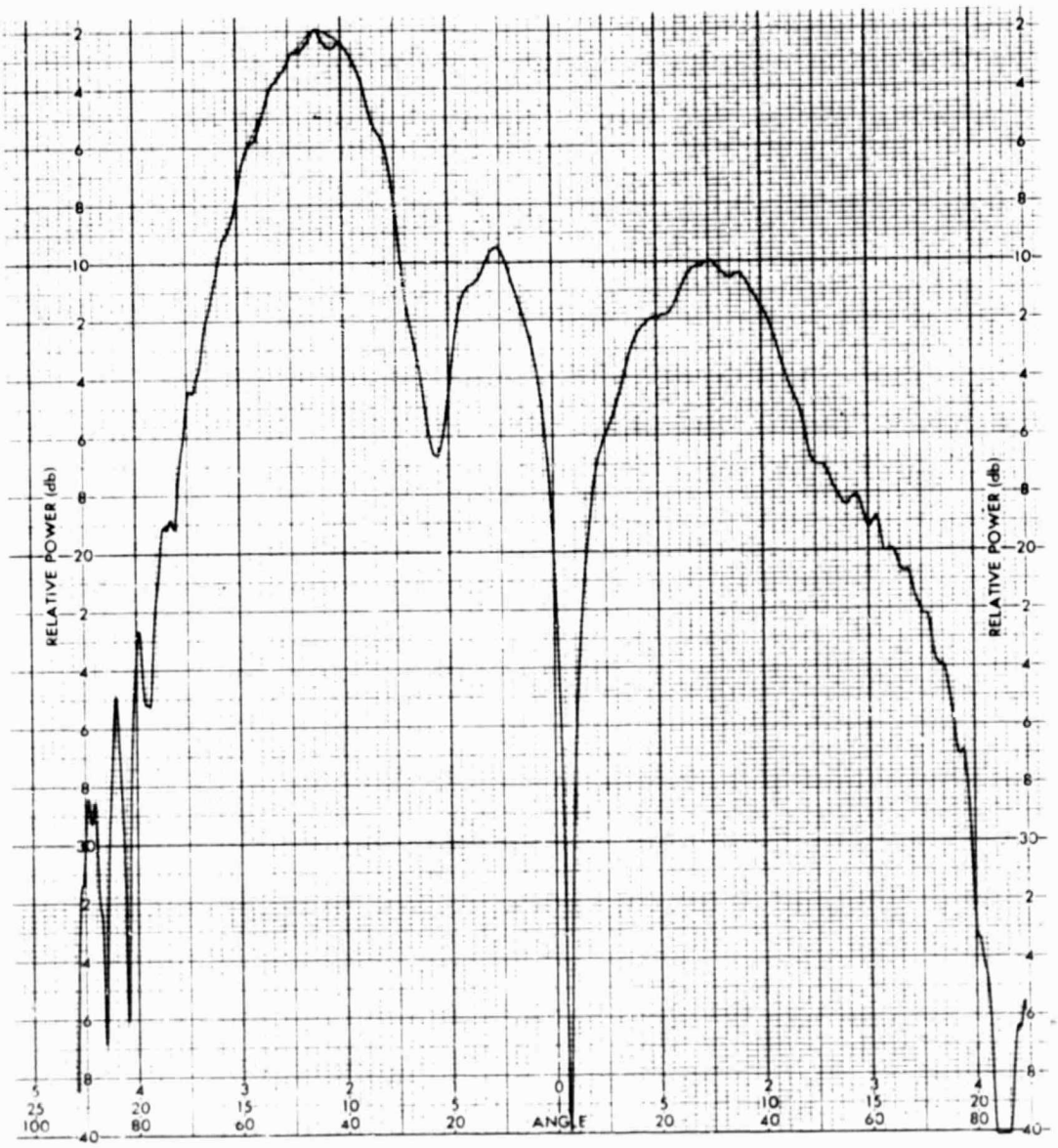

229086

Figure A-42. Measured 14.6-GHz Pattern, Beam Scanned 43 Degrees in Elevation

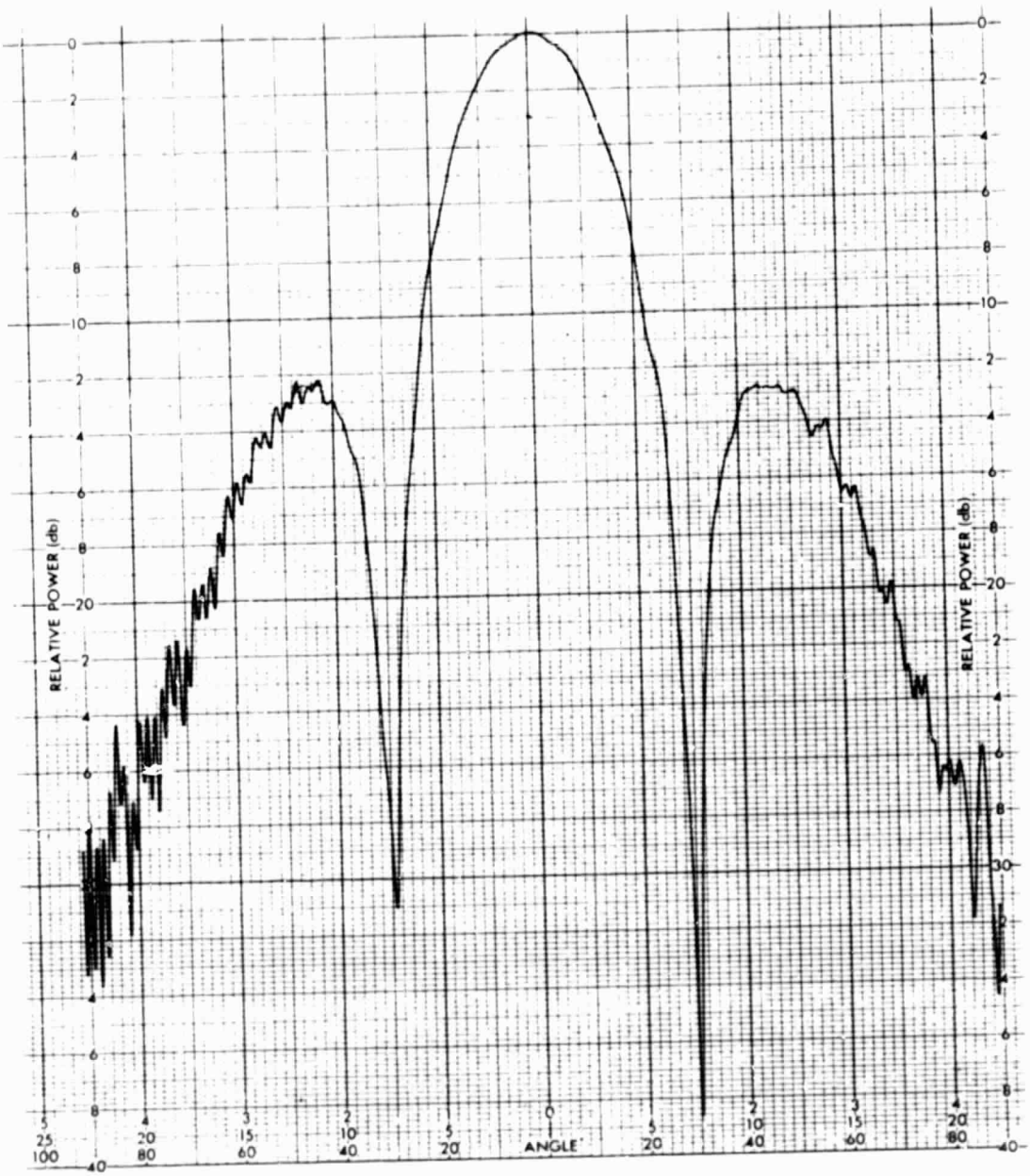

220087

Figure A-43. Measured 14.76-GHz Pattern, Azimuth, No Scan

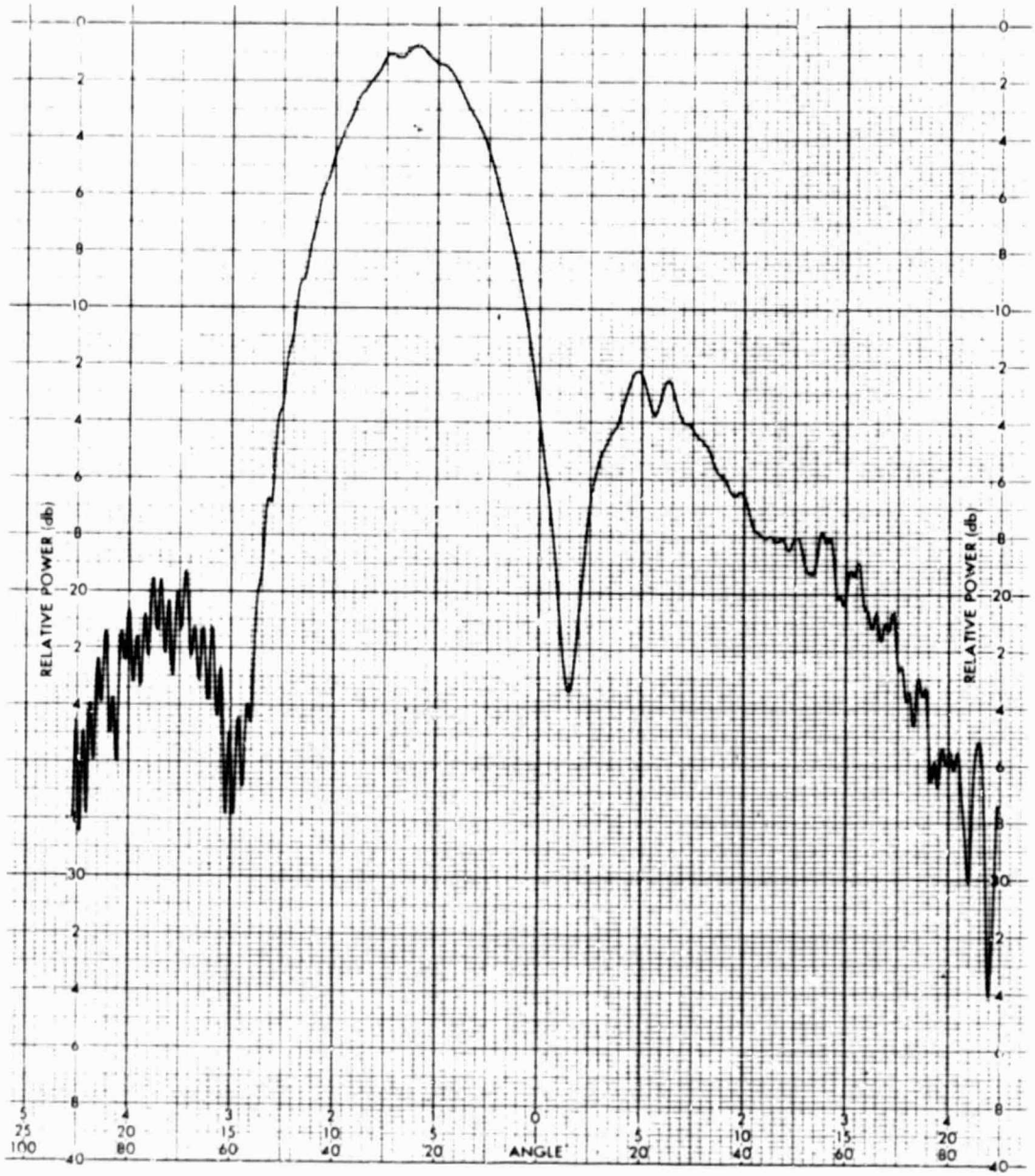

229088

Figure A-44. Measured 14.76-GHz Pattern, Beam Scanned 23 Degrees in Azimuth

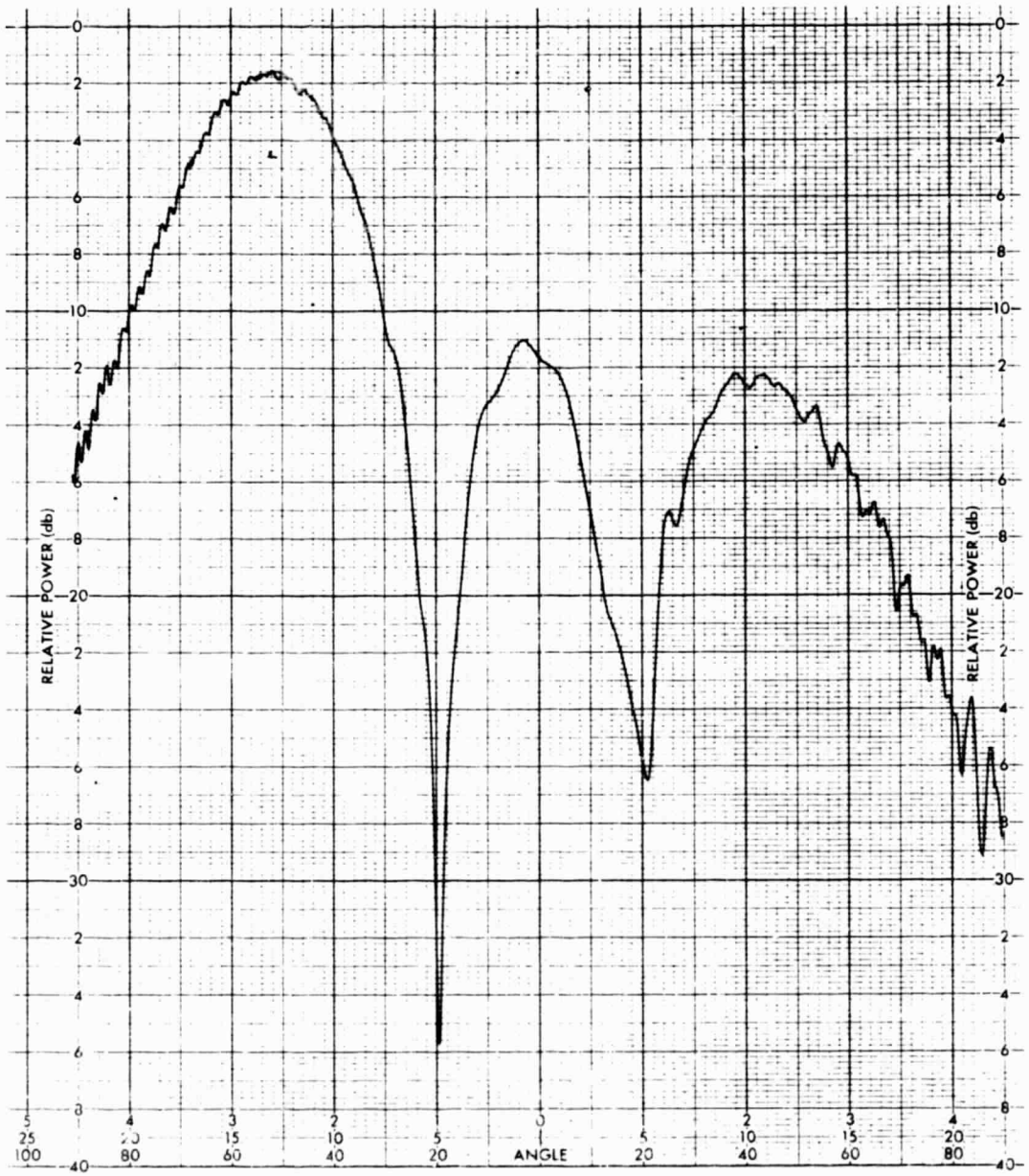

229089

Figure A-45. Measured 14.76-GHz Pattern, Beam Scanned 51 Degrees in Azimuth

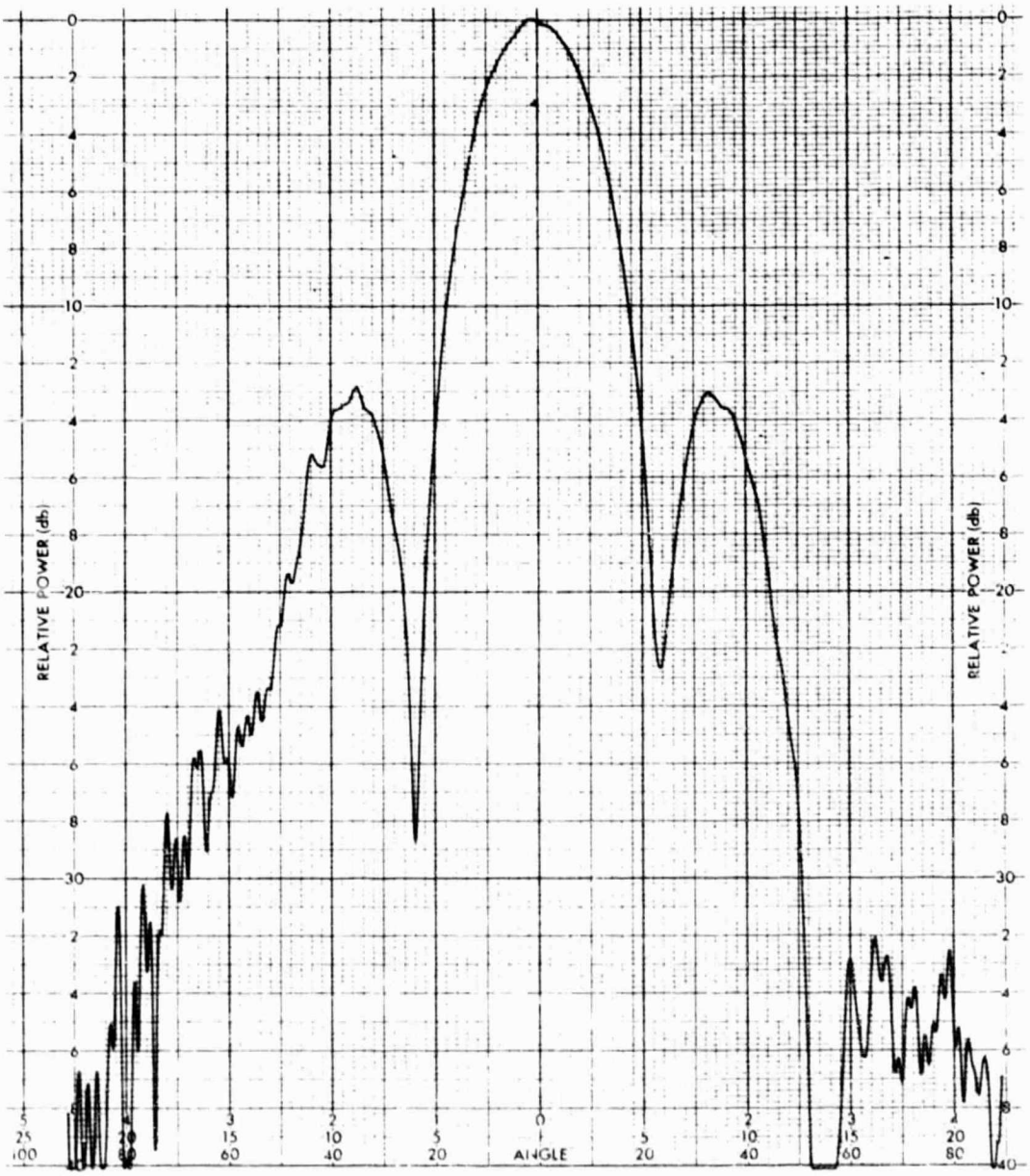

ORIGINAL PAGE IS
OF POOR QUALITY

229090

Figure A-46. Measured 14.76-GHz Pattern, Elevation, No Scan

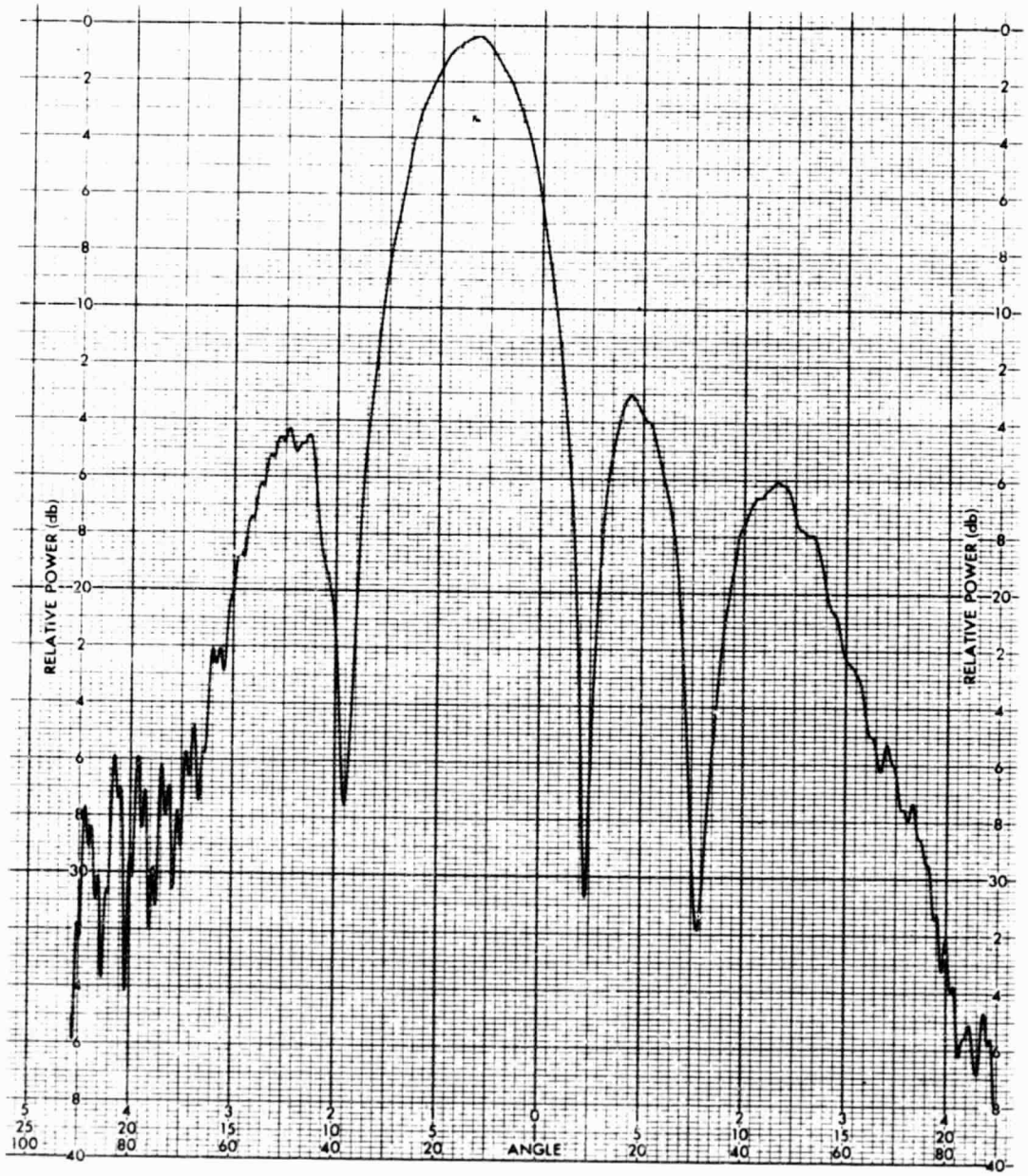

229091

Figure A-47. Measured 14.76-GHz Pattern, Beam Scanned 13 Degrees in Elevation

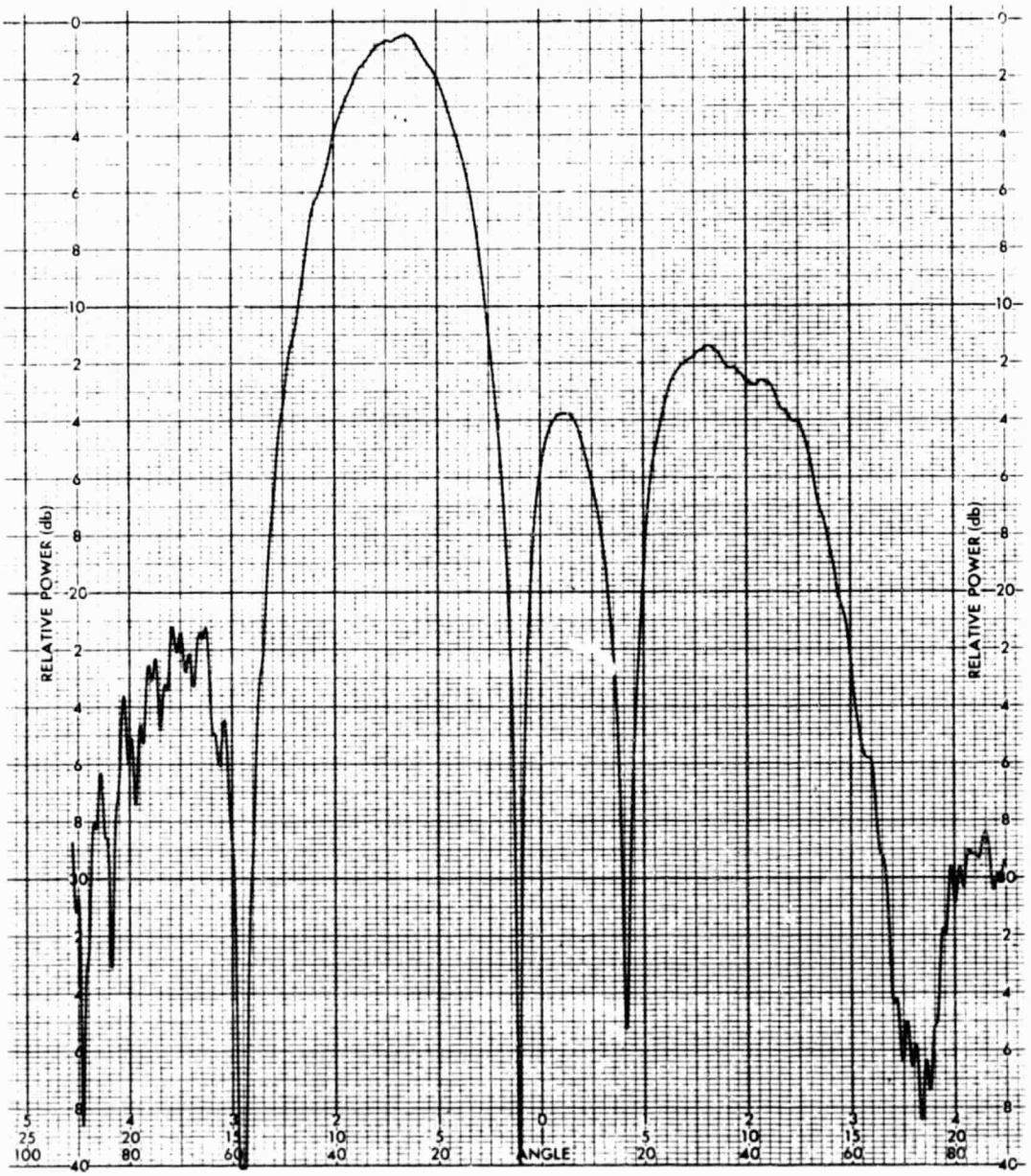

ORIGINAL PAGE IS
OF POOR QUALITY

229092

Figure A-48. Measured 14.76-GHz Pattern, Beam Scanned 27 Degrees in Elevation

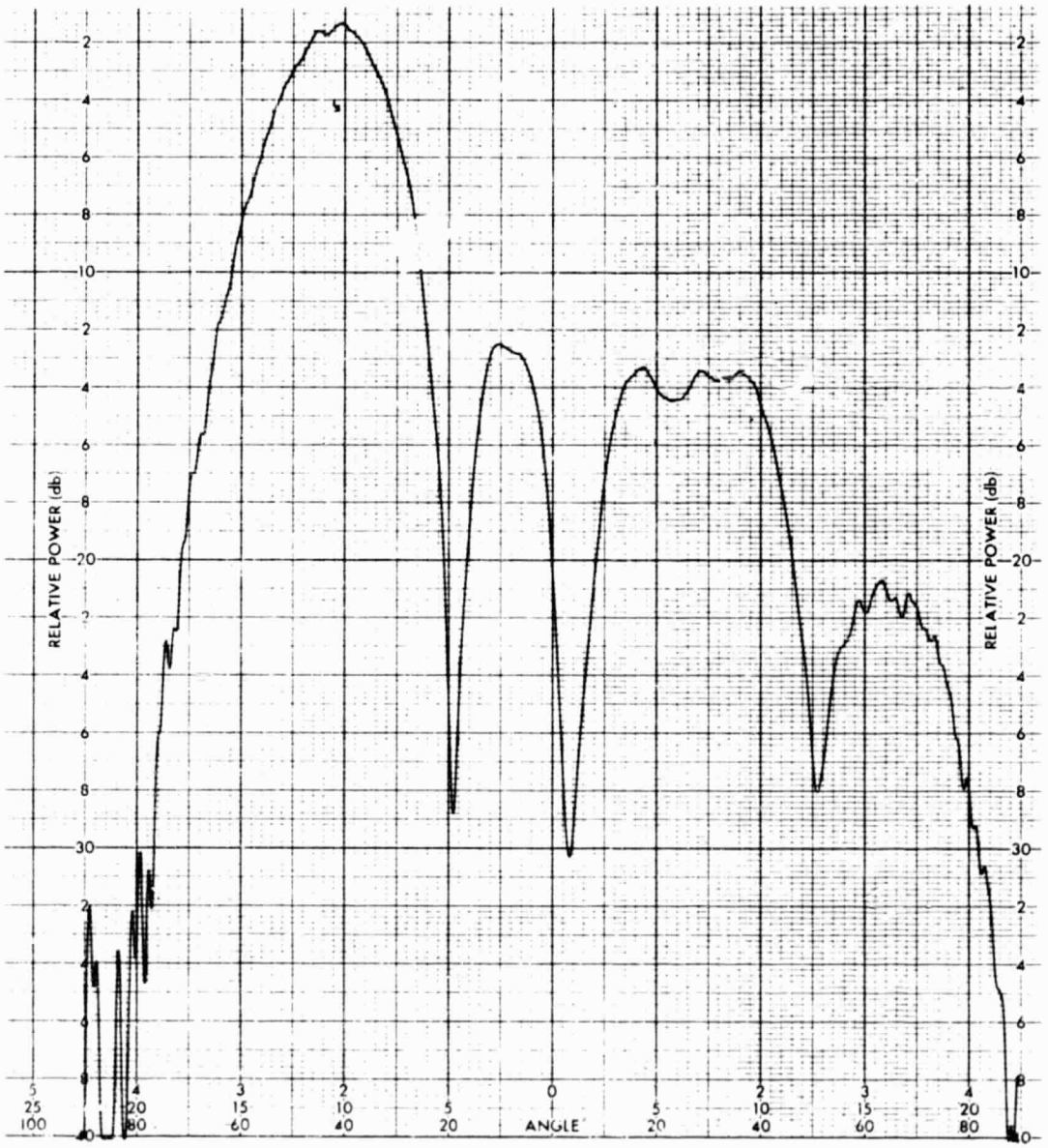

229093

Figure A-49. Measured 14.76-GHz Pattern, Beam Scanned 43 Degrees in Elevation

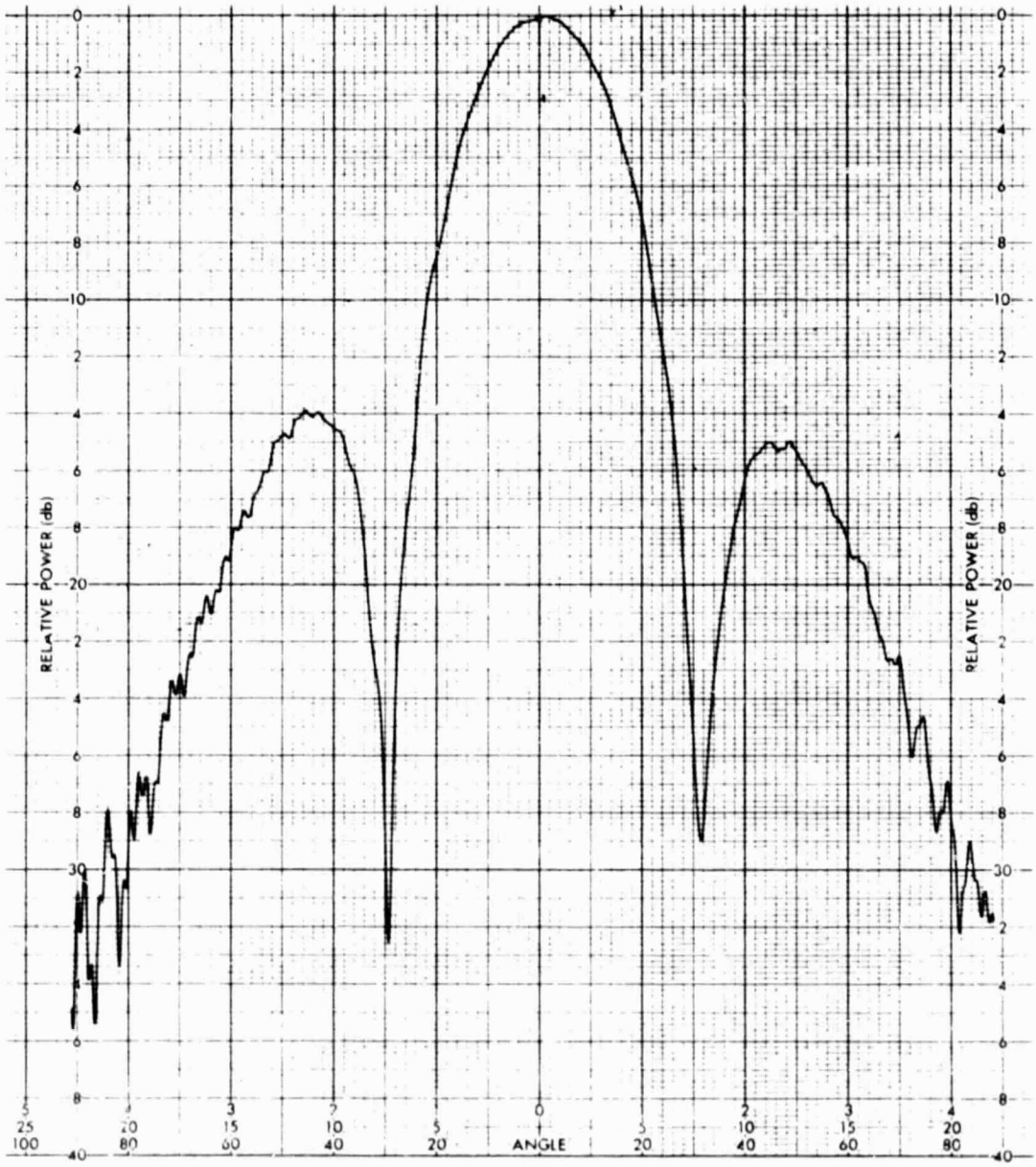

ORIGINAL PAGE IS
OF POOR QUALITY

229094

Figure A-50. Measured 14.9-GHz Pattern, Azimuth, No Scan

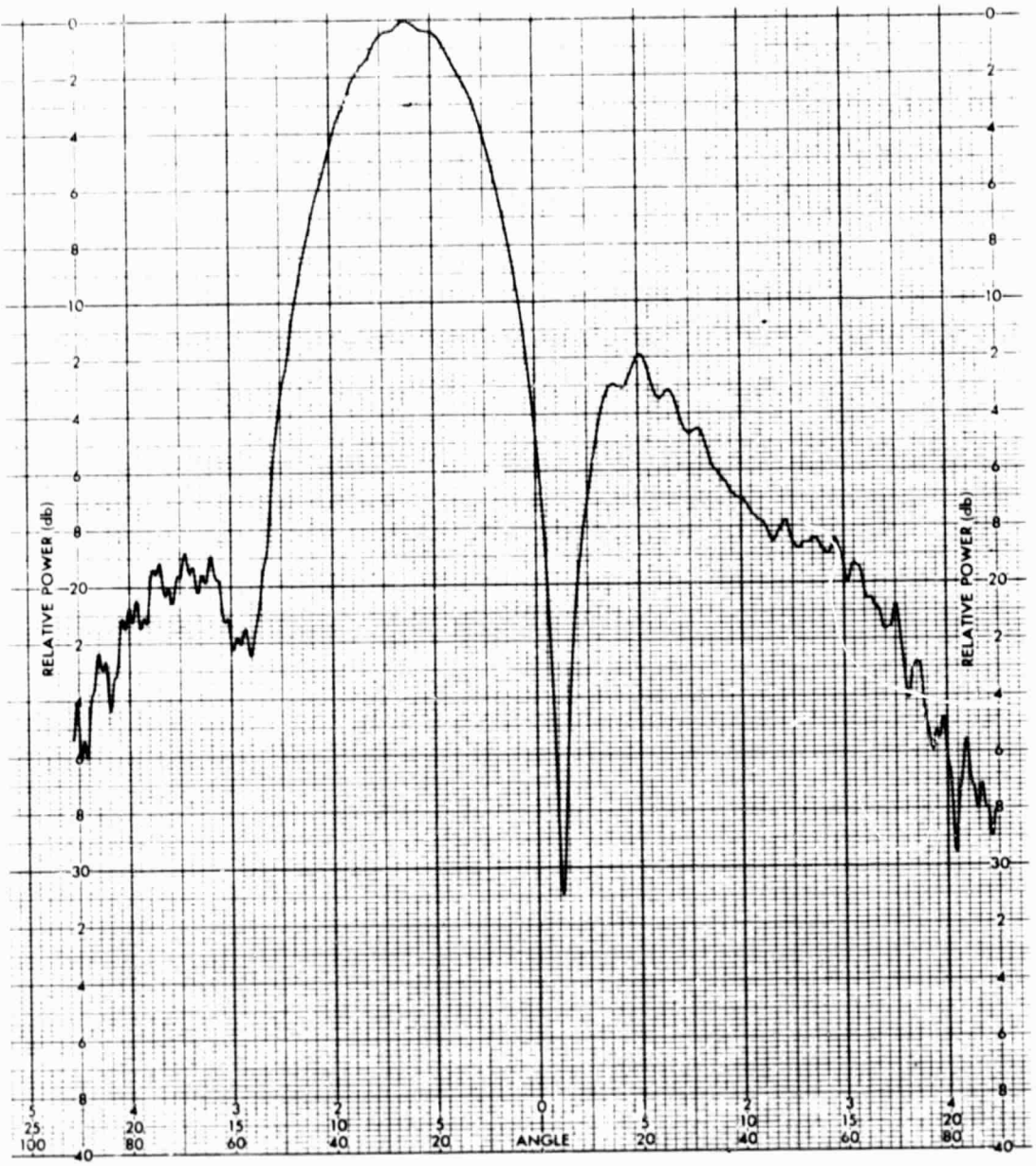

229095

Figure A-51. Measured 14.9-GHz Pattern, Beam Scanned 23 Degrees in Azimuth

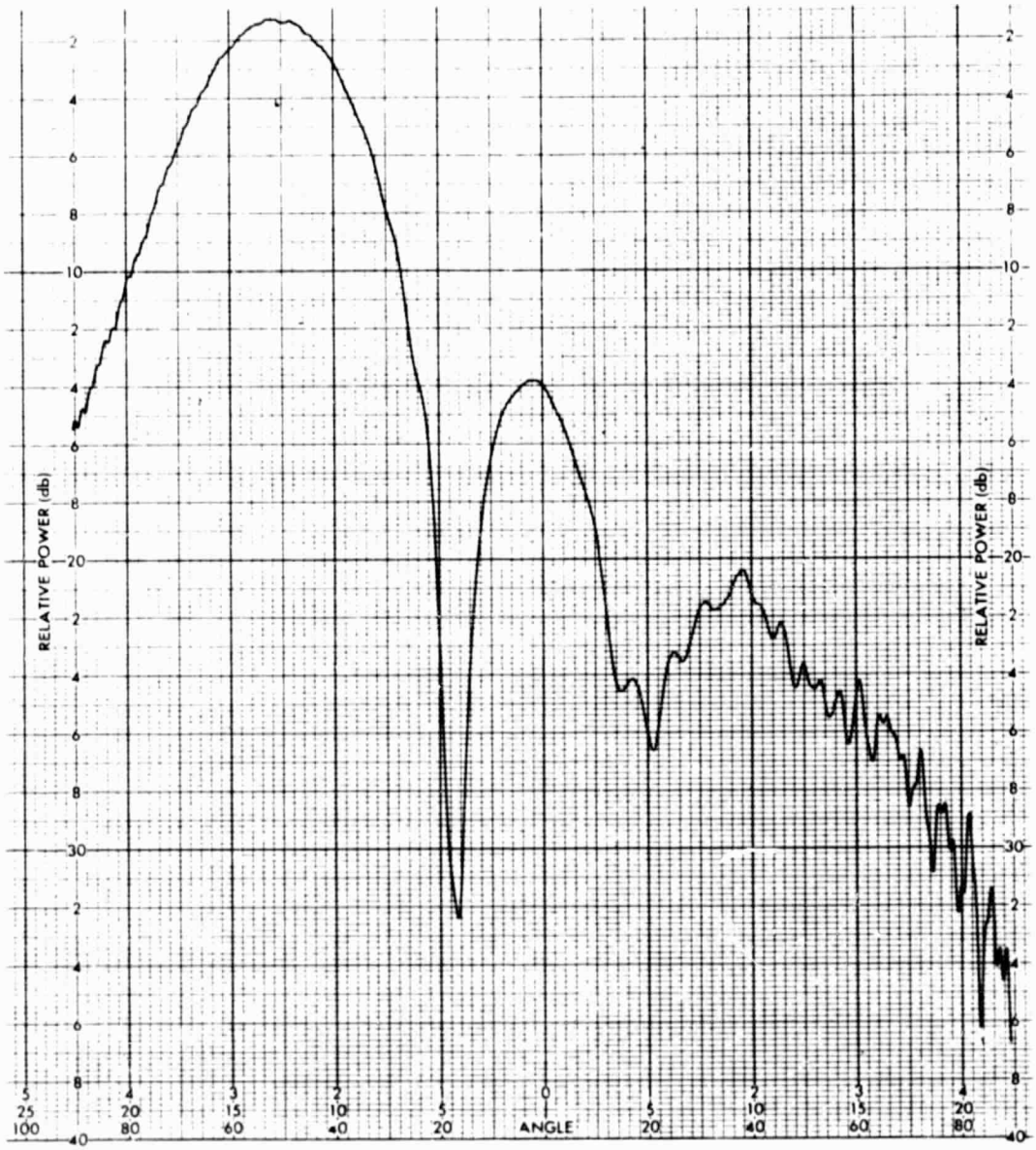

229096

Figure A-52. Measured 14.9-GHz Pattern, Beam Scanned 51 Degrees in Azimuth

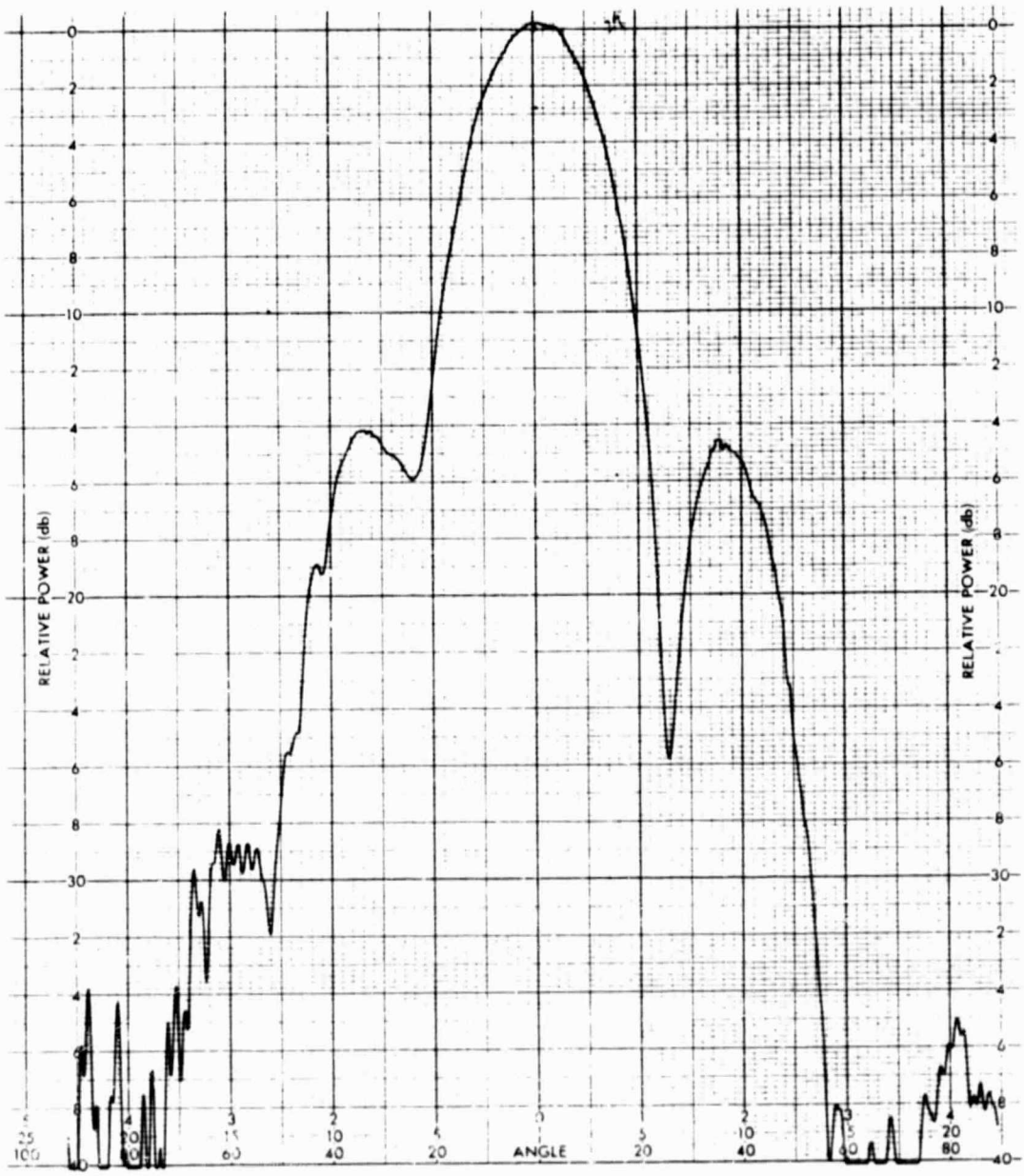

229097

Figure A-53. Measured 14.9-GHz Pattern, Elevation, No Scan

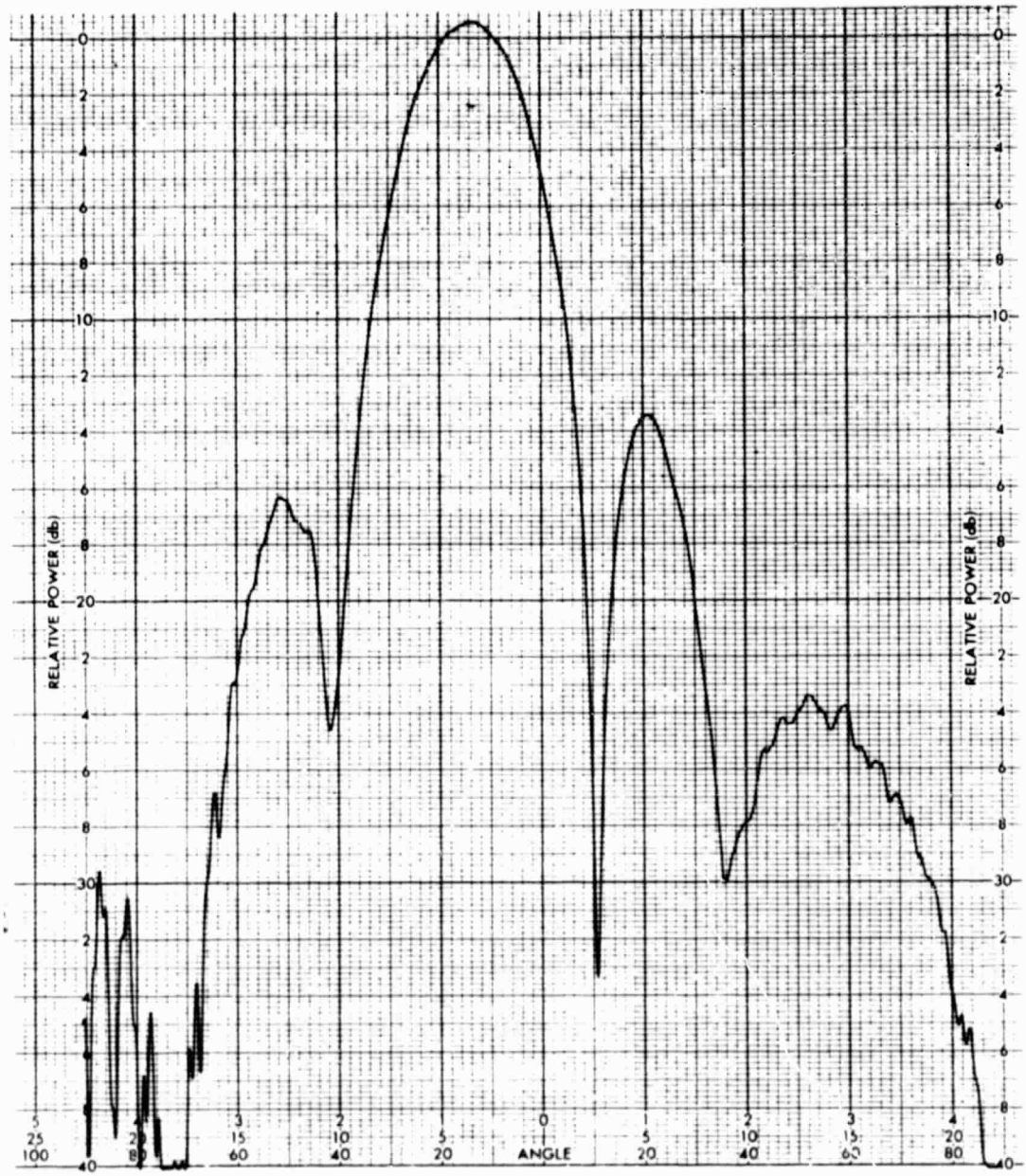

ORIGINAL PAGE IS
OF POOR QUALITY

229098

Figure A-54. Measured 14.9-GHz Pattern, Beam Scanned 13 Degrees in Elevation

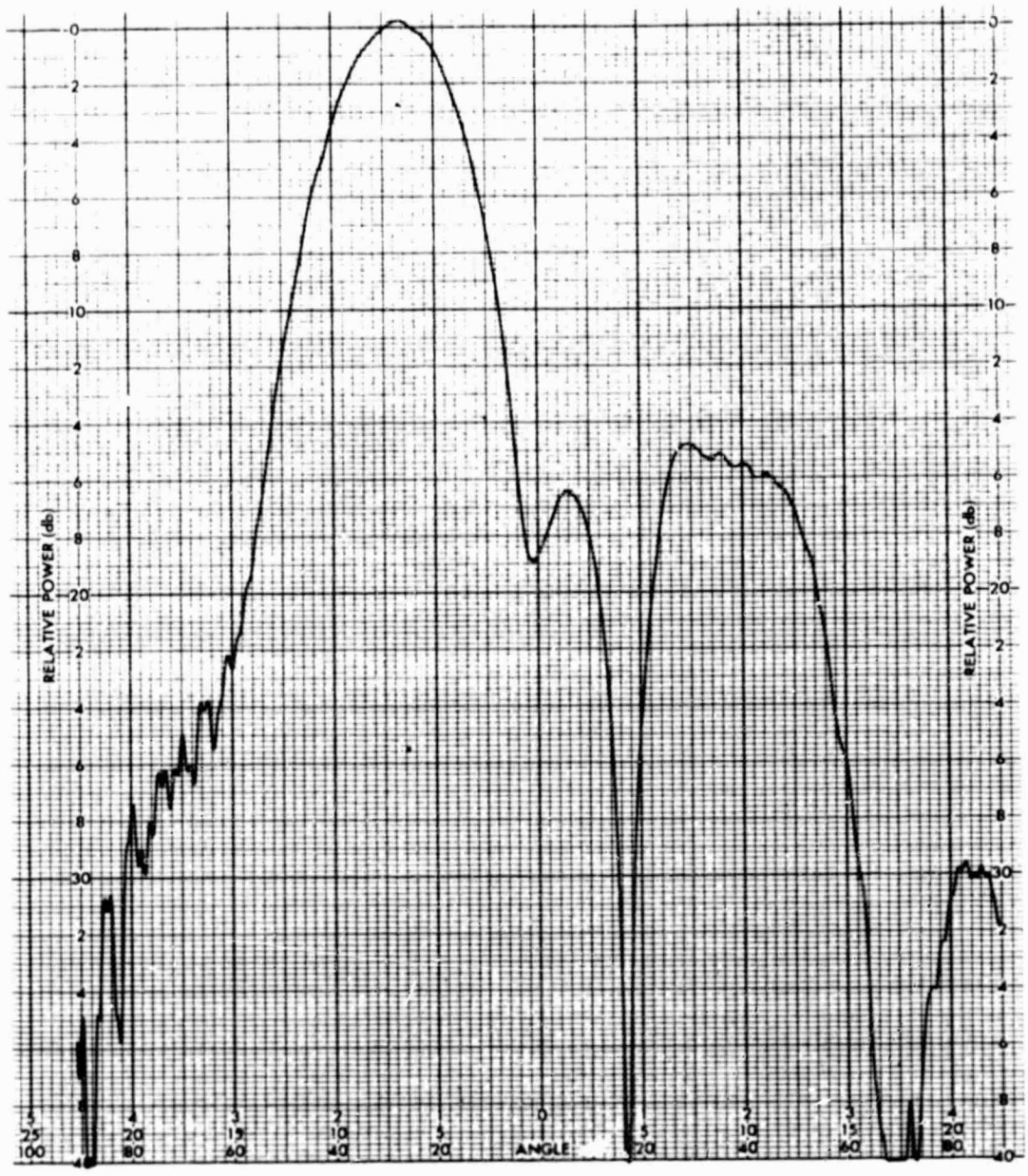

229099

Figure A-55. Measured 14.9-GHz Pattern, Beam Scanned 27 Degrees in Elevation

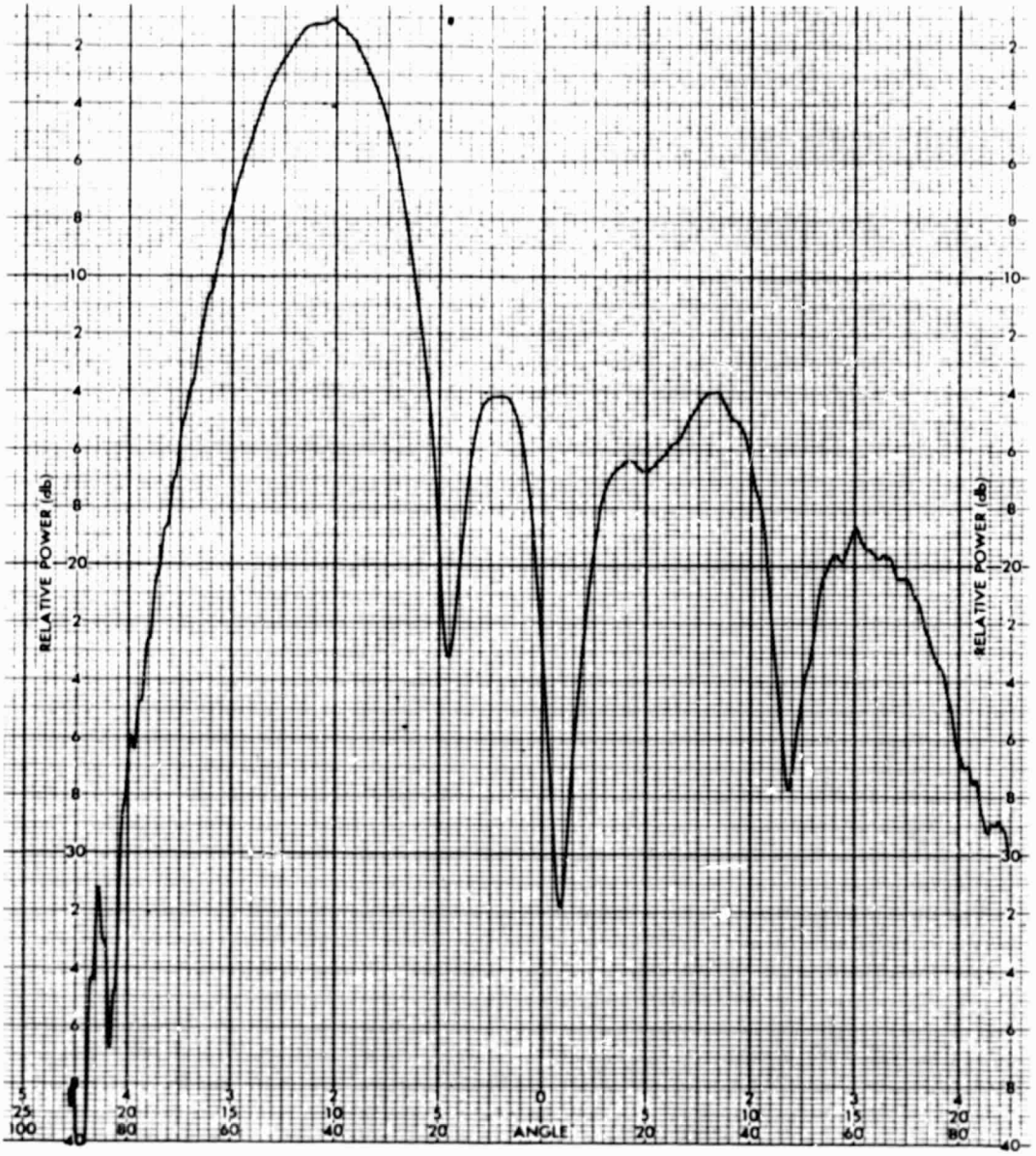

229100

Figure A-56. Measured 14.9-GHz Pattern, Beam Scanned 43 Degrees in Elevation

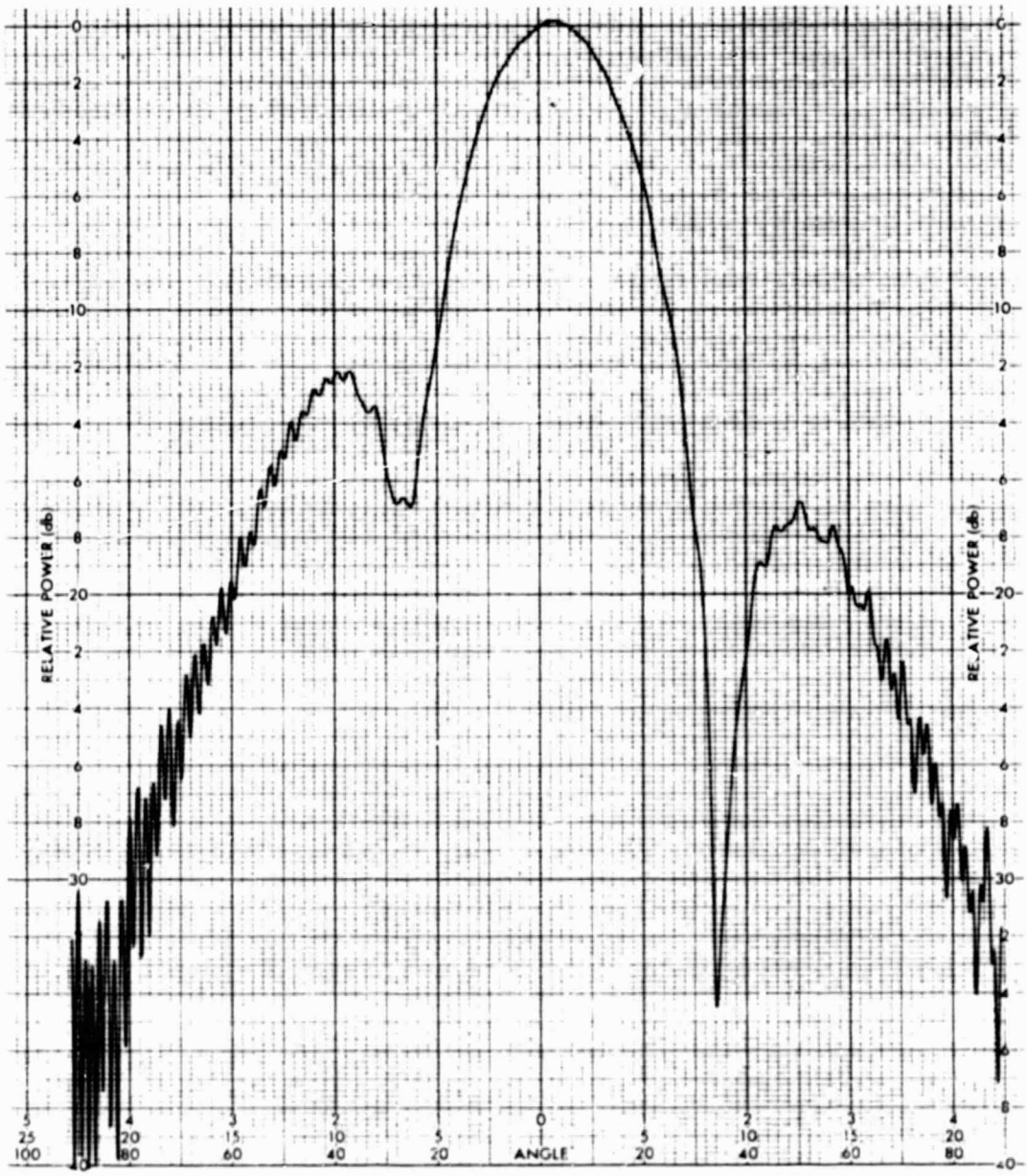

229101

Figure A-57. Measured 15.04-GHz Pattern, Azimuth, No Scan

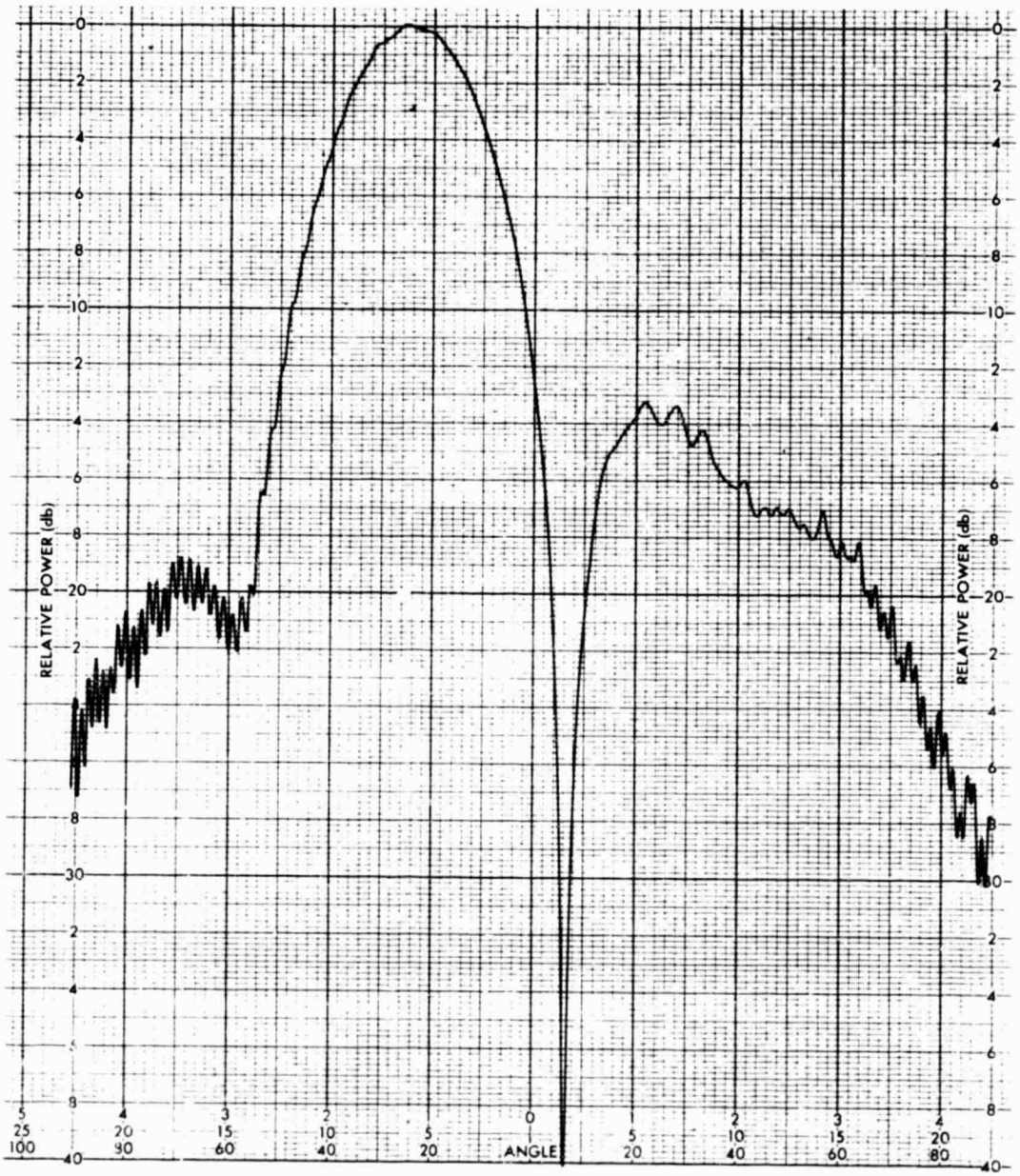

ORIGINAL PAGE IS
OF POOR QUALITY

229102

Figure A-58. Measured 15.04-GHz Pattern, Beam Scanned 23 Degrees in Azimuth

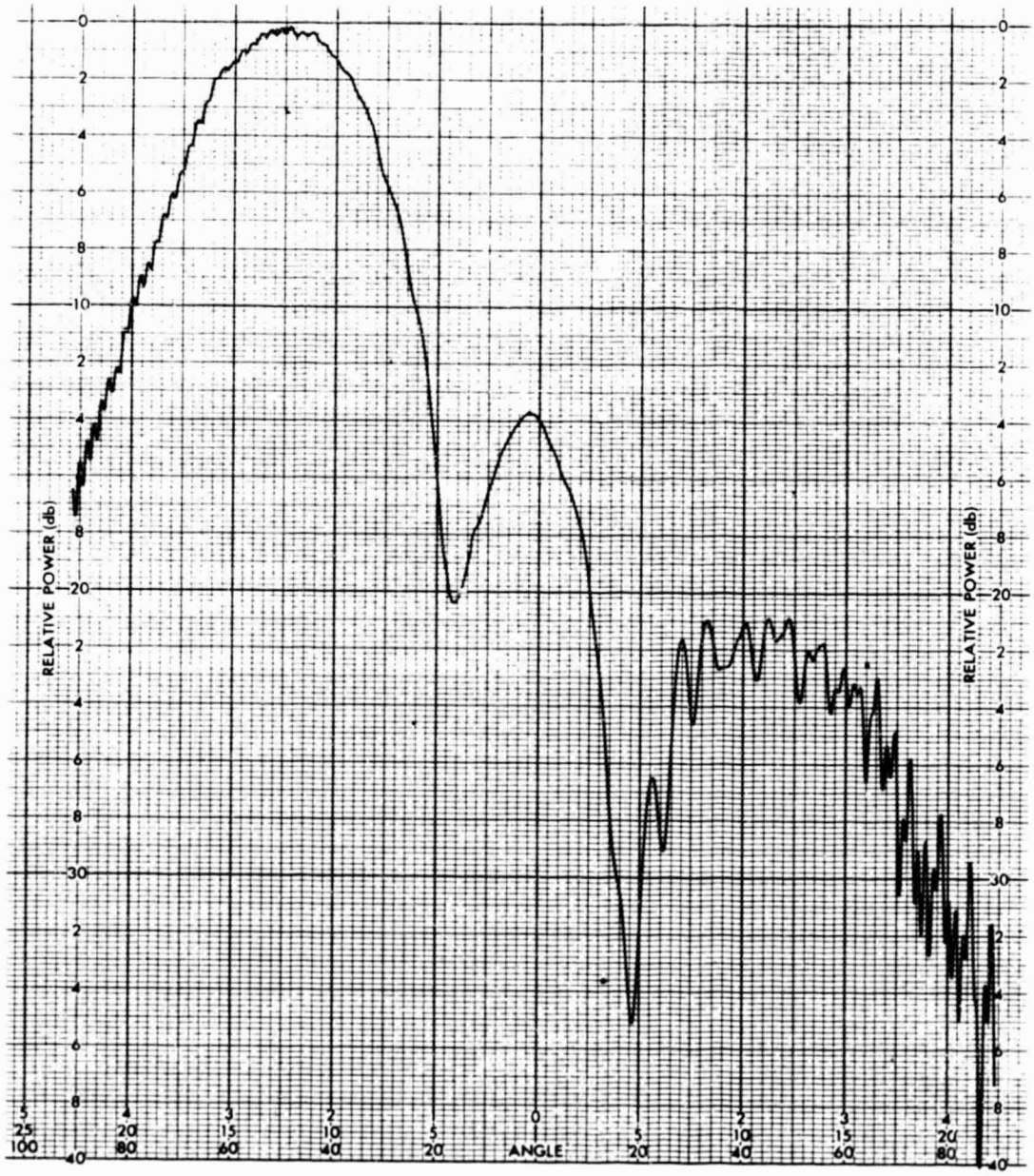

229103

Figure A-59. Measured 15.04-GHz Pattern, Beam Scanned 51 Degrees in Azimuth

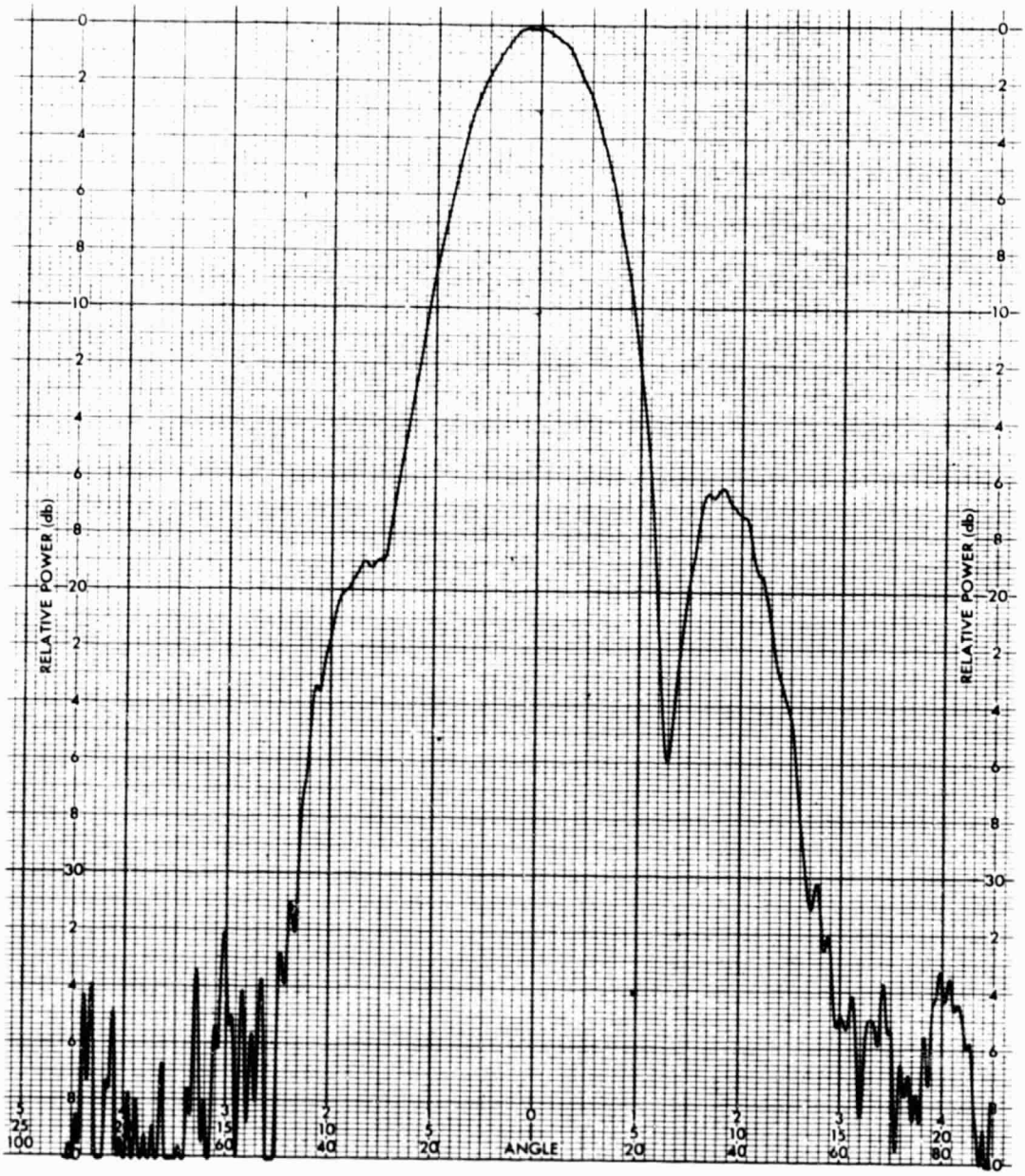

229104

Figure A-60. Measured 15.04-GHz Pattern, Elevation, No Scan

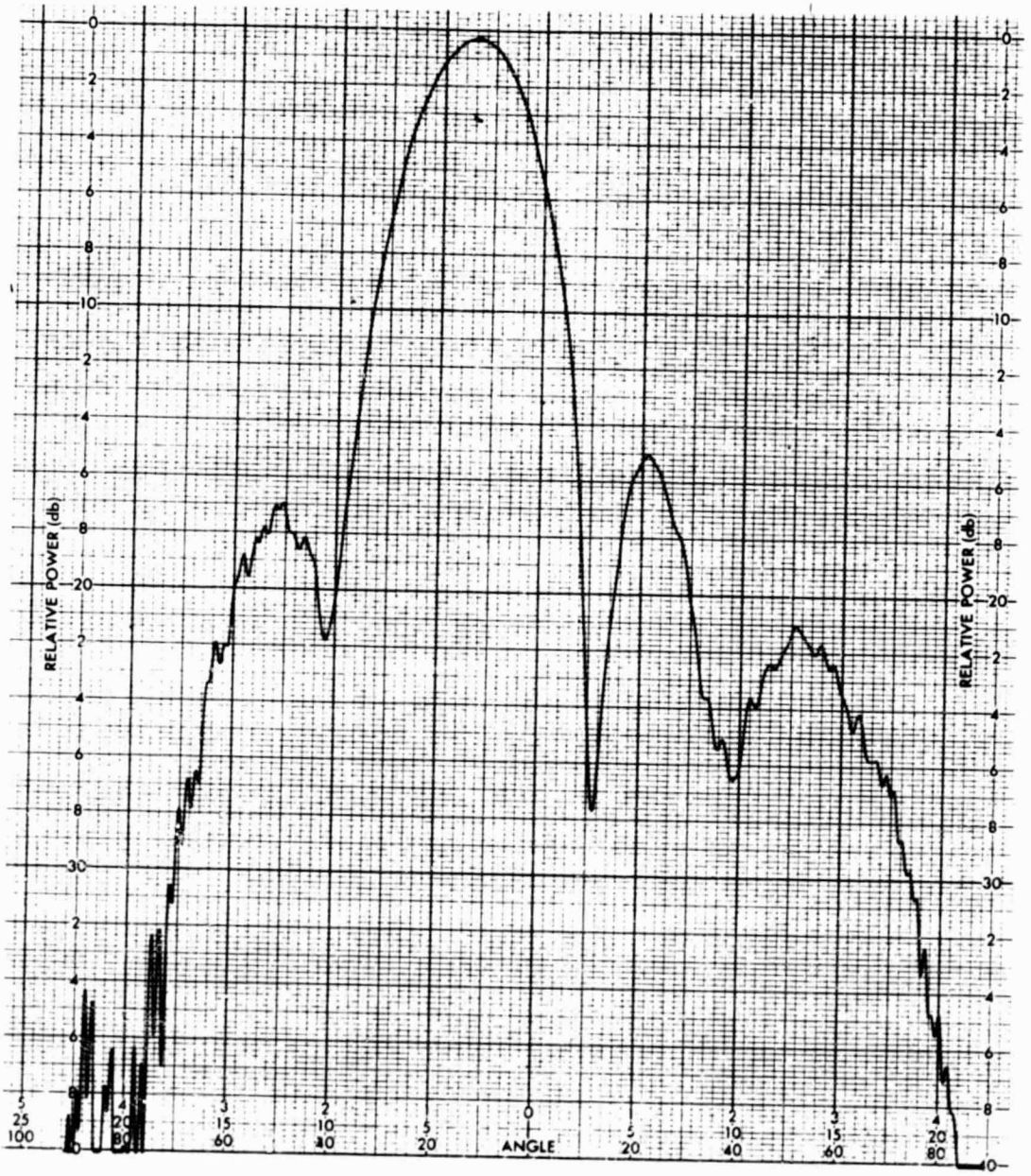

229105

Figure A-61. Measured 15.04-GHz Pattern, Beam Scanned 13 Degrees in Elevation

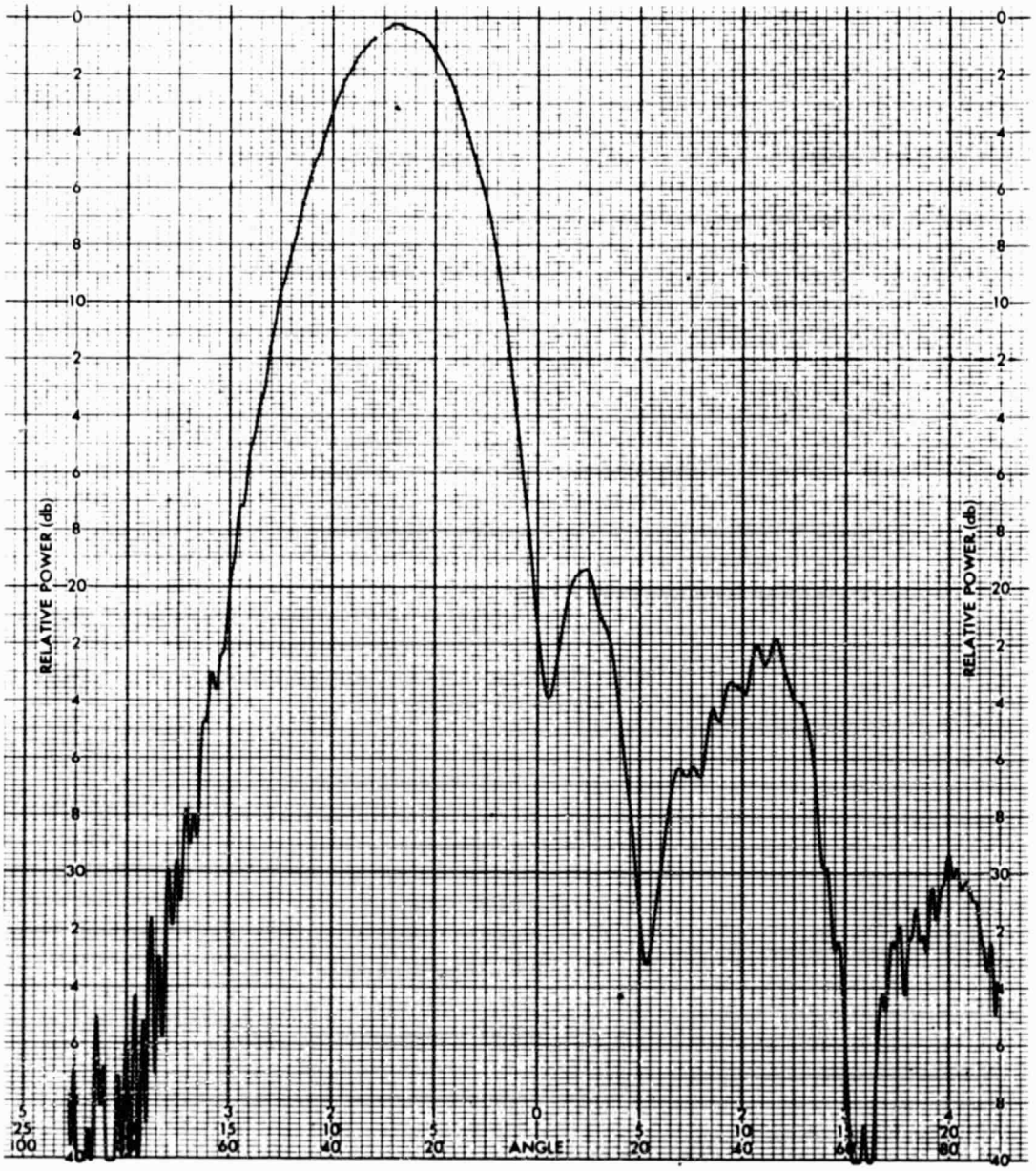

229106

Figure A-62. Measured 15.04-GHz Pattern, Beam Scanned 27 Degrees in Elevation

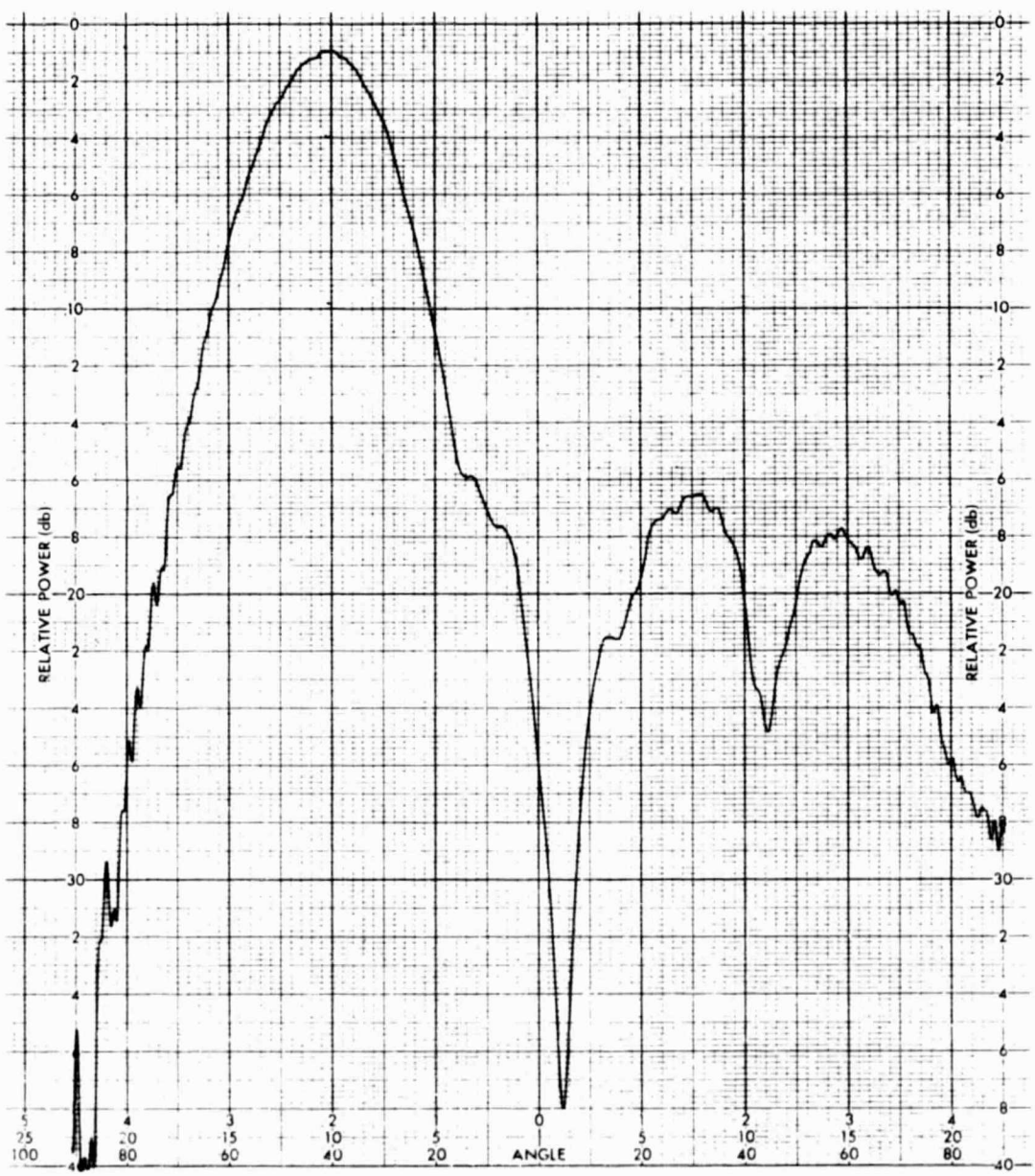

229107

Figure A-63. Measured 15.04-GHz Pattern, Beam Scanned 43 Degrees in Elevation

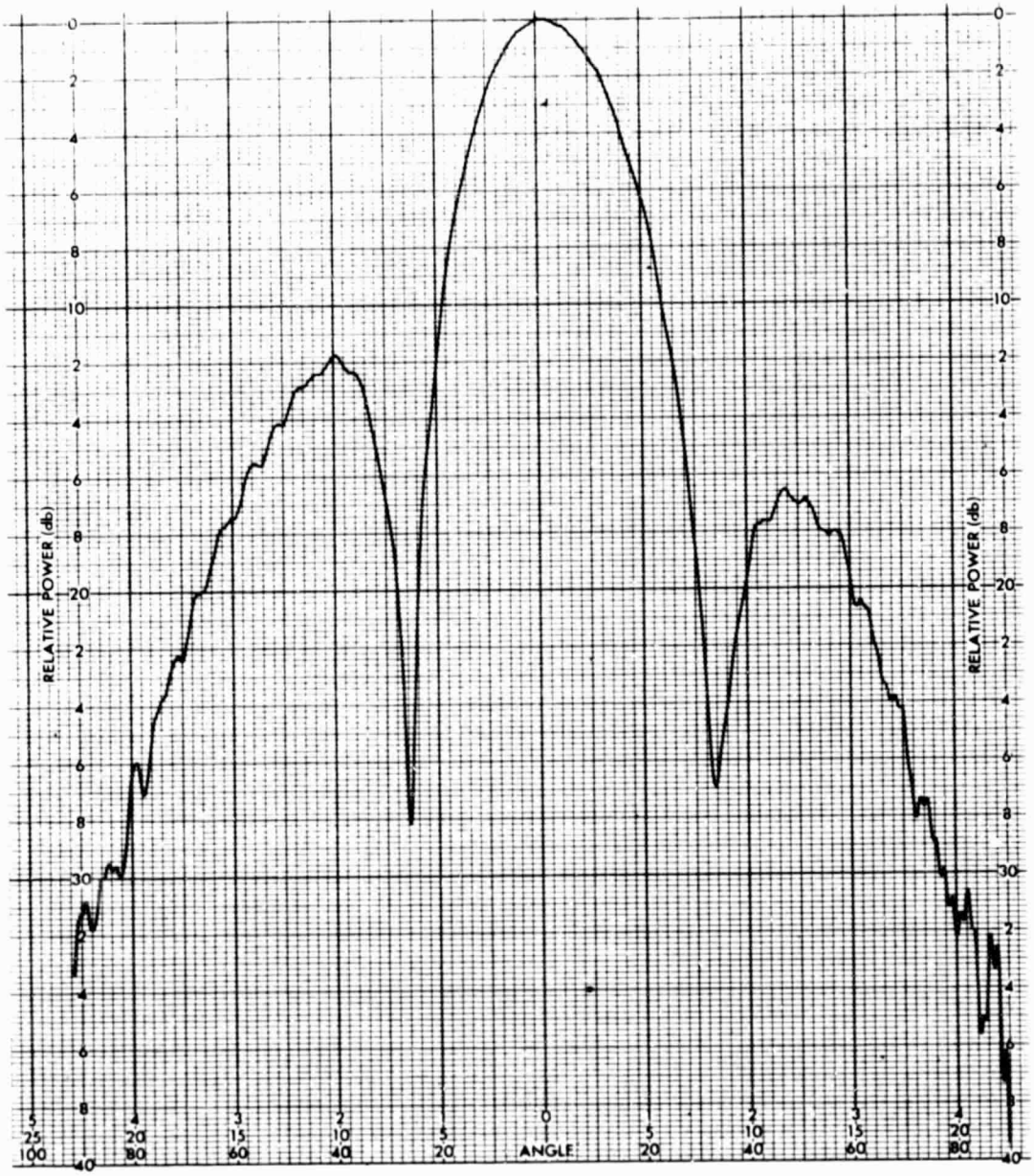

229108

Figure A-64. Measured 15.2-GHz Pattern, Azimuth, No Scan

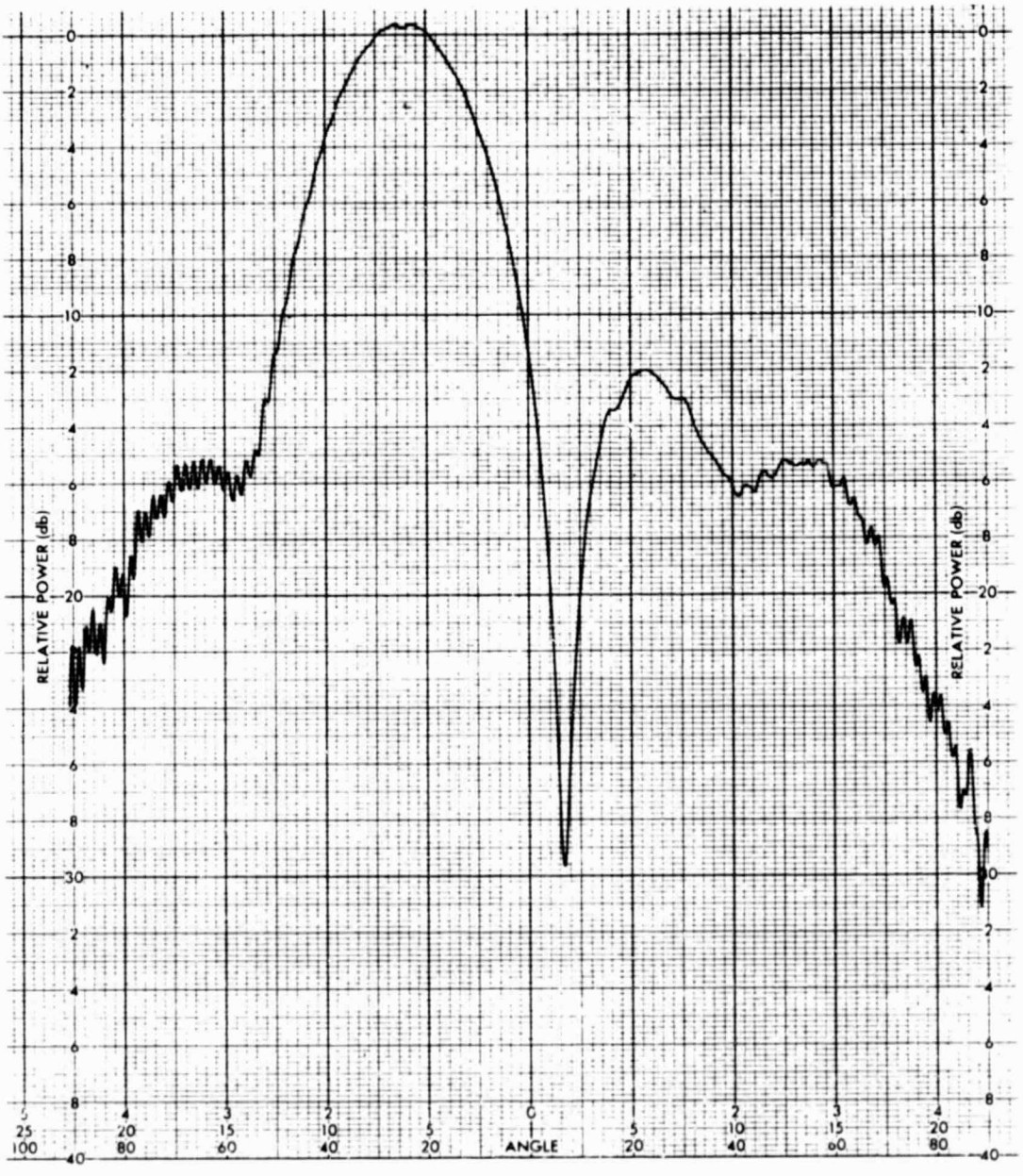

229109

Figure A-65. Measured 15.2-GHz Pattern, Beam Scanned 23 Degrees in Azimuth

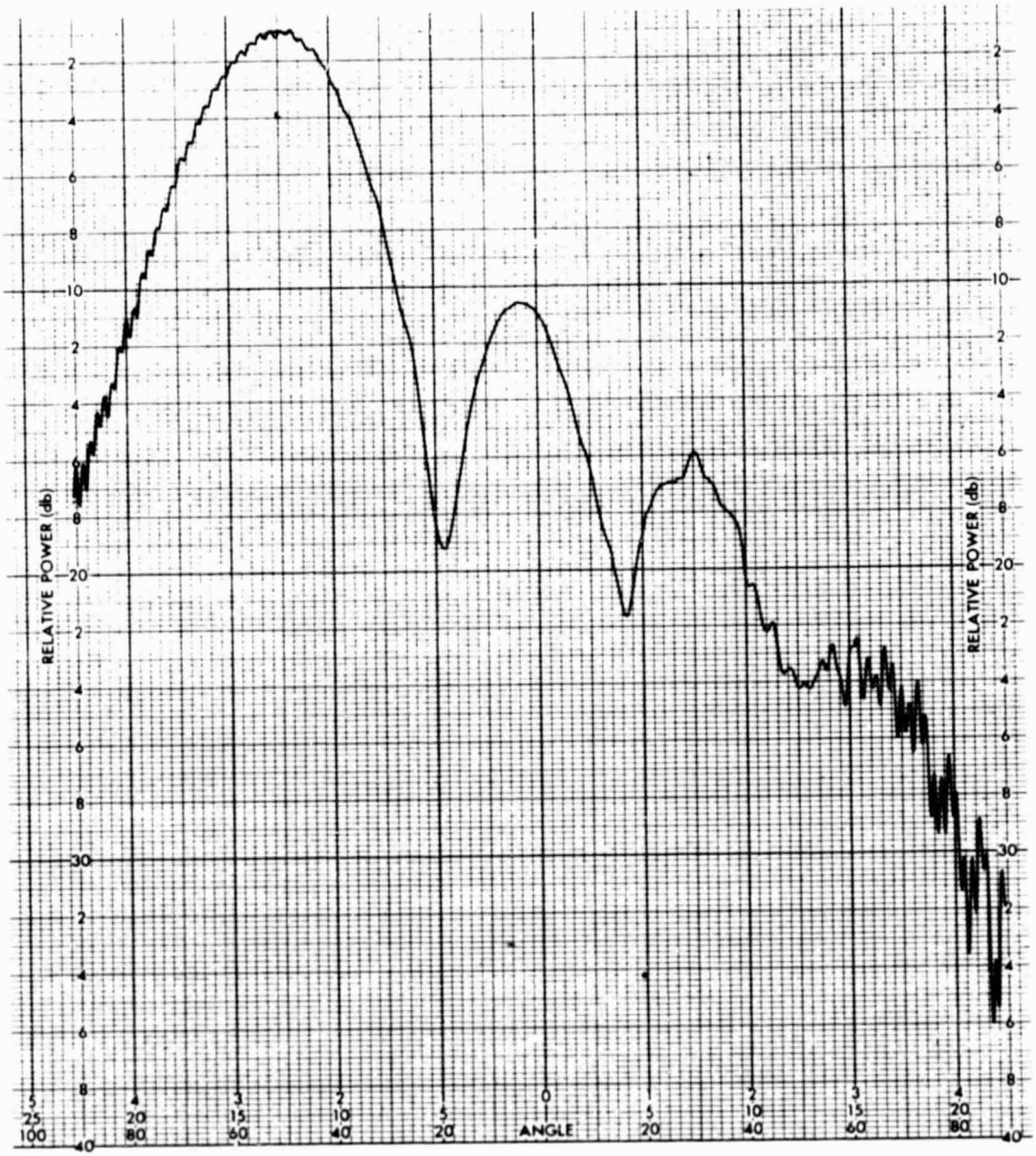

229110

Figure A-66. Measured 15.2-GHz Pattern, Beam Scanned 51 Degrees in Azimuth

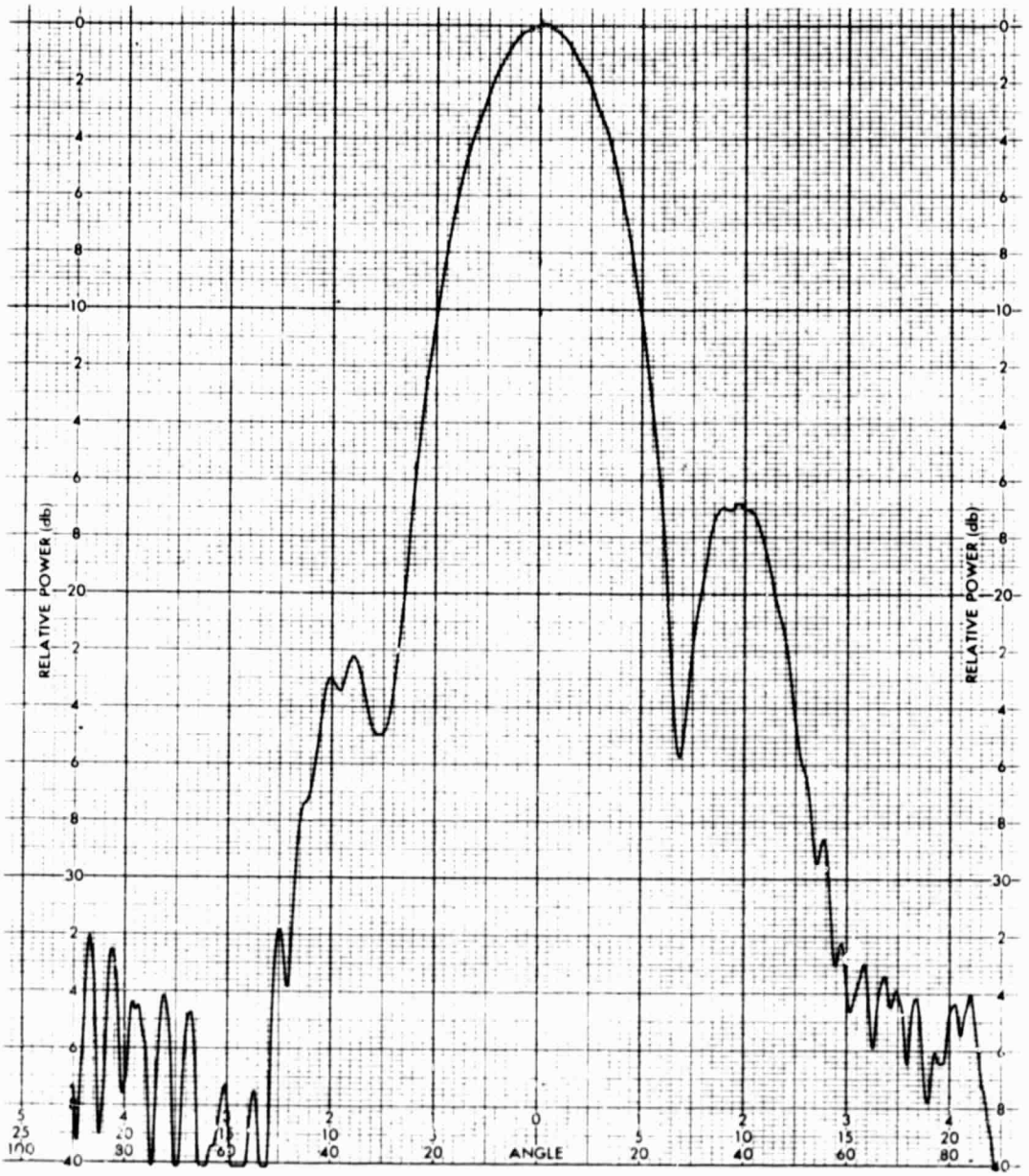

229111

Figure A-67. Measured 15.2-GHz Pattern, Elevation, No Scan

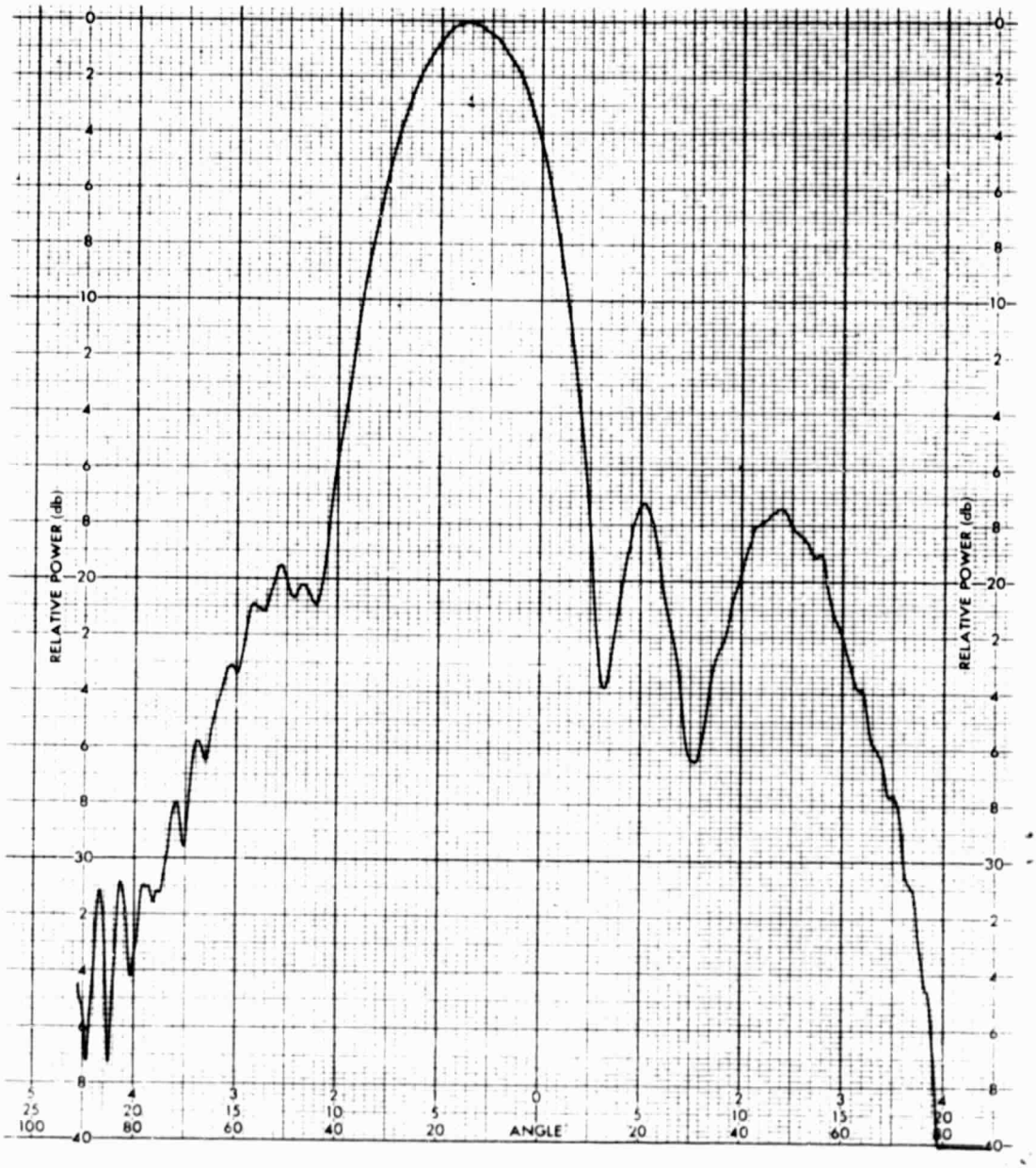

229112

Figure A-68. Measured 15.2-GHz Pattern, Beam Scanned 13 Degrees in Elevation

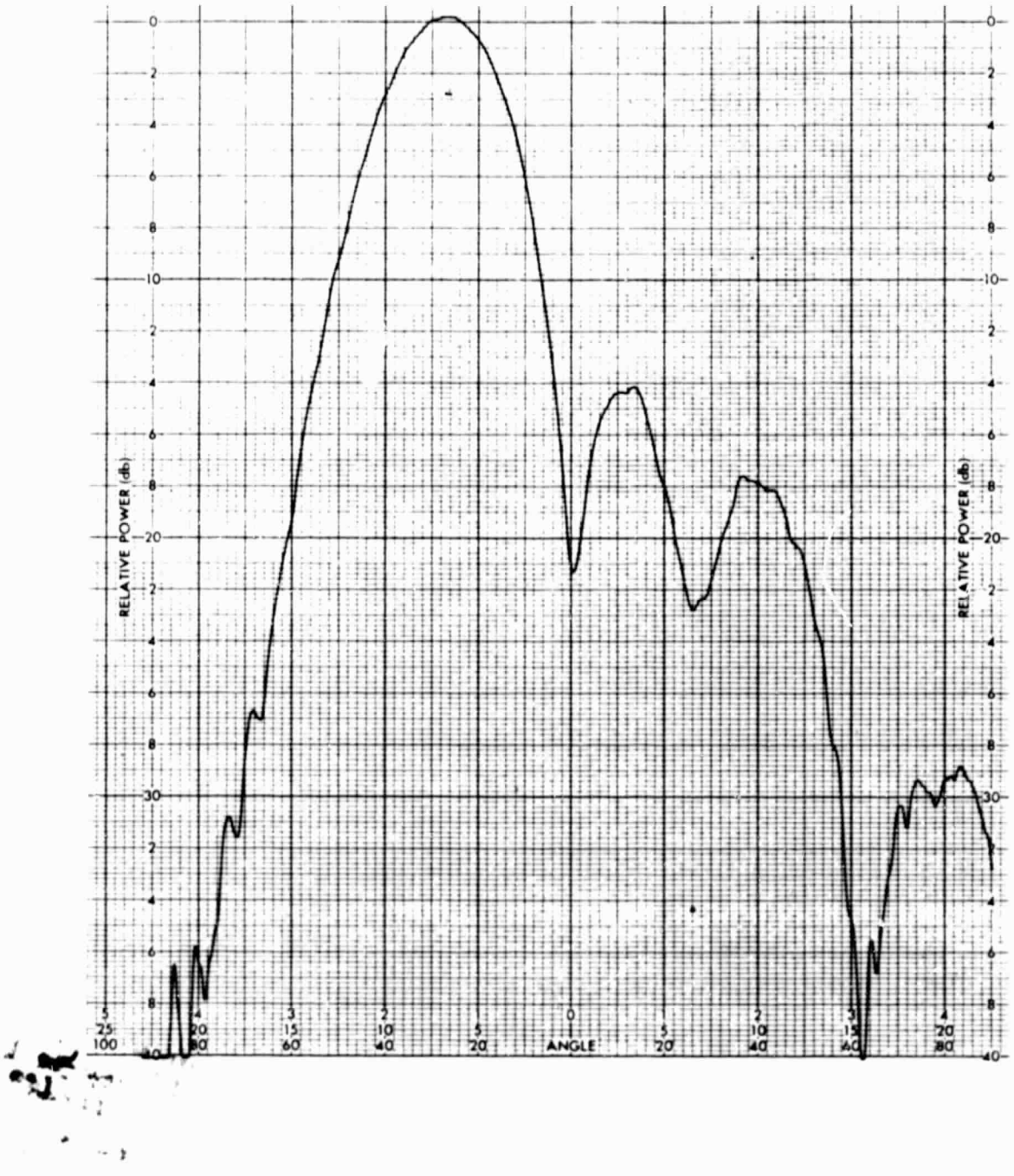

229113

Figure A-69. Measured 15.2-GHz Pattern, Beam Scanned 27 Degrees in Elevation

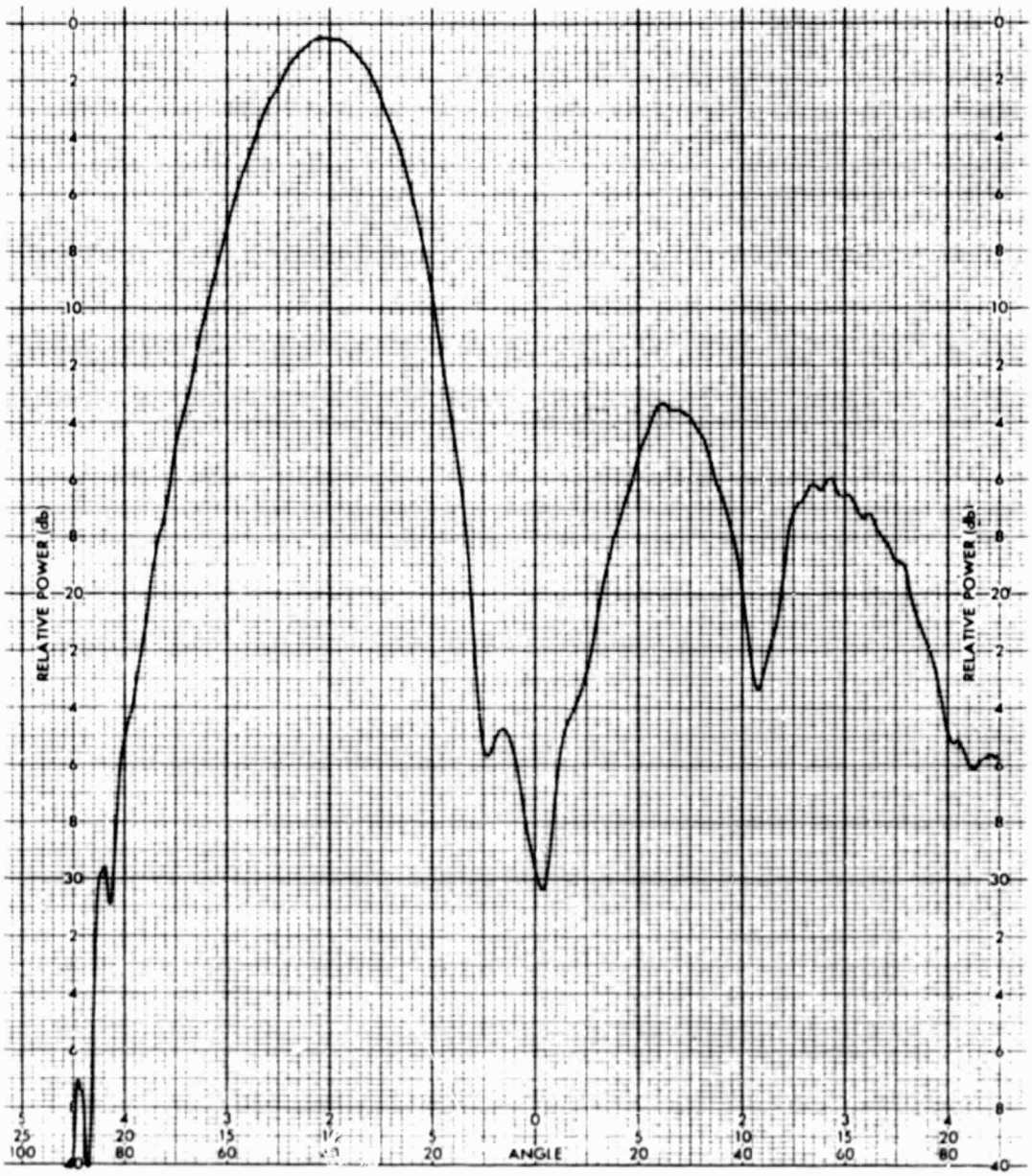

229114

Figure A-70. Measured 15.2-GHz Pattern, Beam Scanned 43 Degrees in Elevation

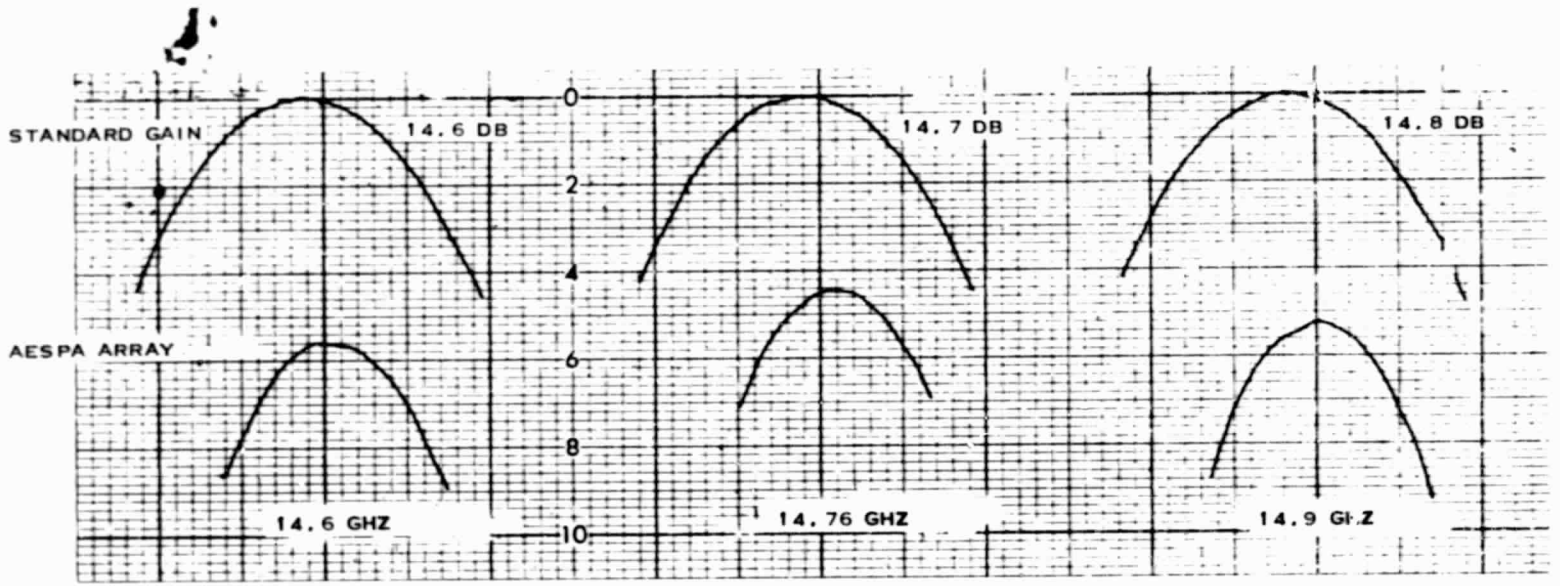

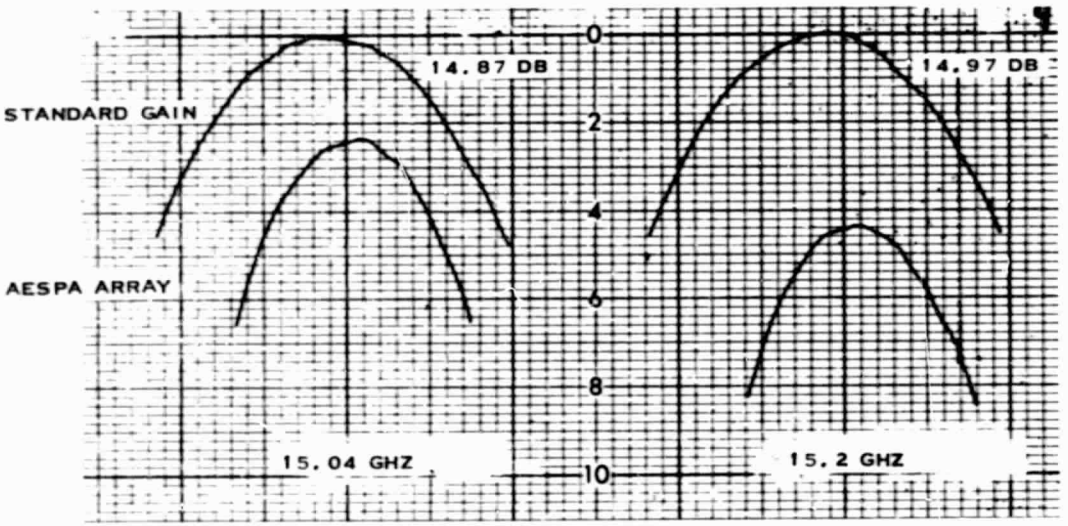

229116

Figure A-71. Array Gain